Studies of the global carbon cycle using atmospheric oxygen and associated tracers

by

Raymond Leonard Langenfelds BSc

Submitted in fulfilment of the

requirements for the Degree of

Doctor of Philosophy

University of Tasmania (September, 2002)

This thesis contains no material which has been accepted for a degree or diploma by the University or any other institution, except by way of background information and duly acknowledged in the thesis, and to the best of my knowledge and belief no material previously published or written by another person except where due acknowledgement is made in the text of the thesis.

Some of the material presented in this thesis has been published in the following articles:

Chapter 3: Langenfelds et al. (1999a; 1999b); Langenfelds (2002b)

Chapter 4: Langenfelds et al. (2002a)

Chapter 5: Langenfelds et al. (1996a; 1996c)

ABSTRACT

This thesis presents research into the global carbon cycle using measurements of atmospheric composition made at the Commonwealth Scientific and Industrial Research Organisation's (CSIRO) Global Atmospheric Sampling LABoratory (GASLAB). The focus is on high precision measurement of atmospheric O_2/N_2 and its application to deduction of carbon fluxes due to surface exchange and atmospheric transport processes. A key theme is the use of multiple species (gas concentrations and isotopomer ratios) constraints to enhance both the interpretation of atmospheric data and the diagnosis of experimental artefacts.

Behaviour of the linked carbon and oxygen cycles in the contemporary atmosphere is examined on three timescales, in each case addressing important but unresolved scientific issues:

- The long term trend in atmospheric O_2/N_2 constrains the partitioning of uptake of anthropogenic CO_2 between the oceans and the land biosphere. The partitioning is deduced here by determination of trends at Cape Grim, Tasmania, based on 5 years of biweekly flask sampling and by reconstruction of a 23-year record using archived air. The results favour a small net global biospheric sink, implying significant oceanic and terrestrial (after allowance for land clearing) carbon uptake between 1978 and 2001.
- More than forty years of atmospheric CO_2 monitoring at Mauna Loa, Hawaii has revealed strong correlation in interannual variability (IAV) of CO_2 growth rate with the El Niño Southern Oscillation (ENSO). GASLAB multi-species measurements during the 1990s showed correlation of ENSO and global IAV in

most of the measured species. They include CO_2, established tracers of terrestrial carbon exchange (O_2/N_2 and $\delta^{13}C$) and other species (H_2, CO and CH_4) whose atmospheric budgets are not as obviously linked to CO_2. A multi-species analysis implicates biomass burning as a major influence on IAV in all species.

- Seasonal cycling in composition of background Southern Hemisphere air is investigated by ground-based flask sampling of the marine boundary layer at Cape Grim and from aircraft-based vertical profiling of the troposphere to altitudes of 6-8 km above Cape Grim. Seasonal variations in the vertical O_2/N_2 gradient are useful as a constraint of vertical mixing rates. Measurements of CO_2, O_2/N_2 and other relevant tracers are used to explore the relative contributions of multiple processes (atmospheric transport, terrestrial and air-sea exchange) to seasonal signals.

Measurement of O_2/N_2 to the precision required for global carbon cycle studies is a major challenge. Extensive consideration is therefore given to the technical aspects of this measurement program, especially in relation to the mass spectrometric analytical technique and to gas handling procedures. Numerous causes of significant O_2/N_2 artefacts were identified, in some cases shedding light on artefacts previously observed, but not understood, for other species (e.g. CO_2).

ACKNOWLEDGEMENT

I am extremely fortunate to have found myself under the supervision of Roger Francey, Paul Steele and Bill Budd in taking on this project. Their knowledge, enthusiasm, support and patience have been remarkable. Without their involvement, the project and I would have faded away a long time ago.

Most of the work was carried out at CSIRO Atmospheric Research in Melbourne, Australia, where I was fortunate to have access to outstanding facilities and people. The gas chromatography and CO_2 isotope data were made available largely through the expertise, hard work and dedication of CSIRO GASLAB staff, from whom I also gained the benefit of regular discussions and assistance. Special thanks go to Lisa Cooper, Darren Spencer, Paul Krummel, Colin Allison, David Etheridge and Bronwyn Dunse. Assistance with the interpretive aspects of this work was provided by the Guesslab team (Peter Rayner, Rachel Law, Cathy Trudinger and Ian Enting), and by Graeme Pearman and Bernard Pak.

I had many valuable discussions and e-mail exchanges with collaborators from other laboratories including Ralph Keeling, Michael Bender, Mark Battle and Andrew Manning regarding O_2/N_2 measurements and the oxygen cycle, and with Jon Lloyd regarding carbon cycle interactions with terrestrial ecosystems and the state of football. Thanks to Laurie Porter and Stuart Baly at CGBAPS for the collection of air samples and quietly suffering endless requests for new experiments.

Finally, thank you to my wife, family and friends for all of their support, and for tolerating my all too frequent withdrawal from society.

TABLE OF CONTENTS

LIST OF TABLES

LIST OF FIGURES

LIST OF ABBREVIATIONS AND SYMBOLS

AIA	CSIRO's site code for aircraft sampling above Cape Grim
Al	aluminium
ALC	CSIRO's site code for Alert, Canada
Ar	argon
C_2H_6	ethane
C_3 plants	plants that use rubisco to make a three-carbon compound as the first stable product of carbon fixation
C_4 plants	plants that use PEP carboxylase to make a four-carbon compound during initial carbon fixation
CFA	CSIRO's site code for Cape Ferguson, Queensland, Australia
CFC	chlorofluorocarbon
CGA	CSIRO's site code for Cape Grim, Tasmania, Australia
CGAA	Cape Grim Air Archive
CH_4	methane
CO	carbon monoxide
CO_2	carbon dioxide
COV	changeover valve of the mass spectrometer
CRC-MATCH	Cooperative Research Centre – Model of Atmospheric Chemistry
CSIRO	Commonwealth Scientific and Industrial Research Organisation
Delta^{plus}XL	the second model of mass spectrometer used for O_2/N_2 measurements at CSIRO
DIC	dissolved inorganic carbon
ENSO	El Niño Southern Oscillation
EPC	CSIRO's site code for Estevan Point, Canada
FID	flame ionisation detection
FPU	flask pump unit
GASLAB	Global Atmospheric Sampling LABoratory
GC	gas chromatograph

GPP	gross primary production
H_2	hydrogen
H_2O	water
HCN	hydrogen cyanide
HNH	high northern hemisphere (approx. 60-90°N)
HSH	high southern hemisphere (approx. 60-90°S)
I	ion beam intensity (current)
IAV	interannual variability
I.D.	inner diameter
IR	infra-red
IRMS	isotope ratio mass spectrometry
m/z	mass/charge ratio
MAA	CSIRO's site code for Mawson Station, Antarctica
MAT252	the first model of mass spectrometer used for O_2/N_2 measurements at CSIRO
MBL	marine boundary layer
MQA	CSIRO's site code for Macquarie Island, Australia
$Mg(ClO_4)_2$	anhydrous magnesium perchlorate (used for drying sample air)
MLU	CSIRO's site code for Mauna Loa, Hawaii, USA
MPI-BGC	Max Planck Institute for Biogeochemistry
MS	mass spectrometer
N_2	nitrogen
N_2O	nitrous oxide
NDIR	non dispersive infra-red
NH	northern hemisphere
NMHC	non-methane hydrocarbon
NO	nitric oxide
NOAA/CMDL	National Oceanic and Atmospheric Administration, Climate Monitoring and Diagnostics Laboratory
NPP	net primary production
O_2	oxygen
O_3	ozone

O.D.	outer diameter
ODR	orthogonal distance regression
OH	hydroxyl radical
PFA	Teflon perfluoroalkoxy
PgC	petagram carbon (10^9 g carbon)
ppb	parts per billion
ppm	parts per million
PTFE	Teflon polytetrafluoroethylene
PU	Princeton University
RGD	reduction gas detection
SA	the sample side gas stream admitted to the mass spectrometer
SF_6	sulfur hexafluoride
SH	southern hemisphere
SIO	Scripps Institution of Oceanography
SIS	CSIRO's site code for Shetland Isles, Scotland
SOI	Southern Oscillation Index
SPU	CSIRO's site code for South Pole Station, Antarctica
SS	stainless steel
ST	the standard side gas stream admitted to the mass spectrometer
STP	standard temperature and pressure
Tg	teragram (10^{12} g)
UAN	Universal Analysis Number (or Sample ID) of CSIRO samples
URI	University of Rhode Island
UV	ultra-violet
V	voltage
VPDB	Vienna Pee Dee Belemnite (carbon isotope reference material)

CHAPTER 1

INTRODUCTION

1.1 The enhanced greenhouse effect

One of the major environmental issues facing the world today is climate change due to the enhanced greenhouse effect. The composition and radiative properties of the Earth's atmosphere are changing at an unprecedented rate due to human activities. Combustion of fossil fuels, deforestation, industrial and agricultural practices all contribute to emission of long-lived greenhouse gases into the atmosphere. These gases are transparent to short-wave solar radiation but intercept some of the long-wave (infra-red) radiation emanating from the Earth's surface, thus heating the atmosphere (Goody and Yung, 1989). The main greenhouse gases include naturally abundant species such as water vapour (H_2O), carbon dioxide (CO_2), methane (CH_4), nitrous oxide (N_2O) and tropospheric ozone (O_3) and groups of predominantly man-made compounds such as the chlorofluorocarbons (CFCs). The largest, direct anthropogenic contribution is from CO_2, which accounts for about 55 % of enhanced radiative forcing since pre-industrial times (Schimel et al., 1996).

Accumulation of these gases in the atmosphere is expected to have major consequences for the Earth's climate, with indirect effects on physical and ecological systems. Projections for the 21st century based on IS92 emission scenarios (Leggett et al., 1992), prepared for the Intergovernmental Panel on Climate Change (IPCC) scientific assessment, include an increase in mean, global surface temperature of between 1 and 3.5°C (Kattenberg et al., 1996), changes in regional climatic patterns with a tendency towards higher frequency of extreme weather events (e.g. high

temperatures, floods, droughts) and a mean sea level rise of 13-94 cm (Warrick et al., 1996) with a small, though not negligible, possibility of a much larger rise of about 5 metres should the West Antarctic Ice Sheet collapse (Oppenheimer, 1998).

There is a growing body of evidence to suggest that anthropogenically-induced climate change has already emerged from the band of natural climate variability (Nicholls et al., 1996). The decade of the 1990s was the warmest on record, extending the trend of rising global temperature that shows an increase of about 0.5°C over the last century. Regional variability is evident, with greatest warming observed over continents of the mid to high latitudes of the Northern Hemisphere (NH). Sea level has risen by 10-25 cm over the last century, due to thermal expansion of ocean waters and retreat of glaciers (Warrick et al., 1996). Impacts of climate change have been observed in the life cycles and migration patterns of many plant and animal species (Peñuelas and Filella, 2001). Evidence for extensive changes to the phenology of terrestrial ecosystems has been captured by the integrating properties of the atmosphere. A trend towards a longer growing season of NH vegetation is manifested in changes to the amplitude and phase of the seasonal cycle of atmospheric CO_2 (C.D. Keeling et al., 1996).

There is growing recognition of the need to ameliorate and/or adapt to climate change, as formalised by the United Nations Framework Convention on Climate Change (UNFCCC) and national and international commitments under the Kyoto Protocol. This process includes research into several key aspects of global atmospheric change, including observation of the natural climate system and anthropogenic perturbations, simulation of climate change using global climate models, studies of potential impacts and assessment of options for mitigation.

One critical element involves monitoring of the spatiotemporal distribution of greenhouse (and related) gases to help identify and quantify the gases' sources and sinks. A broader aim is to establish a mechanistic understanding of the biogeochemical cycles of these gases, including characterisation of the nature of the relevant exchange processes in terms of their dependence on environmental factors such as climate. Developing a sound understanding of the system is important for two reasons. First, it determines our ability to forecast future atmospheric greenhouse gas loading, at least according to assumptions concerning future emissions that are subject to decisions concerning energy and land use practices. This in turn represents a key element in forecasts of future climate change. Second, it may lead to opportunities for mitigating emissions by controlling sources or sinks.

1.2 Evidence of changing atmospheric composition

The prospect of atmospheric composition and hence climate being modified by human activities was first raised in 1896 by the Swedish scientist, Svante Arrhenius (see Crawford, 1996). However, a scientific investigation of the response of natural systems to anthropogenic forcing was not possible until experimental techniques were sufficiently advanced to detect the relevant atmospheric signals. Before the latter part of the 20th Century, sporadic measurements of various trace gases provided an indication of overall atmospheric composition and in some cases identified influence of local sources such as urban areas and terrestrial ecosystems. However, data were neither sufficiently extensive nor precise to provide useful information about spatial or temporal variations in the background atmosphere.

The modern era of research into atmospheric composition began with the commencement of direct, high precision monitoring of CO_2 at Mauna Loa, Hawaii in

1958 and shortly after at the South Pole by the Scripps Institution of Oceanography (SIO; C.D. Keeling et al., 1989). Regular sampling was later extended to a wider network of sites and through air sampling networks operated by other laboratories. Two of the present day networks with extensive geographical coverage are those of the National Oceanic and Atmospheric Administration's Climate Monitoring and Diagnostics Laboratory (NOAA/CMDL) (Conway et al., 1994) and CSIRO (Francey et al., 1996). By 2001, CO_2 was being regularly measured by about 20 individual laboratories at more than 100 surface sites, either by continuous in-situ monitoring or flask sampling.

Monitoring of several other important trace gases has developed in the wake of that for CO_2, but the length of their atmospheric records is shorter and the number of sites where they are measured is fewer than for CO_2. CSIRO's monitoring activities now routinely include measurement of CO_2 and its isotopes $\delta^{13}C$ and $\delta^{18}O$, CH_4, H_2, CO and N_2O in all flask samples collected at global network sites (Francey et al., 1996). Methane and N_2O are strong greenhouse gases in their own right. Hydrogen and CO are not important greenhouse gases, but are linked to carbon cycle processes and have indirect effects on radiative forcing, especially through chemistry involving the hydroxyl radical (OH) and some source processes (e.g. combustion). Isotopes of CO_2 are tracers of exchange processes involving CO_2.

Complementing the direct atmospheric records are reconstructions of past atmospheric composition from ancient air trapped in polar ice sheets and from proxy records such as tree rings, coral and marine sediments. The longest ice core records, such as that from Vostok, Antarctica span more than 400,000 years and reveal strong links between atmospheric CO_2 and climatic variations on timescales up to order 100,000 years for glacial cycles (Petit et al., 1999). Higher resolution time series such

as those from ice cores and firn from Law Dome, Antarctica indicate CO_2/climate links on shorter timescales, such as the Little Ice Age between 1500 and ~1800 AD (Etheridge et al., 1996). They also capture the dramatic increase in CO_2 during the period of industrialisation since ~1800, during which time atmospheric CO_2 rose from its mean pre-industrial level of about 280 ppm to more than 360 ppm by the end of the 20th Century. This increase is due mainly to combustion of fossil fuels and deforestation associated with land use change.

1.3 Key issues for the contemporary carbon cycle

There are two features of the recent atmospheric CO_2 record that highlight gaps in our knowledge of the global carbon cycle and which are addressed in this thesis. They are illustrated by Figure 1.1, which shows the known major CO_2 fluxes and their relationship with the Southern Oscillation Index (SOI). The first point is that the average rate of CO_2 accumulation in the atmosphere is less than half the rate at which CO_2 is emitted by human activities. Independent estimates are available of the history of CO_2 emissions from both fossil fuel usage and land use change. Annual fossil fuel emissions have been determined by inventory-based methods (Marland et al., 2001) to be about 6.5 PgC yr^{-1} in the 1990s. Fluxes from documented land use change, including allowance for removal and oxidation of carbon in the vegetation, subsequent regrowth and changes in soil carbon, have been estimated at ~2 PgC yr^{-1} during the 1990s (Houghton and Hackler, 2000). However, this figure carries larger uncertainty because accounting procedures for land use change are not as precise as those for fossil fuel usage. Of the 8.5 PgC emitted annually by human activity today, on average only 3.5 PgC remains in the atmosphere. The remainder is being removed by the major carbon reservoirs in contact with the atmosphere, namely the oceans and

the land biosphere, but the relative proportions remain uncertain. Modelling of oceanic uptake of anthropogenic CO_2 has for a long time been able to account for some of the difference with estimates of about 2 PgC yr^{-1} uptake for the 1980s-1990s (Sarmiento et al., 1992). However, 3 PgC yr^{-1} remained unaccounted for and became known as the "missing carbon sink".

The second unexplained feature of the atmospheric CO_2 record is the interannual variability (IAV) in growth rate on timescales of 2-5 years. Variations of up to ±2 PgC yr^{-1} are too large to be explained by variability in emissions from fossil fuel use or land use change. Furthermore, the IAV shows strong correlation with the SOI, indicating that the CO_2 flux anomalies are related to climate (Dettinger and Ghil, 1998; Rayner et al., 1999a). Resolution of these questions would reduce some of the remaining uncertainties in our knowledge of carbon cycle processes in today's atmosphere and would thus help to improve forecasts of how the major carbon reservoirs will respond to future changes in atmospheric composition and climate.

1.4 Multiple tracer techniques

Previous studies addressing these questions have often employed constraints imposed by coincident variations in other tracers, such as the isotopomers of CO_2. The $^{13}C/^{12}C$ ratio (expressed as $\delta^{13}C$, a deviation in the ratio from a reference) is a tracer of carbon exchange with biogenic CO_2 and has been widely used to distinguish net oceanic and terrestrial fluxes (e.g. Keeling et al., 1995; Ciais et al., 1995; Francey et al., 1995; Nakazawa et al., 1997). Its suitability for this role is a consequence of photosynthesis by plants discriminating in favour of the lighter carbon isotopomer.

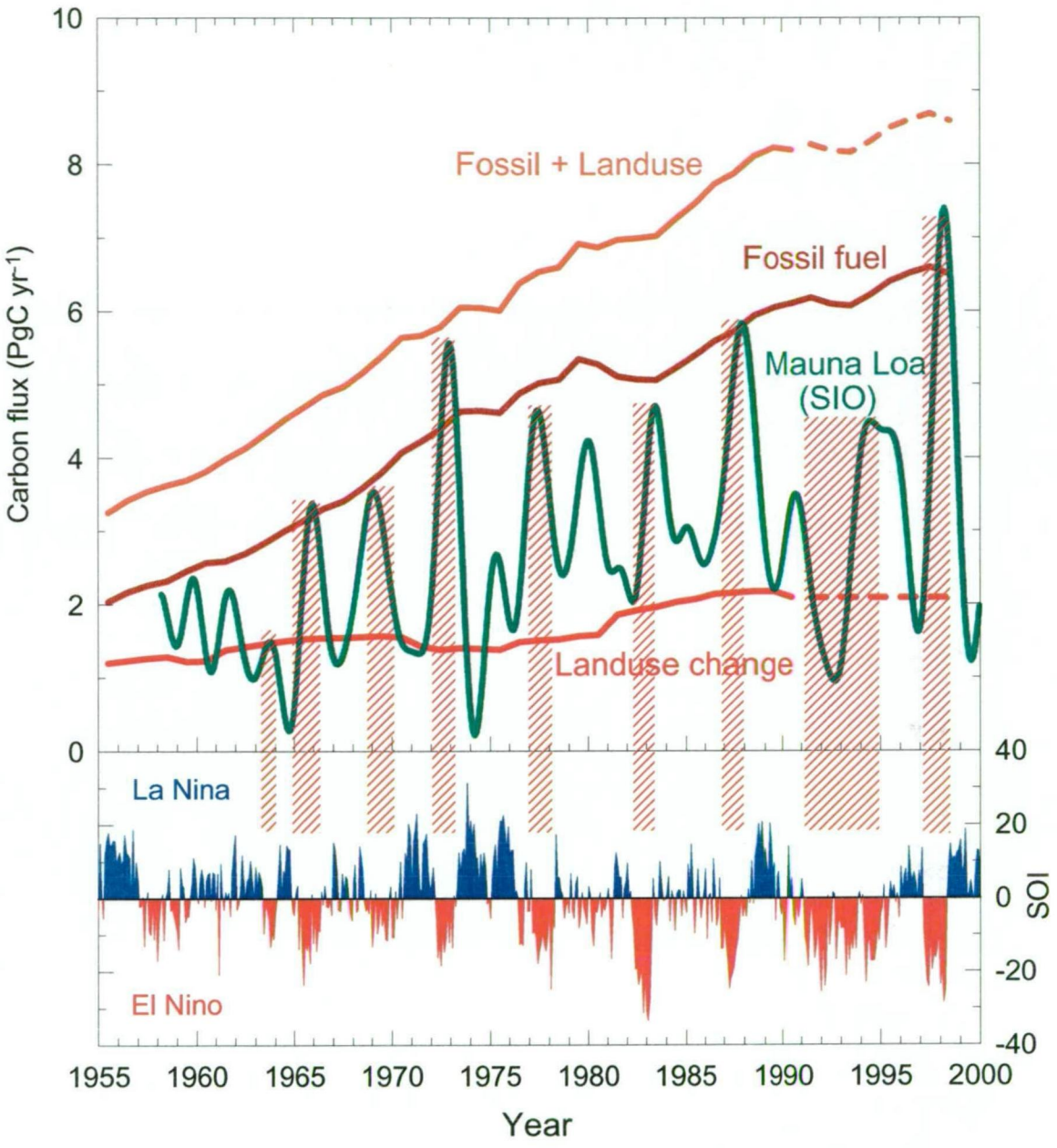

Figure 1.1 Atmospheric CO_2 growth rate from SIO measurements at Mauna Loa (Keeling and Whorf, 2001), rates of emission from fossil fuel use and land use change, and the relationship with the SOI.

By contrast, there is little isotopic signal associated with air-sea exchange of CO_2 because of buffering by the large reservoir of dissolved inorganic carbon (DIC) in seawater.

The $^{18}O/^{16}O$ ratio ($\delta^{18}O$) in CO_2 can be used to distinguish terrestrial CO_2 fluxes due to photosynthesis and total ecosystem respiration, owing to exchange of O atoms in dissolved CO_2 with different isotopically labelled water reservoirs (Francey and Tans, 1987; Peylin et al., 1999). The $^{14}C/^{12}C$ ratio in CO_2 (expressed as $\Delta^{14}C$, percent modern carbon) is a key tracer for calibration of ocean carbon cycle models. It is useful for this purpose because of a dramatic increase in atmospheric ^{14}C from nuclear bomb testing in the atmosphere during the 1950s and 1960s. The rate of oceanic uptake of anthropogenic CO_2 is constrained by observations of the penetration of ^{14}C into the deep ocean. A similar approach was taken by Quay et al. (1992) using oceanic depth profiles of $\delta^{13}C$.

1.5 The use of O_2 as a tracer of carbon cycle processes

Anthropogenic forcing of atmospheric CO_2 has coincident impacts on atmospheric oxygen (O_2). Combustion of fossil fuels and of biomass through deforestation consumes O_2 and produces CO_2 in a stoichiometrically linked relationship (e.g. Keeling, 1988). For fossil fuel hydrocarbons:

$$C_xH_y + (x + \frac{1}{4}y)O_2 \rightarrow x\,CO_2 + \frac{1}{2}y\,H_2O \qquad (1.1)$$

Oxygen and CO_2 are also exchanged through biological cycling. Photosynthesis by plants removes CO_2 from the atmosphere and produces O_2 while exchange is of the opposite sign for respiration of (living and dead) organic matter. For terrestrial

vegetation:

$$CO_2 + H_2O \leftrightarrow CH_2O + O_2 \quad (1.2)$$

An important difference between the two gases is in their solubility in water. CO_2 is highly soluble so that a substantial part of the excess CO_2 in the atmosphere is absorbed by the oceans, and stored mostly in the form of DIC. The equilibrium partitioning ratio for ocean/atmosphere carbon reservoirs is about 50. By contrast, O_2 has low solubility with a partitioning ratio of <0.01. This means that for perturbations in atmospheric O_2, less than 1% of the difference is replenished by degassing of dissolved O_2, after the system returns to equilibrium. It is this feature that makes O_2 especially valuable as a tracer of the global carbon budget. Changes in atmospheric O_2 on multi-annual timescales primarily reflect combustion and terrestrial exchange. When considered in conjunction with concurrent trends in CO_2 and independent estimates of fossil fuel emissions, the system can be solved for the relative rates of uptake of anthropogenic CO_2 by oceans and the land biosphere.

Until relatively recently, an impediment to use of atmospheric O_2 measurements for global carbon cycle studies was the precision with which it could be measured. Because it is highly abundant in the atmosphere with a mole fraction of close to 21% (as compared to CO_2 at 360 ppm, or 0.036%), the proportional changes imparted by carbon cycle processes are very small. For example, current annual CO_2 emissions from fossil fuel combustion equate to about 0.8% of the atmospheric CO_2 burden, whereas the relative change in O_2 is only 0.002%.

During the late 1980s and early 1990s, development of two techniques succeeded in achieving the level of precision (better than 1 part in 10^5) required for

these applications. Both techniques rely on measurement of the O_2/N_2 ratio. One used interferometry to measure relative refraction of light at two different wavelengths (Keeling, 1988; Keeling et al., 1998a), providing the foundation of the O_2/N_2 measurement program now maintained at SIO. The second technique, based on isotope ratio mass spectrometry (IRMS), was developed at the University of Rhode Island (URI; Bender et al., 1994), though the operation has since moved to Princeton University (PU). More recently, high precision techniques have also been developed using gas chromatography (Tohjima, 2000) and paramagnetic methods (Manning et al., 1999; Manning, 2001).

SIO and URI/PU flask sampling records of O_2/N_2 now span more than a decade. The inferred trends have been used to partition terrestrial and oceanic uptake of CO_2 over this period (see Chapter 3). Flask sampling records have also proven useful for other applications. The latitudinal O_2/N_2 gradient has been used to investigate the spatial distribution of net terrestrial CO_2 uptake during the 1990s (R.F. Keeling et al, 1996). Large seasonal air-sea O_2 fluxes have been used to investigate the kinetics of air-sea gas exchange (Keeling et al., 1998b), constrain rates of marine biological production (Bender et al., 1996) and features of oceanic circulation on regional (Stephens et al., 1998) and local (Manning, 2001) scales.

1.6 Incorporating O_2/N_2 into GASLAB measurement programs

This thesis describes the development and first results of a high precision O_2/N_2 measurement capability coordinated within the established CSIRO GASLAB trace gas and isotope measurement program. The initial focus was on compiling time series of O_2/N_2 in background Southern Hemisphere (SH) air, based on flask sampling at Cape Grim and from CSIRO's long-running aircraft program involving

monthly vertical profiles of the troposphere above Cape Grim (Langenfelds et al., 1996a). Principal aims were to investigate the long term O_2/N_2 trend and its implications for uptake of anthropogenic CO_2, and the seasonal cycle of SH O_2/N_2 variations, especially in relation to vertical gradients and their implications for surface exchange and atmospheric transport.

The potential usefulness of O_2/N_2 measurements within the GASLAB program is enhanced by the established capability of high precision measurements for multiple trace gas and isotopic species. It provides a framework for exploring multi-species approaches to quality control of measurements and interpretation of atmospheric data. In the same way that O_2/N_2, $\delta^{13}C$, $\delta^{18}O$ and $\Delta^{14}C$ have previously been used to constrain the global carbon budget, it will be shown that further useful constraints of carbon cycle processes are provided by coincident variations of CO_2 with other trace gases, such as H_2, CO and CH_4. Although the global budgets of these species are largely independent of CO_2, there are some links that can be used to advantage in isolating CO_2 fluxes involving specific processes. Furthermore, the O_2/N_2 data are supported by extensive diagnostic information obtained from regular, concurrent analysis of other molecular ratios including isotopes of O_2 and N_2 and of the inert gas pair Ar/N_2.

1.7 Outline of chapters

Stringent demands are placed on the quality of O_2/N_2 data for them to be useful in constraining the global carbon budget. Acceptable limits for precision and systematic error are of the order of 1 in 10^5, substantially exceeding the requirements for other concentration measurements (e.g. 1 in 10^3 is necessary for CO_2 and achievement of 1 in 10^4 is exceptional). In recognition of the importance of data

quality, Chapter 2 provides extensive documentation of methods used and discussion of the technical issues relating to existing or potential artefacts.

Chapter 3 deals with long term trends in O_2 and CO_2 and their application to partitioning of anthropogenic CO_2 uptake by oceans and the land biosphere. The main emphasis is on reconstruction of a 23-year O_2/N_2 trend from the Cape Grim Air Archive (CGAA). The CGAA is a resource with an unparalleled history of yielding high resolution atmospheric records of a host of trace gas species (Langenfelds et al., 1996b), that are largely free of uncertainties associated with maintaining long term calibration or interfering processes that affect air trapped in firn/ice and other proxy records of atmospheric composition.

The interpretation of IAV in global carbon and oxygen cycles in Chapter 4 is enhanced by a multi-species approach, employing a set of tracers not commonly associated with CO_2. In addition to the established tracers (e.g. O_2/N_2, $\delta^{13}C$), other trace gases (H_2, CO, CH_4 etc.) with global budgets largely independent of CO_2 are found to exhibit IAV that is strongly correlated with that in CO_2. These observations provide new insight into the nature of the CO_2/ENSO link.

The seasonal cycles of O_2/N_2, CO_2 and associated tracers in the SH marine boundary layer and their vertical gradients in the troposphere reflect a combination of seasonally varying fluxes due to multiple processes. Again, a multi-species approach provides an effective means of exploring relative contributions from surface exchange (land and ocean) and atmospheric transport (Chapter 5). O_2/N_2 is particularly useful as a tracer of vertical mixing rates. Finally, a summary of outcomes from this research and their ramifications for carbon cycle research and climate change issues in general are discussed in Chapter 6.

CHAPTER 2

O_2/N_2 MEASUREMENT METHODS AND TESTS

2.1 Measured species and reported units

The main focus of the experimental part of this work is on high precision measurement of the O_2/N_2 ratio in air. Because the technique employed here is isotope ratio mass spectrometry (IRMS), selected samples could also be analysed for other molecular ratios such as $^{40}Ar/^{28}N_2$ (from 1999 only; see Section 2.2), $^{29}N_2/^{28}N_2$ and $^{34}O_2/^{32}O_2$ (all of which are valuable as either tracers of biogeochemical processes or experimental diagnostics); also $^{30}N_2/^{28}N_2$ and $^{33}O_2/^{32}O_2$ which are of less value due to low signal-to-noise relative to signals of interest. All MS measurements are reported as deviations in the ratio from a reference, in delta (δ) notation, such that for relative amounts of substance (N) of two species a and b:

$$\delta(a/b) = \left(\frac{N_{a;\,sample}/N_{b;\,sample}}{N_{a;\,reference}/N_{b;\,reference}} - 1 \right) \times 10^6 \qquad (2.1)$$

The units are "per meg" where 1 per meg = 0.001‰ = 0.0001%. Because the mole fraction of O_2 in the contemporary atmosphere is about 20.946% (in dry air; as measured by Machta and Hughes, 1970), it follows that for small changes in mole fraction, a change of 1 part per million (ppm) O_2 is equivalent to 1 / 0.20946 = 4.8 per meg in $\delta(O_2/N_2)$.

Because two mass spectrometers with different collector configurations were used at different times, O_2/N_2 ratios were inferred from measurement of different molecular pairs. The first instrument (MAT252) was used to simultaneously monitor

ion beam intensity (I) of mass/charge (*m/z*) species 32 and 29, while the second instrument (Delta^{plus}XL) monitored *m/z* 32 and 28. Unless otherwise stated, data relating directly to either instrument (in relation to diagnostics and/or calibration) refer to the measured 32/29 and 32/28 ratios, respectively. However, where data from both instruments are merged (e.g. in atmospheric time series or calibration standard histories), reported O_2/N_2 ratio refers to the most abundant isotopomers of both gases, namely 32/28. This involves an adjustment to MAT252 data (Section 2.6.2). For clarity, reference to measured ratios sometimes explicitly specifies respective masses [e.g., $\delta(^{40}Ar/^{28}N_2)$ is taken to be equivalent to $\delta(Ar/N_2)$; also $\delta(^{29}N_2/^{28}N_2)$ is equivalent to $\delta^{29}N_2$ and $\delta^{15}N$ in N_2; $\delta(^{34}O_2/^{32}O_2)$ is equivalent to $\delta^{34}O_2$ and $\delta^{18}O$ in O_2].

Data are also reported for other trace gas species measured in GASLAB. Quoted mole fractions are relative to dry air, in units of parts per million (ppm; for CO_2) and parts per billion (ppb; for CH_4, H_2, and CO). Data for isotopic ratios of CO_2, namely $^{13}C/^{12}C$ and $^{18}O/^{16}O$ are reported using δ notation as given by Equation 2.1, but on the VPDB scale (Allison and Francey, 1995) and in units of per mil (‰) obtained by using a multiplicative factor of 10^3 rather than 10^6.

2.2 Instrumentation/equipment

2.2.1 Mass spectrometers

Techniques used to analyse O_2/N_2 at CSIRO were adapted from those developed at URI (Bender et al., 1994) based on IRMS. Although the objective of this work is to measure and interpret spatiotemporal trends in atmospheric O_2, the precision required for global carbon cycle studies (about 1 in 10^5) can only be achieved with IRMS by measuring the O_2/N_2 ratio. Biogeochemical forcing of the

atmospheric N_2 mole fraction is negligible with the exception of a small, thermally driven, seasonal, air-sea flux (Keeling et al., 1993). The $^{29}N_2/^{28}N_2$ ratio is also highly stable in the atmosphere so that IRMS measurement of O_2/N_2, referenced against either the mass 28 or 29 N_2 isotopomer, can be used to investigate the biogeochemical influences on atmospheric O_2.

Two mass spectrometers, both manufactured by Finnigan MAT GmbH (Bremen, Germany; http://www.thermo.com) but different models, have been used in the CSIRO program. A MAT252 unit was used from inception of the program in 1995 until 1998, during which time it was shared between the O_2/N_2 and CO_2 isotope measurement programs. A Delta^{plus}XL unit has been used exclusively for the O_2/N_2 program since 1999. The principles of operation are similar for both instruments. Sample gas is ionised by electron bombardment. Resulting ions are accelerated under high voltage through a magnetic field, where they are deflected through an angle that varies with *m/z*. The ion beams of interest are detected using a series of Faraday cups. The main difference between the two instruments is in their mass dispersion. Respective configurations of accelerating voltage, focal length and magnetic field strength and shape yield a *m/z* range of 28-40 on the focal plane of the Delta^{plus}XL but only 29-32 on the MAT252. The ability to simultaneously monitor multiple ion beams is further constrained by the collector cup configuration. For example, the MAT252 allows simultaneous monitoring of either O_2/N_2 ratio (*m/z* species 29 and 32), N_2 isotopes (28, 29) or O_2 isotopes (32, 33, 34).

After commencement of O_2/N_2 measurements on the MAT252, it soon became evident that switching the instrument between respective (air and CO_2) modes of operation was detrimental to analytical performance for both modes. In particular, the switching involved connection/removal of capillaries used for O_2/N_2

analyses, and therefore necessitated venting of the changeover valve (COV), usually with ambient air. Re-equilibration and/or drying of the internal high vacuum surfaces of the ion source, flight tube and detector can take several weeks. By implementing appropriate calibration strategies, it was possible to commence routine analyses within a few days of switching modes but nevertheless, measurements were frequently subject to less than optimal instrument stability: Another drawback of this arrangement was frequent delays in gaining instrument time for O_2/N_2 analyses and resulting degradation of flask samples due to storage-related artefacts.

Commissioning of theDelta^{plus}XL in early 1999 provided several immediate benefits: 1) being dedicated to analysis of O_2/N_2, it eliminated the need to switch between air and CO_2 modes thus improving instrument stability, 2) shorter flask sample storage times, 3) a detector configuration allowing simultaneous monitoring over a wider mass range, most importantly allowing measurement of O_2/N_2 ratio via the most abundant isotopomers at masses 32 and 28, and the capability for concurrent high-precision analysis of Ar/N_2; also isotopes of N_2 (28, 29 and 30) and of O_2 (32, 33 and 34) and 4) improved internal precision for $\delta(O_2/N_2)$ of 4 per meg (mean standard deviation of repeat sample/standard cycles from all analyses between 1999 and 2001) as compared to 16 per meg on the MAT252. These factors helped to achieve marked improvement in precision of atmospheric records and identification of numerous measurement artefacts that might never have been possible with the MAT252. Both mass spectrometers (and other GASLAB analytical instruments) are housed inside an air-conditioned laboratory, where temperature fluctuations are typically controlled to better than ±0.5°C.

2.2.2 Inlet system and working standard

A dedicated, custom made inlet system of glass construction with Viton O-ring seals (Figure 2.1) was used to admit all "unknown" sample air (such as flask samples and external standards) through the COV to the MS ion source. It was used in place of the conventional dual inlet provided with both Finnigan instruments, partly because early tests showed $\delta(^{32}O_2/^{29}N_2)$ to drift rapidly in both variable volumes (by –100 per meg hour^{-1} over several days). The drift was observed both

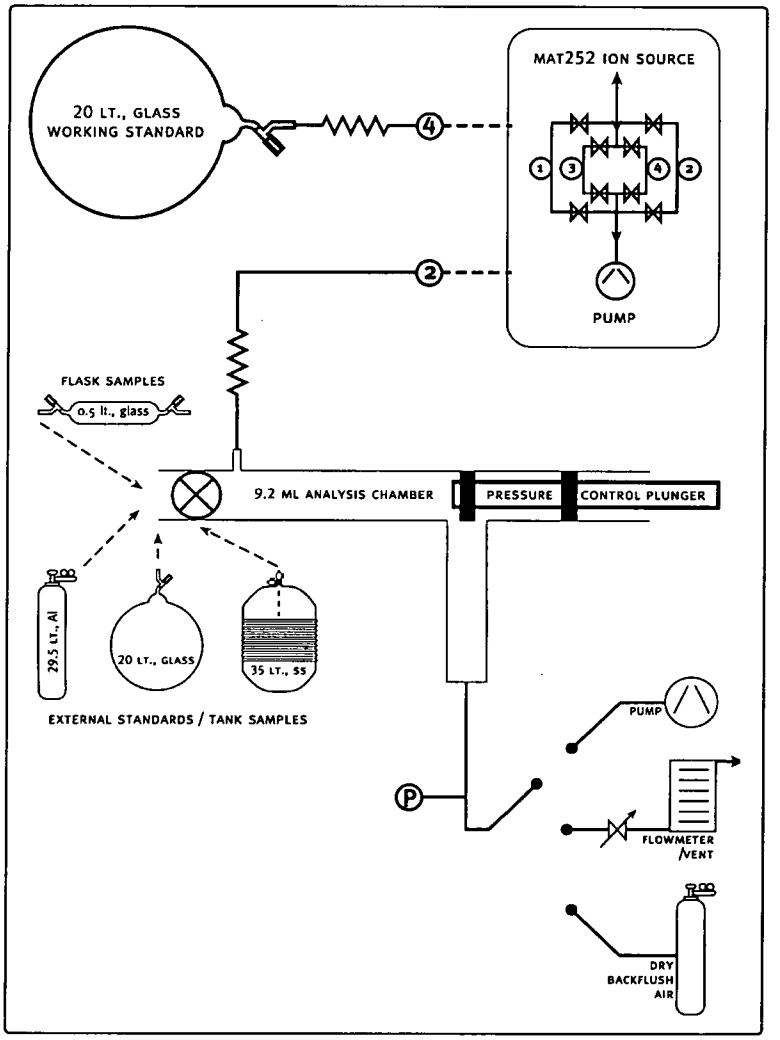

Figure 2.1 A schematic of the inlet system developed for O_2/N_2 analysis, showing the configuration originally used on the MAT252 instrument. Subsequently, a drying tube was inserted upstream of the analysis chamber for routine analyses after October, 1997 and for selected samples before that time.

with the volumes open, thus allowing air to bleed into the COV, or closed. Furthermore, the design provides flexibility both in accommodating samples from a range of containers and pressures, and in options for varying sample loading procedures. Flushing of the analysis chamber is achieved principally by sustained flow of sample air through the length of the chamber ("through-flushing"). This aims to reduce reliance on evacuation and thereby reduce potential for sample modification resulting from non-equilibrium sample flow and surface exchange processes.

An electropolished, stainless steel (SS) plunger provides precise control of sample pressure. It is fitted with two Viton O-rings to seal the analysis chamber from downstream plumbing (during analysis) and the entire system from laboratory air (while flushing). Retraction of the plunger permits either evacuation, through-flushing with measurement of flow rate and/or sample pressure, or conditioning of inlet surfaces by pressurisation with dry, natural ("backflush") air to the operating pressure of the system (~1.25 atm.; i.e. the pressure at which samples are analysed). The inlet to the analysis chamber is sealed by a valve (model RK2 B2-08; Glass Expansion, Melbourne, Australia) also fitted with a Viton O-ring.

Fittings used to connect sample containers to the inlet system are SS. Cajon-Ultratorr ½" fittings equipped with a single oversize Viton O-ring are used at the front end of the glass inlet system and for connecting to CSIRO 0.5 L glass flasks with 11 mm O.D. end stubs. Intermediate fittings and those used to connect to high pressure cylinders are of Swagelok type. After introduction of a drying tube packed with anhydrous $Mg(ClO_4)_2$ (SS, 10 cm length, ¼" O.D., plugged with silanized glass wool) for routine operations (from October, 1997), fittings for all sample types included one quick-connect (Swagelok; part no. SS-QM2-100). Prior to that, 0.5 L

glass flasks were attached using a Cajon-Ultratorr ½" union only. Sample air passes from the inlet system to the COV through a 2.4 m, 25μm I.D. fused silica, polyimide-coated capillary that is insulated and protected by being inside a ¼" O.D. nylon tube. The capillary is attached to the inlet system by a 1/16" Swagelok nut, sealed against the glass by a small Viton O-ring and to the COV by a ¼" Swagelok brass fitting sealed with a Vespel ferrule.

The working (air) standard is contained in a 20 L, glass vessel sealed with a single Viton O-ring valve (Glass Expansion). It was originally filled (in 1994) with dry, natural air to a pressure of 1.3 atm. After 7 years of service its pressure has declined only slightly to 1.25 atm. It is now permanently connected to the COV of the Delta^{plus}XL instrument so that it constantly bleeds through the COV either to the ion source or to waste. On the MAT252 it was used in a similar manner except that the capillary was disconnected from the COV and capped while the MAT252 was used for CO_2 isotope analysis. This reduced its rate of consumption by about 80%. It is connected to the COV by an identical capillary to that used on the sample side inlet and sealed at both ends with ¼" Swagelok brass fittings and Vespel ferrules.

2.2.3 Gas storage vessels and regulators

The types of containers used in GASLAB for storing air samples are described by Francey et al. (1996). For O_2/N_2/Ar specifically, most field samples (and test samples used to evaluate experimental techniques) were contained in CSIRO's 0.5 L glass flasks, which are fitted with two glass valves (Glass Expansion) and sealed with one of three types of O-rings (mostly Viton but also some Teflon, perfluoroalkoxy (PFA) and polytetrafluoroethylene (PTFE)). The relative

performance of different O-ring materials in relation to effects on sample composition during storage is evaluated in Section 2.7.

Air standards are contained in both glass and metal vessels (Table 2.1). There are four 20 L, glass vessels, one of which is used for the working standard, and all of which are fitted with a single glass valve with Viton O-ring (Glass Expansion). The metal cylinders are of three basic types, 1) Al, 29.5 L, manufactured by Luxfer and purchased from Scott Marrin Inc. (Riverside, California, USA), 2) Al, 48 L, manufactured by Commonwealth Industrial Gases (CIG, Sydney, Australia) and treated with their proprietary "Spectra-seal" passivation process, and 3) electropolished, SS, 35 L, manufactured by Essex Cryogenics (Missouri, USA) and fitted with a single SS Nupro bellows valve. Similar SS, 35 L cylinders and older cylinders of similar construction supplied by Biospherics Co. (Oregon, USA) have also been used for archiving of Cape Grim air (Chapter 3).

Most of the high pressure, metal cylinders are fitted with dedicated, two-stage, nickel-plated, brass regulators (series 1000), manufactured by Alphagaz (Walnut Creek, California, USA). Other regulators used for some applications are high purity SS models manufactured by Veriflo (Richmond, California, USA; a division of Parker Instrumentation), APTech (San Rafael, California, USA) and Tescom Corp. (Elk River, Minnesota, USA). No systematic effects have been identified that can be directly attributed to different regulator types, although some effects that are not yet fully understood could be regulator-related. With the exception of tests described in Section 2.6.5, all high pressure cylinders were analysed while in an upright position, by extracting air through a valve at the top of the cylinders, and with no measures taken to insulate regulators and valves from room temperature fluctuations in the laboratory.

UAN	Cylinder Serial No.	Usage	Material	Volume (L)	Valve Type (manufacturer)	Valve Material	Start Date	Start Pressure (psig)	2001 Pressure (psig)
950051	CA01626	Primary standard	Al	29.5	Ceodeux	Brass	02/1995	1940	700
950052	CA01654	Surveillance	Al	29.5	Ceodeux	Brass	02/1995	1110	840
941395	CA01611	Surveillance	Al	29.5	Ceodeux	Brass	02/1995	1590	920
870001	AAL17271	Surveillance	Al	29.5	Sherwood	Brass	06/1996	270	150
880001	CC64041	Surveillance	Al	29.5	Superior	SS	05/1996	940	700
900005	ALVZ864	Surveillance	Al	48	CIG	SS	05/1996	980	770
900006	ALVZ865	Surveillance	Al	48	CIG	SS	06/1996	150	100
941037	CA01655	Surveillance	Al	29.5	Ceodeux	Brass	06/1996	1360	540
950123	CA01642	Surveillance	Al	29.5	Ceodeux	Brass	07/1996	1770	1290
960051	S35L-C24	Surveillance	SS	35	Nupro	SS	01/1996	540	380
941471	G20L-D01	Working standard (ST)	Glass	20	Glass Exp.	Glass	01/1995	4.3	3.6
950545	G20L-D02	Surveillance	Glass	20	Glass Exp.	Glass	05/1995	4.8	1.8
950546	G20L-D04	Surveillance	Glass	20	Glass Exp.	Glass	05/1995	4.2	1.7
960066	G20L-D03	Surveillance	Glass	20	Glass Exp.	Glass	01/1996	4.1	3.0
991291	CA01695	Test flask air	Al	29.5	Ceodeux	Brass	02/2000	1540	10

Table 2.1 Air standards used for $O_2/N_2/Ar$ calibration and/or experimental purposes. "UAN" (Universal Analysis Number) is a unique sample identifier. Start date and pressure refers to the time of first $O_2/N_2/Ar$ analyses.

2.2.4 Other species

This work also refers to measurements of other trace gas species made in GASLAB. Stable isotopes of CO_2 were measured by IRMS, using the MAT252 since 1990 and before that a Vacuum Generators (now Micromass) model 602D instrument (Allison and Francey, 1999). Concentrations of CO_2 and CH_4 were measured by gas chromatography (GC) with flame ionisation detection (FID), using a heated (400°C) nickel catalyst to convert the separated CO_2 to CH_4. Hydrogen and CO were analysed by GC with reduction gas detection (RGD) where heated (175°C) mercuric oxide is reduced to mercury vapour allowing detection of the mercury by UV absorption at 254 nm. A general description of GASLAB operations and analytical facilities is provided by Francey et al. (1996). For specific details of measurement techniques and calibration see Francey et al. (submitted), Allison and Francey (1999) and Langenfelds et al. (in prep.).

2.3 Experimental strategies

2.3.1 Introduction to analytical and calibration procedures

All "unknown" samples are measured directly against the working standard, 941471. This involves alternate admission of sample and standard gas into the ion source, with switching of the COV every 16-48 seconds for routine operations (see Section 2.4.5). These respective gas streams are hereafter referred to as SA and ST. SA $\delta(O_2/N_2)$ values are calculated for each ST/SA/ST cycle relative to the mean of adjacent ST measurements, and are then averaged for each "analysis block" consisting of 8-10 cycles. Typically two $\delta(O_2/N_2)$ blocks are analysed for each sample aliquot admitted to the inlet system. Where multiple blocks are analysed,

mean values are calculated for each aliquot by averaging over all blocks. Isotopic ratios of N_2 and/or O_2 are not measured for all samples, but where they are measured it usually involves a single analysis block.

Because of large variability in the instrumental offset affecting measured $\delta(O_2/N_2)$ between SA and ST sides (akin to a "zero enrichment"; Section 2.6.1), data are referenced against an external ("primary") calibration standard (sample 950051). Stability of the scale is assessed against a suite of other external ("surveillance") standards (Table 2.1). Measurements of calibration standards are processed and reported as daily means by averaging over all individual aliquots analysed per day. Measurements of atmospheric flask samples are processed to give a single value per measured species that is representative of the atmosphere at the time of sample collection. This involves averaging over multiple aliquots, where applicable, and applying corrections for drift during storage (Section 2.7).

The gas handling procedures employed to transfer air from cylinders or flasks into the inlet system have remained virtually unchanged since mid-1995 so as to minimise the chance of introducing systematic errors to the determination of atmospheric O_2/N_2 trends.

In the sections that follow (2.4 – 2.8), various aspects of the experimental techniques are assessed for their influence on $O_2/N_2/Ar$ data. They are addressed in the order in which adjustments/corrections are, or would be, applied if necessary, beginning with analytical techniques (mass spectrometry, inlet system and gas handling), followed by stability of sample composition during storage and sample collection techniques. This chapter deals principally with calibration and routine (i.e. glass flask) field sampling activities. Other technical issues relating to specific applications and/or individual samples are discussed elsewhere (primarily Chapter 3).

2.3.2 Multi-species diagnostics

The potential for modification of O_2/N_2 during analysis of air samples by various fractionating processes, such as diffusion and surface adsorption, has been noted previously (Bender et al., 1994; Keeling et al., 1998a; Manning, 2001). Such effects on the composition of gases have also been observed in nature, for example in the diffusive columns of air in both firn (Craig et al., 1988) and sand dunes (Severinghaus et al., 1996). It will be shown that measurements presented here are also subject to modification by such processes and that an understanding of the underlying causes is beneficial to interpretation of atmospheric data.

A useful approach for identifying (or apportioning) effects of different fractionating processes is to take advantage of the ability to precisely measure multiple molecular and isotopic ratios in the same air samples. The isotopic ratios $^{29}N_2/^{28}N_2$ and $^{34}O_2/^{32}O_2$ compare chemically and geometrically like molecules and are not subject to any significant biogeochemically forced variations in the contemporary free atmosphere. They thus serve as useful tracers of mass-dependent fractionation associated with experimental techniques and some natural processes. The ratio $^{40}Ar/^{28}N_2$ compares two inert gases with only second order variations in the free atmosphere resulting from seasonal variations in air-sea flux due to temperature dependence of their solubility in seawater. The Ar/N_2 ratio is strongly sensitive to mass-dependent fractionation processes owing to the large 12-unit mass difference by comparison to other molecular pairs dealt with here.

It is useful to identify the processes that might affect measurements, and their expected signatures in terms of relative changes among the different molecular and isotopic ratios. The relative change in ratio of two pairs of molecules (a and b, c and d) can be calculated from Equation 2.1 and from the relationship:

$$\frac{\Delta N_1}{\Delta N_2} = f_{12}\frac{N_1}{N_2} \tag{2.2}$$

where N is amount of substance and ΔN are perturbations subject to a fractionation factor f for a pair of species 1 and 2. For small perturbations and specifying all fractionation factors relative to species d, one obtains the approximation:

$$\frac{\delta(a/b)}{\delta(c/d)} \approx \frac{f_{ad} - f_{bd}}{f_{cd} - 1} \tag{2.3}$$

Fractionations associated with kinetic processes reflect varying rates of diffusion among different species, resulting from gradients in pressure, concentration or temperature, and where diffusivities are dependent on mass, molecular geometry and intermolecular forces. The general equation of diffusion for a binary mixture is given by Chapman and Cowling (1970) as:

$$C_1 - C_2 = -(x_1 x_2)^{-1} D_{12}\{\nabla x_1 + \frac{n_1 n_2 (m_2 - m_1)}{n\rho}\nabla \ln p - \frac{\rho_1 \rho_2}{\rho p}(F_1 - F_2) + k_T \nabla \ln T\} \tag{2.4}$$

where subscripts denote species 1 and 2, C is mean velocity, x is mole fraction, D_{12} is the diffusion coefficient, n is number density, m is mass, p is pressure, ρ is mass density, F represents external forces, k_T is the thermal diffusion ratio and T is temperature. The four terms in the bracket at the right hand side represent components due to gradients in concentration, pressure, external forces and temperature respectively. If the molecules are assumed to behave as rigid elastic spheres, the diffusion coefficient is approximated by:

$$D_{12} = \frac{3}{8n\sigma_{12}^2}\left\{\frac{kT(m_1 + m_2)}{2\pi m_1 m_2}\right\}^{\frac{1}{2}} \quad (2.5)$$

where σ_{12} is the mean diameter of species 1 and 2, and k is the Boltzmann constant. Mass is a key parameter, especially for isotopic (geometrically and chemically like) pairs where relative fractionation among multiple molecular ratios can be reasonably approximated from consideration of relative mass alone. However, for ratios involving different gases, such as O_2, N_2 and Ar, the molecules' geometric properties may also become significant. For example, some experimental evidence attributes a higher diffusivity to O_2 than N_2 in some circumstances (e.g. Severinghaus et al., 1996), despite O_2 having the greater mass. This might be explained by the dependence of D_{12} on molecular diameter and the smaller diameter of O_2 relative to N_2, though noting that published values of the relative diameters of O_2, N_2 and Ar also vary substantially (Moore, 1962; Chapman and Cowling, 1970; Roth, 1976) with significant implications for relative diffusivities. Approximate diameters as quoted by Chapman and Cowling (1970) are 3.64, 3.66 and 3.78 x 10^{-10} m for O_2, Ar and N_2 respectively.

Some processes with the potential to significantly impact on results from this study are addressed below, with expected multi-species signatures listed in Table 2.2.

Pressure diffusion

In the presence of a pressure gradient, diffusion causes heavier molecules to preferentially accumulate in the region of higher pressure. At equilibrium, diffusion in one direction due to the pressure gradient is balanced by an opposing flux due to the gradient in concentration. One example of fractionation induced by pressure

gradients is in the "gravitational settling" of heavier molecules towards the base of air columns where gas transport is dominated by diffusion, such as observed in firn and in sand dunes. Craig et al. (1988) described the gravitational equilibrium in terms of the barometric equation:

$$P = P_0 e^{mgz/RT} \tag{2.6}$$

where P is partial pressure, P_0 is partial pressure at the surface, g is gravitational acceleration, R is the gas constant. He showed that enrichment in the ratio of any two components with depth is approximately proportional to mass difference. As discussed by Keeling et al. (1998a), this mechanism is also potentially significant for gas handling procedures employed in measuring O_2/N_2. Fractionation occurs in flow-related pressure gradients but is attenuated by turbulent mixing and advection of the air sample. Relative fractionation among two pairs of species can be estimated on the basis of mass difference alone.

Thermal diffusion

Under a thermal gradient, heavier molecules generally (but not always) preferentially accumulate in the colder region. As for pressure diffusion, at equilibrium there is a balance in opposing fluxes, in this case due to thermal and concentration gradients. Fractionation effects can be calculated in terms of a thermal diffusion factor α (Grew and Ibbs, 1952; Chapman and Cowling, 1970). Ratios in Table 2.2 are calculated from values of α, determined experimentally for temperatures of ~293K, as summarised for most of the key molecular pairs

considered here by Severinghaus et al. (1996) and taken from Chapman and Cowling (1970, page 278) for Ar/N_2.

Effusion

Gas molecules escaping from a pressurised vessel through a tiny orifice are subject to a type of diffusion called molecular effusion (also known as Knudsen diffusion). This process occurs when the size of the orifice is small compared to the mean free path between molecular collisions so that most collisions are with the walls of the orifice. The rate of effusion is inversely proportional to the square root of the mass as described by Graham's Law for a pair of gases a and b:

$$\frac{\text{effusion rate of a}}{\text{effusion rate of b}} = \left(\frac{m_b}{m_a}\right)^{\frac{1}{2}} \tag{2.7}$$

The derivation of this relationship, for example as given by Moore (1962), does not allow for any dependence on molecular geometry, yet it is possible that geometry could have significant influence on effusion rates. For example, Battle et al. (1996) observed fractionation of O_2/N_2 in South Pole firn air that they attributed to the ability of the more prolate O_2 molecules to preferentially escape through channels separating air bubbles from open firn during the bubble close-off process. Thus Graham's Law might be more robust for fractionation ratios involving pairs of isotopic species rather than pairs of different gases.

Permeation

This process is discussed in more detail in Section 2.7 in relation to stability of sample air composition in CSIRO's 0.5 L glass flasks sealed with elastomeric O-

rings. Storage tests involving Viton and PFA O-rings showed that changes in $\delta(O_2/N_2)$ of sample air due to permeation are about 3.5 times larger than corresponding changes in $\delta(Ar/N_2)$ and with no detectable influence on $\delta^{29}N_2$ and $\delta^{34}O_2$.

Solubility

The composition of air that contacts liquid water with which it has not equilibrated will be modified due to the varying solubility of different gases. At equilibrium, the amount of gas dissolved is proportional to its solubility and its partial pressure in the air and is also a function of temperature (Lide, 1993). This process impacts on atmospheric O_2/N_2 and Ar/N_2 ratios, especially on seasonal timescales due to cycling in sea surface temperatures. It can also modify air samples, for example in circumstances where sample pressure is changed in the presence of water. Relative changes in $\delta(O_2/N_2)$ and $\delta(Ar/N_2)$ are calculated from the solubility data of Lide (1993).

Surface adsorption

A further potentially important process is the adsorption of gases on solid surfaces. Of most interest here are the interactions of $O_2/N_2/Ar$ with wetted materials used in the experimental equipment, in particular glass, SS, Al and especially the elastomers (Viton, PFA, PTFE etc.) used to seal flasks, cylinders, the inlet system and the mass spectrometer vacuum system. Adsorption bears some parallels with dissolution in water, in that the equilibrium partitioning of gases between gaseous and adsorbed phases is sensitive to pressure and differentiates between chemically

different species. However, its effects cannot be easily characterised in terms of multi-species signatures because they depend heavily on the combination of gas and surface material, and data characterising such interactions are not readily available. Adsorption may involve either physisorption, which results from weak intermolecular forces and is generally reversible, or chemisorption which involves stronger bonding between molecules and is generally irreversible (Moore, 1962). What can be said is that because adsorption is likely to be primarily a function of gases' chemical properties rather than mass or diameter, one would expect resulting fractionations among $O_2/N_2/Ar$ to be decoupled from those of the isotopic tracers $\delta^{29}N_2$ and $\delta^{34}O_2$. Such behaviour was observed for permeation through Viton and PFA (Section 2.7) and might also be indicative of adsorption effects on these materials because permeability constants are specific to the combination of gas and solid, and are a function of solubility. Modification of O_2/N_2 by surface adsorption was identified by Keeling et al. (1998a) in tests involving exposure of air samples to a large number of Viton O-rings. Two processes were identified, 1) preferential physisorption of O_2 relative to N_2, characterised by depletion of sample O_2/N_2 and CO_2 and 2) chemisorption characterised by declining O_2/N_2 and increasing CO_2 and attributed to oxidation of the Apiezon grease used to lubricate the Viton O-rings.

Comparison of values in Table 2.2 suggests that the ability to distinguish between pressure diffusion, thermal diffusion and effusion using multi-species information may be limited even if the ratios calculated here are robust, whereas changes in $O_2/N_2/Ar$ due to permeation or dissolution in water are better distinguished from the purely diffusive processes.

Molecular ratios	Pressure diffusion	Thermal diffusion	Effusion	Permeation[a] (Viton, PFA)	Water Solubility
$\delta(^{40}Ar/^{28}N_2) / \delta(^{32}O_2/^{28}N_2)$	3.0	3.9	2.8	0.3	1.2
$\delta(^{40}Ar/^{28}N_2) / \delta(^{29}N_2/^{28}N_2)$	12.0	10.3	11.1		
$\delta(^{32}O_2/^{29}N_2) / \delta(^{29}N_2/^{28}N_2)$	3.0	1.6	2.9		
$\delta(^{32}O_2/^{28}N_2) / \delta(^{29}N_2/^{28}N_2)$	4.0	2.6	3.9		
$\delta(^{34}O_2/^{32}O_2) / \delta(^{29}N_2/^{28}N_2)$	2.0	1.6	1.7		

Table 2.2 Approximate fractionation ratios for molecular pairs expected from different processes. [a]obtained experimentally for permeation through Viton and PFA (see Section 2.7).

2.4 Mass spectrometer performance and artefacts

2.4.1 Precision

Raw measurement precision typical of the two mass spectrometers used here is listed in Table 2.3. It is defined here as the standard deviation of repeat ST/SA/ST cycles, where each ST and SA measurement involved idle and integration times of 40 and 8, 8 and 8 seconds for the MAT252 and Delta^{plus}XL respectively. Data in Table 2.3 were obtained by averaging over all analysis blocks within extended periods of about 1 year of high performance operation for each instrument. Implied standard errors for a single block of 8 and 10 cycles respectively represent the precision to which mean values from a single block would be known if all of the noise were assumed to be random. For the key $\delta(O_2/N_2)$ measurement, the precision achieved using the Delta^{plus}XL is clearly superior that of the MAT252, by close to a factor of 4. This likely reflects the ability of the Delta^{plus}XL to simultaneously monitor $^{32}O_2$ and the more abundant N_2 isotopomer, $^{28}N_2$, rather than $^{32}O_2$ and $^{29}N_2$ as done on the MAT252. For the isotopic ratios, $\delta(^{29}N_2/^{28}N_2)$, $\delta(^{33}O_2/^{32}O_2)$ and $\delta(^{34}O_2/^{32}O_2)$, the MAT252 achieved marginally higher precision.

	MAT252		Delta^{plus}XL	
	Standard deviation of repeat cycles	Standard error of mean of one block of 8 cycles	Standard deviation of repeat cycles	Standard error of mean of one block of 10 cycles
$\delta(^{32}O_2/^{29}N_2)$	16.2	5.7		
$\delta(^{32}O_2/^{28}N_2)$			4.3	1.4
$\delta(^{40}Ar/^{28}N_2)$			12.6	4.0
$\delta(^{29}N_2/^{28}N_2)$	10.8	3.8	16.1	5.1
$\delta(^{30}N_2/^{28}N_2)$			114.3	36.1
$\delta(^{33}O_2/^{32}O_2)$	70.5	24.9	101.4	32.1
$\delta(^{34}O_2/^{32}O_2)$	30.3	10.7	40.0	12.6

Table 2.3 Typical raw measurement precision of the two mass spectrometers. All units are per meg.

2.4.2 Pressure imbalance

Bender et al. (1994) identified sensitivity of $\delta(O_2/N_2)$ in URI measurements to the difference in pressure (or ion beam intensity) between SA and ST gas streams entering the ion source. This phenomenon is puzzling as measurements compare O_2/N_2 ratio on SA and ST sides and one would expect this ratio to be independent of pressure. The implication is that their relative ion beam intensities are non-linear with pressure.

Both mass spectrometers used here exhibit similar effects, not only for $\delta(O_2/N_2)$ but all measured ratios. As was the case at URI, the routine procedure adopted here for dealing with this effect was to closely balance measured ion beam intensity on SA and ST sides and apply a correction for small, actual differences. In the GASLAB system, balance is achieved by carefully positioning the plunger on the

SA side so as to match measured voltage (e.g. of *m/z* 28, V_{28}) with that of the ST side where gas flow is effectively constant. The two voltages are generally balanced to better than ±0.005V (out of about 4V) for $O_2/N_2/Ar$ analysis. It has been customary to balance the voltage of the lowest measured *m/z* species only, i.e. V_{29} for measurement of 32/29 ratio, V_{28} for 40/32/28 and 30/29/28, V_{32} for 34/33/32, rather than ion source pressure or a voltage integrated over all measured species.

The magnitude of the pressure imbalance effect was regularly monitored for all measured species. This was conveniently achieved with the GASLAB inlet system by analysing air from a single sample aliquot over a period of typically 3 hours during which time sample pressure decays by about 3%. Repeated measurements during this time give a distribution of measured $\delta(O_2/N_2)$ etc. for deviations within ±1.5% of pressure balance. These experiments were performed on average about twice a week. A set of results from one such test is shown in Figure 2.2. Time variation in the magnitude of the effect is plotted in Figure 2.3, showing the slope of sensitivity obtained from linear regressions fitted to data from each individual experiment. Corrections are routinely applied to data for all measured species using sensitivity values obtained either by interpolating between points in Figure 2.3 where both points lie within a week on either side, or alternatively by extrapolating from the nearest point.

There is a lot of structure in Figure 2.3 that holds clues as to the processes responsible, yet the inter-species relationships are variable and not consistent with any single, simple explanation. General observations are that sensitivities can vary

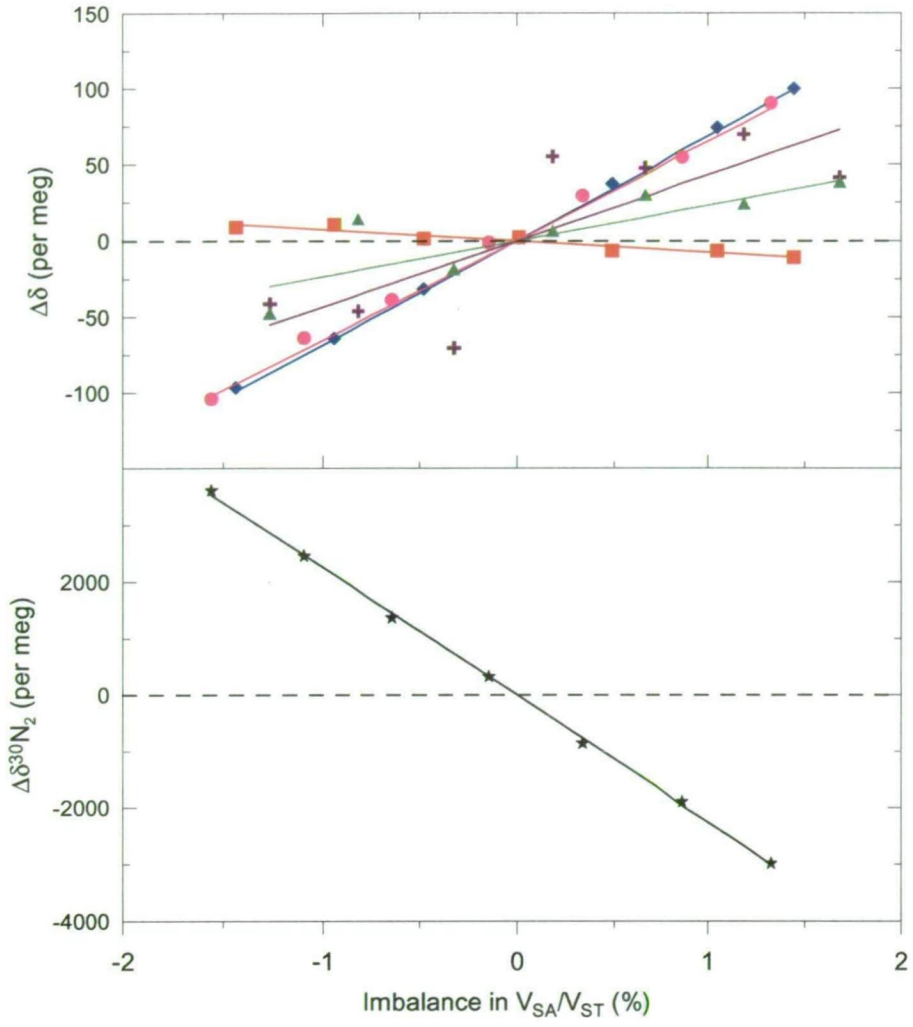

Figure 2.2 Anomalies (in per meg) for $\delta(^{32}O_2/^{28}N_2)$ (blue diamonds), $\delta(Ar/N_2)$ (red squares), $\delta^{29}N_2$ (pink circles), $\delta^{33}O_2$ (magenta crosses), $\delta^{34}O_2$ (green triangles) and $\delta^{30}N_2$ (black stars) as a function of pressure imbalance between SA and ST sides as measured on 28-May-2001.

dramatically and can even change sign, emphasising the need for ongoing monitoring. The magnitude of $\delta(O_2/N_2)$ corrections for imbalance in V_{28} (or V_{29}) of 0.005V are on average about 5 per meg and at times have been as large as 16 per meg. There are some specific features in Figure 2.3 worthy of comment:

1. The multi-species variations are not consistent with mass-dependence. For example, $\delta(O_2/N_2)$ and $\delta(Ar/N_2)$ usually have slopes of opposite sign. Neither the

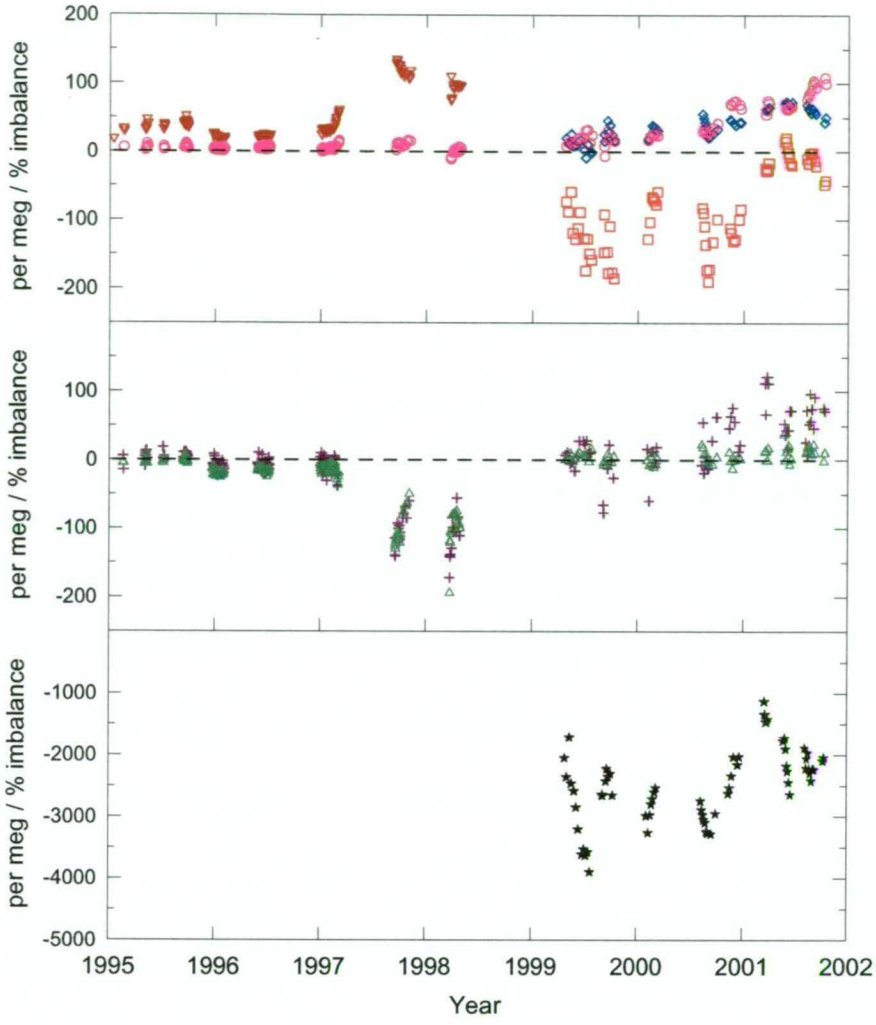

Figure 2.3 The slope of sensitivity (in per meg / % imbalance) from all individual pressure imbalance tests. Symbols are as for Figure 2.2 above with addition of $\delta(^{32}O_2/^{29}N_2)$ (brown inverted triangles).

isotopes of O_2 or of N_2 show relative distributions that could be linked only to mass difference.

2. By far the strongest sensitivity is observed for $\delta^{30}N_2$. It is decoupled from $\delta^{29}N_2$ and from other ratios involving *m/z* 28, indicating the largest influence from pressure imbalance at *m/z* 30 for which the signal is dominated by $^{14}N^{16}O^+$ (Section 2.4.6). It may reflect varying NO production through differential response of O_2 and N_2 to pressure changes, for example from perturbations to adsorption of O_2 and N_2 on ion source surfaces.

3. There is strong correlation among positive $\delta(^{32}O_2/^{29}N_2)$ and negative $\delta^{33}O_2$ and $\delta^{34}O_2$ anomalies in 1997/98, and all ratios show changes of similar magnitude. This strongly suggests an interference involving *m/z* 32, which is common to all three ratios. If so, it could be explained by either 1) an additional contribution to ion beam intensity at *m/z* 32, perhaps from stray ions of another *m/z* species and where the additive component is preferentially increased relative to $^{32}O_2$ with increasing sample pressure or 2) partial loss (i.e. ions not detected) of the *m/z* 32 ion beam where the proportional magnitude of the loss increases with decreasing sample pressure. A complication with this hypothesis is that different collector cups were used for monitoring of *m/z* 32 when analysing $\delta(O_2/N_2)$ and O_2 isotopes on the MAT252 so that the effect on *m/z* 32 is not just related to one single cup.
4. $\delta^{29}N_2$ and $\delta(^{32}O_2/^{28}N_2)$ show similar long term variations in Delta^{plus}XL measurements, consistent with a common interference at *m/z* 28 and with the inference drawn above for *m/z* 32 in 1997/98. However, in this case the sign of the pressure dependence in additive or lost components would be of the opposite sense. On shorter time scales, for example in late 2001, there is evidence of divergence in $\delta^{29}N_2$ and $\delta(^{32}O_2/^{28}N_2)$ pressure imbalance sensitivity, indicating a contribution from other processes or interference at *m/z* species other than 28.
5. $\delta(Ar/N_2)$ shows greater variability than all other species except $\delta^{30}N_2$. This suggests either interference specific to *m/z* 40 and/or a process that chemically distinguishes Ar from both O_2 and N_2.
6. Analysis of high purity (99.999 %) N_2 against the (air) working standard in March, 2000 showed similar pressure imbalance sensitivity in $\delta^{29}N_2$ to that observed for comparison of air on both SA and ST sides. This indicates the effect

for $\delta^{29}N_2$ is not simply related to chemistry involving gases other than N_2 present in the SA gas stream. It also limits the number of species that might potentially contribute to additive interference at *m/z* 28 or 29 to isotopomers of N_2 or species with significant background presence (e.g. H_2O).

These observations cannot be easily reconciled with any single process or simple explanation. It may be that more than one process is responsible. A better understanding of the causes of this effect is desirable to ensure that it does not introduce any significant error. For example, it is not certain that balancing SA and ST voltage of the lowest *m/z* species is the best procedure. There is some evidence linking non-linearity of $\delta^{29}N_2$ and $\delta^{34}O_2$ (with respect to O_2/N_2) to the pressure imbalance effect (Section 2.4.3). Anomalous results have been observed to correlate with changes in pressure imbalance sensitivity for samples with "unusual" O_2/N_2, where the practice of balancing voltages of lowest *m/z* species results in strong imbalance in SA/ST ion source pressure. It is noted though that these anomalies were not removed by making allowance for pressure imbalance sensitivity and calculated SA/ST ion source pressure difference. A final point is that although the effect remains unexplained, any errors affecting data reported here are likely to be small because SA/ST differences in $O_2/N_2/Ar$ composition are always small for air sampled directly from the atmosphere.

2.4.3 Instrument non-linearity

Measurement of differences in the chemical composition of gases can be subject to error from uncharacterised non-linearity in instrument response (i.e. as a function of the concentration or ratio of the species being measured). This is an

important issue for many trace gas measurement techniques, such as GC and NDIR. For some species measured by GC in GASLAB, non-linearity can be as large as 20% of sample/standard difference (e.g. for N_2O by electron capture detection or H_2 and CO by reduction gas detection; Langenfelds et al., in prep.). If left uncorrected, this would directly translate to comparable errors in quantification of spatial or temporal gradients in atmospheric composition. Mass spectrometric detectors are generally assumed to have a linear response, but for O_2/N_2 (and other species analysed by MS in GASLAB, e.g. isotopes of CO_2), verification of linearity is made difficult by the requirement for a suite of mixtures whose difference in composition can be reliably established by independent means at a sufficiently high level of precision. At present, CSIRO does not have access to "absolute" techniques (e.g. gravimetric, manometric) for directly linking O_2/N_2 ratios to fundamental constants.

The O_2/N_2 linearity of the MAT252 instrument was tested using a batch of six glass flask samples with $\delta(O_2/N_2)$ spanning a range of more than 12‰. These samples were prepared by combining varying amounts of two primary mixtures, one being zero air (with O_2/N_2/Ar in proportion to natural air but with most other trace constituents removed) and the other a volumetrically prepared mixture of high purity CO_2 (5.34 ± 0.05%) and N_2 (94.66 ± 0.05%). Both were purchased from Scott-Marrin Inc. The ratio of the two primary components in each of the six flask samples, and hence "true" $\delta(O_2/N_2)$ relative to the zero air (no added CO_2/N_2), was calculated using GC measurements of CO_2 mole fraction (range 0 – 548 ppm), with due allowance made for isobaric interference on $\delta(O_2/N_2)$ from CO_2 (Section 2.4.6) and for non-linearity in CO_2 measurement. Anomalies in measured $\delta(O_2/N_2)$ relative to "true" values calculated using CO_2, are shown in Figure 2.4. They are scattered

around zero to within measurement precision (~±10 per meg), thus indicating no systematic deviation from linearity. The main source of uncertainty with this approach stems from uncertainty in the CO_2/N_2 ratio of the Scott-Marrin Inc. primary mixture. The confidence intervals assigned by Scott-Marrin Inc. imply that MS linearity cannot be established to better than ±1 % of SA/ST difference (as shown by the solid lines in Figure 2.4), even though the distribution of data points is indistinguishable from the zero line to better than ±0.1 % of SA/ST difference. Contributions to uncertainty from other sources, such as residual O_2 in the CO_2/N_2 mixture (< 0.4 ppm) and non-linearity correction for CO_2 (±0.02 % of the range in CO_2) are of second order importance, together accounting for less than 20 % of the uncertainty due to that from the CO_2/N_2 ratio.

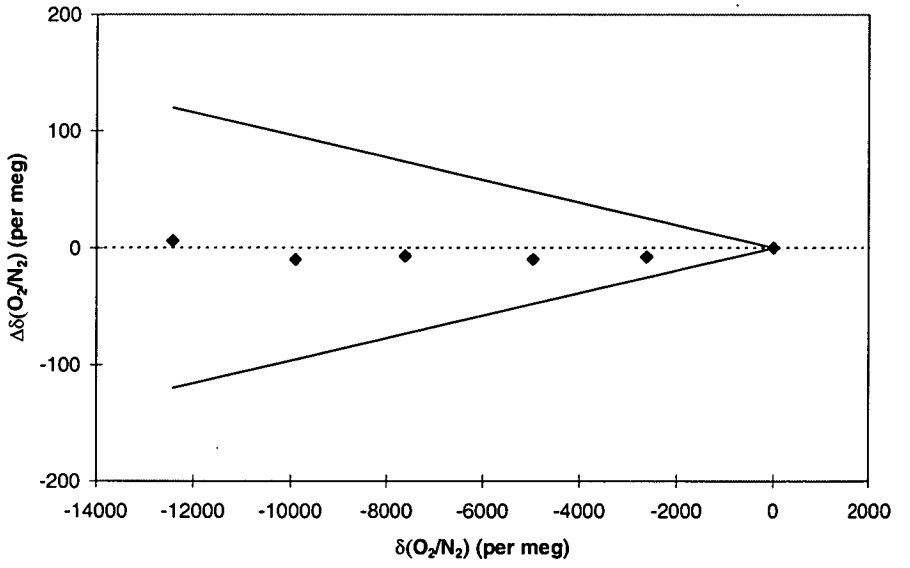

Figure 2.4 The error in measured $\delta(O_2/N_2)$ as a function of $\delta(O_2/N_2)$ due to instrument non-linearity, inferred from one experiment carried out on the MAT252 on 13-Feb-97. Diamonds are $\delta(O_2/N_2)$ anomalies (measured – true) for six individual samples of varying but known composition. The range of uncertainty is bounded by the solid lines.

Because this experiment was carried out on one occasion only, the results only provide a snapshot of instrument linearity at that time. Variations over longer periods are constrained by regular analysis of two high pressure cylinder standards with $\delta(O_2/N_2)$ significantly depleted relative to current background atmospheric levels, namely 880001 (-28 ‰) and 870001 (-5 ‰) (see Figure 2.18 in Section 2.6.7). The range of measured $\delta(O_2/N_2)$ in 880001 between 1995 and 2001 is about 300 per meg with most of the variability observed between October 1997 and April 1998, coinciding with a large perturbation in pressure imbalance sensitivity of $\delta(O_2/N_2)$ (see Figure 2.3 in Section 2.4.2). This range is much larger than anything observed in air standards with $\delta(O_2/N_2)$ close to current atmosphere. Data for 870001 show similar variability but with magnitude smaller by a factor of 5. This is consistent with the magnitude of variability being proportional to SA/ST $\delta(O_2/N_2)$ difference and thus points to the presence of a variable non-linearity, possibly associated with the pressure imbalance effect. It implies an uncertainty in measurements, and consequently in estimates of spatial or temporal $\delta(O_2/N_2)$ gradients, of within ±1 % of SA/ST difference, at least for the period of anomalous pressure imbalance sensitivity. Excluding this period, the range in $\delta(O_2/N_2)$ of 880001 is much smaller (within 90 per meg), implying an uncertainty due to non-linearity of within ±0.3 % of SA/ST difference.

Sowers et al. (1989) reported non-linearity of measured $\delta^{34}O_2$ and $\delta^{29}N_2$ with respect to $\delta(O_2/N_2)$ in their Finnigan MAT251 mass spectrometer. The effect was observed in tests where aliquots of pure N_2 were added to dry sample air. The proportionality factor for $\Delta\delta^{34}O_2/\Delta\delta(O_2/N_2)$ was about 0.05, significant to their

determination of $\delta^{34}O_2$ in air extracted from polar ice sheets, where $\delta(O_2/N_2)$ was fractionated by up to about 10 ‰. Dependence of $\delta^{29}N_2$ on $\delta(O_2/N_2)$ was also reported but was less sensitive, with a proportionality factor of ≤ 0.004.

A similar test was conducted on CSIRO's MAT252 instrument. It showed $\Delta\delta^{34}O_2/\Delta\delta(O_2/N_2)$ to be about 0.02, of the same sign as reported by Sowers et al. but with smaller magnitude. There were no tests of corresponding sensitivity in $\delta^{29}N_2$. Measurements reported here focus on the contemporary atmosphere with much smaller variation in O_2/N_2, and the isotopic measurements are only used for diagnostic purposes. Hence non-linearity in $\delta^{34}O_2$ and $\delta^{29}N_2$ is not as important an issue and is not examined in detail.

However, brief mention is warranted of some circumstantial evidence linking this effect to the "pressure imbalance effect" discussed in Section 2.4.2. For example, measured drifts in $\delta^{29}N_2$ and $\delta^{34}O_2$ in 880001 and 870001 (Figure 2.5) are correlated with changes in pressure imbalance sensitivity (Figure 2.3). This contrasts with high stability of both ratios in the other air standards with $\delta(O_2/N_2)$ much closer to the working standard. The magnitude of drift is larger for 880001 than 870001, certainly for $\delta^{29}N_2$, consistent with it having the larger $\delta(O_2/N_2)$ deviation from ST air. It is also significant that largest deviations from zero in Figure 2.5 tend to occur at times of largest pressure imbalance sensitivity (Figure 2.3). Both 870001 and 880001 are expected to have "true" $\delta^{29}N_2$ and $\delta^{34}O_2$ close to ST (or atmospheric values) because they contain background air, diluted with small amounts of high purity N_2 that is also expected to be negligibly fractionated with respect to atmospheric $\delta^{29}N_2$ and $\delta^{34}O_2$. Records of other species in these standards rule out the possibility of the drifts being due to fractionation.

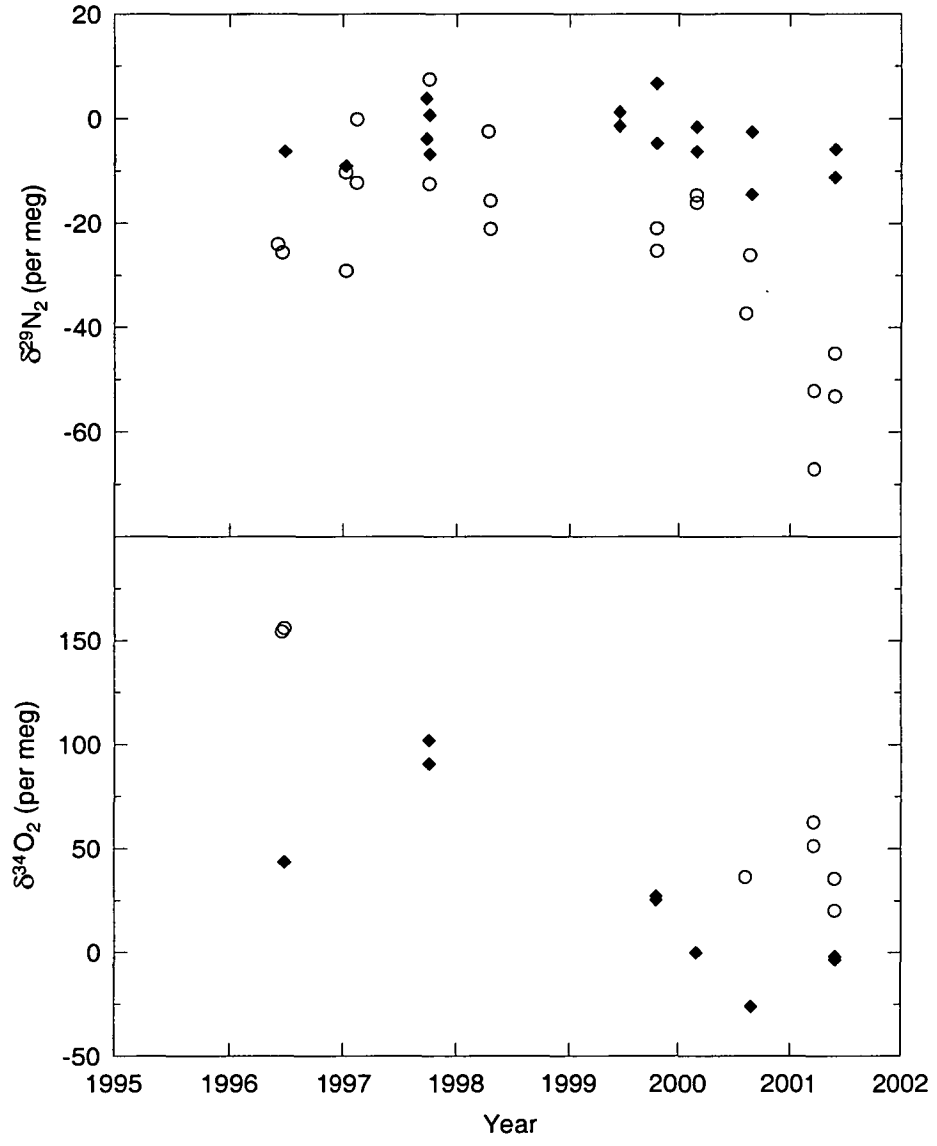

Figure 2.5 Measured $\delta^{29}N_2$ and $\delta^{34}O_2$ of two air standards, 870001 (diamonds) and 880001 (circles).

Further evidence comes from analyses of firn air retrieved from Law Dome, Antarctica. Measurements made on multiple occasions within a 2-year period (unpublished data) showed large variations, especially in $\delta^{34}O_2$ and to a lesser extent in $\delta^{29}N_2$ that also correlated with variations in pressure imbalance sensitivity. Calculations were made to test whether the $\delta^{29}N_2$ and $\delta^{34}O_2$ drifts/anomalies could be explained by applying pressure imbalance corrections relative to SA/ST balance in

ion source pressure rather than in V_{28} or V_{32}. This did result in substantial differences at times of significantly non-zero pressure imbalance sensitivity. However, the measurement anomalies could not be accounted for by this change in data processing alone, indicating that if non-linearity is linked to pressure imbalance, the nature of the link is more complex.

2.4.4 Sample/standard mixing in the ion source

Mixing of SA and ST gas in the MS ion source, associated with switching of the COV has been identified as an important source of systematic bias in CO_2 isotope measurements (Francey and Allison, 1994; Meijer et al., 2000). Incomplete removal of the previous gas from the ion source before measurement of the incoming gas causes the difference between SA and ST to be underestimated. The magnitude of the error is inversely related to idle time (the length of time between admission of a new sample into the source and the commencement of analysis).

The importance of this effect for O_2/N_2 measurements was investigated on the MAT252 using two surveillance standards, one (941395) with $\delta(O_2/N_2)$ almost identical to the working standard (within 200 per meg subject to variability in zero enrichment) and the other strongly depleted (880001; -28 ‰). Tests were conducted at varying times after switching the instrument from CO_2 to O_2/N_2 analysis mode. Thus the tests addressed sensitivity of $\delta(O_2/N_2)$ to three parameters: idle time, SA/ST difference and the state of ion source "conditioning".

The results indicate some sensitivity to all of these parameters (Figure 2.6). Within the first day after switching analysis modes, both standards showed dependence of $\delta(O_2/N_2)$ on idle time that was of opposite sign to what would be

expected from SA/ST mixing. This signal was slightly larger for 941395 than 880001. After conditioning of the source for longer periods, the idle time dependence observed for 941395 diminished to near zero while that for 880001 changed sign. One could speculate that under these conditions, the dominant process affecting 880001 data was SA/ST mixing. If so, the results for short conditioning times point to the effects of a different process that is not as sensitive to SA/ST difference but is sensitive to pressure perturbations (e.g. physisorption of gases on source surfaces).

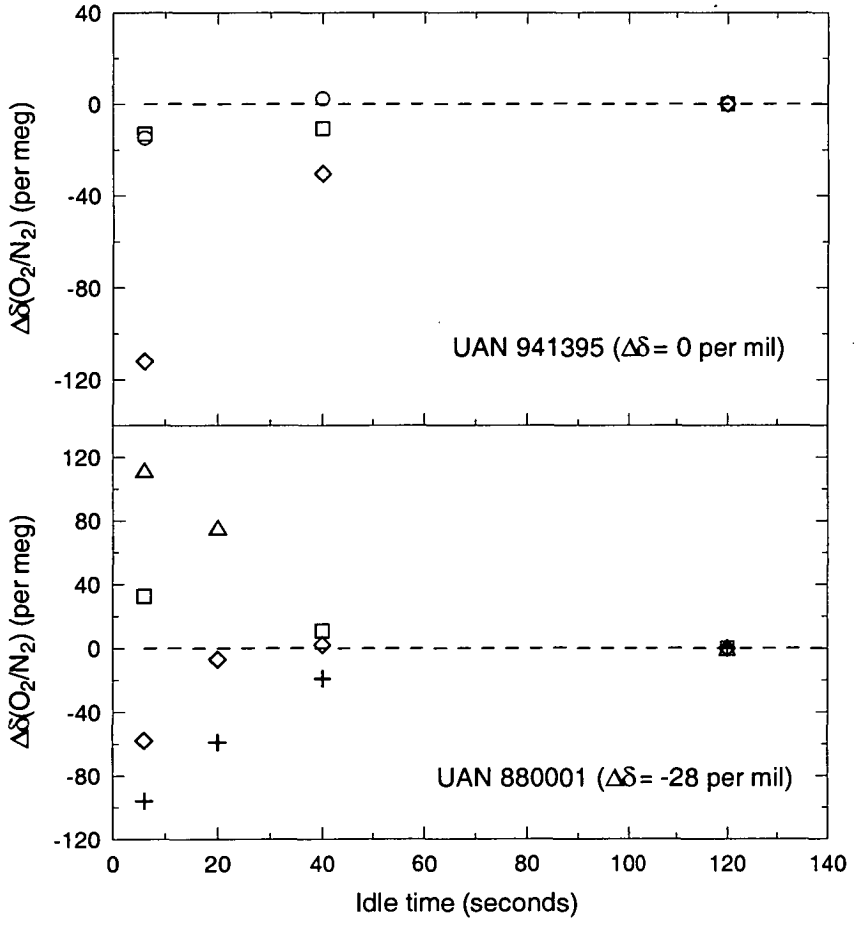

Figure 2.6 Variations of $\delta(O_2/N_2)$ as a function of idle time, measured in two standards (941395, 880001) that deviate from $\delta(O_2/N_2)$ of the working standard by different amounts (0, -28‰ respectively). Sets of measurements were made at varying times after switching analysis modes from CO_2 to air: 0 days (diamonds), 1(crosses), 5 (circles), 25 (squares) and 46 (triangles). Data for each set are plotted as deviations from values obtained at the maximum idle time of 120 seconds.

As long as consistent idle/integration times are used for all SA and ST air, there should be negligible systematic bias for routine measurements of O_2/N_2 in air. Any bias relating to SA/ST difference that does exist would be manifested as a non-linearity (with respect to SA/ST difference) and is constrained by the results for 880001 in Figure 2.6 to be within ±0.5% of SA/ST difference. This is consistent with the conclusions drawn in Section 2.4.3.

Biases relating to the significant idle time dependence observed for short conditioning times (even for $\delta(O_2/N_2)$ close to the working standard) would be manifested as a "zero enrichment". They would be largely accounted for by the practice adopted here of referencing all data to an external standard (950051) rather than the working standard. Measurements made during times of rapidly drifting idle time dependence could be subject to significant errors due to relatively infrequent (e.g. once a day) analysis of 950051. However, this is unlikely to be a serious concern for data reported here because of the common practice of conditioning the source for several days after switching analysis modes before commencing routine analyses.

2.4.5 Idle and Integration times

Measurements were initially made on the MAT252 using routine idle and integration times of 40 and 8 seconds respectively. The relatively long idle time was employed to guard against the possibility of systematic biases due to mixing of SA and ST gases in the ion source. Such biases are exacerbated by short idle times. After establishing that idle time had relatively little impact on mean $\delta(O_2/N_2)$ even where the sample and working standard are very different (Section 2.4.4), the idle time was reduced to a lower, but still conservative, 20 s (from September 1997). On

commissioning of the Delta^{plus}XL instrument, further tests were carried out to assess the influence of idle and integration times on precision. Over two days in April 1999, multiple (5-12) blocks were analysed for each idle/integration time combination listed in Table 2.4. Variations in precision were relatively small but suggested improving precision with longer integration times and, if anything an optimal idle time near 8 s, at least in the $\delta(Ar/N_2)$ results. Times of 8 s were adopted for both parameters for routine analyses thereafter. Although precision might be marginally improved with longer integration times, the choice of 8 s also took into account sample throughput efficiency, which is favoured by shorter integration times.

Idle time (sec)	Integration time (sec)	$\delta(^{32}O_2/^{28}N_2)$ precision (per meg)	$\delta(^{40}Ar/^{28}N_2)$ precision (per meg)
2	2	7.8 ± 4.9	21.0 ± 9.6
2	8	6.0 ± 1.3	16.1 ± 4.2
8	2	7.6 ± 1.7	19.6 ± 10.4
8	4	3.9 ± 0.9	17.0 ± 6.9
8	8	5.1 ± 1.8	13.2 ± 5.3
8	16	4.1 ± 1.9	12.3 ± 3.9
16	8	5.6 ± 1.7	15.6 ± 3.8
40	8	6.4 ± 2.0	20.6 ± 6.7

Table 2.4 Delta^{plus}XL measurement precision as a function of idle and integration times. Listed values are the mean of standard deviations from multiple analysis blocks. Uncertainties are the standard error of the mean.

2.4.6 Isobaric interferences

Isotopomers of O_2 and N_2 are subject to isobaric interference from either fragmentation of CO_2 or production of NO in the ion source (Bender et al., 1994). The ion beams measured for N_2 are not distinguished from those due to fragments of CO_2 at *m/z* 28 ($^{12}C^{16}O^+$), 29 ($^{13}C^{16}O^+$and $^{12}C^{17}O^+$) and 30 ($^{13}C^{17}O^+$and $^{12}C^{18}O^+$), while O_2 fragments derived from CO_2 interfere with the primary O_2 signal.

NO is generated in the presence of N_2 and O_2 and interferes with $^{30}N_2$ (due to $^{14}N^{16}O^+$) and $^{32}O_2$ (mainly $^{14}N^{18}O^+$). Delta^{plus}XL measurements show the NO contribution to ion beam intensity (I) at *m/z* 30 to be about 100 times larger than that expected for $^{15}N^{15}N$ (calculated from natural isotopic abundances relative to $^{14}N^{14}N$). Hence isobaric interference at *m/z* 30 due to CO_2 is not considered further here. The effect of NO interference at *m/z* 32 on measured $\delta(O_2/N_2)$ is expected to be negligible for atmospheric samples because $^{14}N^{18}O^+$ is present in the source at only about 4 ppm (calculated from the Delta^{plus}XL measurements and scaling by $^{18}O/^{16}O$ abundance) and its contribution to *m/z* 32 should be almost identical for both "unknown" air samples and the air working standard.

Of most importance here are effects on $\delta(O_2/N_2)$, $\delta^{29}N_2$ and $\delta(Ar/N_2)$ due to CO^+ interference at *m/z* 28 and 29. For these species:

$$I_{28} \propto Z_{N_2}[^{14}N^{14}N] + Z_{CO}F_{CO}[^{12}C^{16}O] \tag{2.8}$$

$$I_{29} \propto Z_{N_2}[^{14}N^{15}N] + Z_{CO}F_{CO}([^{13}C^{16}O] + [^{12}C^{17}O]) \tag{2.9}$$

where Z is the ionisation factor and F_{CO} is the fraction of CO_2 fragmented to CO.

These relationships are only approximate as they neglect possible variations in Z and F among isotopomers of CO or N_2. Mass spectra for pure CO_2 measured on the MAT252 gave a ratio for I_{28}/I_{44} of 0.067, lower than the value of 0.11 reported by Bender et al. (1994), and only minor production of O_2 fragments (I_{32}/I_{44} = 0.0015), indicating that interference with O_2 at *m/z* 32 is only of second order importance. Using Equations 2.8 and 2.9, corresponding formulae for other *m/z* species, estimates of F_{CO} etc. from the measured mass spectra and Z_{CO}/Z_{N2} = 1.25 (Beaumont et al., 1994), it is possible to predict the sensitivity of measured O_2/N_2/Ar ratios to CO_2 mole fraction (Table 2.5).

	MAT252 (11-Feb-1997)	Delta^{plus}XL (11-Oct-2001)	Predicted
$\delta(^{32}O_2/^{29}N_2)$	-0.24 ± 0.02		-0.12
$\delta(^{32}O_2/^{28}N_2)$		-0.10 ± 0.03	-0.07
$\delta(^{40}Ar/^{28}N_2)$		-0.03 ± 0.12	-0.08
$\delta(^{29}N_2/^{28}N_2)$	0.105 ± 0.007	0.105 ± 0.007	0.044
$\delta(^{34}O_2/^{32}O_2)$		-0.04 ± 0.06	0.00
$\delta(^{34}O_2/^{32}O_2)$		0.07 ± 0.02	0.00

Table 2.5 Sensitivity of measured ratios to isobaric interference from fragmentation of CO_2 in the ion source (in units of per meg / ppm CO_2). Uncertainties are standard errors of the linear regressions.

The sensitivity of both mass spectrometers was tested experimentally by preparing subsamples of zero air spiked with varying amounts of high purity CO_2 with near-atmospheric isotopic composition (Table 2.5, Figure 2.7). The results gave almost identical slopes for $\delta^{29}N_2$ on the two instruments and showed slopes of

consistent sign but generally larger magnitude than what was predicted, at least for those species where the CO_2 dependence is well resolved, namely $\delta(O_2/N_2)$ and $\delta^{29}N_2$. The slopes for $\delta(Ar/N_2)$ and to a lesser extent $\delta(^{32}O_2/^{28}N_2)$ are not as well defined as could be expected from raw measurement precision alone, almost certainly due to noise associated with fractionation of air samples as they are introduced to the inlet system.

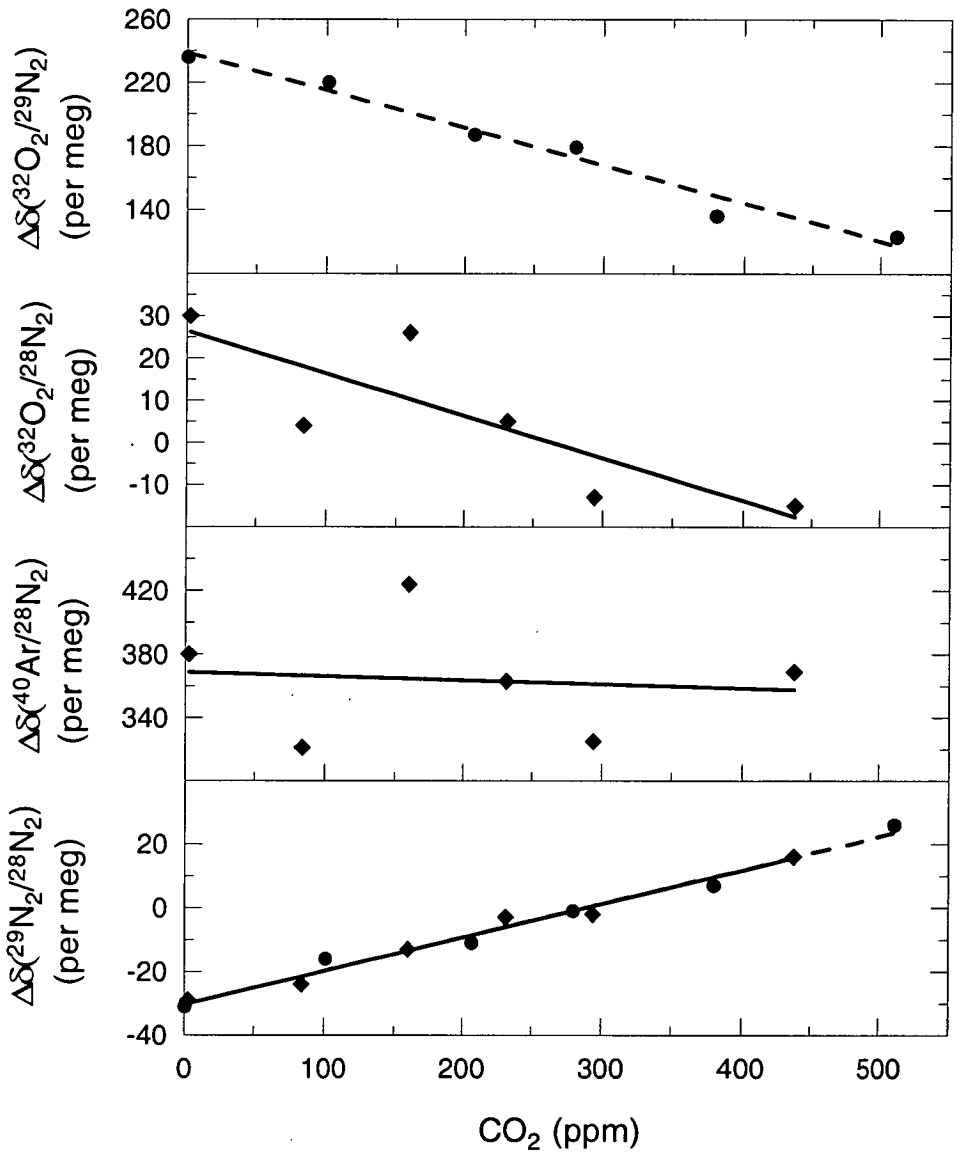

Figure 2.7 Experimentally-derived sensitivity of measured ratios to CO_2 due to isobaric interference with CO^+ and O_2^+ for the MAT252 (circles; linear regressions indicated by dashed lines) and Delta^{plus}XL (diamonds; solid lines).

The experimentally derived values are used to correct all $\delta(O_2/N_2)$, $\delta^{29}N_2$ and $\delta(Ar/N_2)$ data relative to a "reference" CO_2 mole fraction of 360 ppm. Sample CO_2 values are taken from GC analysis where available. For Cape Grim or aircraft-based samples not analysed for CO_2, values are taken from CSIRO's smoothed Cape Grim flask sampling record. For atmospheric records reported here, CO_2 mole fraction spans a range of about 40 ppm, so that uncertainty in correcting for isobaric interferences (e.g. estimated from comparison of observed and predicted slopes) is small. For example, the uncertainty that applies to partitioning of global oceanic and terrestrial carbon uptake (Chapter 3) is less than 0.1 PgC yr^{-1}. Although a significant, non-zero slope is implied for $\delta^{34}O_2$, it is doubtful whether this is real, as differences in the isotopic composition of O in O_2 and in CO_2 are much too small to account for the observed slope.

2.4.7 Moisture-related artefacts

Systematic biases in some measured ratios were at times observed to correlate with variations of the amount of moisture in the ion source (as inferred from ion beam intensity at *m/z* 18, I_{18}, and measured as a voltage, V_{18}), and more specifically with differences in moisture between SA and ST sides (ΔV_{18}). A substantial background signal in V_{18} has always been present in both mass spectrometers, even at times when no air was admitted to the ion source (i.e. COV closed). This reflects 1) the strong tendency of moisture to adsorb onto surfaces and slowly desorb under vacuum and 2) ongoing supply of moisture to the ion source from both SA (especially before introduction of in-line drying as a fixed component of the inlet system) and ST (no drying) sides, even though the vast majority of analysed air

samples and standards were dried to dewpoints of –70°C or lower during sampling or preparation.

Relative V_{18} of SA and ST gas streams has been regularly monitored. Invariably, V_{18} is high after the ion source has been vented and thus exposed to moist, laboratory air. It then subsides over a period of several weeks as moisture levels approach an equilibrium where the rate of surface desorption and evacuation is in balance with the inflow of moisture from SA and ST air (Figure 2.8a). During such periods, it is typical for $\delta^{29}N_2$ and $\delta^{33}O_2$ to be positively correlated with ΔV_{18} (Figure 2.8b; expressed as a percentage of V_{32} to allow for variations in instrument sensitivity). Similar correlations have been observed when undried air was introduced on the SA side, with perturbations in $\delta^{29}N_2$ of as much as ~100 per meg in some cases. This behaviour can be explained by protonation of the highly abundant species $^{28}N_2$ and $^{32}O_2$ due to the presence of water, thus producing ions with *m/z* 29 and 33.

This process has important implications for MAT252 measurement of $\delta(^{32}O_2/^{29}N_2)$, as interference of $^{14}N^{14}NH^+$ with $^{29}N_2$ leads to underestimation of the measured O_2/N_2 ratio. The variation of $\delta(^{32}O_2/^{29}N_2)$ with time in Figure 2.8 is of opposite sign to that in $\delta^{29}N_2$. This is consistent with interference at *m/z* 29, though noting that the magnitude of the change is smaller for $\delta(^{32}O_2/^{29}N_2)$ and that the relationship between $\delta(^{32}O_2/^{29}N_2)$ and ΔV_{18} has not always been consistent at other times. On some occasions both $\delta(^{32}O_2/^{29}N_2)$ and $\delta^{29}N_2$ appeared to be positively correlated with ΔV_{18}, although moisture-related effects could not be clearly distinguished from other possible influences at those times. Even though some of these observations remain unexplained, there are strong reasons to suggest that

variable moisture levels in the ion source can lead to significant biases in $\delta(^{32}O_2/^{29}N_2)$ measurements.

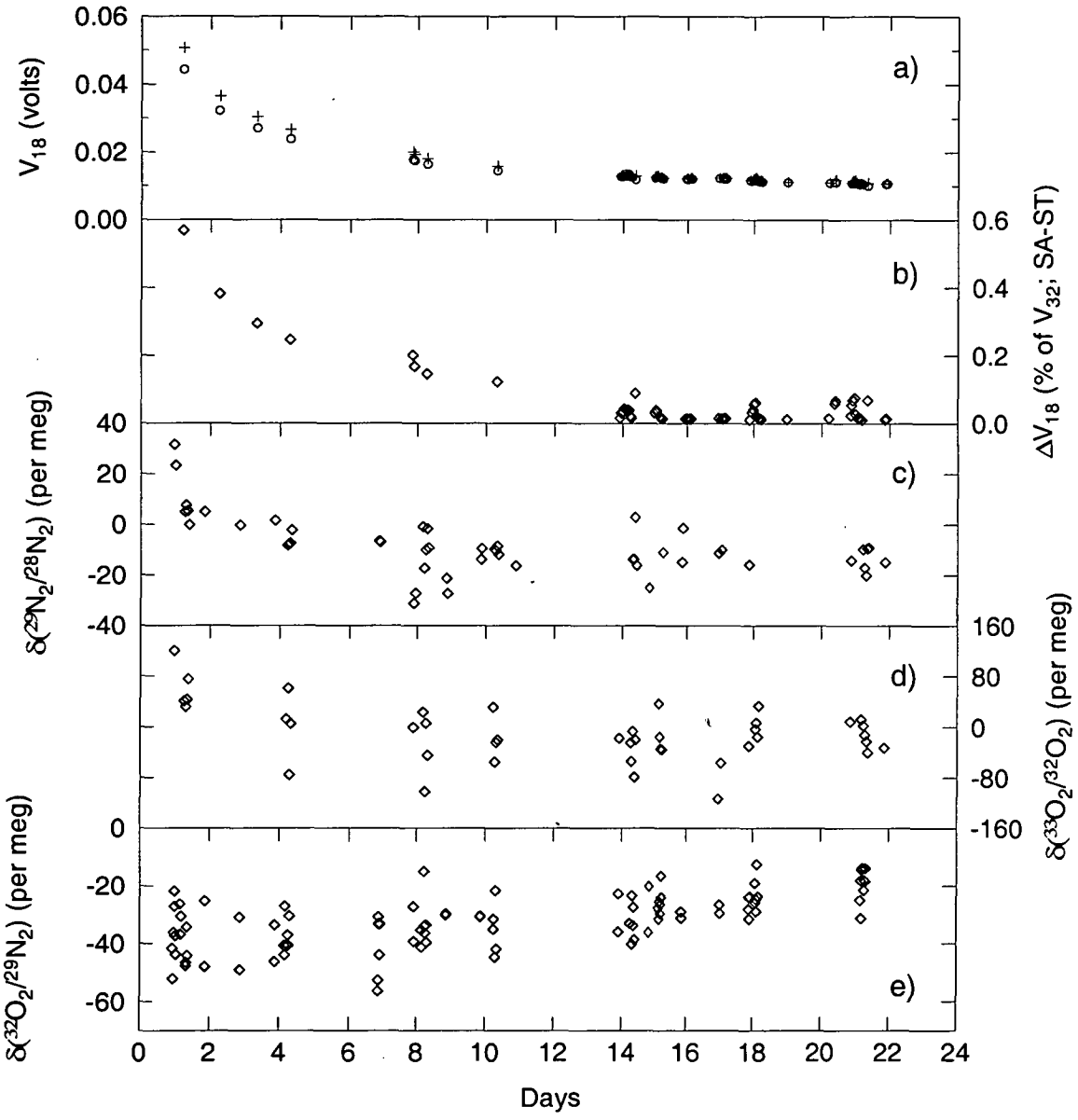

Figure 2.8 A typical example of the evolution of a) ion beam intensity at *m/z* 18, expressed here as V_{18}, the measured voltage, b) the difference in V_{18} (SA-ST) of gas streams entering the source, expressed as a percentage of V_{32}, c-e) $\delta(^{29}N_2/^{28}N_2)$, $\delta(^{33}O_2/^{32}O_2)$ and $\delta(^{32}O_2/^{29}N_2)$ respectively of individual analysis blocks from 950051 relative to the working standard for a period of several weeks on the MAT252. The time axis represents days after venting of the source and resumption of vacuum (commencing 15 September, 1997).

For comparisons of dried air, moisture-induced artefacts are largely accounted for by referencing all unknown samples to the external standard, 950051. However, errors could still result from a systematic offset in V_{18} between 950051 and other (e.g. flask) samples and by any change in this offset with time. The period between September and November, 1997 which includes the measurements in Figure 2.8, provides useful constraints of the magnitude of this offset because the anhydrous $Mg(ClO_4)_2$ drying tube was first installed for routine operation on 3 October (at 18.2 days on the time axis of Figure 2.8) and V_{18} was measured for a large number of 950051 and flask samples around this time.

Mean V_{18} offsets relative to 950051 in glass flask samples are listed in Table 2.6. They do show significant differences, with systematically higher V_{18} in glass flask samples loaded to the inlet system without drying. The intermediate offset observed for (occasional and random) analyses of undried flask air relative to dried 950051 air is probably due to a time lag in the increase of V_{18} after introduction of a sample containing higher moisture. Such time delays were observed on several occasions where very moist air was admitted to the ion source. They probably result from selective adsorption of moisture onto surfaces of the inlet system, capillary and COV so that the true sample moisture levels are not immediately registered at the detector.

Elevated moisture levels in flask samples relative to 950051 may result from one or more factors: 1) if a glass flask has previously contained a "wet" sample, moisture adsorbed onto the flask surfaces is unlikely to be effectively removed by the relatively short flushing before collection of a new sample, 2) moisture will desorb from the external part of the flask valve that is exposed to ambient air, while sample air is extracted for analysis, 3) the volume and flow rate of sample air used to flush

In-line drying?		Dates	Mean ΔV_{18} (glass flasks - 950051; % of V_{32})
glass flasks	950051		
no	no	29-Sep to 3-Oct, 1997	0.022 ± 0.010 (n=15)
no	yes	13-Oct to 5-Nov, 1997	0.009 ± 0.009 (n=28)
yes	yes	13-Oct to 5-Nov, 1997	-0.002 ± 0.002 (n=41)

Table 2.6 Statistics of the relative difference of V_{18} measured in glass flask samples with respect to 950051 analysed on the same day.

the inlet system is smaller for glass flasks than for high pressure cylinders, thus inhibiting exclusion of moisture.

The sensitivity of $\delta^{29}N_2$ to ΔV_{18} (estimated at 44±6 per meg $\%^{-1}$ using an ODR fit to data in panels b and c of Figure 2.8) can be used to constrain the magnitude of biases resulting from this effect. A difference of 0.024 in mean ΔV_{18} implies a systematic offset of –1 per meg in $\delta(^{32}O_2/^{29}N_2)$ and +1 per meg in $\delta^{29}N_2$ for glass flask samples analysed before introduction of the drying tube. Flask data are not adjusted for this offset, but it does contribute uncertainty, for example to determination of the atmospheric $\delta(O_2/N_2)$ trend from Cape Grim flask samples (Chapter 3). This effect will also contribute random noise to flask data due to variations in the moisture content of aliquots drawn from different flasks, even among samples that would be considered well-dried. This is reflected in the scatter of ΔV_{18} in Figure 2.8 (e.g. between days 14 and 22) which shows a range of about 0.08%, equivalent to a range in $\delta(O_2/N_2)$ of about 4 per meg. Effectiveness of the in-line drying in reducing bias and noise is demonstrated by the near zero mean ΔV_{18}

and low standard deviation of comparisons where both flask samples and 950051 were actively dried.

In summary, the presence of moisture in the ion source can cause significant interference with ion beams at *m/z* 29 and 33. This effect could lead to large errors in $\delta(^{29}N_2/^{28}N_2)$, $\delta(^{33}O_2/^{32}O_2)$ and $\delta(^{32}O_2/^{29}N_2)$ if data were referenced against the working standard rather than an external standard, or if samples are not adequately dried before analysis. Even if all analysed samples are believed to have been dried at the time of collection, there can be no guarantees that the drying procedures are infallible. If a moist sample is unwittingly introduced, large errors may result and may go unnoticed if V_{18} is not routinely monitored. Furthermore, slow stabilisation of V_{18} on SA and ST sides can also lead to errors in measurements of subsequent samples. MAT252 measurements of glass flask samples admitted to the ion source without active drying on the inlet system were probably subject to small systematic bias (~1 per meg) and random noise (~±2 per meg). These effects were reduced to insignificant levels after introducing routine drying of all air admitted to the sample side inlet from 3 October 1997.

2.5 Inlet and gas handling

2.5.1 Stability of sample air stored in the inlet

After sample air has been admitted to the sample side inlet for analysis, it can potentially be modified by two processes. One is fractionation of air passing through the capillary to the COV of the mass spectrometer. An example of this effect has been reported by Allison and Francey (1999) for $\delta^{13}C$ in CO_2 using the same MAT252 instrument but with smaller CO_2 reservoirs and crimped SS capillaries. The

other is interaction with the surface materials (glass, Viton, Apiezon grease, SS) to which samples are exposed. Of main interest are changes occurring on time scales characteristic of sample analysis, namely from a few minutes up to a few hours, although sample stability has been tested for periods up to several days.

Significant changes in $\delta(O_2/N_2)$ are observed within the first 20 minutes after a new sample has been admitted to the inlet, but only if substantial time has elapsed since loading of the previous sample (Figure 2.9). In these circumstances, continuous flow of sample air from the inlet volume to the COV has caused inlet pressure to decay significantly below the operating pressure of 1.25 atm. This effect was characterised using data from a large number of occasions where a sample was analysed after idle periods of either about 15 hours (overnight) or 63 hours (over a weekend) and multiple O_2/N_2 measurements were made over a period of at least 30 minutes. It was established that immediately after loading the sample, $\delta(O_2/N_2)$ is measurably depleted and that the anomaly decays exponentially to be no longer detectable after about 20 minutes. The magnitude of the initial depletion is proportional to the time elapsed since the previous sample was loaded (and inlet pressure was set to 1.25 atm.). All data are thus routinely corrected using the following relationship:

$$\delta(O_2/N_2) = \delta(O_2/N_2)_{measured} + 0.72\, h\, e^{-0.15m} \qquad (2.10)$$

for m minutes ($0 < m < 20$) since sample loading, and h hours since loading the previous sample. There is no measurable effect in $\delta(Ar/N_2)$ or in $\delta^{29}N_2$, suggesting the changes in O_2/N_2 are not the result of mass-dependent fractionation but rather equilibration of the inlet surfaces to higher pressure when a new sample is

introduced. This observation also suggests that for materials used in this inlet system, surface adsorption effects are probably larger for O_2/N_2 than for Ar/N_2, consistent with observations of permeation through Viton and PFA O-rings (Section 2.7).

Numerous tests of sample storage in the inlet system for periods up to several days show only minor drifts in $\delta(O_2/N_2)$, $\delta(Ar/N_2)$, and $\delta^{29}N_2$ (Table 2.7), indicating that the combination of surface interactions (after the initial 20 minutes) and

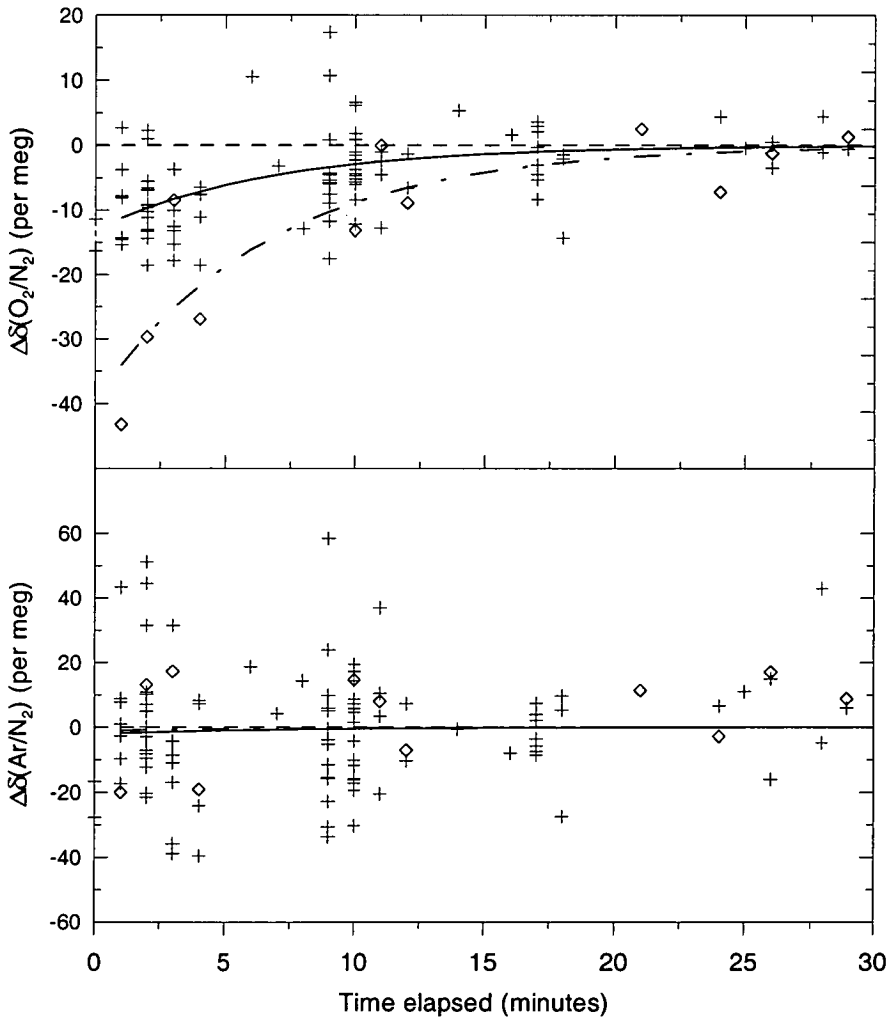

Figure 2.9 Anomalies in $\delta(O_2/N_2)$ (upper panel) and $\delta(Ar/N_2)$ (lower panel) in air stored in the sample side inlet either overnight (crosses; mean storage time 15 hours) or over a weekend (diamonds; 63 hours). Anomalies are determined with respect to the mean of measurements made more than 30 minutes after pressure adjustment and are fitted by solid (15 hours) and dash-dot (63 hours) exponential curves of the form described by Equation 2.10.

fractionation related to sample consumption is negligible for periods of up to a few hours. The majority of analyses are completed within 1 hour of samples being loaded. Data from samples stored more than 4 hours are rejected.

	Mean Drift Rate (per meg hour^{-1})	
	After 15 hours	After 63 hours
$\delta(^{32}O_2/^{28}N_2)$	-1.1 ± 0.2 (n = 8)	-0.7 ± 0.5 (n = 8)
$\delta(^{40}Ar/^{28}N_2)$	0.1 ± 0.2 (n = 4)	0.5 ± 0.2 (n = 4)
$\delta(^{29}N_2/^{28}N_2)$	0.6 ± 0.2 (n = 9)	0.1 ± 0.1 (n = 3)

Table 2.7 Mean drift rates for air stored in the sample side inlet either overnight (mean storage time 15 hours) or over a weekend (63 hours). These values were calculated after correction for pressure re-equilibration effects as described by Equation 2.10. Uncertainties are the standard error of the mean.

2.5.2 Drying

The recognition that variable moisture levels between different types of samples could introduce significant bias and/or noise in measurements of $\delta(O_2/N_2)$ and $\delta^{29}N_2$ etc. (Section 2.4.7) led to the addition of an anhydrous $Mg(ClO_4)_2$ drying tube as a fixed component of the sample side inlet system from 3 October, 1997 and for selected samples (known to be undried) before that time. This action successfully reduced the mass spectrometric, moisture-induced artefacts to insignificant levels. However, it introduced a possibility of other artefacts related to chemical properties of the drying agent. In particular, a serious concern only recognised at a later time was that $Mg(ClO_4)_2$ is classified as an oxidizing agent and thus presented a risk that it might liberate O_2 on reaction with water.

Various tests of the suitability of $Mg(ClO_4)_2$ were conducted in the laboratory around the time of its addition to the inlet system, and subsequently also involving field samples in relation to drying techniques employed for sample collection (Section 2.8.2). The laboratory tests involved analysis of dry cylinder air (950051), moist cylinder air (960051; filled at Cape Grim without drying but partially dried by pressurisation to 30 atm.) and a batch of glass, 0.5 L flasks filled with dry air from a cylinder, where each of these samples was admitted to the inlet system with and without the in-line drying tube (Table 2.8). Mean differences were small for all tests. The only statistically significant result was for moist cylinder air where marginally lower $\delta(O_2/N_2)$ was indicated for dried aliquots. If this represents a real bias, it is of the wrong sign for liberation of O_2 by the $Mg(ClO_4)_2$ or from isobaric interference at *m/z* 29 only. More than 2 years of sampling (moist air) at Cape Grim using anhydrous $Mg(ClO_4)_2$ and Nafion in parallel, and with occasional comparisons against a cryogenic drying technique showed no detectable bias in $\delta(O_2/N_2)$ between the three techniques (Section 2.8.2).

Sample type	$\Delta\delta(O_2/N_2)$ (per meg)
Dry cylinder air	0.3 ± 2.2
Moist cylinder air	-4.9 ± 1.9
Dry glass flask samples	4.3 ± 6.5 (n = 12)

Table 2.8 Mean $\delta(O_2/N_2)$ differences between aliquots of the same sample loaded to the inlet system with and without in-line drying. All differences are in the sense of [dried minus undried]. Uncertainties are the standard error of the mean.

2.5.3 Cylinder (via regulator) sample loading procedures

Most of the high pressure, $O_2/N_2/Ar$ cylinder standards are fitted with dedicated, permanently attached regulators (Section 2.2.3) that are handled in ways to minimise artefacts due to pressure-dependent, surface adsorption effects. The high pressure side is always exposed to full cylinder pressure, even when the cylinder is not in use and the valve is closed. The low pressure side is also left pressurised, generally to the delivery pressure required for $O_2/N_2/Ar$ purposes.

Sample loading procedures consist of some combination of three parts: 1) removal of resident air by draining all overpressure from the regulator with the cylinder valve closed ("pressure drain"); this provides effective removal of "old" air from any dead volumes such as gauges, 2) "venting" of cylinder air through the regulator at constant pressure, with cylinder valve open and 3) "through-flushing" of the inlet system at a (constant) set pressure and flow rate.

The main variation to the procedure relates to the "pressure drain" step. This step is always performed if air has resided in the regulator for several hours or more, for example ahead of the first load from a cylinder on any day. It is otherwise applied randomly, partly to test for sensitivity of measurements to variations in the procedure. After regulator pressure has been drained, the cylinder valve is immediately opened and air is vented to atmosphere at constant pressure for long enough to (twice or more) replace the volume of air that may have been modified by pressure-dependent effects when expanded into the drained regulator (step 2). For most cylinders this involves venting for 40 seconds at flow rates estimated to be in excess of 1 L min^{-1}. The flow is then directed through the inlet with regulator delivery pressure and the needle valve of the inlet system set to maintain 1.25 atm. in the analysis chamber and a flow rate of 200 ml min^{-1} (step 3). The delivery pressure is

usually already set at the appropriate level but is fine tuned at this point if necessary. The inlet is generally flushed in this way for 2 minutes.

For the occasions where step 1 is bypassed, steps 2 and 3 are carried out in immediate succession. Sometimes, a variation of the procedure was tested by draining the regulator (steps 1 and 2), then leaving the regulator to condition for periods of minutes to hours before proceeding with step 3. In these cases, step 2 was repeated immediately before step 3.

Initial tests on the MAT252 instrument, mostly using the primary standard 950051, did not reveal any sensitivity of measured ratios to various parameters associated with loading procedures. The one notable exception was depletion in measured $\delta(O_2/N_2)$ if too little air was vented through the regulator after a pressure drain. Similar tests were later performed with several cylinders on the Delta^{plus}XL, with the advantages of higher precision and ability to measure Ar/N_2. Those results did identify sensitivity of O_2/N_2 and Ar/N_2 to flushing flow rate that varied strongly between cylinders (Section 2.6.5).

A large body of statistics relating measurements to variations in loading procedures has been compiled for the frequently analysed primary standard, 950051. The variability in measurements is too small to detect in isolated tests but some systematic differences do emerge in long term averages. There is some evidence linking depletion of $\delta(O_2/N_2)$ and $\delta(Ar/N_2)$ to the pressure drain step and also to the order of successive aliquots with the first aliquot after a period of inactivity (usually a day) being depleted relative to one or more subsequent aliquots. Qualitatively similar order dependence was also reported by Keeling et al. (1998a). At this stage the statistics are insufficient to clearly separate the relative contributions. However, a

clear signal is observed for those cases where both conditions are satisfied (Table 2.9).

$\delta(^{32}O_2/^{29}N_2)$	$\delta(^{32}O_2/^{28}N_2)$	$\delta(^{40}Ar/^{28}N_2)$	$\delta(^{29}N_2/^{28}N_2)$
–4.9 ± 1.4 (n = 61)	–5.1 ± 0.5 (n = 116)	–9.5 ± 1.3 (n = 116)	0.3 ± 0.6 (n = 151)

Table 2.9 Mean deviations (in per meg) of the first of two or more successive aliquots from 950051 using a sample loading procedure that includes draining overpressure from the regulator, relative to subsequent aliquots (usually analysed within the following 1-2 hours and mostly without the pressure drain step).

The observed $\delta(O_2/N_2)$ anomaly is similar for independent data sets obtained with the two mass spectrometers. A significant anomaly is also evident in $\delta(Ar/N_2)$ but not in $\delta^{29}N_2$. The multi-species signature does not clearly distinguish between a mass-dependent fractionation and a surface, chemical effect. For diffusive fractionation one would expect: 1) the $\delta(Ar/N_2)/\delta(O_2/N_2)$ ratio in Delta^{plus}XL data to be slightly higher than what is observed (1.9 ± 0.3, c.f. Table 2.2), 2) the $\delta(O_2/N_2)$ anomaly in MAT252 data to be smaller than for the Delta^{plus}XL owing to the smaller measured mass difference (3 and 4 mass units respectively); this is not indicated by the mean values in Table 2.9, though noting that a MAT252 value of -3.8 would be expected relative to the higher precision Delta^{plus}XL value and this is accommodated by the confidence intervals and 3) relative to $\delta(Ar/N_2)$ one would expect a $\delta^{29}N_2$ anomaly of about –0.9 which lies 2σ from the mean. Thus the data are neither strongly supportive of nor clearly inconsistent with mass-dependent fractionation. It seems likely that these effects are a symptom of the same process causing the flow rate dependence described in Section 2.6.5 as both sets of observations relate to air

flow through regulators and are characterised by a $\delta(Ar/N_2)/\delta(O_2/N_2)$ ratio close to 2. If they are linked it would be easier to explain both results in terms of diffusive processes, for example involving thermal diffusion. However, some contribution from surface adsorption effects cannot be ruled out.

Corrections for $\delta(O_2/N_2)$ and $\delta(Ar/N_2)$ of 5 and 10 per meg are applied accordingly to 950051 data. This is done mainly to avoid systematic bias in atmospheric time series of $\delta(O_2/N_2)$ due to variation in the analysis protocol for 950051. In particular, during analysis sessions on the MAT252, it was common to load a single 950051 aliquot per day, usually with steps 1-3 carried out in immediate succession. More extensive analysis of 950051 has been possible on the Delta^{plus}XL, with usually 2 aliquots analysed per day and more variation in loading procedures. After allowance for this correction, uncertainty in long term $\delta(O_2/N_2)$ calibration due to these effects is within ±2 per meg. The main component of remaining uncertainty relates to the question of whether the observed anomalies are due to diffusive or chemical processes. If the anomalies are mainly due to surface effects, a similar $\delta(O_2/N_2)$ correction would be appropriate for both mass spectrometers. If, on the other hand, they are due to mass-dependent fractionation, the 5 per meg correction for MAT252 data would be too large by more than 1 per meg.

Measurements from other high pressure cylinders (standards and Cape Grim Air Archive (CGAA) samples) were also scrutinised for evidence of similar regulator effects. There was significant variability between cylinders and between sets of analyses of those cylinders. Some showed little or no variation, comparable to 950051, while others showed $\delta(O_2/N_2)$ variations of up to around 20 per meg. Where variability was observed, it was generally the first of several successive aliquots that

showed the largest anomaly relative to subsequent aliquots and generally in the sense of O_2/N_2 depletion. The occurrence of such variability tended to be more prevalent in CGAA samples, though it is not clear if this was due to higher moisture levels in these cylinders, generally shorter conditioning times of regulators attached to these cylinders, use of generally different regulators to those tested on 950051 and most other standards, or some other factor. No corrections have been directly applied for cylinders other than 950051 but in cases where large anomalies were observed only in the first of several aliquots, data from the first aliquot have been rejected.

2.5.4 Flask sample loading procedures

The single largest source of noise in flask measurements reported here is the process of transferring air from the flask into the analysis chamber of the inlet system. Unlike high pressure cylinders, there is relatively little air available for flushing and conditioning of inlet plumbing. Samples are thus more susceptible to surface effects and/or mass-dependent fractionation associated with the transfer procedures. For example, Bender et al. (1994) reported preferential adsorption of O_2 relative to N_2 onto Viton O-ring surfaces as air was expanded into vacuum.

Two main variations to flask sample loading procedures were introduced to accommodate samples of different pressure (i.e. above-ambient, sub-ambient). A further variation applies to each of these procedures, depending on whether the air being transferred is from a "fresh" flask sample, thus replacing air from a different sample in the analysis chamber (refer to Figure 2.1), or a repeat aliquot from the same flask sample.

Introduction of a fresh flask sample always involves: 1) backflushing of the inlet plumbing with dry, background air from a high pressure cylinder, 2) evacuation

for 10 seconds to a vacuum of about 0.01 atm. and expansion of sample air into the 13 ml volume consisting of the flask neck, drying tube (if present) and connecting fittings up to the Glass Expansion (GE) valve located at the entrance to the analysis chamber (2 cycles), 3) conditioning of inlet surfaces for 2 minutes with sample air in the flask neck, and backflush air in the analysis chamber at the operating pressure of 1.25 atm., 4) evacuation of the analysis chamber and expansion of sample air into the analysis chamber and pressure gauge.

The steps that follow differ for the two procedures. If sample pressure is > 1 atm., air may be swept through the analysis chamber ("through-flushed") for 90 seconds at a flow rate of 20 ml min^{-1}. If sample pressure is ≤ 1 atm. (though above-ambient pressure sample are also sometimes loaded this way), the plunger is used to seal the analysis chamber from downstream plumbing (volume 22 ml), which is evacuated and then sealed from the pump. The plunger is retracted to expand sample air into the downstream volume, and thus sweep fresh sample air through the analysis chamber at near-constant pressure. Both procedures aim to enclose a parcel of air in the analysis chamber that has not been subjected to any substantial pressure change (i.e. from evacuation/expansion), thus minimising potential for modification of O_2/N_2 by pressure-dependent surface adsorption effects. For repeat aliquots of the same sample, steps 1-3 are omitted and either of the two procedures can again be followed, depending on remaining sample pressure. Finally, the plunger is used to adjust sample pressure so that SA ion beam intensities are matched to that of the ST side. For ≤ 1 atm. samples, this step does subject the enclosed air parcel to a pressure change of ≥ 0.25 atm. The volume of air used per aliquot ranges from 80-130 ml STP depending on flask volume and initial pressure.

Memory effects

The efficiency of removal of previous inlet contents was tested on two occasions by introducing multiple, successive aliquots of standard air after filling the inlet system with high purity N_2. Multiple analysis blocks were measured for each aliquot. One of the tests employed the flushing procedure used for cylinders (i.e. through-flushing 400 ml of air) and the other involved a glass flask with only a single evacuation and expansion step. On both occasions, $\delta(O_2/N_2)$ of the first aliquot was initially depleted by 100-200 per meg (implying uncertainty due to memory effects from the previous sample of within ±0.02 %) and $\delta(O_2/N_2)$ drifted higher during the first analysis block suggesting that some time is required to equilibrate capillary and COV surfaces to a new sample. This behaviour is not observed when successive samples have similar O_2/N_2. The magnitude of the memory effect is negligible for routine operations, for example implying an error of < 6 per meg for a difference of 28 ‰ (as applies to standard 880001).

Test flasks

A key strategy for assessing O_2/N_2 effects due to flask sample loading procedures is through analysis of "test flasks" containing air decanted from a high pressure cylinder where the cylinder contents have been precisely and directly measured. Test flasks are "sausage-filled", usually in batches of six, by connecting them in series to output flow from the cylinder. Where targeted sample pressure was above 1 atm., a back pressure regulator was attached downstream of the flasks to maintain constant pressure in the flasks throughout the flushing/filling procedure. Typically 60 L of air (20 minutes at 3 L min^{-1}) was flushed through each batch of

flasks, thus ensuring at least a 10-fold replacement (for flasks filled to 2 atm.) of air in each of the six flasks. Previous tests for other trace gas species (e.g. CO_2) indicated that at these flow rates, a replacement factor of about 6 was sufficient to reduce the previous sample contents to below detection limits.

Test flask results give a clear indication of biases with respect to measurements directly from cylinders but give ambiguous results about possible systematic biases between loading procedures. For example, some batches suggest biases of up to about 10 per meg in $\delta(O_2/N_2)$ associated with loading procedure variations. This includes comparison of repeat aliquots from the same samples using "above-ambient" and "sub-ambient" procedures or between first and subsequent aliquots. However, the indicated biases are not sufficiently consistent over different subsets of flask samples (e.g. test flasks, field samples or comparing data from the two mass spectrometers) to be clearly attributed to these factors. The implication is that other unidentified factors are also involved.

Flask air-sharing intercomparisons similar to that of NOAA/CMDL and CSIRO (Masarie et al., 2001) have been maintained for O_2/N_2 between CSIRO and URI/PU since 1995 and between CSIRO and SIO since 1997, using URI/PU and SIO flasks filled at Cape Grim (Cooper et al., 2001). Large, systematic and consistent $\delta(O_2/N_2)$ differences have emerged between CSIRO measurements of these flask samples (filled to 1 atm. pressure for both laboratories) and CSIRO's 0.5 L flask samples, even when the same ("sub-ambient") loading procedure is used. $\delta(^{32}O_2/^{28}N_2)$ measurements from the URI/PU and SIO samples are depleted relative to CSIRO samples by on average 34 and 48 per meg respectively in Delta^{plus}XL measurements. There are associated anomalies in $\delta(Ar/N_2)$ (-130 and -179 per meg) and $\delta^{29}N_2$ (-7

and -12 per meg) that suggest the main influence is from mass-dependent fractionation. These anomalies exist despite there being little difference in flask materials or in fittings used to connect respective flask types to the inlet system (especially for URI/PU and CSIRO flasks for which the fittings are identical). The implication is that subtle differences in the geometry of flask valves (GE, Louwers-Hapert and J.Young valves used for CSIRO, URI/PU and SIO flasks respectively), end stubs or valve actuation may affect air flow and induce fractionations of different magnitude. Although the cause of these differences is not known, the observations do reinforce the point that significant O_2/N_2 artefacts can easily be incurred from gas handling procedures.

Mean test flask differences relative to direct measurement of the parent cylinder show depletion of $\delta(O_2/N_2)$ but enrichment of $\delta(Ar/N_2)$, $\delta^{29}N_2$ and $\delta^{34}O_2$ (Table 2.10). This distribution implies a contribution from mass-dependent fractionation but is inconsistent with this being the only influence. It suggests a likely contribution from surface exchange, perhaps involving the Viton O-rings present in the inlet system. A further complication is that the general assumption of air drawn from a cylinder being precisely representative of cylinder contents may not be valid (Sections 2.6.4 and 2.6.5). Fractionation of air extracted either for analysis or for decanting into test flasks might account for much of the differences in Table 2.10. For example, it is plausible that the decanted air is, on average, depleted relative to true cylinder contents by about 40, 3 and 6 per meg in $\delta(Ar/N_2)$, $\delta^{29}N_2$ and $\delta^{34}O_2$ respectively, thus accounting for all of the flask/cylinder difference in these species. If this were the case, $\delta(O_2/N_2)$ would be depleted by about 13 per meg due to

fractionation and would thus require a depletion of 24 (13 + 11) per meg due to other, e.g. surface influences.

In order to simplify comparison of flask and cylinder samples (e.g. filled at a common site like Cape Grim), the test flask results are used as a basis for adjusting flask data so as to be consistent with cylinder data. Corrections of +11, -40, -3 and –6 per meg are applied to $\delta(O_2/N_2)$, $\delta(Ar/N_2)$, $\delta^{29}N_2$ and $\delta^{34}O_2$ respectively. The $\delta^{34}O_2$ correction is smaller than indicated in Table 2.10 but is within uncertainty and more consistent with the fractionation implied by both $\delta(Ar/N_2)$ and $\delta^{29}N_2$ results. Thus if the test flask results reflect biases due to flask loading procedures only, flask and cylinder data would be directly comparable after these adjustments. On the other hand, if either the cylinder measurements or the air decanted to test flasks is fractionated, errors will be propagated to flask/cylinder differences.

$\delta(^{32}O_2/^{29}N_2)$	$\delta(^{32}O_2/^{28}N_2)$	$\delta(O_2/N_2)$	$\delta(^{40}Ar/^{28}N_2)$	$\delta(^{29}N_2/^{28}N_2)$	$\delta(^{34}O_2/^{32}O_2)$
–6.2 ± 3.1 (n = 36)	–10.5 ± 2.1 (n = 39)	–11.0 ± 2.5 (n = 46)	40.5 ± 7.2 (n = 39)	2.8 ± 1.4 (n = 39)	12.1 ± 8.1 (n = 7)

Table 2.10 Mean deviations (in per meg) of measurements from test flasks relative to direct measurements from the parent cylinder. The value for $\delta(O_2/N_2)$ was obtained by merging $\delta(^{32}O_2/^{28}N_2)$ data from the Delta^{plus}XL with the sum of $\delta(^{32}O_2/^{29}N_2)$ and $\delta^{29}N_2$ from MAT252 data where both species were measured (see Section 2.6.2). Uncertainties are the standard error of the mean.

Finally, the multi-species characteristics of noise introduced by flask sample loading procedures can be examined by plotting differences between multiple aliquots extracted from the same flask sample (Figure 2.10). The $\delta(^{40}Ar/^{28}N_2)/\delta(^{32}O_2/^{28}N_2)$ relationship is very well defined with a slope of 3.4, consistent with diffusive fractionation. The slopes indicated for other pairs of ratios are also in the

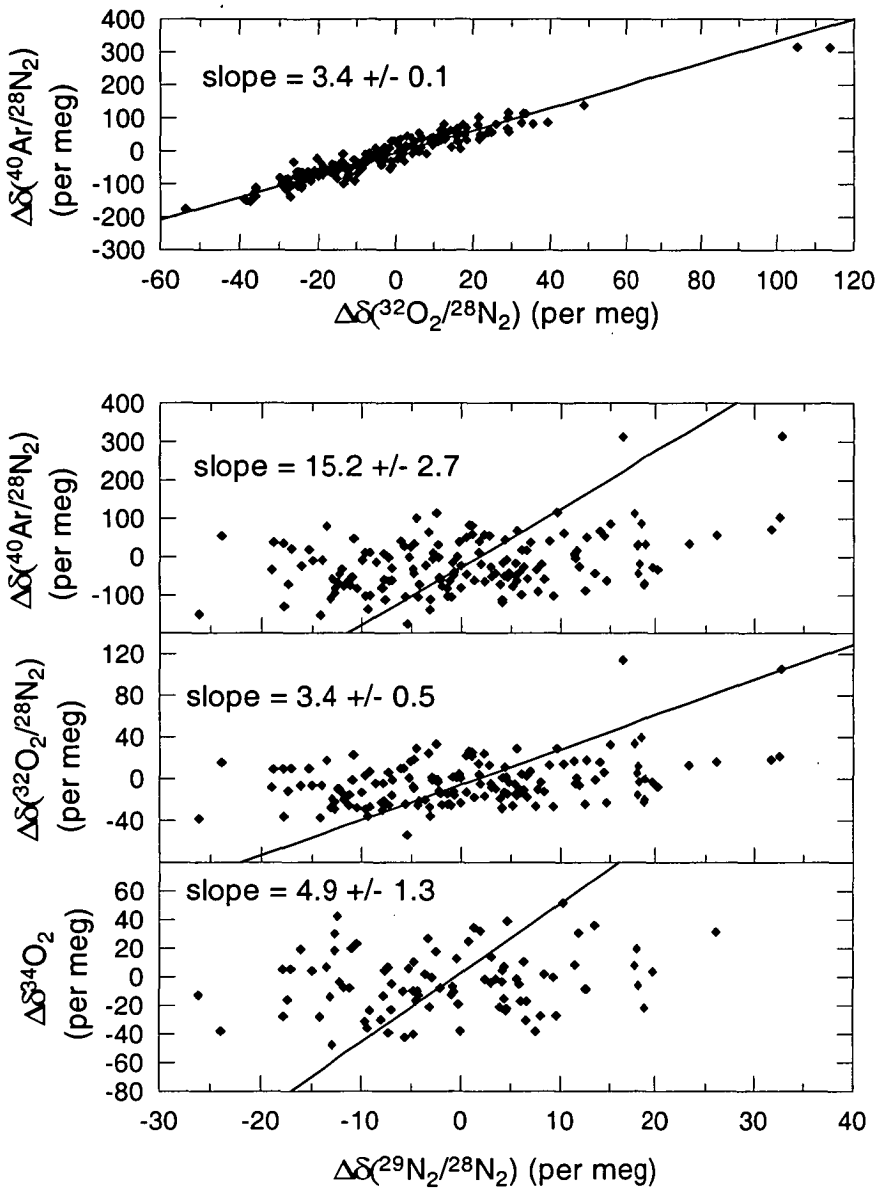

Figure 2.10 Inter-species relationships of differences between repeat aliquots of the same flask sample with lines of best fit obtained by ODR.

vicinity of what is expected from mass dependence. These results suggest that even if there is a surface exchange component to mean $\delta(O_2/N_2)$ differences, most of the variability in differences is related to mass-dependent processes. Note that some ODR fits do not appear to closely match the data. This reflects strong sensitivity of the fit to relative uncertainties of each ratio pair, and the range of variation in $\delta^{29}N_2$ being comparable to measurement uncertainty. Assigned uncertainties are taken from

the standard deviation of test flask differences relative to their parent cylinders after allowance for all flask-related corrections (Table 2.11). These values also provide a measure of reproducibility for flask samples of this type.

$\delta(^{32}O_2/^{29}N_2)$	$\delta(^{32}O_2/^{28}N_2)$	$\delta(^{40}Ar/^{28}N_2)$	$\delta(^{29}N_2/^{28}N_2)$	$\delta(^{34}O_2/^{32}O_2)$
16	14	47	9	23

Table 2.11 External reproducibility (in units of per meg) of glass, 0.5 L flask sample measurements as given by the standard deviation of test flask differences relative to their parent cylinders.

2.6 Calibration

2.6.1 Instrumental offset between SA and ST sides

Measurements of all species for 950051 against the working standard (941471) are displayed in Figure 2.11 so as to demonstrate the variability of instrumental offsets between SA and ST sides. This plot includes some data that are otherwise rejected for calibration purposes, such as from periods of instability after venting of the ion source. The $\delta(O_2/N_2)$ data span a range of more than 200 per meg. Even within individual analysis sessions where the instruments were considered to be operating well, changes in $\delta(O_2/N_2)$ were sometimes as large as 40 per meg. Significant variability was observed in data from both mass spectrometers but was smaller for the Delta^{plus}XL, at least partly because of the lower frequency of ion source venting. These results underscore the importance of maintaining a calibration strategy that accommodates variability in the zero enrichment. This is achieved here by referencing all data to the external standard, 950051.

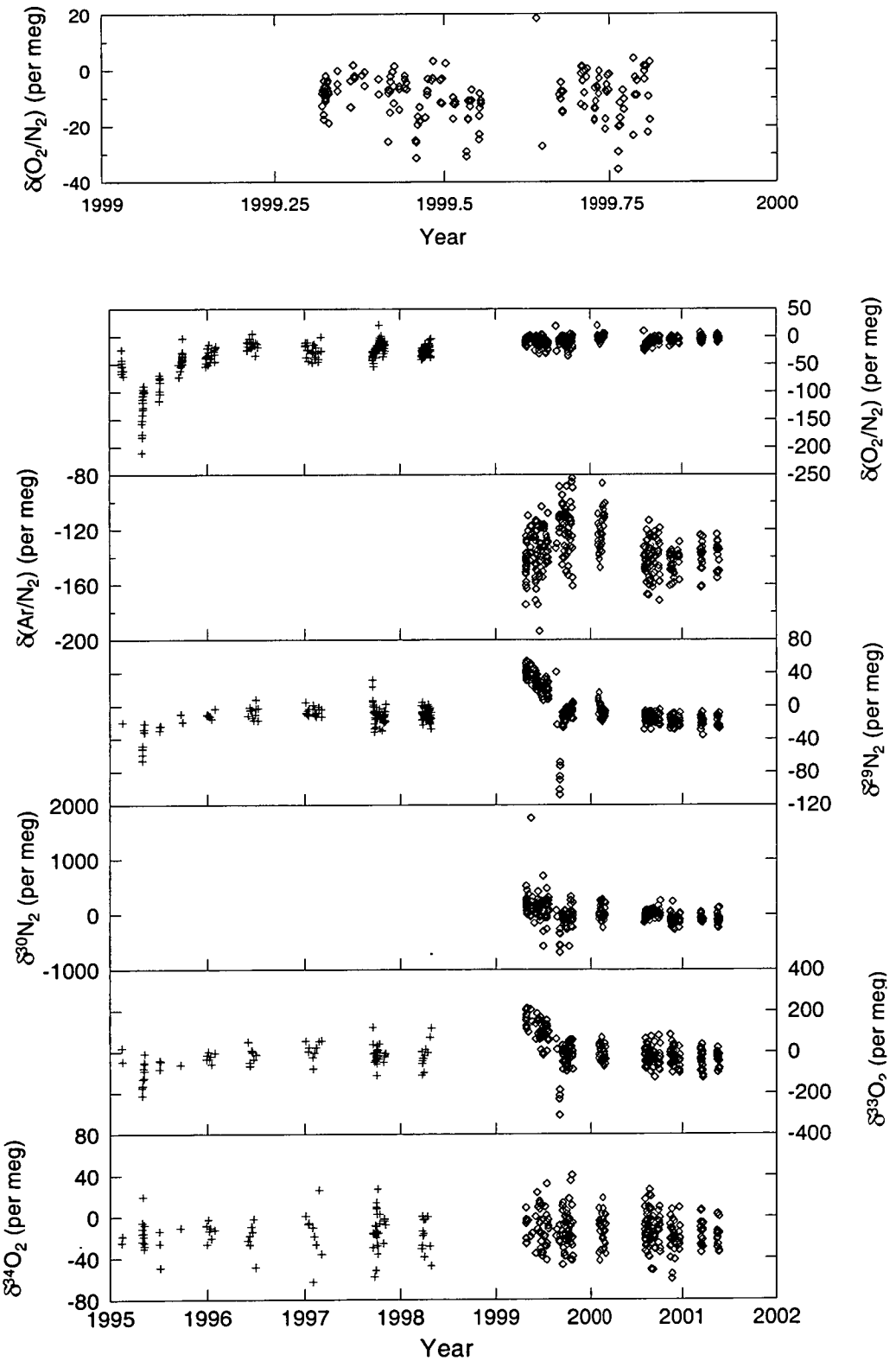

Figure 2.11 Variability in measured offsets between SA and ST sides of the MAT252 (+) and Delta^{plus}XL (◊) as displayed by measurements of 950051 against the working standard, 941471. The uppermost panel shows $\delta(O_2/N_2)$ only over a single year (1999) of Delta^{plus}XL measurements to illustrate the magnitude of shorter term variability.

There is also significant structure evident in records of other measured ratios. Inter-species relationships provide some insight into possible causes. In some cases, for example in 1995, changes in $\delta(O_2/N_2)$ are correlated with $\delta^{29}N_2$ in a way that is consistent with mass-dependent fractionation. However, $\delta^{34}O_2$ shows little change at this time, and certainly not a drift of ~100 per meg that would be predicted from mass dependence based on the $\delta(O_2/N_2)$ and $\delta^{29}N_2$ results. Early Delta^{plus}XL data in 1999 exhibit a correlated drift in $\delta^{29}N_2$ and $\delta^{33}O_2$, suggesting influence of moisture related artefacts (see also Section 2.4.7). Other features, for example variability in $\delta(Ar/N_2)$ in 1999/2000, are not obviously linked to other species, indicating that other, as yet unidentified processes are also at work.

2.6.2 Merging $\delta(^{32}O_2/^{29}N_2)$ and $\delta(^{32}O_2/^{28}N_2)$ records

A complication applying to the measurement of $\delta(^{32}O_2/^{29}N_2)$ on the MAT252 is that it only gives an accurate measurement of relative $\delta(O_2/N_2)$ if there is no relative difference in $\delta(^{29}N_2/^{28}N_2)$. In practice, $\delta(^{29}N_2/^{28}N_2)$ differences do exist between 950051 and either field samples or other standards, in part due to fractionation associated with gas handling procedures. In some cases, $\delta(^{29}N_2/^{28}N_2)$ may also be changing with time. This is a critical issue for merging of data from MAT252 and Delta^{plus}XL instruments, where the integrity of long term records is important, particularly for measuring atmospheric trends or determining calibration standard histories.

The protocol adopted here is to convert measured $\delta(^{32}O_2/^{29}N_2)$ to $\delta(^{32}O_2/^{28}N_2)$ using knowledge of the deviation in $\delta(^{29}N_2/^{28}N_2)$ from the reference scale defined by 950051. Writing Equation 2.1 in terms of the ratio of amount of substance (N) in

sample air for mass pairs 32/29 and 29/28 gives:

$$\frac{N_{32;sample}}{N_{29;sample}} = [\delta(^{32}/_{29}) \times 10^{-6} + 1] \times \frac{N_{32;reference}}{N_{29;reference}} \quad (2.11)$$

$$\frac{N_{29;sample}}{N_{28;sample}} = [\delta(^{29}/_{28}) \times 10^{-6} + 1] \times \frac{N_{29;reference}}{N_{28;reference}} \quad (2.12)$$

Substituting into:

$$\frac{N_{32}}{N_{28}} = \frac{N_{32}}{N_{29}} \frac{N_{29}}{N_{28}} \quad (2.13)$$

for both sample and reference air and finally substituting into Equation 2.1 for masses 32 and 28 reduces to:

$$\delta(^{32}/_{28}) = \delta(^{32}/_{29}) + \delta(^{29}/_{28}) + [\delta(^{32}/_{29})\delta(^{29}/_{28}) \times 10^{-6}] \quad (2.14)$$

For atmospheric measurements dealt with here, the product term at the right hand side of Equation 2.14 can be safely ignored, thus giving the simple approximation:

$$\delta(^{32}/_{28}) = \delta(^{32}/_{29}) + \delta(^{29}/_{28}) \quad (2.15)$$

This equation is applied to MAT252 data, thus generating consistent records of measured $\delta(^{32}O_2/^{28}N_2)$ for both mass spectrometers. For cases where further corrections are necessary to allow for modification of atmospheric O_2/N_2 ratio by fractionation of sample air, $\delta(^{32}O_2/^{29}N_2)$ data are first converted to $\delta(^{32}O_2/^{28}N_2)$ using Equation 2.15 and then corrected for fractionation, calculated for a 4 mass unit difference and applied relative to measured $\delta^{29}N_2$ or $\delta(Ar/N_2)$.

2.6.3 Air standards

A key requirement for reliably quantifying temporal trends in atmospheric O_2/N_2 is the stability of O_2/N_2 in calibration standards. To this point in time, no "absolute" O_2/N_2 reference scale has been established along the lines of those adopted by the international CO_2 measurement community (Zhao et al., 1997) and by various other trace gas measurement programs (e.g. Matsueda, 1993; Prinn et al., 2000). This mainly stems from the technical difficulties involved in either preparing or analysing (in absolute terms) O_2/N_2 standards at the high precision required for contemporary global carbon cycle studies. In the absence of links to fundamental constants, existing O_2/N_2 monitoring programs have relied on relative stability among some number of air standards as a constraint of absolute stability. A similar approach was taken here, using a suite of 15 air standards stored in a variety of containers and with different pressure histories (Table 2.1). The rationale for maintaining some diversity in cylinder/sample conditions is to guard against concerted (and thus unidentified) drifts occurring among a group of like standards and to help isolate the cause of any drifts that might be observed.

Regular analysis of laboratory gas standards is an integral part of calibration strategies for many trace gas measurement programs, and there are numerous cases where standards have been shown to drift. Such drifts have usually been attributed to surface interactions, for example involving physisorption (e.g. for some halocarbon species; Yokohata et al., 1985; Fraser et al., 1991; Thompson et al., 1994) or chemisorption (e.g. production of CO through oxidation of surface organic residues; Langenfelds et al., in prep.). Drifting standards have long been recognised as a major issue for high precision monitoring of atmospheric CO_2 (e.g. Thoning et al., 1987) and have been one impediment to achieving the long-standing WMO target for inter-

comparability among CO_2 measuring laboratories of ±0.1 ppm. Experience at CSIRO suggests that CO_2 instability in high pressure cylinder standards is in some cases related to cylinder type and possibly also to moisture levels. For example, drifts of several ppm CO_2 have been observed in some stainless steel cylinders used by CSIRO (L.P. Steele, personal communication; Langenfelds et al., in prep).

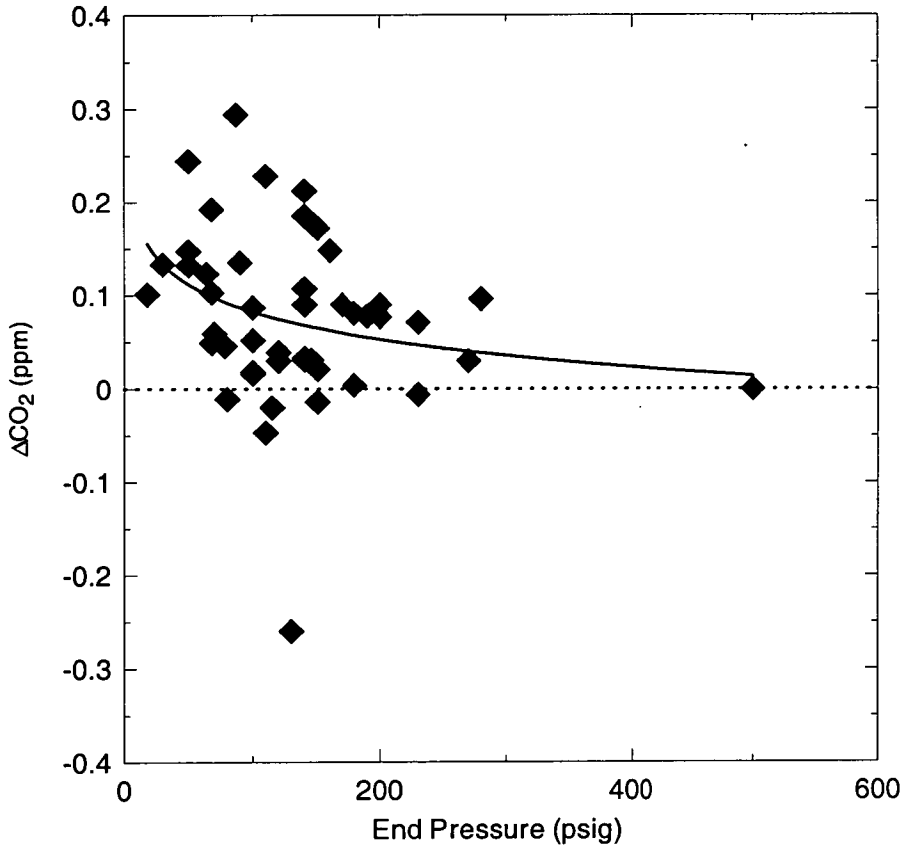

Figure 2.12 The change in CO_2 in dry, natural air standards supplied by GASLAB to Cape Grim. The standards are in service for 2-4 months during which time most of the initial contents (1500-2100 psig) are consumed. The solid curve is a logarithmic fit to the data, highlighting the trend towards increasing CO_2 enrichment with lower end pressures.

Standards contained in 29.5 litre, Luxfer aluminium cylinders that are currently used by CSIRO, the Central CO_2 Calibration Laboratory (CCCL) and distributed by the CCCL to other CO_2 measuring laboratories have been found to be

generally more stable, at least if the air is carefully dried. Nevertheless, many such standards exhibit measurable and significant drift and the cause(s) have not yet been clearly identified. The main indication of CO_2 drift in CSIRO standards occurs as a function of pressure (or usage) rather than time, as observed in air standards used for the Cape Grim in-situ CO_2 monitoring program. These standards are analysed in GASLAB before and after deployment at Cape Grim, and show a systematic bias towards CO_2 growth during their short (2-4 months) period of service as standards (Figure 2.12). Assessment of both the relative stability of $O_2/N_2/Ar$ standards, and of processes that could potentially modify these and other measured ratios are important issues to be addressed here.

2.6.4 Mass-dependent drift in cylinders

The history of one cylinder standard (991291) is of critical importance to the question of long term stability of $O_2/N_2/Ar$ standards. This standard was unusual in that it was drained from 2000 to 10 psig in 2 years, mainly through short bursts of high flow rates (3-4 litres min^{-1}) for filling test flasks, and that because of its test flask role for several GASLAB measurement programs it was regularly analysed for $O_2/N_2/Ar$, isotopes of O_2 and N_2, concentration of CO_2 and other species. Measurement histories for selected species are shown in Figure 2.13 as a function of cylinder pressure. The data show enrichment of $\delta(Ar/N_2)$, $\delta(O_2/N_2)$, $\delta^{29}N_2$, $\delta^{34}O_2$ and CO_2 as cylinder pressure was consumed, and acceleration in the drift at very low pressures, at least for $\delta(Ar/N_2)$ and $\delta(O_2/N_2)$ where the magnitude of the drift is large compared to measurement uncertainty.

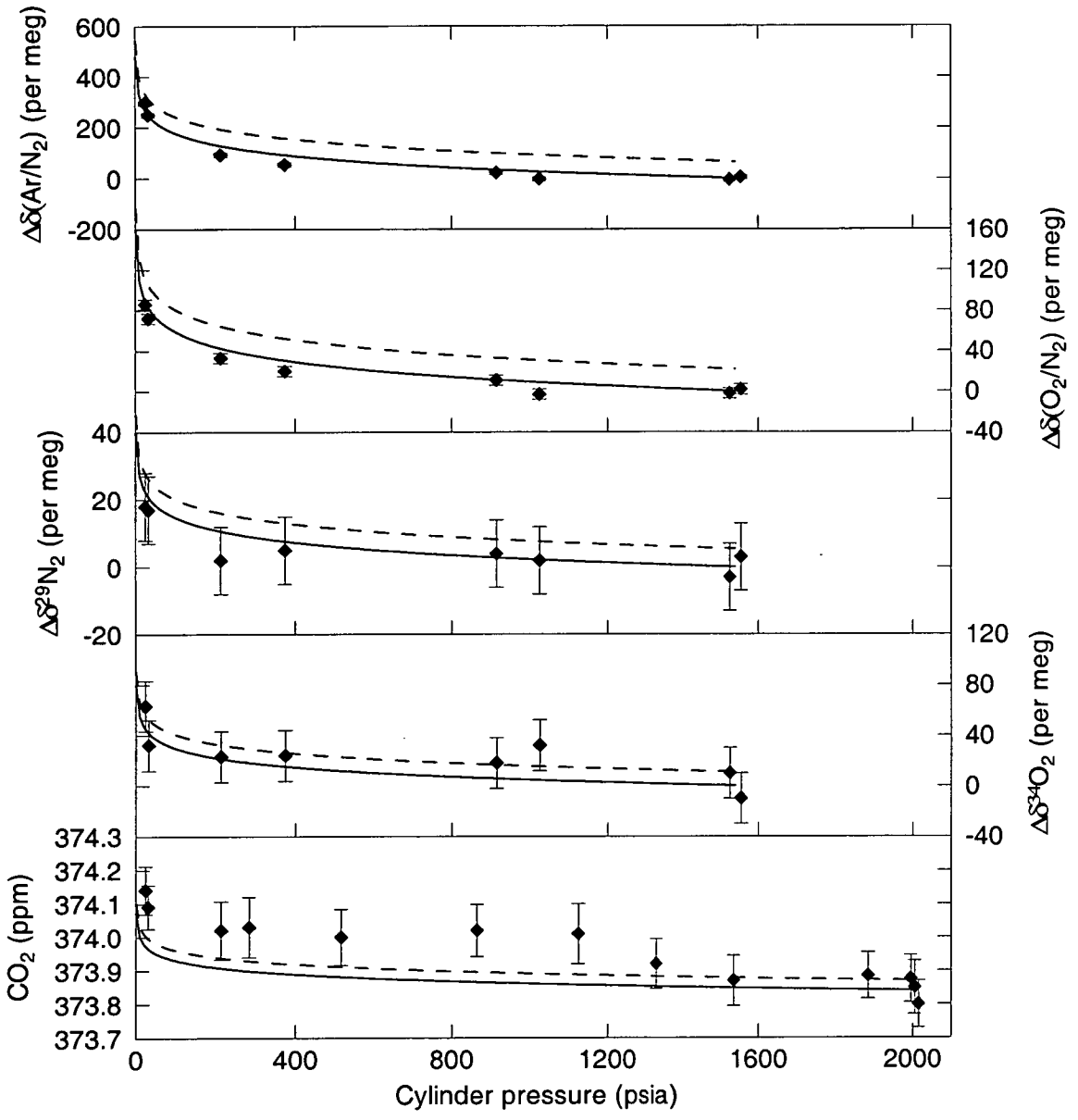

Figure 2.13 Multi-species measurements from one cylinder standard (UAN 991291) as a function of cylinder pressure. Data for species other than CO_2 are plotted as deviations from the mean of measurements at highest cylinder pressure (1525-1555 psia). Error bars represent typical uncertainties for daily mean values and are within the symbol size for $\delta(Ar/N_2)$ and $\delta(O_2/N_2)$. For $\delta(Ar/N_2)$, the solid curve approximates the change with pressure in air drawn from the cylinder, assuming a constant fractionation relative to bulk cylinder contents (dashed curve). Curves for other species are predicted from $\delta(Ar/N_2)$ assuming fractionation exactly proportional to mass difference, and fixed to pass through the mean of data points at highest cylinder pressure.

The fact that all ratios, including the purely isotopic tracers, show progressive enrichment in the heavier species points to the signature of a mass-dependent process (see also inter-species scatter plots and ODR-derived relationships in Figure 2.14). This can be explored further by assuming that air drawn from the cylinder was fractionated with respect to its bulk contents by a constant amount over the life of the standard. It is by no means certain that this assumption is accurate, as fractionation factors may have varied with cylinder pressure (and/or other parameters such as flow rate etc.) but nevertheless it provides a useful benchmark against which to assess the observed multi-species drifts. One can exploit the fact that the product of cylinder pressure P and the ratio R of any two species is conserved, analogous to the case for amount of CO_2 and its isotopic labelling (i.e. $[CO_2] \times \delta^{13}C$; Tans et al., 1993). Thus for a change in cylinder pressure of dP from P_0 to P_1 that is accompanied by a fractionation causing R to change in the cylinder by an amount dR from R_0 to R_1:

$$R_0P_0 = R_{out}dP + R_1P_1 \tag{2.16}$$

If the two-species ratio in the gas removed from the cylinder (R_{out}) is modified by a fractionation factor α with respect to the ratio in the cylinder such that:

$$R_{out} = \alpha R_0 \tag{2.17}$$

and ignoring the second order term dR.dP, Equations 2.16 and 2.17 give the relationship:

$$\frac{dR}{dP} = \frac{R(\alpha - 1)}{P} \tag{2.18}$$

and a solution for R :

$$R = e^{[(\alpha - 1)\ln P + k]} \quad (2.19)$$

Two curves of this form are shown for the $\delta(Ar/N_2)$ data in Figure 2.13. One (solid line) represents $\delta(Ar/N_2)$ of the air that is drawn from the cylinder and is analysed. The curve is constrained to pass through the mean of data pairs at maximum and minimum cylinder pressure. The other (dashed) curve is offset by a constant amount, in this case 65 per meg, to represent $\delta(Ar/N_2)$ of air remaining in the cylinder. Although the modelled curves slightly underestimate acceleration of $\delta(Ar/N_2)$ drift at low cylinder pressure, they nevertheless suggest that the assumption of a constant fractionation factor over the life of this standard is reasonable.

Similar curves are plotted for other species in Figure 2.13 but where the magnitude of drift is predicted from $\delta(Ar/N_2)$ data and assuming that fractionation is exactly proportional to mass difference. This would imply fractionation of -22 per meg (-65 x 4 / 12) for $\delta(O_2/N_2)$, -5 and –11 per meg respectively for $\delta^{29}N_2$ and $\delta^{34}O_2$, and –0.03 ppm for CO_2 with respect to air. All solid curves are constrained to fit the mean of points near maximum cylinder pressure only. The modelled curves provide a good fit to data for all species with the exception of CO_2 for which the measurements show a larger drift than what is predicted from mass-dependence alone. At minimum cylinder pressure the observed CO_2 enrichment is 2.1 times that predicted. The cause of this discrepancy is not clear. One possible explanation relates to the significantly larger molecular diameter of CO_2 (i.e. 4.64×10^{-10} m as quoted by Chapman and Cowling, 1970) as compared to the other three gases ($3.64\text{-}3.78 \times 10^{-10}$). Although the impact of this difference cannot be easily quantified, it would be expected to reduce the diffusion coefficient of CO_2 (see Section 2.3.2) and thus favour a larger

fractionation than expected from consideration of mass alone. Alternatively, the possibility of other measurement artefacts, such as pressure-dependent surface effects involving regulators, cannot be dismissed, especially as there is a suggestion of significant CO_2 drift between 1500 and 1100 psia that conflicts with the shape of the modelled curves.

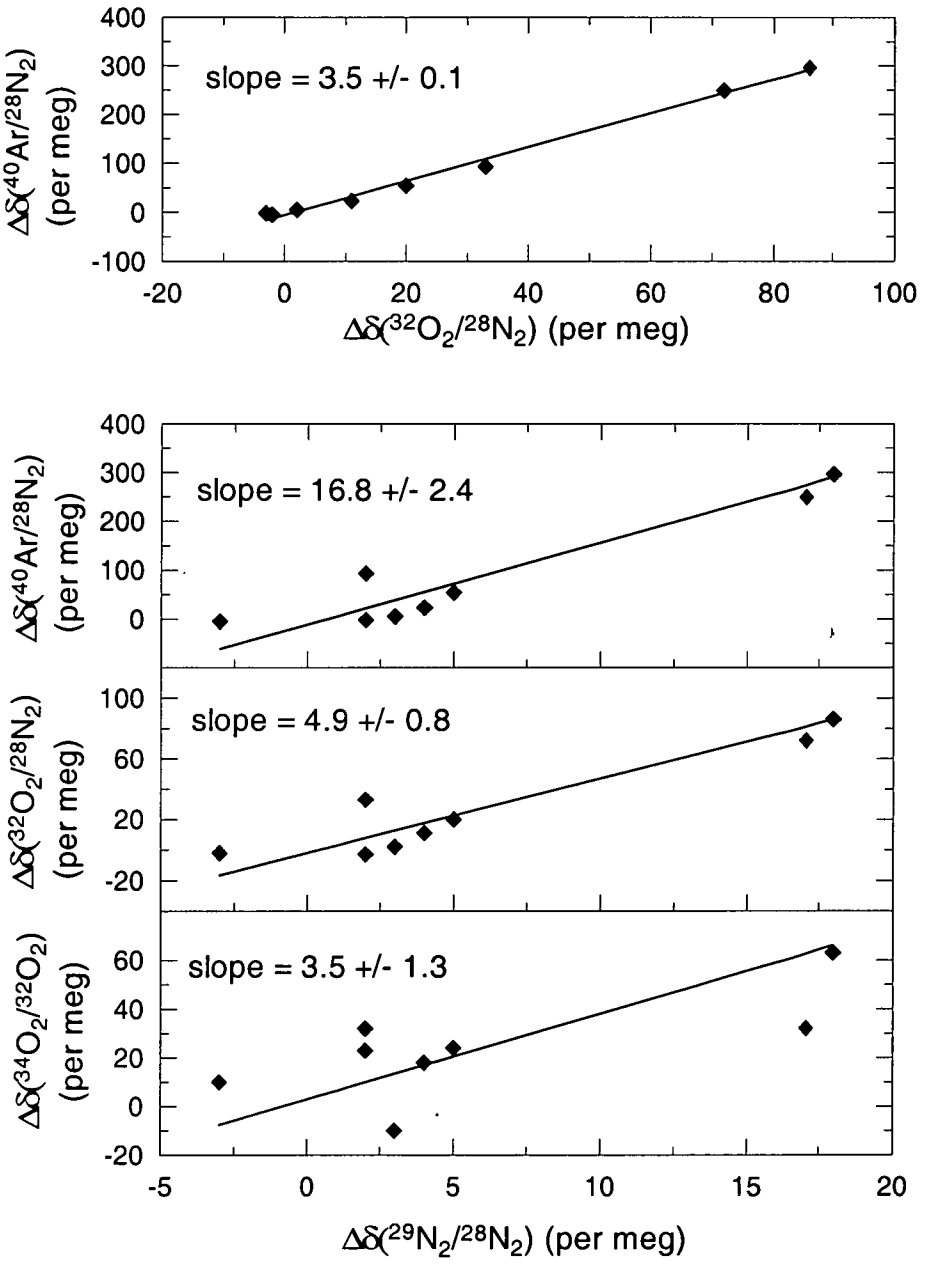

Figure 2.14 Inter-species relationships of concurrent measurements from standard 991291 with ODR fits and slopes.

The drifts observed in standard 991291 have major implications for calibration of atmospheric records for some trace gas species. If similar fractionations have occurred in the primary $O_2/N_2/Ar$ standard (950051), for which cylinder pressure has fallen from 1940 to 700 psia in 6.5 years, an error of –3 per meg yr^{-1} would apply to the measured trend in atmospheric $\delta(O_2/N_2)$. This would translate to an error of more than 1 PgC yr^{-1} in partitioning of oceanic and terrestrial carbon fluxes. Drifts in $\delta(Ar/N_2)$ and the isotopic ratios are potentially significant, especially if they are to be useful as tracers of fractionation associated with other experimental procedures. The CO_2 drift (with respect to cylinder pressure) in 991291 is of the same sign and with magnitude near the upper end of the range observed in the Cape Grim standards (Figure 2.12 above). This suggests that mass-dependent fractionation is probably a major, and perhaps dominant, cause of CO_2 instability in high pressure cylinders and that measurements of $O_2/N_2/Ar$ can play a valuable role in 1) constraining CO_2 drifts in the event that CO_2 cannot be measured as precisely as $\delta(Ar/N_2)$ and 2) development of techniques to improve stability of CO_2-in-air standards.

While the causes of observed drifts in 991291 are yet to be resolved, two possible mechanisms have been identified and are being investigated through further experiments. One relates to fractionation occurring during passage of air either through the cylinder valve or the regulator. Both environments are characterised, at least part of the time, by narrow pathways and gradients in pressure and temperature (e.g. due to adiabatic cooling of expanding air), factors that may promote fractionation.

The other involves gravitational settling of air inside a cylinder. In relation to this mechanism it is important to reiterate that 991291 and all other high pressure O_2/N_2/Ar standards have valves located at the top of the cylinders and have always been used and stored in a vertical position. Keeling et al. (1998a) calculated that at barometric equilibrium, $\delta(O_2/N_2)$ would be enriched at the top of a 1 m column by 17 per meg. However, it would take 1 year to achieve this equilibrium and the gradient would likely be strongly diminished by mixing due to other influences such as convection due to differential heating or cooling of different parts of the cylinder.

Effects on measured $\delta(O_2/N_2)$ due to changes in experimental procedures that have been observed by other laboratories may be related to one or both of these mechanisms. Keeling et al. (1998a) reported shifts of +10 per meg in cylinder standards moved from an upright position on the laboratory floor to lying horizontally inside a thermally insulated box. The changes in O_2/N_2 were accompanied by small, positive deviations in CO_2 (R.F. Keeling, SIO, personal communication), of sign consistent with mass-dependent fractionation. Thereafter, relative stability among these standards was very good, within about ±5 per meg for $\delta(O_2/N_2)$ and ±0.02 ppm CO_2 over periods of up to 10 years and/or down to pressures below 3300 kPa (480 psi). These results indicate O_2/N_2 and CO_2 stability in the SIO standards was significantly superior to that observed in 991291 and in CO_2-in-air standards employed at Cape Grim. They further imply that the measured SIO standard air was probably being fractionated while the cylinders were vertical and that the fractionation was reduced or eliminated when the cylinders were horizontal and insulated. If so, it is not clear whether the fractionation was due to thermal diffusion effects or gravitational settling. More evidence of O_2/N_2 dependence on

cylinder orientation and insulation has been gathered from experiments performed at Max Planck Institute for Biogeochemistry (MPI-BGC; W. Brand, personal communication). Effects of fractionation due to effusive and thermal diffusion processes related to experimental procedures, but not specifically involving extraction of air from high pressure cylinders, have also been demonstrated by Bender et al. (1994) and Manning (2001).

2.6.5 Flow rate dependence

At the time of writing, there are several experiments in progress at CSIRO investigating fractionation of air drawn from high pressure cylinder standards. Preliminary results from one test are described here because they demonstrate high sensitivity to at least one parameter.

During 1995/96, several tests were conducted on the MAT252 to investigate dependence of $\delta(O_2/N_2)$ in cylinder air on the flow rate used to flush the sample side inlet prior to isolating a sample aliquot for analysis. Three different standards (950051, 941395 and 960051) were tested, but no systematic and repeatable bias was observed over a flow rate range of 10 – 200 ml min^{-1}. A similar test was conducted on the Delta^{plus}XL with higher precision and also measuring $\delta(Ar/N_2)$. Four cylinders were tested, 950051 (still upright and fitted with an Alphagaz series 1000 regulator that is mounted directly to the cylinder valve by way of a 7 cm brass nipple), and three cylinders of similar construction but which were stored horizontally for 18-23 days up to and during this test and fitted with Tescom regulators connected to the cylinder valve by 1 m lengths of 1/16" O.D. electropolished, SS tubing. Successive aliquots were taken from each cylinder with flushing flow rates ranging from 25 –

600 ml min^{-1}. Target flow rates were achieved by adjusting the regulator delivery pressure and the needle valve restriction on the outlet of the inlet system such that pressure in the analysis chamber (see Figure 2.1) was maintained during flushing at the (analysis) operating pressure of 1.25 atm. Prior to loading of each sample aliquot, regulators were flushed by venting air to the room for 40-140 seconds at flow rates estimated to be upwards of 1 L min^{-1}. Air was then flushed through the inlet system for periods ranging from 2-5 minutes. In each case, vent/flush times were inversely related to flushing flow rates.

Measurements revealed dramatic dependence of both $\delta(O_2/N_2)$ and $\delta(Ar/N_2)$ on flow rate (Figure 2.15) with differences of up to 50 per meg in $\delta(O_2/N_2)$ observed for one cylinder (994025) over the full range of flow rate. All four cylinders showed a dependence of similar shape with higher O_2/N_2 and Ar/N_2 ratios at low flow rates, but there were differences of up to a factor of 5 in the magnitude of variations. The three cylinders fitted with Tescom regulators and stored horizontally showed the largest variations. For these cylinders the test was repeated the next day, with a different order of analysis (and of flushing flow rates among successive aliquots), but with little or no difference in results. The relationship between $\delta(O_2/N_2)$ and $\delta(Ar/N_2)$ again suggests a likely contribution from mass-dependent fractionation, although the slope of 2.2 ± 0.2 (Figure 2.16) is slightly lower than expected for diffusive processes (Table 2.2). The isotopic ratios, $\delta^{29}N_2$ and $\delta^{34}O_2$ were not measured with sufficient precision in this test to provide any meaningful quantification of their relationship with O_2/N_2 or Ar/N_2.

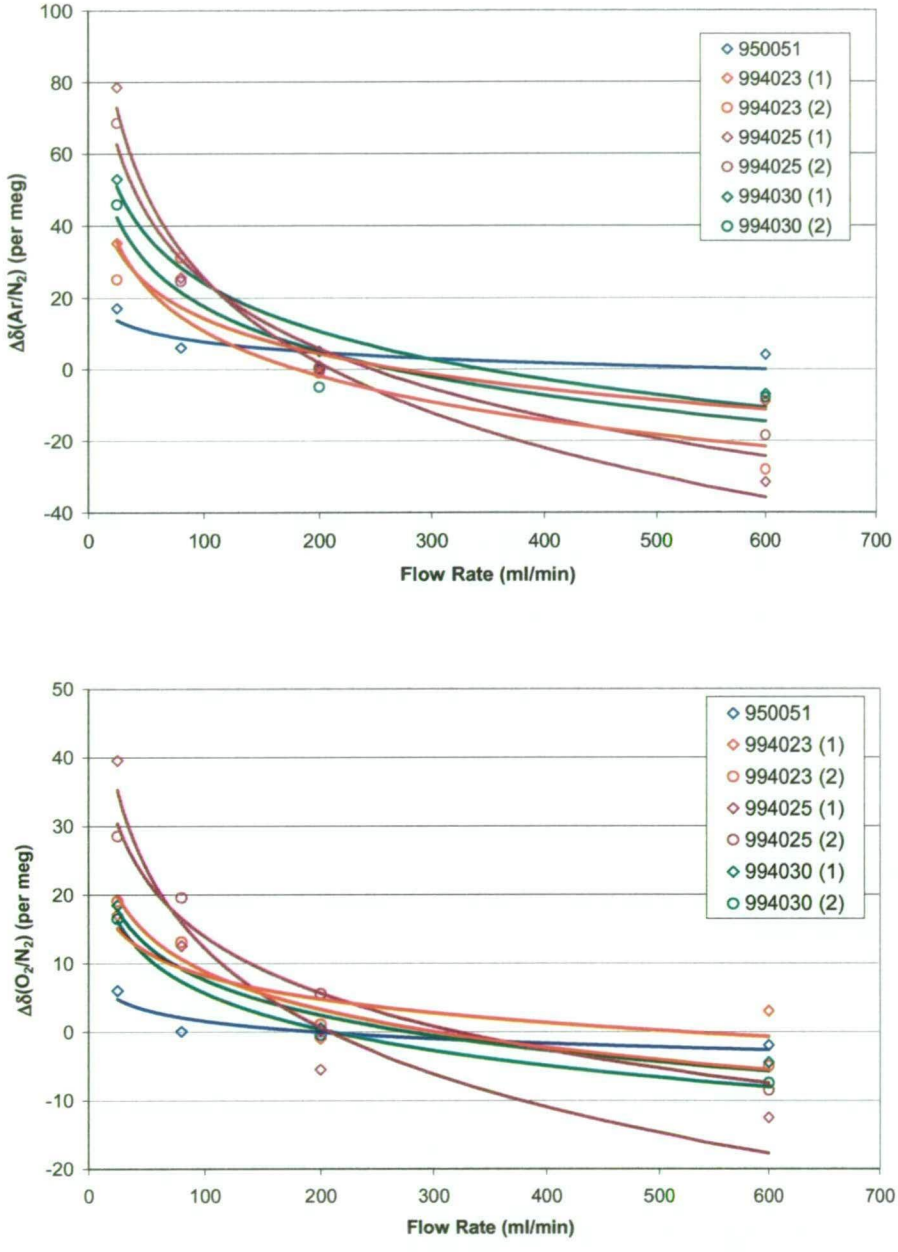

Figure 2.15 Measurements of $\delta(O_2/N_2)$ and $\delta(Ar/N_2)$ from four cylinders of air (950051 etc.) analysed on two separate days (1 and 2) as a function of flow rate used to flush the analysis chamber of the inlet system. Data are plotted as deviations from the mean of values for each cylinder at the normal operating flow rate of 200 ml min^{-1}. The curves are logarithmic fits to each of the seven data sets.

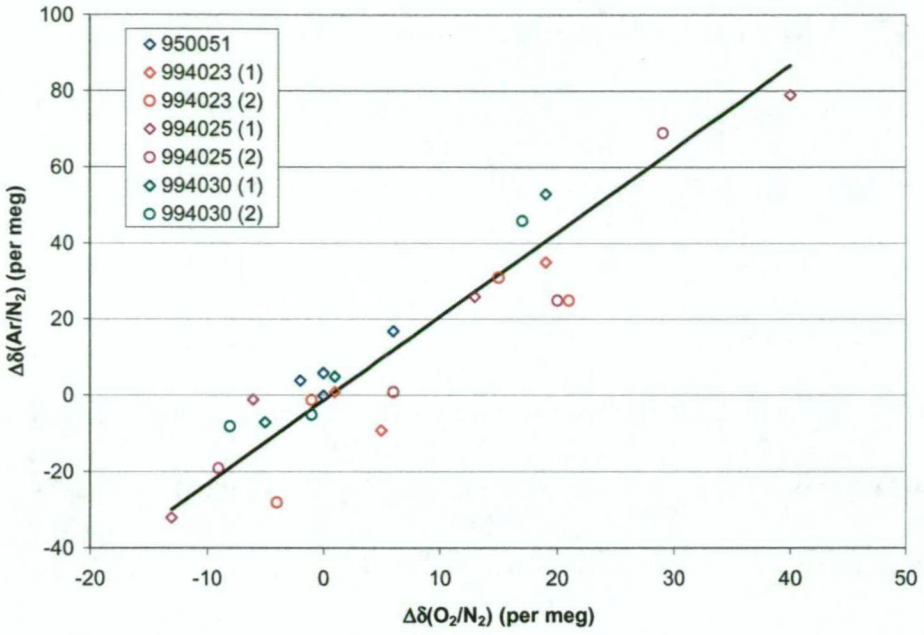

Figure 2.16 The relationship of $\delta(Ar/N_2)$ vs $\delta(O_2/N_2)$ for the data plotted in Figure 2.15. The solid line shows an ODR fit to the composite data set.

The fact that the four standards tested showed very different sensitivity of O_2/N_2 and Ar/N_2 to flow rate indicates that the sensitivity is not related to the inlet system but rather to the cylinders or regulators. If it is assumed that any fractionation of sample air is in the sense of lighter molecules preferentially escaping the cylinder, then it follows that the degree of fractionation increases with flow rate. This would be consistent with the changing composition of 991291 (Figure 2.13) and the observation of CO_2 enrichment with falling pressure in Cape Grim standards (Figure 2.12).

The standard (994025) that exhibited the largest $O_2/N_2/Ar$ sensitivity to flow rate was additionally analysed for CO_2 using the GC technique. Aliquots were introduced to the sample loop either with or without "extra" flushing of the regulator immediately before injection. "Extra" flushing involved venting sample air at > ~2 L min^{-1} for long enough to ensure replacement of air inside the regulator (120 atm. x ~5

ml = 600 ml STP) at least twice. The regulator outlet was then reconnected to the GC inlet system where a further 30 ml of air, flowing at about 60 ml min^{-1}, was used to flush the GC sample loop. Where no extra flushing was applied to the regulator, only 30 ml of air was removed for each sample aliquot. Fresh sample aliquots were analysed every 20 minutes.

The CO_2 in aliquots preceded by the extra (high-flow rate) regulator flushing was systematically lower (by 0.15 ppm; Figure 2.17). The sign of the difference is consistent with the flow rate dependence observed for $O_2/N_2/Ar$. It implies significant fractionation of CO_2 relative to air for this cylinder at high flow rates. Another feature of this plot that might be important is the absence of "ramping" between the two concentration levels. Thus, while extra flushing of the regulator leads to markedly lower measured CO_2, the anomaly does not appear to be even partly sustained in following aliquots with no extra flushing, despite the fact that only around 5 % (30 / 600 ml) of air residing in the regulator is replaced per aliquot. It has been established from other tests that minimal exchange of air occurs between the regulator and the main body of the cylinder in 20 minutes. This implies that the fractionation indicated by these measurements must occur with respect to air residing in the regulator and near the regulator outlet. The regulating valve orifice is the most likely point of fractionation as the volume of air contained in the low pressure side of the regulator is only about 5 ml STP and should be well flushed by removal of 30 ml STP of air per injection. The present hypothesis to explain these observations is that the air is fractionated as it passes through this orifice due to thermal gradients induced by adiabatic cooling of air that is most pronounced at high flow rates, and that no fractionation is observed 20 minutes later due to dissipation of the temperature anomaly.

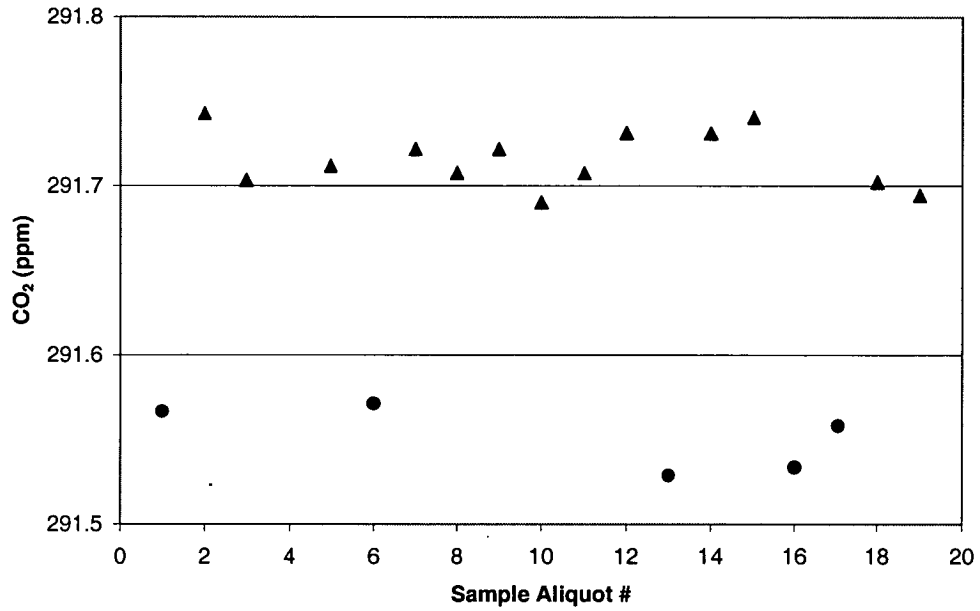

Figure 2.17 Measurements of CO_2 from 994025 from successive aliquots injected 20 minutes apart with either "extra" (high flow rate) flushing of the regulator immediately preceding injection (circles) or no extra flushing aside of the 30 ml required to flush the sample loop (triangles).

2.6.6 Surface processes

The composition of air standards could also be modified by surface processes. Physisorption onto metal, glass or elastomeric surfaces is likely to depend on gases' chemical properties and could thus fractionate gas phase $O_2/N_2/Ar$ ratios. With regard to long term stability of standards, any pressure dependence of physisorption effects is important as this could also contribute to changes in $O_2/N_2/Ar$ as a function of standard pressure or usage. It may be difficult to identify such effects because their signatures in $O_2/N_2/Ar$ are not known and may differ according to surface material. However, some observations (e.g. Section 2.5.1) argue for greater impact on O_2/N_2 than Ar/N_2, at least for some materials.

On the other hand, a multi-species approach provides more scope for constraining the impact of chemisorption effects. One would expect that O_2, being more reactive than the inert gases Ar and N_2, would be most affected. Consumption of O_2 during oxidation of organic surface residues is constrained by measurements of other trace gases in the same air standards. Oxidation of hydrocarbons produces CO_2 and CO, concentrations of which have been monitored over the life of these standards. Drifts in these species are within ±0.04 ppm yr^{-1} (for CO_2) and ±0.8 ppb yr^{-1} (CO), indicating negligible oxidative consumption of O_2, providing that a non-trivial fraction of oxidation products are present in the gas phase.

2.6.7 Stability of O_2/N_2/Ar scales

All data are referenced against the most frequently analysed high pressure cylinder standard, 950051. Typically two aliquots from 950051 were analysed on each day that routine O_2/N_2/Ar analyses were conducted. However, on some occasions samples were analysed without analysis of 950051 on the same day. To accommodate these varying circumstances and to improve precision of calibration by averaging 950051 measurements over neighbouring days, 950051 reference values for any given day take into account two values, 1) the daily mean for 950051 analysed on the same day and 2) a value obtained by linearly interpolating in time between the nearest 950051 daily means from preceding and following days, if both occurred within 7 days. The 950051 reference value was then calculated by averaging 1) and 2) where both were available, or alternatively by using the single available value.

The air standards used to assess stability of the scale are listed in Table 2.1. All are natural air with the only notable modifications relating to drying, and to

dilution of two of the standards (870001 and 880001) with residual N_2 not removed from the cylinders before they were originally filled. All high pressure, metal cylinders were dried on collection to below about 0.5 ppm H_2O, with the exception of 960051 which was collected at Cape Grim without drying. The 20 L, glass flasks were washed, baked (while flushed with dry air), briefly exposed to laboratory air, then filled with dry air from high pressure cylinders but with no drying during the transfer. Water vapour concentration has not been measured in these standards but is likely to be somewhat higher than in dried cylinder air. Occasional water vapour measurements have favoured a higher concentration in the glass, 20 L working standard as compared to the dried cylinder standards.

The $\delta(O_2/N_2)$ records for all standards with respect to 950051 are plotted in Figure 2.18. Two standards (950052 and 941395) have the highest measurement frequency. Plotted on this scale, the 950052 record shows good stability against 950051, while significant variability is evident for 941395 in the first two years of monitoring. The reasons for this discrepancy are unclear and somewhat surprising given that the materials and gas handling procedures for the three standards were nominally identical. The strong relative stability between 950051 and 950052 was a key factor in the selection of 950051 (rather than 941395) as the primary reference standard. Of the other standards, 870001 and 880001 show the largest variability, most likely associated with variations in instrument non-linearity (Section 2.4.3).

Relative stability among the suite can be examined by comparing spline fits to each of the records, excluding 870001 and 880001 (Figure 2.19). Here the data represent stability against 950051, relative to the mean difference in 2000/2001. The glass, 20 L standards have been adjusted for a small depletion in $\delta(O_2/N_2)$ due to

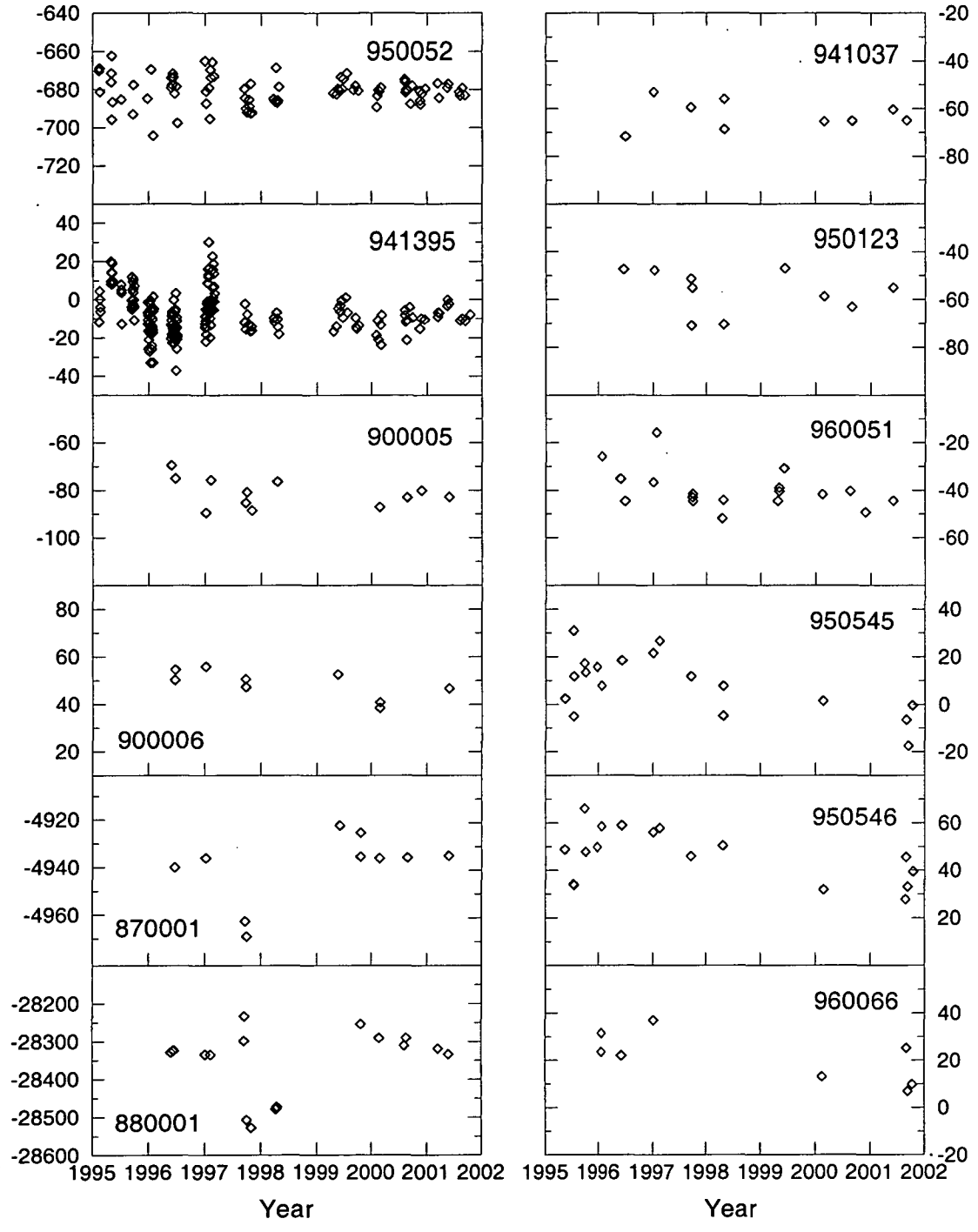

Figure 2.18 $\delta(O_2/N_2)$ measurements of surveillance standards relative to 950051.

permeation through the Viton O-ring (see Section 2.7). The adjustments were calculated for each of the three standards individually, based on permeation rates determined from storage tests involving glass, 0.5 L flasks with dual Glass

Expansion valves. Inferred drift rates in the 20 L standards were obtained by scaling for flask volume, number of valves and sample pressure using recorded pressure histories of the standards. In each case, the calculated cumulative change between 1995 and 2001 was about –2 per meg.

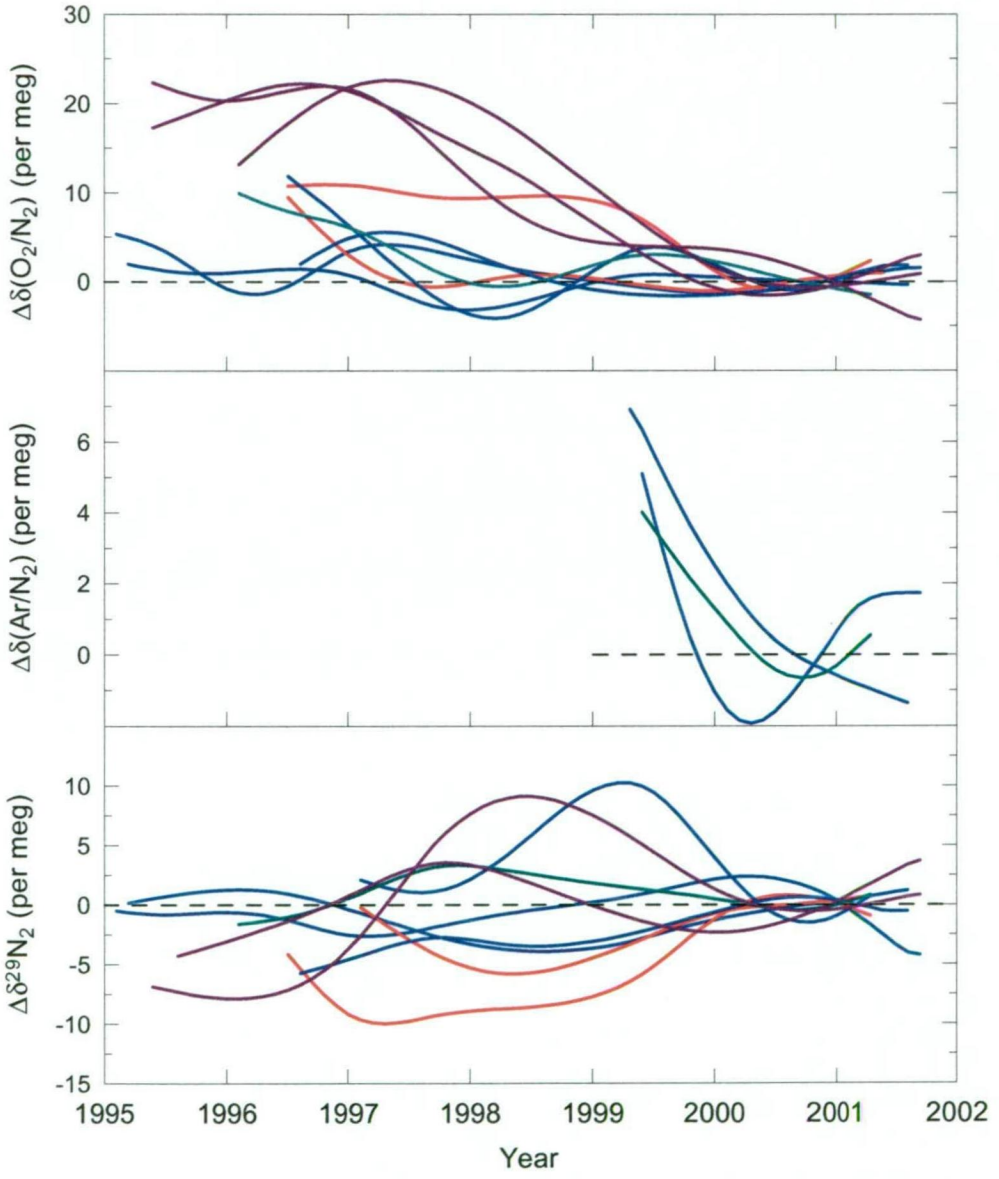

Figure 2.19 The deviation of surveillance standard measurements from the mean difference relative to 950051 in 2000/01, plotted as spline fits to the data with 50 % attenuation at 3 years. Curves represent Al, 29.5 L cylinders (blue), Al, 48 L (red), SS, 35 L (green) and glass, 20 L (magenta). $\delta(Ar/N_2)$ data are from 950052, 941395 and 960051. No $\delta^{29}N_2$ are shown for 960066 due to sparse data (a single point) before 2000.

There are several important features in the $\delta(O_2/N_2)$ plot. First, there is a general bias towards negative drifts in the surveillance standards. It is likely that this at least partly reflects a progressive enrichment in $\delta(O_2/N_2)$ of 950051, consistent in sign with the pressure-dependent enrichment observed for 991291 (Sections 2.6.4 and 2.6.5). If the magnitude of drift were similar to that for 991291, the modelled curve in Figure 2.13 would imply a $\delta(O_2/N_2)$ drift in 950051 of +22 per meg for a pressure drop from 1940 to 700 psig between 1995 and 2001. However, a smaller drift is more probable as the CO_2 drift in 991291 was at the upper end of the range observed in a large number of similar cylinder standards used at Cape Grim (Figure 2.12).

The high pressure surveillance standards are likely to be affected by the same process but all have experienced smaller proportional pressure change than has 950051 over the period of interest. Thus there may be concerted drift among these standards with only differences in drift rates being captured by assessment of relative stability. The two standards with longest records and highest analysis frequency show smallest differences and are almost indistinguishable from 950051 (e.g. within 2 per meg for 950052 in 1995 as compared to a difference of 16 per meg that would be expected from the above assumptions). However, the other five surveillance standards that were analysed less frequently show differential drift of up to about 12 per meg between 1996 and 2000/01.

If all of these cylinders were assumed to be equally susceptible to fractionation (as a function of pressure) and if all the variability in Figure 2.19 were attributed to relative differences in fractionation corresponding to relative rates of consumption, it should be possible to use data for each cylinder to independently

estimate the drift rate in 950051. The smallest predicted difference (2 per meg in 1996 relative to 2000/01) applies to 941037 for which the proportional pressure change has been almost as large as that in 950051. The observed difference is similar within uncertainty. This is consistent with similar drift in both standards but is of little use in constraining the magnitude of any drift. Data from the other six standards imply $\delta(O_2/N_2)$ drift in 950051 of between 0.5 and 2.1 (average 1.5) per meg yr^{-1}, and a cumulative drift of about –9 per meg in 6.5 years.

Largest differences are seen for the three glass, 20 L flasks. All are consistent in indicating a differential drift of about 20 per meg relative to 950051. If the glass flask standards are infact stable, it would indicate a $\delta(O_2/N_2)$ enrichment in 950051 of 20 per meg, and larger, correlated enrichment in the other high pressure standards than expected from their pressure histories. If the curves in Figure 2.19 reflect instability of the glass flask standards it would require $\delta(O_2/N_2)$ to be falling more rapidly (by an order of magnitude) than expected from permeation through the O-ring. Loss of O_2 through oxidative processes is not supported by measurements of CO_2 and CO in these standards. There was negligible change in either species over 6 years. Another possible explanation might be changes in gas handling procedures, such as the introduction of active drying of sample air being admitted to the sample side inlet system from October, 1997. The glass flask records in Figure 2.19 do not exclude the possibility of a step change at that time. However, if moisture-related effects were responsible, the impact on $\delta(O_2/N_2)$ would have to be significantly greater than indicated by other evidence (Sections 2.4.7 and 2.5.2)

Also plotted in Figure 2.19 are differential drift curves for $\delta(Ar/N_2)$ and $\delta^{29}N_2$. Few of the standards provide a useful constraint of Ar/N_2 stability due to the

shorter period of measurements. The three curves based on sufficient data points show mean $\delta(Ar/N_2)$ drift of about 5 per meg between 1999 and 2001, consistent with enrichment of 950051, but with insufficient statistics to usefully constrain the magnitude of any $\delta(O_2/N_2)$ drift. On the other hand, there is no systematic bias evident in $\delta^{29}N_2$ that would support significant fractionation of 950051, though noting that such a signal may be difficult to detect. For example, a difference of 20 per meg in $\delta(O_2/N_2)$ due to fractionation would correspond to just 5 per meg in $\delta^{29}N_2$.

In summary, these data favour a progressive enrichment in $\delta(O_2/N_2)$ of 950051. The high pressure standard results are broadly consistent with effects of fractionation, although some contribution from other processes (e.g. desorption of gases from cylinder surfaces with falling pressure) is also possible. A large difference in relative stability exists between standards in high pressure cylinders and in glass, 20 L flasks, the cause of which is uncertain. Allowance is made for a best estimate of the drift of 1.5 per meg yr^{-1}, but where the correction carries an uncertainty of ±1.5 per meg yr^{-1}. The CSIRO2001 $\delta(O_2/N_2)$ scale is thus defined with reference to 950051, allowing for drift in this standard of +1.5 per meg yr^{-1} relative to 1996.0 and for other systematic adjustments described in this chapter (such as those for isobaric interference relative to CO_2 = 360 ppm, and variations in $\delta(O_2/N_2)$ associated with regulator effects). Scales for other measured ratios are defined in a similar way but with no corrections applied for drift in 950051. A $\delta(O_2/N_2)$ drift in 950051 of +1.5 per meg yr^{-1} due to fractionation would imply a corresponding drift in $\delta(Ar/N_2)$ of

about +4.5 per meg yr^{-1}. This may have significant implications for $\delta(Ar/N_2)$-based correction of atmospheric $\delta(O_2/N_2)$ data and is considered further in Chapter 3.

2.7 Glass flask storage drift

Laboratory experiments were conducted to test stability of measured molecular and isotopic ratios in CSIRO's 0.5 L glass flasks. These flasks are each fitted with two valves (Glass Expansion) which for these experiments were sealed with a selection of O-ring materials, Viton, PFA and PTFE. Stability was tested at a range of sample pressures from 1-2 atm. with highest sample density at 1.5 atm. corresponding to the pressure routinely used in field sampling programs. Several such experiments were carried out over several years, both to improve statistics and to additionally test Ar/N_2 stability after the Delta^{plus}XL instrument was commissioned.

Test samples were prepared by decanting air from a high pressure cylinder, of measured composition, under conditions of steady flow as described for test flasks in Section 2.5.4. Each experiment typically involved about 12 flasks. Typically 2 samples were analysed within 2 days to check the integrity of the sample preparation (within uncertainty limits due to other experimental factors) and to establish a starting point for stability tests. The remaining 10 samples were each analysed on a single occasion, after varying storage periods up to 15 months. In other words, all samples were stored for the duration of the test at their original fill pressure, thus reproducing conditions experienced by field samples.

Results showed O_2/N_2 and Ar/N_2 ratios became depleted with time in pressurised flasks, with large dependence on material and sample pressure (Figures

2.20 and 2.21, Table 2.12). Drift rates were significantly higher for PFA and PTFE O-rings than for Viton. There was little or no change in $O_2/N_2/Ar$ of 1 atm. samples, or in the isotopic ratios ($\delta^{29}N_2$ and $\delta^{34}O_2$) regardless of pressure. The results are

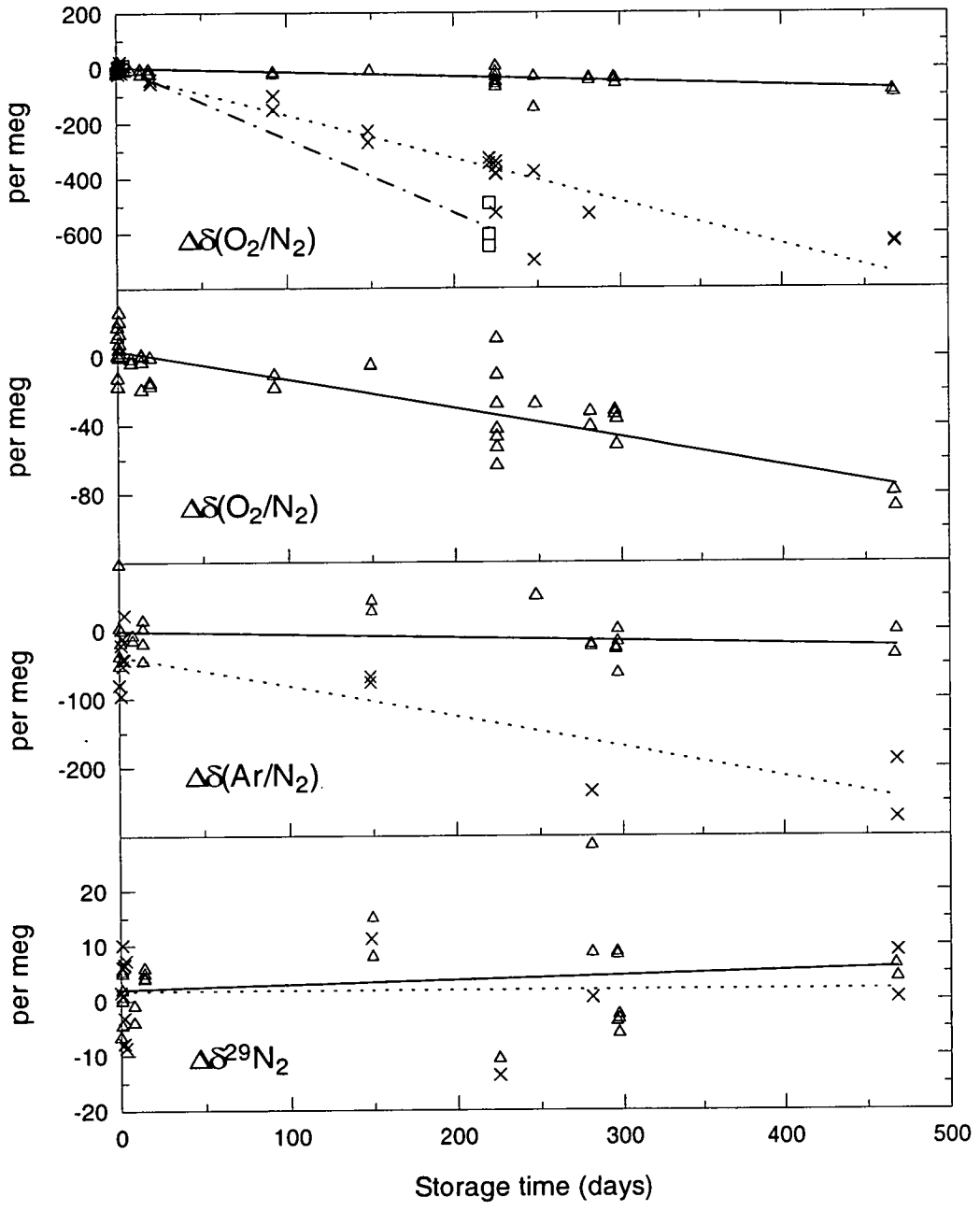

Figure 2.20 Changes in $\delta(O_2/N_2)$, $\delta(Ar/N_2)$ and $\delta^{29}N_2$ of air due to storage in 0.5 L, glass flasks filled to 1.5 atm. and sealed with Viton (△; with linear regression represented by the solid line), PFA (x; dashed) or PTFE (□; dash-dot) O-rings. Viton O-ring data are plotted in the two uppermost panels on different scales.

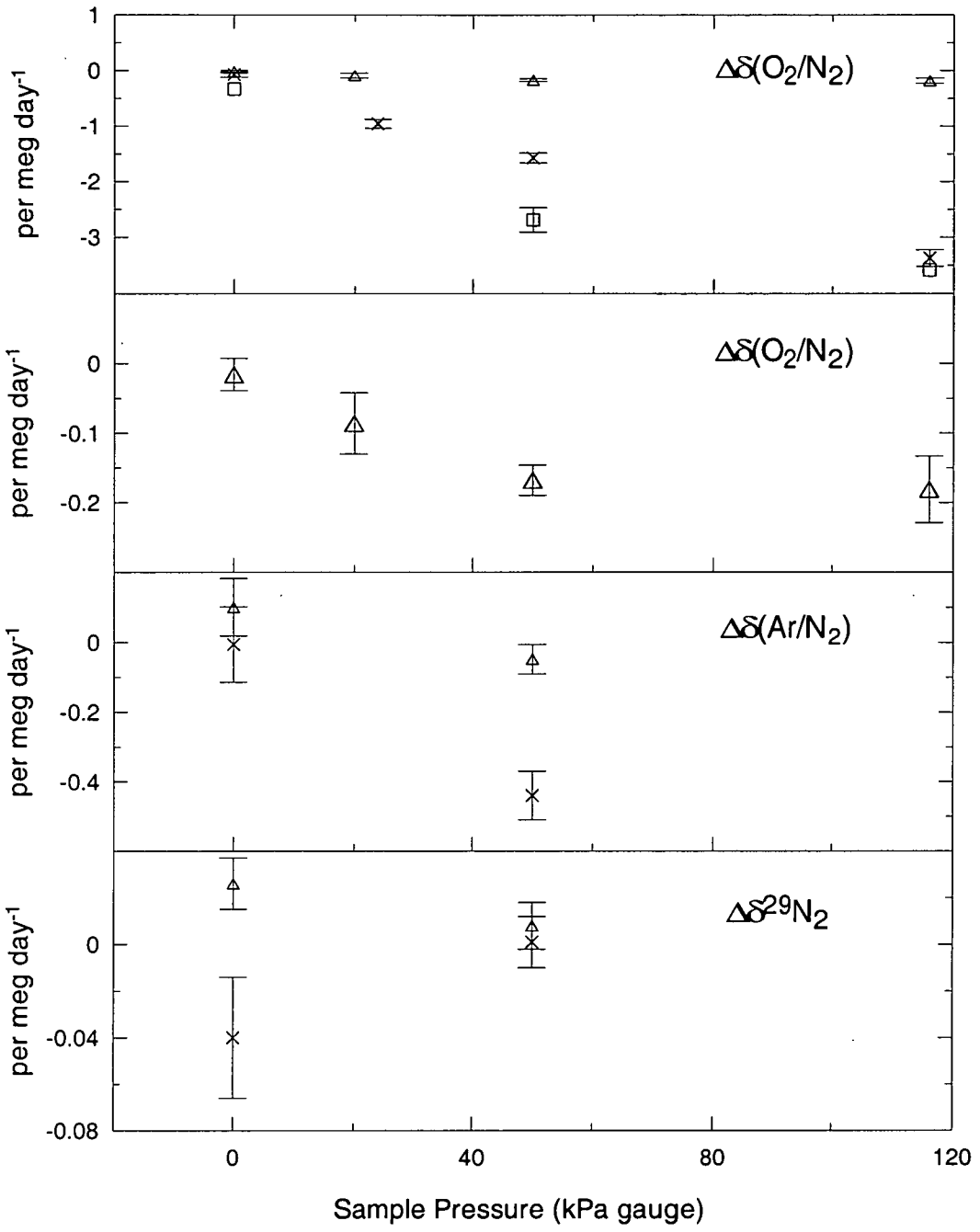

Figure 2.21 The rate of drift in $\delta(O_2/N_2)$ as a function of pressure and O-ring material (symbols as for Figure 2.20), as determined by linear regression to data in Figure 2.20 (for 1.5 atm.) and data for other sample pressures (not shown). Error bars denote standard error. No error bars are shown for data sets of only 2 points. Regressions were not forced to zero at zero days because non-zero y-intercepts are likely to reflect other influences unrelated to flask storage drift.

	Viton	PFA	PTFE
$\delta(O_2/N_2)$	-0.168 ± 0.022	-1.57 ± 0.09	-2.69 ± 0.22
$\delta(Ar/N_2)$	-0.048 ± 0.042	-0.44 ± 0.07	
$\delta^{29}N_2$	0.008 ± 0.010	0.001 ± 0.011	
$\delta(Ar/N_2) / \delta(O_2/N_2)$	0.29	0.28	

Table 2.12 Mean drift rates of $\delta(O_2/N_2)$, $\delta(Ar/N_2)$ and $\delta^{29}N_2$ (in per meg day^{-1}) and the ratio for $\delta(Ar/N_2)/\delta(O_2/N_2)$ as obtained from laboratory storage tests of air in CSIRO 0.5 L glass flasks sealed with different O-ring materials and filled to 1.5 atm. pressure.

consistent with the dominant modification process being a preferential loss of O_2 and Ar, relative to N_2, due to permeation through the O-rings. The flux (F) due to permeation (O'Hanlon, 1989) is given by:

$$F = K\frac{PA}{d} \tag{2.20}$$

where K is the permeability constant for the gas/solid pair (given by the product of the diffusion constant and the solid solubility), P is partial pressure difference, A is surface area and d is thickness of material.

It is possible to calculate predicted rates of $\delta(O_2/N_2)$ drift, applicable to the glass flasks tested here. Estimates of K are available for some combinations of gas and O-ring material, for example 15 and 4.4 x 10^{-10} cc.(STP)/cm^2/mm/sec/cm H_g for O_2 and N_2, respectively, in Viton at 20-30°C (Lebovits, 1966). For samples at 1.5 atm., P is precisely known for O_2 and N_2 as there is negligible proportional change of these gases in ambient laboratory air. The same is not true for trace gases such as CO_2, for which proportional changes in laboratory or urban air can be substantial (e.g. CO_2 changes of 50% above background are common in GASLAB).

There is significant uncertainty in A and d as these quantities are strongly dependent on compression of the O-rings in the tapered shaft of the Glass Expansion valves fitted to CSIRO flasks. The compression can vary between actuations and is likely to also be operator-dependent. Higher compression both increases the distance (d) that gases must travel to permeate the O-ring and reduces the surface area (A), thus reducing the gas flux. It is plausible that K might also be dependent on the extent of compression. A and d were measured for a small set of randomly selected flasks and the ratio A/d was found to vary by more than a factor of 2, implying similar variability in F. Using approximate values for compressed Viton O-rings of 0.2 cm^2 and 2.0 mm for A (per O-ring) and d respectively, the predicted rate of $\delta(O_2/N_2)$ drift in 1.5 atm. samples is –0.86 per meg day^{-1} as compared to –0.17 obtained experimentally. The predicted and observed drift rates differ by a factor of 5, probably reflecting uncertainty in A/d and K. It seems very unlikely that some other process could be offsetting a larger rate of drift due to permeation as any such process would also have to be proportional to partial pressure difference but with opposite sign and similar magnitude. Permeation is the likely major cause of the observed drifts in $\delta(O_2/N_2)$.

It is possible that secondary effects on O_2/N_2 may result from other processes, such as oxidation of grease used to lubricate the Viton O-rings. Keeling et al. (1998) reported depletion of up to 160 per meg over 313 days storage in SIO 5 L glass flasks fitted with Viton O-rings and filled to 1 atm. pressure with 20 extra greased O-rings inserted in the flasks. Flasks with no extra O-rings were stable to better than 10 per meg over a similar period, although depletion of about 40 per meg was observed within 4 days after the flasks were filled. The initial offset was considered likely to

be an artefact of sample preparation and not related to flask storage. Bender et al. (1996) found no significant drifts in URI/PU 2 L glass flasks, also fitted with Viton O-rings and filled to 1 atm., over a storage period of 109 days. In terms of the permeation identified in CSIRO flasks, a key difference in SIO and URI/PU programs is that their flasks are routinely filled only to 1 atm. pressure so that O_2 and N_2 partial pressure differences are very small under normal storage conditions. Furthermore, flask volumes are larger, also serving to reduce effects of permeation, although this might be partly offset by larger surface area of O-rings, at least in SIO flasks.

Experimental uncertainty in CSIRO field sampling related to flask storage could be reduced by collecting samples at 1 atm. pressure, especially if long storage times are anticipated. However, there are competing factors to consider, such as sample volume and pressure required for the range of laboratory procedures. It should also be noted that sampling to 1 atm. would not eliminate all potentially significant impacts of permeation. For example, sampling to 1 atm. and storage at the high altitude (3397 m) site, Mauna Loa, (or sampling to ambient pressure at Mauna Loa with storage at sea level) in CSIRO flasks would induce a $\delta(O_2/N_2)$ drift of –0.14 and +0.14 per meg day^{-1} respectively (scaled relative to drift rates obtained from laboratory tests).

All O_2/N_2 and Ar/N_2 data from CSIRO flask samples are routinely corrected for drift during storage according to the results in Table 2.12. Assumed drift rates are O-ring dependent, proportional to sample pressure difference with respect to 1 atm. and tuned to exactly match test results at 1.5 atm. pressure. Although the drift in Ar/N_2 in Viton O-ring flasks is not as well resolved as for O_2/N_2 due to slower drift

and poorer overall precision, the ratio of drift rates given by $\delta(Ar/N_2)/\delta(O_2/N_2)$ is similar to that observed in PFA O-ring flasks where drift rates are higher. This provides confidence that the correction for Viton O-ring flasks is reasonable, as relative rates of permeation of different gases are generally similar for different membranes, for example within a factor of 3 or less for O_2, N_2, CO_2 and H_2S (Lebovits, 1966).

Finally, it is also interesting to consider effects of permeation on other trace gases measured in GASLAB. For CO_2 in Viton at 20-30°C, $K = 78 \times 10^{-10}$ (Lebovits, 1966), implying drift of -5.7×10^{-4} ppm day^{-1} (or -0.21 ppm yr^{-1}; again scaled for experimental O_2/N_2 results) in CSIRO (Viton; 1.5 atm.) flasks if they are assumed to be stored at sea level with "background" CO_2 levels of ~370 ppm. This is similar to the drift rate of -8×10^{-4} observed in laboratory tests. For flasks sealed with PFA O-rings, and filled to about 1.85 atm., as most commonly used by CSIRO for CO_2 measurements, the drift attributable to permeation is even larger. Values of K for CO_2 (also O_2 and N_2) are available (2001-02 Product Catalogue, Cole Palmer International, IL, USA, page 734), however there may be an error in the quoted units as loss of > 0.3 ml day^{-1} of sample air and drift in $\delta(O_2/N_2)$ of –529 per meg day^{-1} is implied. Both estimates are shown by the tests reported here to be overestimated by orders of magnitude. Nevertheless, if the relative values of K for O_2, N_2 and CO_2 are correct (and they are consistent with relative values for other materials), it is possible to estimate the rate of CO_2 drift by scaling to observed changes in $\delta(O_2/N_2)$. This gives a value of -3.7×10^{-3} ppm day^{-1} (-1.4 ppm yr^{-1}) steeper than that observed in laboratory storage tests of -1.0×10^{-3}. However, for CO_2, the actual drift rate will be sensitive to the mean CO_2 mole fraction of the ambient air in which the flasks are

stored. For example, 50% elevation of CO_2 (as has been observed for daytime laboratory air in GASLAB) would eliminate CO_2 partial pressure difference (and the net permeation flux) in 1.5 atm. samples or reduce the predicted drift rate in flasks with PFA O-rings at 1.85 atm. to -1.5×10^{-3} ppm day^{-1}. In practice, the CO_2 partial pressure differences experienced by these flasks is likely to vary with location (e.g. whether they are stored in a laboratory frequented by people or in a better ventilated storage area) and also diurnally, depending on the presence of people and on meteorological conditions that will affect the influence of other urban sources and sinks on the CO_2 concentration of ambient air. Thus, while it is difficult to accurately predict CO_2 permeation fluxes, these calculations demonstrate that permeation is probably also a major influence on CO_2 stability in CSIRO's glass flask air samples.

Permeation of CO_2 through the O-rings also has the potential to modify the isotopic composition of CO_2 in flask samples. Ignoring any fractionation associated with the permeation process itself, no change in isotopic composition of the sample would occur when CO_2 of sample and surrounding air is isotopically similar, even if there is a partial pressure difference in CO_2. However, changes will occur if flasks are stored in an environment such as GASLAB, that on average is almost certainly enriched by biogenic CO_2. Assuming an average enrichment in GASLAB air of 50 ppm CO_2 with $\delta^{13}C$ = -25 ‰ (compared to –8 ‰ for background air) and an upper limit for CO_2 drift in glass (PFA, 0.5 litre, 1.85 atm.) flasks of –1.4 ppm yr^{-1}, the rate of drift in $\delta^{13}C$ would be about –0.01 ‰ yr^{-1}. This is of little concern for storage in GASLAB where field samples are generally stored for days to weeks but it could potentially become significant if samples were stored at (e.g. Antarctic) field sites for long periods in a CO_2-rich environment.

2.8 Sample collection

2.8.1 Pump units

Flask samples were collected at Cape Grim (site code CGA) using a GASLAB Flask Pump Unit (FPU; Francey et al., 1996), modified to incorporate an absolute pressure relief device (Tavco Inc., Chatsworth, CA, USA). This device maintains constant pressure (set to 1.5 atm.) in flasks during and after flushing, so as to minimise any pressure-dependent surface effects. Flasks were filled specifically for O_2/N_2 analysis, in parallel with established GASLAB sampling activities focusing on other trace gas species. Figure 2.22 shows a schematic of the system used for O_2/N_2 sampling. The unit is constructed around a diaphragm pump (Model N05STI.9, KNF Neuberger, Princeton, NJ, USA) fitted with a Teflon-coated, Viton diaphragm. Plumbing materials are mainly SS with a Dekabon tube intake.

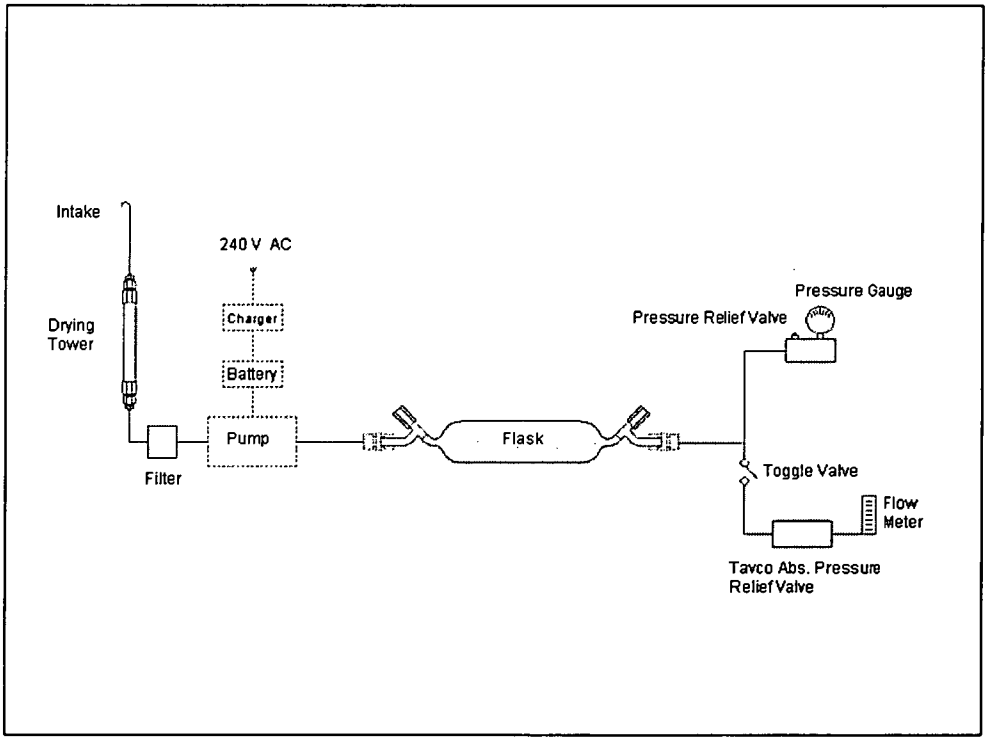

Figure 2.22 A schematic of the pump unit used for collection of flask samples at Cape Grim.

The configuration of pump units used for aircraft-based sampling (site code AIA) is very similar, except that the anhydrous $Mg(ClO_4)_2$ is contained in a glass tube sealed with Viton O-rings (rather than an SS tube on the FPU) and much of the inlet/outlet tubing is Nylon. Further details of aircraft sampling equipment have been presented elsewhere (Langenfelds et al., 1996a; 1996c; 2001c).

2.8.2 Drying

All CGA and AIA glass flask samples were dried, in most cases using anhydrous $Mg(ClO_4)_2$. This drying agent has been used extensively within GASLAB's established sampling programs, with no evidence of it modifying composition in relation to the species of interest under normal operating conditions. Modification of some species (depletion of CO_2 and N_2O) has only been observed on the few occasions where the drying agent was located between the pump and the flask and was subjected to large pressure changes during flask pressurisation (Langenfelds et al., 2001c). These conditions do not apply to the O_2/N_2 sampling considered here.

Before routine sampling was commenced at CGA, an initial comparison of CGA and AIA pump units and of the pump unit used at Cape Grim for collection of O_2/N_2 samples for SIO and URI/PU was conducted at Cape Grim on 4 December, 1995. The experiment also tested three different drying techniques including the "cryocooler" routinely used for the SIO and URI/PU programs. Multiple flask samples were collected with different pump/drying combinations over an 8 hour period under baseline conditions (Table 2.13). No significant differences were observed with the only marginal outlier being the phosphorus pentoxide (P_2O_5) drier

which returned mean $\delta(O_2/N_2)$ values enriched by about 7 per meg relative to the other techniques.

Early results from CGA sampling showed some unexplained $\delta(O_2/N_2)$ variability (Chapter 3), with the chemical drying being suspected as a possible cause. Further tests were carried out by co-collection (same hour) or alternate collection (week to week) of samples dried by anhydrous $Mg(ClO_4)_2$ and by a Nafion drier (Perma Pure Inc., Toms River, NJ, USA; model MD-110-144S) purged with a counter-flow of dried ambient air. Over 2½ years of parallel sampling between September, 1998 and April, 2001, and involving about 100 samples collected with each technique, the mean $\delta(O_2/N_2)$ difference was -1.2 ± 1.1 per meg (std. error; Nafion - $Mg(ClO_4)_2$). On six individual days during this period, successive pairs of flasks were collected within a 2 hour period, using anhydrous $Mg(ClO_4)_2$, Nafion and cryocool drying (Table 2.14). There was no evidence of significant mean differences for $\delta(O_2/N_2)$ or other species, nor of any correlation with season (and atmospheric humidity). All of the tests described here suggest there is no discernible effect on $\delta(O_2/N_2)$ from any of the pump units or drying techniques that were tested.

Pump unit	Drying	Mean $\Delta\delta(O_2/N_2)$ (per meg)
FPU	$Mg(ClO_4)_2$	0.0 ± 3.6 (n = 8)
FPU	Cryocool (-63°C)	-1.4 ± 11.7 (n = 2)
FPU	P_2O_5	6.4 ± 5.8 (n = 4)
Aircraft	$Mg(ClO_4)_2$	-2.1 ± 5.0 (n = 6)

Table 2.13 Mean $\delta(O_2/N_2)$ differences in flask samples collected with different pump units and drying techniques, shown as anomalies relative to the FPU/$Mg(ClO_4)_2$ mean. Uncertainties are the standard error of the mean.

Drying	Mean $\Delta\delta(O_2/N_2)$ (per meg)	Mean $\Delta\delta(Ar/N_2)$ (per meg)	Mean $\Delta\delta^{29}N_2$ (per meg)
Nafion	1.9 ± 2.4	9 ± 18	6.2 ± 3.3
Cryocool (-75°C)	3.0 ± 2.4	-14 ± 19	-0.1 ± 2.6

Table 2.14 Mean differences in six pairs of flask samples collected in parallel with different drying techniques, shown as anomalies relative to anhydrous $Mg(ClO_4)_2$. Uncertainties are the standard error of the mean.

2.8.3 Sampling procedures

Glass flasks are deployed to the field pre-conditioned with dry, natural air to 1.5 atm., the same pressure to which they will be filled with sample air. At CGA, flasks are flushed for 10 minutes at a nominal flow rate of 4 L min^{-1} before closing off the valves. AIA flasks are flushed for varying times, with a minimum of 3 minutes at lowest altitudes (i.e. near 150 m) scaled up to longer times at high altitudes (e.g. 7+ minutes at 6-8 km).

High pressure cylinders are filled at Cape Grim as part of the air archiving program by various techniques. Specific details of the procedures and their effect on sample O_2/N_2 ratio are discussed in Chapter 3.

2.9 Summary

The information presented in this chapter emphasises the challenge of measuring O_2/N_2 ratio to the exacting specifications necessary for global carbon cycle studies. There are many potential pitfalls relating to mass spectrometry, to selection of materials for storage of air samples and to gas handling procedures.

There are several aspects of overall experimental technique that impose limitations on data usefulness, depending on the specific application. The most important of these are summarised here. For "short-term" precision (i.e. differences between flask samples) the major source of noise is in the transfer of sample air from flasks into the MS inlet system. This noise appears to be mainly from mass-dependent fractionation but might also include some contribution from pressure-dependent surface adsorption effects. The quality of long-term calibration is limited by potential drift in air standards. There is compelling evidence of significant fractionation occurring in some high pressure cylinder standards as a function of cylinder pressure and/or in the air extracted from cylinders as a function of flow rate. An important problem specific to flask sampling records is O_2/N_2 drift due to permeation through O-rings, especially when storage times are long, such as occurred for Cape Grim samples in 1998/99 where samples were stored for more than a year before analysis. In such cases, errors in storage corrections undoubtedly contribute both to short-term noise and to spurious perturbations in atmospheric time series.

CHAPTER 3

DECADAL TRENDS IN ATMOSPHERIC O_2 AND CO_2

3.1 Introduction

It has long been suspected that atmospheric O_2 levels are being altered by human activities. A declining trend is expected from the anthropogenic perturbation to rates of combustion of biogenic material. Fossil fuels (coal, oil, natural gas) have been the primary energy source over the period of industrialization. Rates of land clearing have increased in tandem with world population growth and expansion of agriculture. Oxidation of this organic material consumes O_2 from the atmosphere. Earlier, though as yet unsupported concerns existed over diminution of O_2 through other processes, such as a possible decline in phytoplankton stocks due to pollution of the oceans. A few decades ago, there was speculation that O_2 losses might be large enough to have detrimental environmental consequences. Extreme predictions warned of a catastrophic O_2 decline that could threaten the habitability of the planet. These fears were demonstrated to be unwarranted by theoretical calculations of oxygen cycle processes (Broecker, 1970) and subsequent measurement of actual changes in the atmosphere.

Before the 1980s, there were no ongoing O_2 monitoring programs. Measurements were sporadic and obtained by different researchers at various times and geographical locations. In a review of measurements reported to 1970, Machta and Hughes (1970) concluded that O_2 had been stable at 20.95% between 1910 and 1970, with any trend too small to be resolved by available data. Since then, advances

in measurement technologies have achieved much higher precision, revealing small trends that would previously have escaped detection.

Contemporary, high-precision, O_2/N_2 measurement programs were pioneered by groups at SIO and URI (now based at PU). The primary aim was to establish the global, long term trend of atmospheric O_2/N_2, which provides a key constraint of the relative rates of uptake of fossil CO_2 by the oceans and the land biosphere. The carbon and oxygen cycles are intimately linked through combustion of fossil fuels and biomass, and in the cycling of biomass through photosynthesis and respiration. However, unlike CO_2, O_2 has low solubility in seawater. Large seasonal, air-sea fluxes of O_2 are driven by cycling of marine biological production and ventilation of near-surface waters, but changes in the oceanic O_2 inventory on interannual time scales are relatively small. Thus trends in atmospheric O_2 are mainly attributed to two processes, fossil fuel combustion and exchange with the land biosphere. The global average stoichiometry of O_2/CO_2 exchange can be estimated for both processes, as can the rate of CO_2 emission from fossil fuel use. Thus the O_2 trend directly constrains the rate of change of the size of the land biosphere, and together with the concurrent global trend in CO_2, can be used to solve for the rate of oceanic CO_2 uptake.

The flask sampling records of SIO (R.F. Keeling et al., 1996; Manning, 2001) and URI/PU (Battle et al., 2000) now span more than a decade. Both indicate significant roles for both oceans and land biota in the uptake of anthropogenic CO_2 during the 1990s. Nevertheless, there are limitations with the flask sampling approach in terms of the timespan of records and the challenge of maintaining stable calibration over many years. Experience from the CSIRO measurement program (Chapter 2) underscores the demanding nature of this task.

Battle et al. (1996) report an O_2 trend from Antarctic firn air for the period 1977-1985, but difficulties in calibrating the different methodologies prevent a close link to the modern records. In this case, the atmospheric O_2 trend is not directly measured, but is inferred from measurements of O_2/N_2 in the firn, that are corrected for modification by diffusive, gravitational and bubble exclusion processes. Fractionating processes, probably related to molecular geometry, that affect O_2/N_2 at lower depths of the firn, limit the length of the Battle et al. record and have also prevented recovery of any meaningful trends from air sealed in ice (Craig et al., 1988; Bender et al., 1995).

The trend in atmospheric O_2/N_2 is examined here using CSIRO data obtained by two approaches. One involves measurements from ground and aircraft-based flask sampling in the Cape Grim region between 1995 and 2001. The second aims to reconstruct a longer, 23-year trend from analysis of the Cape Grim Air Archive (CGAA), a suite of air samples collected at Cape Grim since 1978 and maintained as an archive of "background" atmospheric composition (Langenfelds et al., 1996b). The CGAA continues to provide high precision reconstructions of many atmospheric trace gas species, including SF_6 (Maiss et al., 1996), many long-lived halocarbon species (e.g. Oram et al., 1995; 1996; Fraser et al., 1996) and greenhouse gases and their isotopes (Etheridge et al., 1998; Francey et al., 1999a; 1999b). Advantages of the CGAA approach for determination of O_2/N_2 trends are its long timespan (now 23 years), the ability to analyse all samples against a common calibration scale over a short period of time and less interference of diffusive processes that affect air retrieved from firn and ice. This air archive provides a unique opportunity to confirm and extend knowledge of the change in atmospheric O_2 and behaviour of the global carbon cycle over the last two decades.

This chapter updates and extends the flask sampling and CGAA results first reported by Langenfelds et al. (1999a, 1999b). The main differences are:

1. Data are reported here into 2001, extending the earlier published records that ended in 1997.
2. The previously reported data were obtained from MAT252 measurements only. Some CGAA cylinders have since been analysed on the Delta^{plus}XL instrument, thus providing first $\delta(Ar/N_2)$ measurements of CGAA air.
3. Data processing algorithms have been revised in accordance with the definition of calibration scales, experimental effects and associated corrections described in Chapter 2.

3.2 Methods

3.2.1 Sampling

Flask sampling equipment and techniques are described in Sections 2.7 and 2.8. All of the data reported here are from CSIRO's 0.5 L, dual-stopcock, glass flasks. During the first year of sampling starting in January, 1995, stopcocks were fitted with one of three O-ring materials (PFA, PTFE, Viton). Of these materials, Viton was found to provide best O_2/N_2 stability of sample air during storage and was thus used exclusively for all field sampling from 1996. Flask samples were collected at Cape Grim in pairs, on average once a fortnight. Members of each pair were filled separately but in immediate succession, usually about 10 minutes apart. Aircraft-based samples were collected less frequently, on average once a month through 1998. Thereafter, flights were more sporadic, did not always include collection of samples by techniques used specifically for O_2/N_2 analysis (i.e. in relation to pressure control

during sampling and O-ring material etc.) and were suspended from October, 2000. Further details of aircraft sampling operations are provided in Chapter 5.

A general description of the range of sampling techniques employed in the CGAA program has been documented previously (Weeks et al., 1992; Langenfelds et al., 1996b). The majority of cylinders were filled cryogenically by immersion in liquid nitrogen, with flow into the cylinder assisted by a small metal bellows pump. A small number were dried through glass U-traps immersed in ethanol cooled to about -75°C with dry ice or liquid N_2, while most were filled "wet". Some specific features of pre-sampling and sampling procedures are discussed in detail below where they are relevant to observed anomalies in O_2/N_2 or other diagnostic tracers.

3.2.2 Analysis

General flask and cylinder analysis procedures are described in Chapter 2. Some unusual characteristics of the CGAA suite required modification of standard analytical procedures. First, unlike glass flask samples and the majority of O_2/N_2 cylinder standards, most CGAA samples were filled without drying. Thus all CGAA air extracted for analysis was dried during transfer to the inlet system through a small tube containing anhydrous $Mg(ClO_4)_2$, even before the chemical drier was introduced as a permanent component of the inlet system in October 1997. The air was dried to minimise possible measurement bias due to varying moisture levels in the inlet or in the mass spectrometer source regions.

The pressure of CGAA samples varies widely among cylinders. Most were analysed using a limited number of pressure regulators that were rotated among a large number of cylinders. Consequently, regulator conditioning times were relatively short, in contrast to normal practice for O_2/N_2 cylinder standards, which are fitted

with dedicated regulators. Once fitted to CGAA cylinders, regulators were exposed to full sample pressure for at least 3 hours (though usually at least 1 day) before analysis, during which time they were occasionally flushed to promote surface conditioning. Immediately prior to introduction of sample air to the inlet system, air contained within the internal volume of the regulator was replaced many-fold by flushing through the regulator, while maintaining constant (full cylinder) pressure on the high pressure side of the regulator. Air from CGAA cylinders with pressure below about 5 psig was transferred to the inlet system without regulators, and using only a length of stainless steel, capillary tubing. For all cylinders, the delivery pressure and/or flow rate of sample air was adjusted, as far as possible, to maintain pressure in the analysis chamber of the inlet system at about 1.25 atm. during sample introduction as described in Section 2.5.3.

3.3 Flask sampling data

3.3.1 Cape Grim and aircraft-based sampling

CSIRO data from flask sampling at Cape Grim and from aircraft-based vertical profiling of the troposphere above Cape Grim are plotted in Figure 3.1a. The aircraft-sourced data shown here are from the marine boundary layer (MBL) in the 0-1 km altitude range (see Chapter 5 for further details of aircraft sampling procedures). Also plotted in Figure 3.1a are the Cape Grim records of SIO (Manning, 2001) and URI/PU (Battle et al., 2000). To date, the three laboratories have reported data on in-house scales relative in each case to a value within the range of observed, current atmospheric $\delta(O_2/N_2)$. Records are merged here by adjustment to the SIO scale on the basis of average differences over the period of overlap. The adjustment to CSIRO data of –122 per meg is calculated from Cape Grim surface data, from four

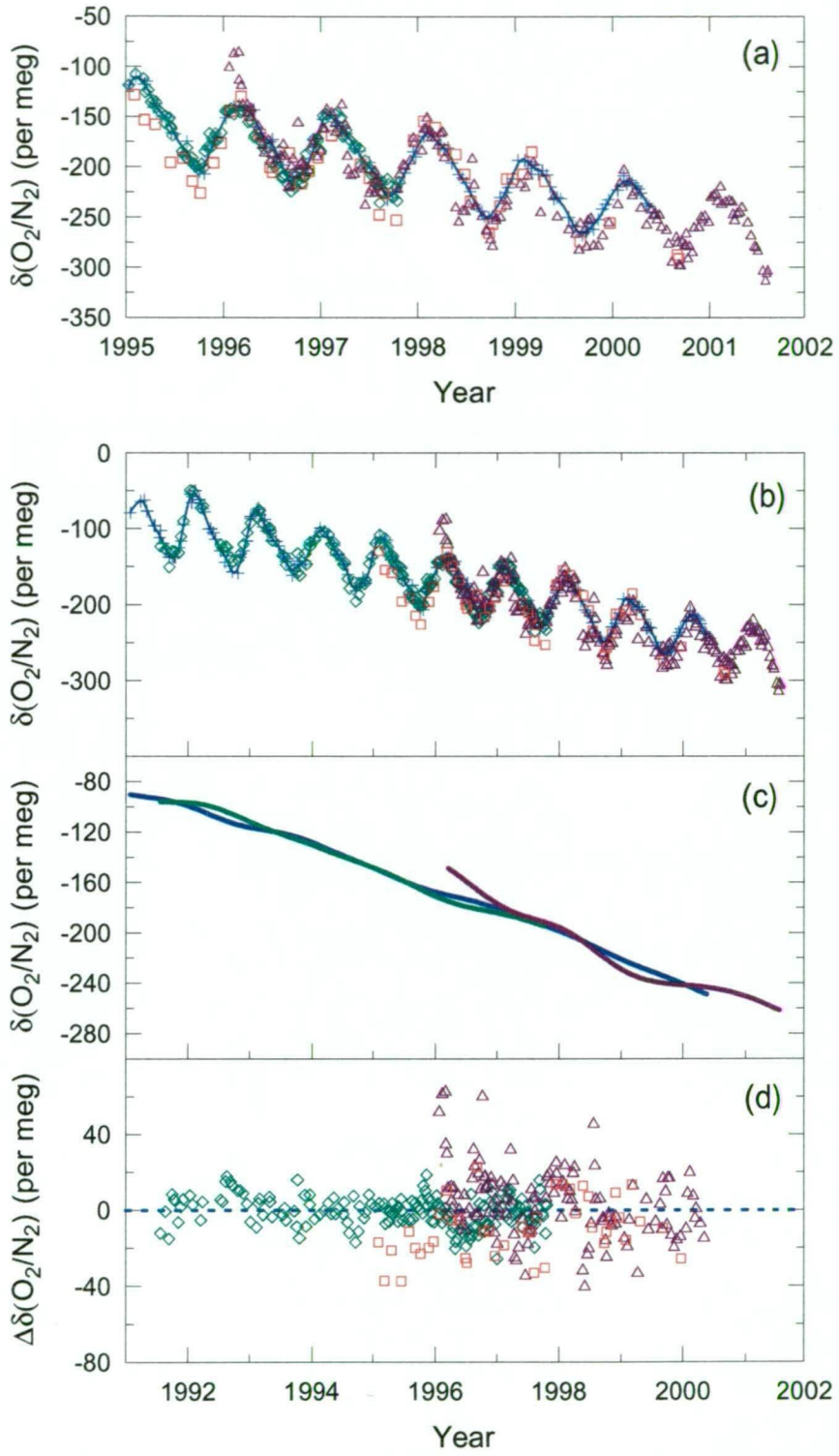

Figure 3.1 a) Cape Grim $\delta(O_2/N_2)$ data from analysis of surface flask samples by SIO (blue crosses), URI/PU (green diamonds) and CSIRO (magenta triangles) and from CSIRO aircraft-based sampling 35 km to the west of Cape Grim in the 0-1 km altitude band (red squares). Data are shown as daily means of multiple collections. CSIRO and URI/PU data have been adjusted to the SIO calibration scale (see text). The SIO data are fitted by a smooth curve (blue line); b) as for panel (a) but over the longer period 1991-2002; c) Trend curves of SIO (blue), URI/PU (green) and CSIRO (magenta) records from surface sampling; d) Residuals of CSIRO and URI/PU data from the SIO smooth curve. Symbols are as for panel (a).

years of overlap between 1996 and 2000. The adjustment to URI/PU data of –66.7 per meg was calculated by Battle et al. (2000) also from Cape Grim surface data with 5 years of overlap. All records show a declining trend and well-defined seasonal cycle.

Subsequent data analysis uses curves fitted to the data to describe the long-term trend, interannual variations (specifically addressed in Chapter 4) and the seasonal cycle (Chapter 5). This is achieved here using the curve-fitting routine of Thoning et al. (1989). First, a curve comprising a quadratic function and 4 harmonic terms is fit to the data:

$$f(t) = at^2 + bt + c + \sum_{i=1}^{4}[d_i \sin(2\pi it) + e_i \cos(2\pi it)] \qquad (3.1)$$

Residuals from the fit are then smoothed by a low pass filter with cutoff times of both 80 days and 650 days (1.8 years). A "smooth curve" is generated by adding the 80-day smoothed residuals to the function f(t). The smooth curve describing the SIO $\delta(O_2/N_2)$ record is shown as the solid line in Figure 3.1a. A "trend curve" is generated by adding the 1.8-year smoothed residuals to the quadratic component of f(t), thus showing the long-term trend with mean seasonal cycle removed (Figure 3.1b). The mean seasonal cycle is defined by the harmonic component of f(t).

Inter-laboratory differences can be examined by plotting residuals of CSIRO and URI/PU data from the SIO smooth curve (Figure 3.1c). The residuals show the CSIRO data to have the largest scatter of the three records. Figure 3.1c also suggests systematic differences between the CSIRO surface and aircraft-sourced data. This feature is examined further in Chapter 5. Evidence of experimental artefacts such as

these in the CSIRO data and other limitations identified in Chapter 2, and the superior precision of and agreement between SIO and URI/PU records suggests that the SIO and URI/PU flask sampling records provide a more reliable representation of atmospheric $\delta(O_2/N_2)$ at Cape Grim over the last decade. These records are thus used as a benchmark for assessment of CSIRO data in subsequent discussion.

For the purpose of establishing the long-term trend in $\delta(O_2/N_2)$, subsequent analysis of CSIRO data uses only the surface record owing to its longer timespan, better continuity and greater consistency in sampling procedures. Data from the first five sampling events (spanning six weeks) at Cape Grim are rejected on grounds of highly anomalous results with respect to both SIO and URI/PU records. They are plotted in Figures 3.1a and 3.1c but are excluded from the CSIRO trend curve in Figure 3.1b. The discrepancy is presumably due to start-up sampling problems, although the exact cause has not been identified.

3.3.2 Mass-dependent artefacts

The relationship of CSIRO flask pair differences in $\delta(O_2/N_2)$, $\delta(Ar/N_2)$, $\delta^{29}N_2$ and $\delta^{34}O_2$ (Figure 3.2) indicates most of the scatter in the Cape Grim record is due to mass-dependent fractionation, probably introduced during transfer of sample air from flasks into the MS inlet system (Section 2.5.4). The $\delta(Ar/N_2)/\delta(O_2/N_2)$ plot, in particular, shows a well-defined relationship with a slope of 3.9 ± 0.2 determined by the ODR fit. As was the case in Section 2.5.4 and Figure 2.10, the lines of best fit involving $\delta^{29}N_2$ data do not appear to closely match the data, because 1) they are sensitive to uncertainties assigned to x and y variables and 2) the range of variation in $\delta^{29}N_2$ is comparable to measurement uncertainty.

The $\delta(Ar/N_2)/\delta(O_2/N_2)$, $\delta(Ar/N_2)/\delta^{29}N_2$ and $\delta(O_2/N_2)/\delta^{29}N_2$ slopes all deviate from values proportional to mass difference (e.g. that are expected for pressure diffusion; Section 2.3.2) in a sense that favours the signature of thermal diffusion. The $\delta(Ar/N_2)/\delta(O_2/N_2)$ slope for differences in measurements of repeat aliquots of the same flask samples (Figure 2.10) was also relatively high (3.4 ± 0.1). These results suggest that thermal diffusion may be an important influence on fractionation of sample air during transfer to the MS inlet system.

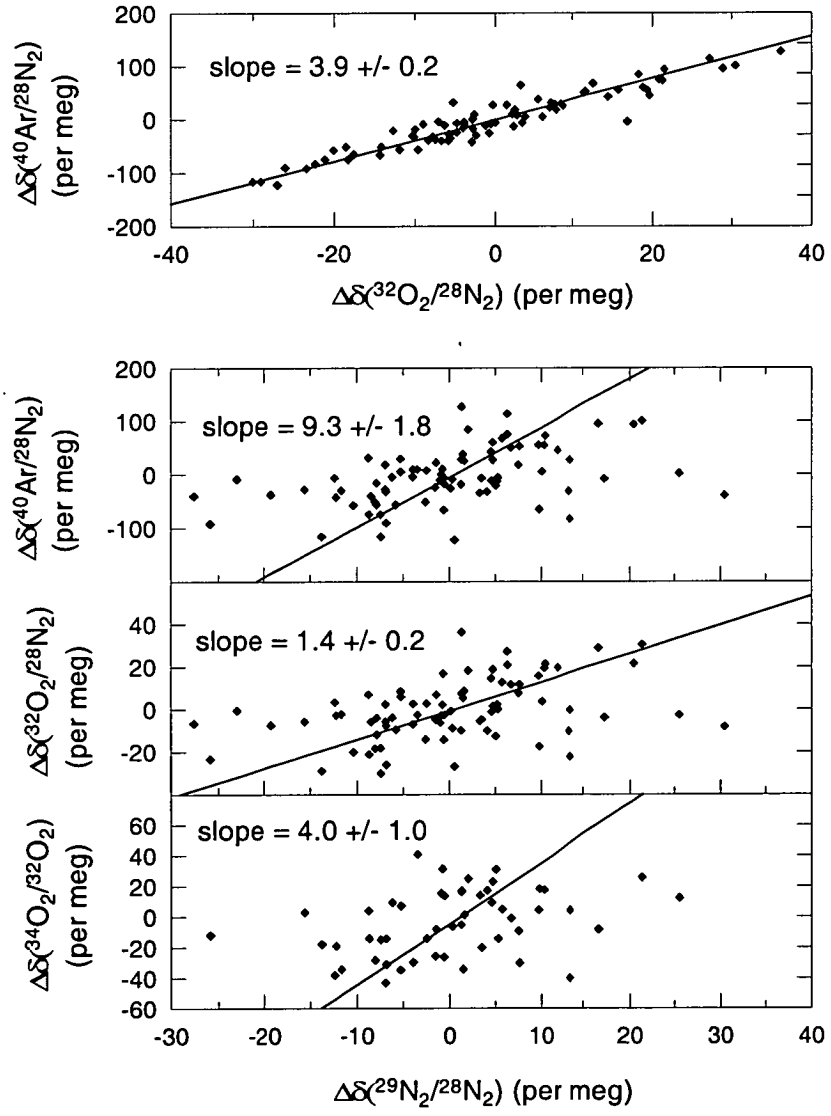

Figure 3.2 Inter-species relationships of differences between flask sample pairs collected at Cape Grim, with lines of best fit obtained by ODR.

Given that most of the scatter in $\delta(O_2/N_2)$ and $\delta(Ar/N_2)$ of flask sample data is due to mass-dependent fractionation, there is potential to use the $\delta(Ar/N_2)$ measurements to correct for fractionation in $\delta(O_2/N_2)$ and thus improve precision of the atmospheric records. The mass spectrometric precision of $\delta(Ar/N_2)$ measurements (e.g. 4 per meg as defined by the standard error of the mean of one analysis block of 10 cycles; Table 2.3) could potentially limit uncertainty in $\delta(O_2/N_2)$ due to fractionation to within ±2 per meg, an order of magnitude lower than the scatter in Figure 3.2. For such corrections to be reliable would require:

1. assumed knowledge of $\delta(Ar/N_2)$ variations in the atmosphere. There is assumed to be negligible long-term trend, but there may be a significant seasonal cycle due to thermally forced air-sea fluxes. Fractionation-related scatter in the 3-year CSIRO record obscures any atmospheric variations (Figure 3.3). A harmonic fit to these data yields a seasonal cycle that suggests a summer maximum and winter minimum, but uncertainties are large (Figure 3.4).
2. assumed knowledge of the $\delta(Ar/N_2)/\delta(O_2/N_2)$ ratio of anomalies caused by the fractionation. This varies among diffusive processes (Table 2.2), however the values from theory and from the various empirical results relating to gas handling that are reported in this thesis all lie in the range 2.2 – 3.9. This range is sufficiently tight for $\delta(Ar/N_2)$ to usefully constrain O_2/N_2 fractionation artefacts in flask sampling data.
3. limits on uncertainty in stability of the $\delta(Ar/N_2)$ scale. There is reason to suspect that $\delta(Ar/N_2)$ in the primary reference standard (950051) may be drifting at about 4.5 per meg yr^{-1} due to usage-related fractionation (Section

2.6.7), even though the scale is defined assuming no drift in 950051. Any such drifts would impact on inferred trends in atmospheric $\delta(O_2/N_2)$.

The possibility of using the $\delta(Ar/N_2)$ data in this way is flagged as a possibility for the future, but no such adjustments have been made to $\delta(O_2/N_2)$ data from glass flask sampling reported in this thesis.

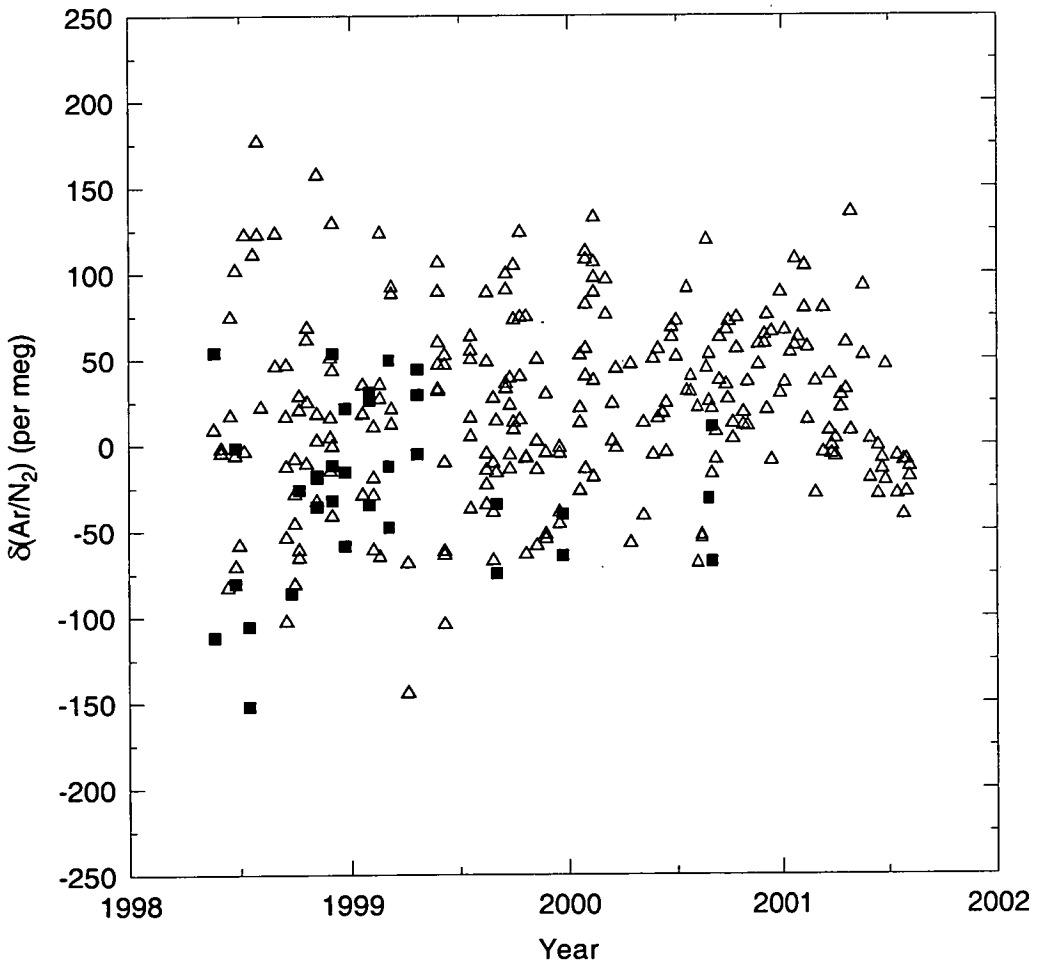

Figure 3.3 CSIRO measurements of $\delta(Ar/N_2)$ in individual flasks from Cape Grim (triangles) and aircraft-based sampling (squares).

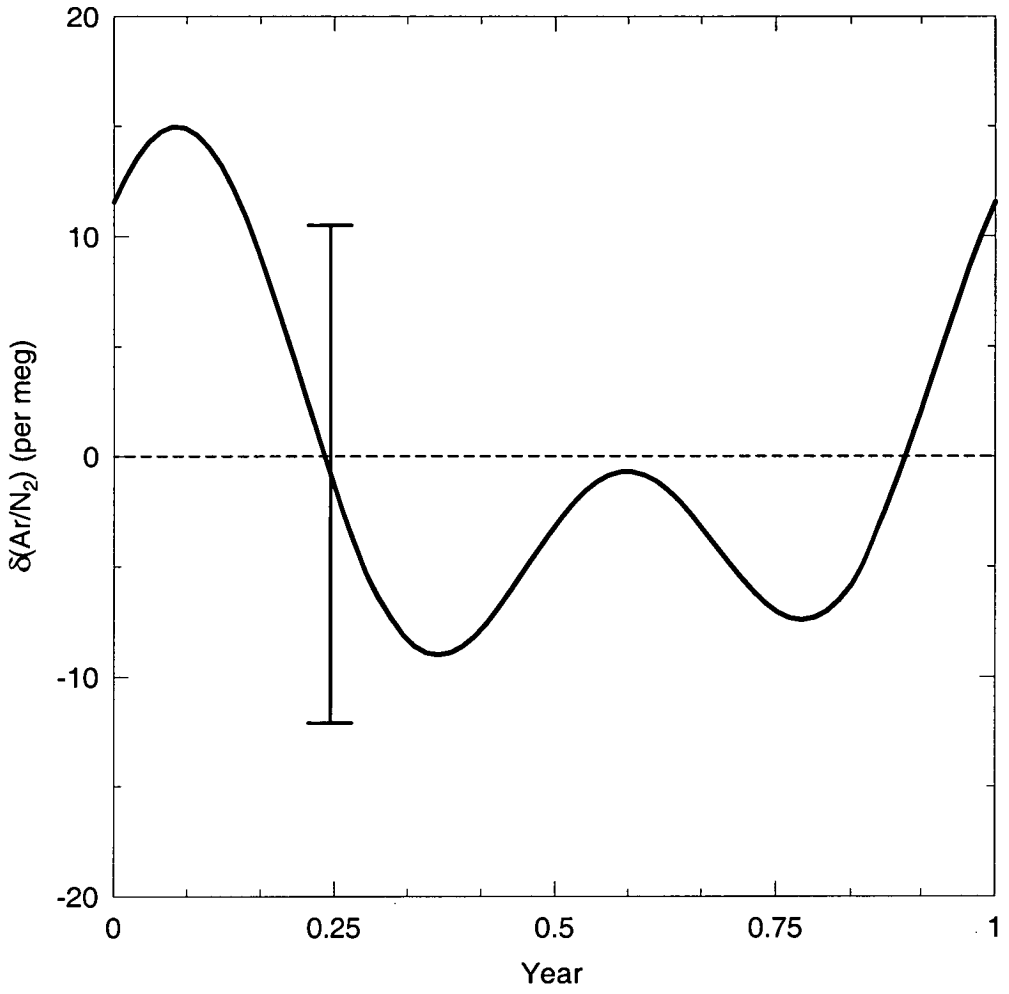

Figure 3.4 The seasonal cycle of $\delta(Ar/N_2)$ at Cape Grim from the harmonic component of a curve fit to CSIRO Cape Grim data. Error bars represent 1 standard error uncertainty of monthly mean observed values.

3.3.3 Storage drift correction artefacts

Another likely contributor to scatter in the CSIRO flask data is the drift of $\delta(O_2/N_2)$ in flasks during storage that results from differential permeation of O_2 and N_2 through the elastomeric O-ring seals. Storage drift corrections derived from laboratory tests (Section 2.7) are applied to data from CSIRO's 0.5 L glass flasks based on O-ring type, sample pressure and length of storage. However, the true rate of drift in individual samples could deviate from average behaviour indicated by the laboratory tests for several reasons, especially the degree of compression of the O-rings sealing the stopcocks. Any errors in correction would be accentuated by long storage times.

Before 1999, limited access to the MAT252 instrument resulted in relatively long and variable storage times for O_2/N_2 flask samples (Figure 3.5). In particular, samples collected from April, 1998 were stored for up to a year before analysis. Data from these samples show larger scatter in Figure 3.1c. There is also a suggestion of a time-dependent anomaly in the residuals for data collected between April 1998 and mid-1999, which is consistent with a systematic error in storage drift correction for these samples. The mean deviation of CSIRO data from the SIO curve from April to June 1998 is –7 per meg, equivalent to 1σ uncertainty in the rate of $\delta(O_2/N_2)$ drift observed for similar flask samples in the laboratory tests. Storage-related errors are probably the main cause of the discrepancy between CSIRO and SIO trend curves during 1998/99 (Figure 3.1b). The same feature appears as an anomaly in $\delta(O_2/N_2)$ growth rate curves inferred from CSIRO data, thus masking any growth rate variations that could plausibly be attributed to biogeochemical processes (see Chapter 4).

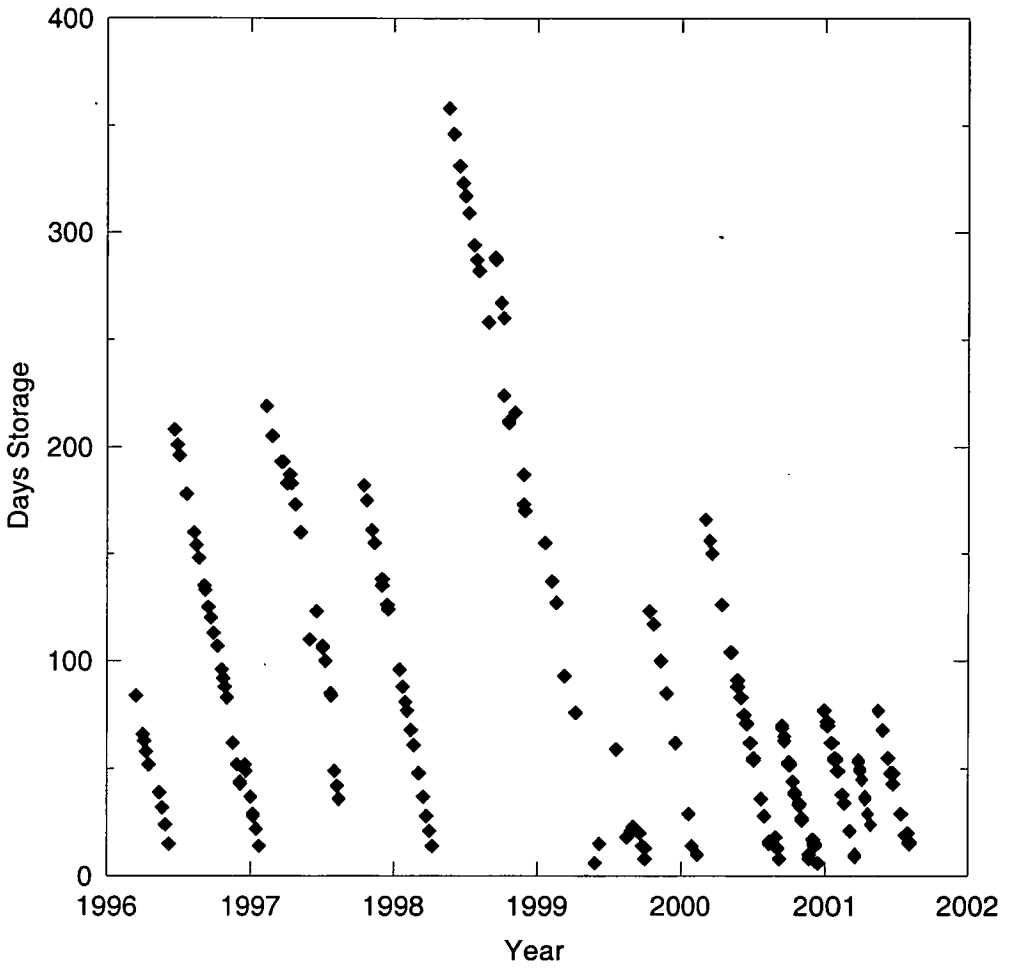

Figure 3.5 Storage time between collection and analysis of Cape Grim flask samples, plotted as a function of collection date.

3.4 Cape Grim Air Archive data

A plot of raw CGAA $\delta(O_2/N_2)$ data (Figure 3.6a) alongside the flask sampling records shows scatter in CGAA data several orders of magnitude larger than that required for constraining the global carbon budget. Inspection of sample collection records and measurements of other trace gas species enable identification of factors responsible for O_2/N_2 modification in subsets of samples. Table 3.1 shows the relevant diagnostic information. Data are rejected or corrected in the following sequence with progressively reduced scatter displayed in successive panels of Figure 3.6.

3.4.1 Fractionation by effusion

Measurements of $\delta^{29}N_2$, $\delta^{34}O_2$ and $\delta(Ar/N_2)$ reveal many samples to be heavily enriched. Most of these samples are low in pressure and are contained in the oldest batch of 35 litre cylinders (prefix"S35L-A"), many of which are known to have developed small leaks through surface rust. Rejected $\delta(O_2/N_2)$ data from these cylinders are identified in Figure 3.6a. Multi-species relationships are shown in Figure 3.7 and are consistent with mass-dependent fractionation resulting from molecular effusion through the leaks, as governed by Graham's Law for molecules escaping from a vessel of gas under pressure through a tiny orifice (see Section 2.3.2). Observed values for the $\Delta\delta(Ar/N_2)/\Delta\delta^{29}N_2$ and $\Delta\delta^{34}O_2/\Delta\delta^{29}N_2$ ratios of 10.8 and 1.8 are close to those predicted from theory (11.1 and 1.7).

Measurements of the isotopic composition of O_2 and N_2 can be influenced by the elemental composition of the gas mixture through an artefact of the mass spectrometric technique, as reported by Sowers et al. (1989) and discussed in Section 2.4.3. However, if the magnitude of the effect quantified on one occasion (in April, 1998) for the MAT252 instrument is assumed to be representative of instrument behaviour at the times of CGAA analyses, then the impact on multi-species relationships of drifts in CGAA samples is negligible.

Unlike $\delta(Ar/N_2)$, $\delta^{29}N_2$ and $\delta^{34}O_2$, variations in atmospheric $\delta(O_2/N_2)$ are large compared to experimental precision and may become significant in empirically assessing effects of effusion or other interfering processes. Therefore to examine the relationship of $\delta(O_2/N_2)$ with $\delta(Ar/N_2)$ and $\delta^{29}N_2$, the $\delta(O_2/N_2)$ residuals are calculated relative to a hypothetical curve extrapolated back to 1978. This approach is ineffective for small residuals that are of comparable magnitude to the uncertainty

UAN	Cylinder ID	Collection Date	Flushing Procedure	Dry/ Wet	Fill Pressure	Analysis Pressure	$\delta(O_2/N_2)$	δ^{29}_{N2}	$\delta^{34}O_2$	$\delta(Ar/N_2)$
					(psig)	(psig)	[.....(per meg).....]			
780001	S35L-A01	26-Apr-78	through-flush		320	90	276	1	5	
780002	S35L-A02	7-Jul-78	through-flush		320	110	106	1	7	
780003	S35L-A03	30-Oct-78	through-flush			0	3106	779		
790001	S35L-A04	6-Feb-79	through-flush		430	110	245	-1	-2	
800003	S35L-A06	3-Sep-80	through-flush	wet	430	3	1034	79	113	
810002	S35L-A09	5-Oct-81	through-flush		400	39	258	36	76	
820001	S35L-A10	23-Feb-82	through-flush			0	1083	337		
830002	S35L-A13	1-Aug-83	through-flush		420	11	3761	812	1377	
840001	S35L-A14	20-Jan-84	through-flush	wet	430	0	460	326		
840002	S35L-A15	20-Jan-84	through-flush		400	1	2113	525	989	5634
840003	S35L-A16	4-Apr-84	through-flush	wet	420	0	2872	718		
840004	S35L-A17	23-May-84	through-flush	wet	410	315	130	12	-27	
840008	S35L-A20	28-Aug-84	through-flush	wet	460	2	2295	175	318	
840010	S35L-A22	20-Dec-84	through-flush	wet	410	30	881	173	349	
850003	S35L-A25	8-Aug-85	through-flush	wet	440	2	900	195	342	
850006	S35L-A28	10-Dec-85	through-flush	wet	90	4	4307	997	1740	
860001	S35L-A29	6-Feb-86	through-flush	wet	350	260	111	1	12	
860002	S35L-A30	6-Feb-86	through-flush	wet	360	70	123	4	-7	
860005	ALVM0005	12-Nov-86	evac./P&V	dry	480	430	193	-8	-2	
870002	ALVM0002	8-Jan-87	evac./P&V	dry	420	380	-2418	-6		
870003	ALVM0003	9-Jan-87	evac./P&V	dry	375	310	-2662	-14	69	
870004	S35L-A33	24-Mar-87	through-flush	dry		3	251	36	97	
870006	ALVM0006	28-May-87	evac./P&V	dry	360	310	-624	1		
870007	S35L-A07	2-Oct-87	through-flush	wet	405	3	7019	1568	2727	
880002	ALVM0001	21-Jun-88	evac./P&V	dry	480	320	42	1		
880003	S35L-A36	21-Jun-88	evac./P&V	dry	420	235	204	-5	40	
890002	ALVT531	28-Apr-89	evac./P&V	dry	1000	47	-909	-23		
890004	ALVM0004	19-May-89	evac./P&V	dry	1020	880	-109	-5		
890005	ALVT566	8-Nov-89	evac./P&V	dry	1080	930	-413	-10	11	
900005	ALVZ864	15-Nov-90	evac./P&V	dry	1600	770	-76	1	-7	-104
900006	ALVZ865	14-Nov-90	evac./P&V	dry	1600	100	52	6	22	17
900027	ALVT567	16-Feb-90	evac./P&V	dry	500	320	-541	-16		
900039	S35L-B06	18-Dec-90	evac./P&V	dry	580	17	-31	49	58	231
900048	ALVT568	26-Apr-90	evac./P&V	dry	920	780	-82	1		
900050	ALTH8462	15-Nov-90	evac./P&V	dry	1500	520	-99	-8		
900051	ALTH8457	15-Nov-90	evac./P&V	dry	1000	380	-47	-3		
910361	S35L-B07	29-Aug-91	evac./P&V	dry	500	55	-39	10	-17	-44
910375	S35L-B04	31-Oct-91	evac./P&V	dry	560	7	-94	32	-4	-76
920408	S35L-B02	8-Apr-92	evac./P&V	wet	520	30	-4	3	9	43
920469	S35L-C09	18-Mar-92	evac./P&V	dry	320	65	17	9	1	-18
920655	S35L-C11	23-Sep-92	evac./P&V	wet	520	140	50	1	1	51
930279	S35L-C13	2-Mar-93	evac./P&V	wet	600	70	-278	2	-15	-283
931007	S35L-C14	11-Aug-93	evac./P&V	wet	480	1	-118	-7	23	
940159	S35L-C15	1-Nov-93	evac./P&V	wet	620	65	-85	-3	-11	-85
940160	S35L-C17	17-Dec-93	evac./P&V	wet	640	12	-66	5	7	38
940378	S35L-C16	11-Feb-94	evac./P&V	wet	600	75	-8	5	0	-46
940379	S35L-C19	15-Mar-94	evac./P&V	wet	650	30	-94	-3	-27	-160
940678	S35L-C20	27-Apr-94	evac./P&V	wet	595	30	-90	-5	16	-118

UAN	Cylinder ID	Collection Date	Flushing Procedure	Dry/ Wet	Fill Pressure	Analysis Pressure	$\delta(O_2/N_2)$	$\delta^{29}N_2$	$\delta^{34}O_2$	$\delta(Ar/N_2)$
					(psig)	(psig)	[.....(per meg).....]			
940679	S35L-C21	27-Apr-94	evac./P&V	wet	680	65	-55	12	-18	-79
940720	S35L-C10	1-Jun-94	evac./P&V	wet	600	8	-63	0	16	88
940851	S35L-B10	9-Jun-94	evac./P&V	wet	550	20	483	129	204	1153
941096	ALTH8473	4-Oct-94	evac./P&V	dry	1015	930	-157	0		
941413	S35L-C08	7-Dec-94	evac./P&V	wet	645	48	-249	-5	9	
950241	S35L-B03	8-Feb-95	evac./P&V	wet	615	70	-9	0	-6	
950527	ALVV126	13-Mar-95	evac./P&V	dry	435	400	-96	-8		
950789	S35L-B09	13-Jun-95	evac./P&V	wet	620	555	-61	4	-1	-50
960051	S35L-C24	4-Dec-95	evac./P&V	wet	520	380	-35	0	4	-8
960115	ALVU427	24-Oct-95	evac./P&V	dry	675	650	-107	-3	9	
960619	CA01606	7-Mar-96	evac./P&V	dry	620		-165	-2	0	
960957	S35L-C28	28-May-96	evac./P&V	wet	600	505	-72	-1	12	-30
961164	S35L-C30	21-Aug-96	evac./P&V	wet	580		-126	-3		
961408	S35L-C29	2-Oct-96	evac./P&V	wet	620	610	-213	-12		
961409	S35L-C31	3-Oct-96	evac./P&V	wet	640		-130	1		
970007	S35L-C33	7-Jan-97	through-flush	wet	730	730	-55	-5	-14	
970008	S35L-C34	7-Jan-97	through-flush	wet	780	700	-57	4	14	-34
970010	S35L-C36	7-Jan-97	through-flush	wet	720	720	-78	7	-5	-76
970011	S35L-C37	7-Jan-97	through-flush	wet	760	750	-95	4	-17	-123
970012	S35L-A34	7-Jan-97	through-flush	wet	24		-19	9		
970013	S35L-C38	8-Jan-97	through-flush	wet	130	130	-53	-6	15	
970014	S35L-C39	8-Jan-97	through-flush	wet	72	72	-63	-2	-22	
970015	S35L-C40	8-Jan-97	through-flush	wet	270	270	-71	-13	22	
970092	S35L-C41	20-Nov-96	through-flush	wet	620	570	-110	3	-7	-82
970259	S35L-C43	26-Feb-97	through-flush	wet	670		-61	7		
970380	S35L-C44	13-Mar-97	through-flush	wet	650	600	-66	1	7	-40
970754	S35L-C45	4-Apr-97	through-flush	wet	620	500	-84	-1	-10	-72
970756	S35L-C47	30-May-97	through-flush	wet	630	395	-97	5	-5	-44
971115	S35L-C50	15-Jul-97	through-flush	wet	620	580	-122	-1	9	-69
980429	S35L-C52	18-Dec-97	through-flush	wet	560		-116	0		
980724	S35L-C56	15-Apr-98	through-flush	wet	640	580	-105	3	7	-76
980918	S35L-C51	25-Jun-98	through-flush	wet	640	615	-138	3	7	-105
981531	S35L-C60	5-Oct-98	through-flush	wet	320	305	-164	10	-44	-38
981563	S35L-C61	15-Oct-98	through-flush	wet	630	590	-156	6	32	-67
991060	S35L-C65	17-Feb-99	through-flush	wet	420	380	-114	-4	-3	-70
991381	S35L-C40	4-Aug-99	through-flush	wet	430	390	-169	-6	17	-64
992045	S35L-C38	16-Nov-99	through-flush	wet	450	480	-187	-9	4	-96
993562	S35L-C55	29-Sep-00	through-flush	wet	460	360	-199	-7	4	-87
993563	S35L-B05	15-Jan-01	through-flush	wet	540	500	-142	-2	3	-70

Table 3.1 Collection and preliminary analysis data for all analysed CGAA samples. Cylinders are either stainless steel, 35 L (prefix "S35L"), aluminium, 48 L ("ALV") or aluminium, 24 L ("ALTH"). Blank entries in "Dry/wet" and "Fill pressure" columns denote information not available from sampling records. Entries under "Flushing procedure" refer to flushing large volumes of ambient air at 1 atm. pressure (through-flush; see Section 3.2.2), and evacuation followed by multiple pressurise/vent cycles (evac./P&V). Where samples were analysed on both MAT252 and Delta^{plus}XL instruments, it is the Delta^{plus}XL data shown here, except for "S35L-A" cylinders, many of which leak and were strongly fractionated over about 4 years between analyses on the two instruments. All analysis data are expressed here on the CSIRO scales. All $\delta(O_2/N_2)$ data refer to the relationship of *m/z* ratios 32 and 28.

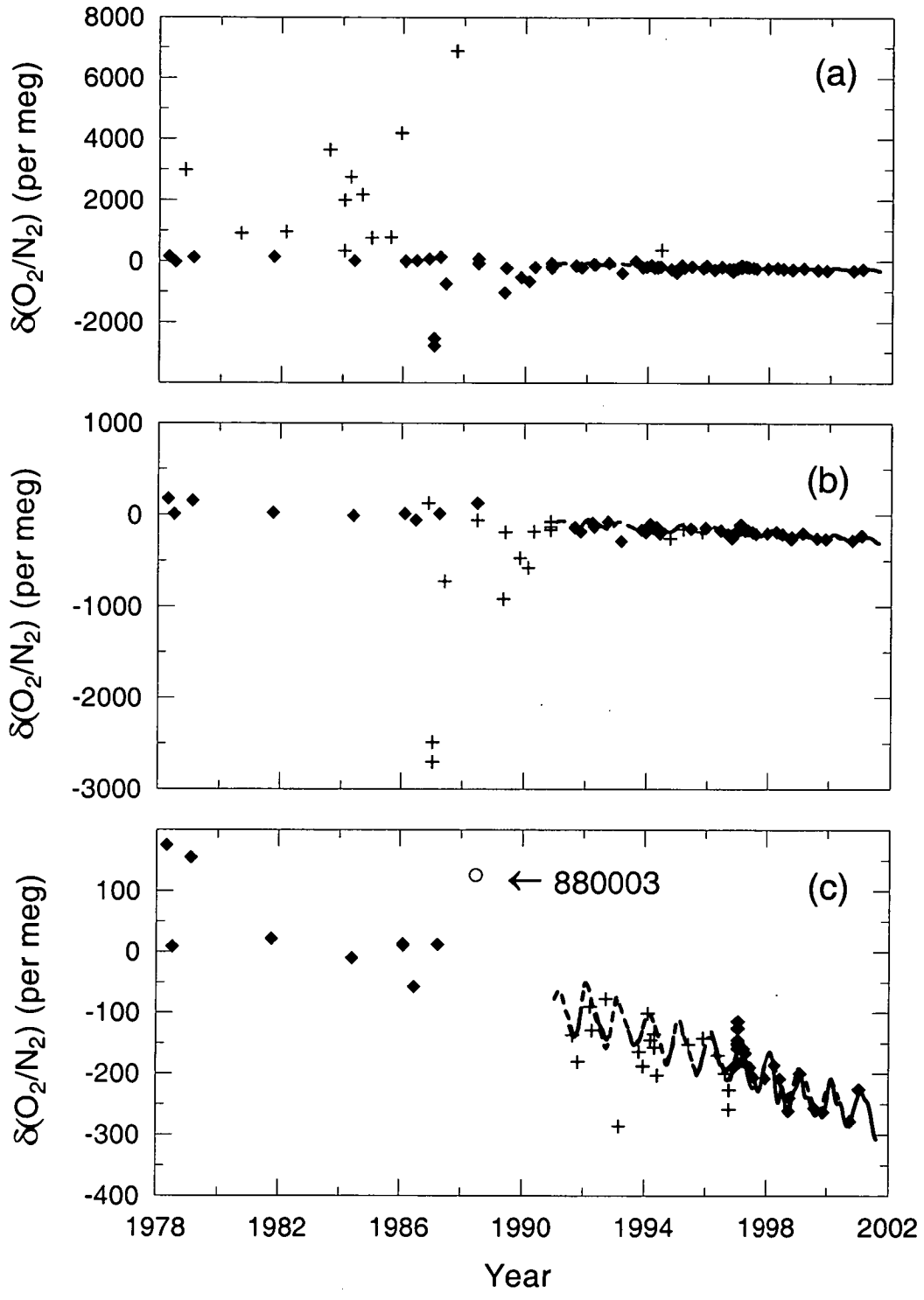

Figure 3.6 Cape Grim $\delta(O_2/N_2)$ from CGAA and glass flask data. CGAA data are distinguished according to retained (diamonds) and rejected (crosses or circles) status at successive steps of quality assessment. Rejected data in respective panels represent samples with a) $\delta^{29}N_2$ enriched by > 37 per meg, b) collection in cylinders pre-filled with pure N_2 and c) sampling error (circle) and pre-fill evacuation through liquid N_2 (crosses). Lines are smoothed curve representations of SIO (dash), URI (dot-dash) and CSIRO (solid) glass flask data.

in the hypothetical $\delta(O_2/N_2)$ curve, but becomes effective for the heavily fractionated samples. The curve is constructed by fitting a smoothed curve to the SIO flask record and linearly extrapolating from 1991 back to the first CGAA sample in 1978 (Sample ID 780001) with seasonality defined by the harmonic component of the curve-fit to the SIO record. Excluded from this comparison are those samples with O_2/N_2 modified by other processes listed below and four samples with enriched $\delta^{29}N_2$ but with pressure already decayed to 1 atm. For each of the 1 atm. samples, $\Delta\delta(O_2/N_2)/\Delta\delta^{29}N_2$ is lower than for samples still pressurised. The discrepancy is attributable to depletion in sample O_2/N_2 caused by exchange between sample and laboratory air at CSIRO. Laboratory air has been shown to be consistently depleted in O_2/N_2 by ~1 ‰.

Anomalies in $\delta(O_2/N_2)$ and $\delta^{29}N_2$ are related by a factor 4.6 (Figure 3.8), larger than the value of 3.9 predicted for effusive fractionation. The observed $\Delta\delta(Ar/N_2)/\Delta\delta(O_2/N_2)$ ratio of 2.4 is lower than the predicted value of 2.8. Discrepancies in both ratios are proportionally larger than for the $\Delta\delta(Ar/N_2)/\Delta\delta^{29}N_2$ and $\Delta\delta^{34}O_2/\Delta\delta^{29}N_2$ ratios in Figure 3.7. If these differences are real, they may reflect influences other than effusion, for example involving molecular shape and size, and possibly surface chemical influences for some species. The possibility of O_2 consumption by chemisorption onto cylinder surfaces is addressed below.

A possible influence involving molecular geometry relates to the large O_2/N_2 fractionation observed in the firn/ice column of polar ice sheets. It has been suggested that the effect is primarily dependent on molecular geometry rather than mass (Battle et al., 1996 and references therein). This hypothesis contends that as

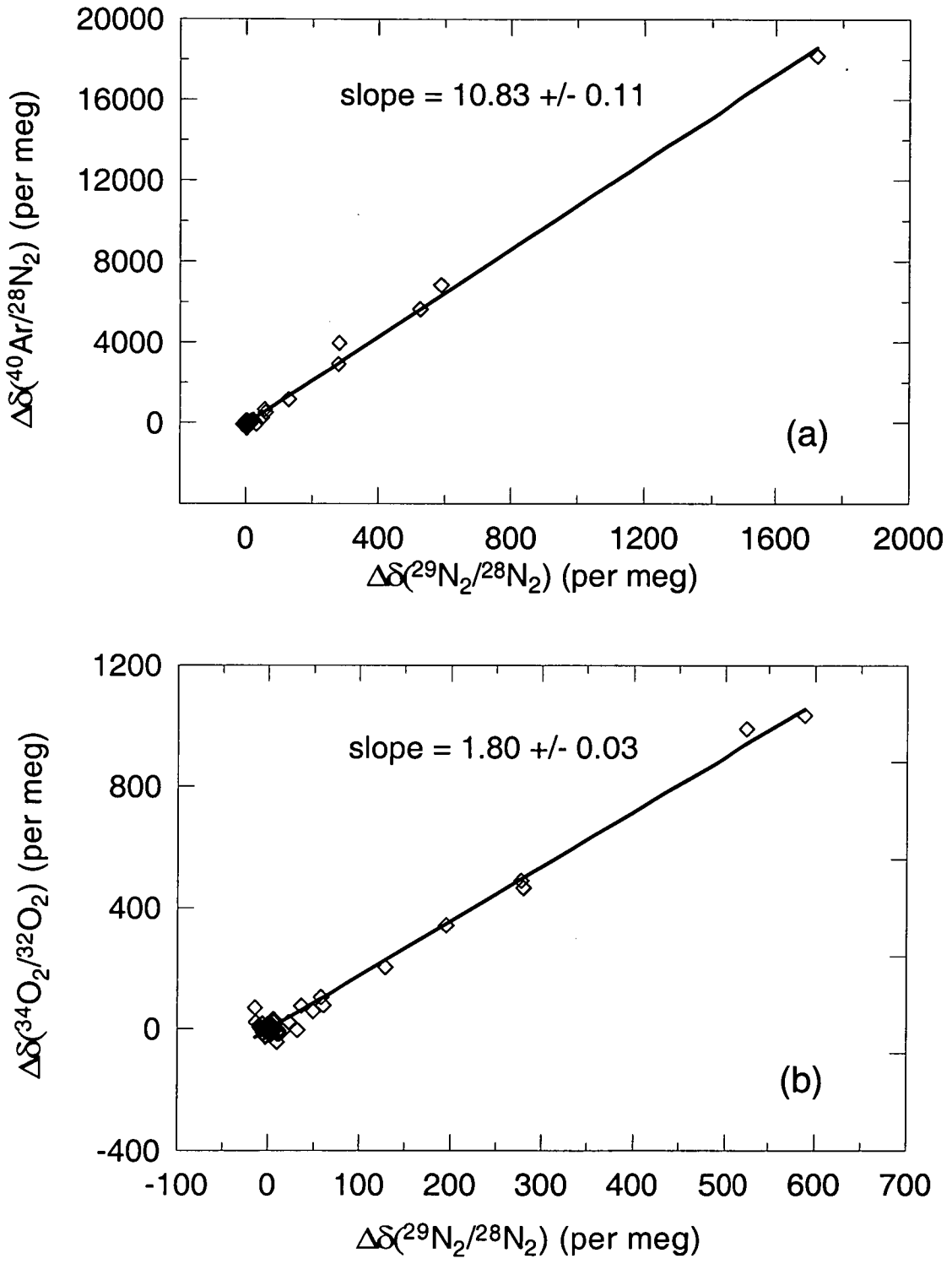

Figure 3.7 Inter-species relationships of $\delta(Ar/N_2)$ and $\delta^{34}O_2$ with respect to $\delta^{29}N_2$ of CGAA samples, with lines of best fit obtained by ODR.

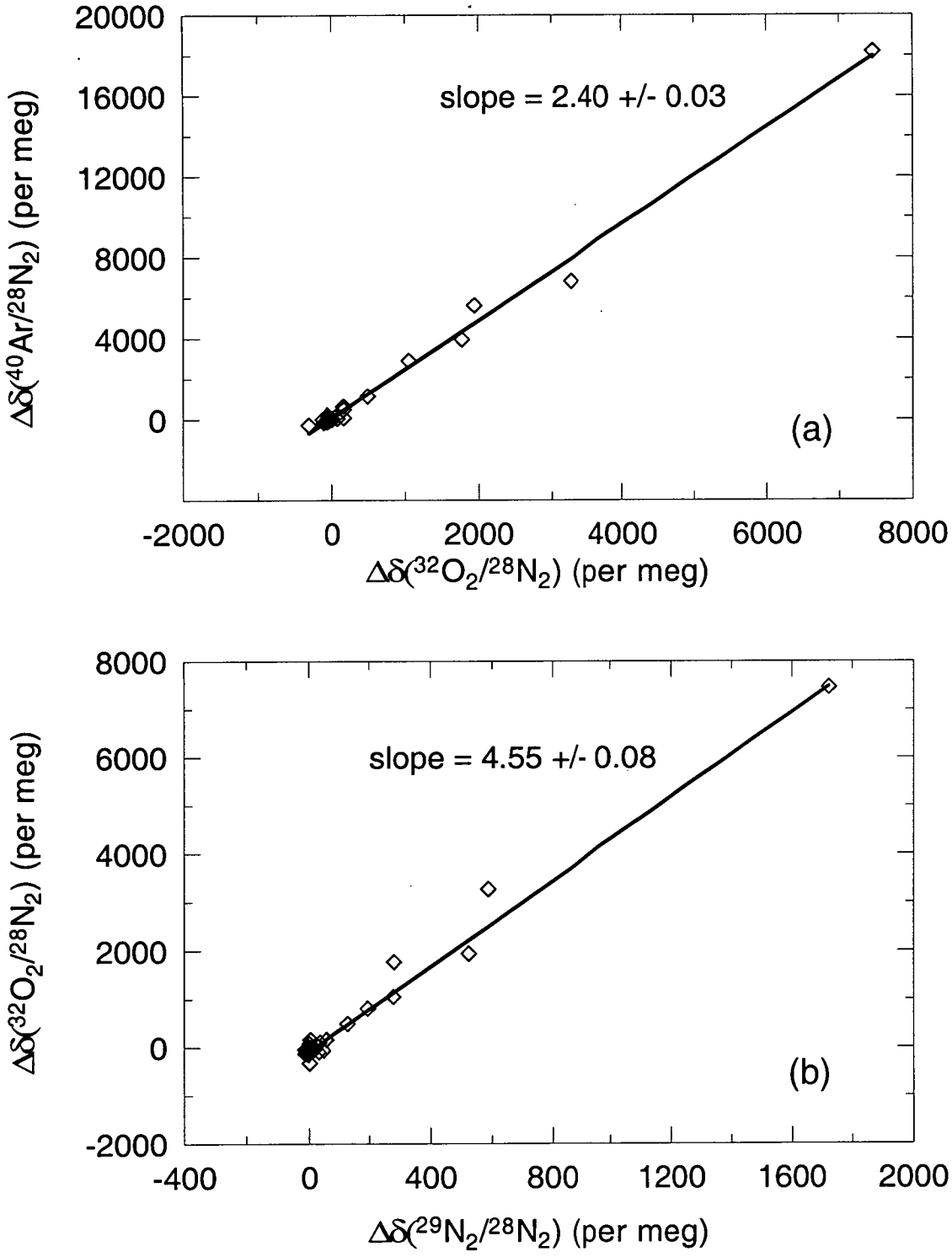

Figure 3.8 Inter-species relationships of $\delta(O_2/N_2)$, $\delta(Ar/N_2)$ and $\delta^{29}N_2$ of CGAA samples, with lines of best fit obtained by ODR. The $\delta(O_2/N_2)$ residuals are calculated here with respect to a hypothetical back-extrapolated curve giving a preliminary estimate of atmospheric $\delta(O_2/N_2)$ at Cape Grim.

bubbles close off at the base of the firn layer, the pressure gradient drives a net O_2/N_2 flux from the bubbles into the open porosity of the firn. The more prolate O_2 molecules are preferentially excluded from the bubbles as channels of molecular size are formed. One could imagine that similar conditions might exist for escape of air through narrow pores in leaking CGAA cylinders. If so, this process would deplete O_2 relative to N_2 in measured CGAA air and cause $\Delta\delta(O_2/N_2)/\Delta\delta^{29}N_2$ points in Figure 3.8b to fall below a line of slope 3.9 that describes the relationship expected from effusion alone. There is no clear evidence for such behaviour, suggesting that molecular geometry is not a dominant factor.

The CGAA $\delta(O_2/N_2)$ data from samples subject to large enrichment in $\delta^{29}N_2$ are rejected, and retained values are corrected using measurements of $\delta^{29}N_2$ and/or $\delta(Ar/N_2)$. Selection of a rejection threshold requires "trading off" a reduction in number of points against increased uncertainty due to correction. Samples with $\delta^{29}N_2$ enrichment of up to 37 per meg are retained. Beyond this, sample density becomes very sparse. Preliminary corrections are applied to the $\delta(O_2/N_2)$ data plotted in Figures 3.6b and 3.6c using $\Delta\delta(O_2/N_2)/\Delta\delta^{29}N_2$ and $\Delta\delta(Ar/N_2)/\Delta\delta(O_2/N_2)$ ratios of 3.9 and 2.8 respectively, based on the theoretical values for effusion. The corrections are applied relative to reference values of 23.7 and 6.3 per meg for $\delta(Ar/N_2)$ and $\delta^{29}N_2$ respectively (on the CSIRO2001 scales defined by 950051), so that CGAA and flask sampling records are directly comparable under the assumption that mean $\delta(Ar/N_2)$ and $\delta^{29}N_2$ differences between techniques are due to mass-dependent fractionation. The mean CGAA/flask differences were calculated from 1996-2001 data. There has been little consumption of air from CGAA samples collected during this period, either through usage or leaks, so that CGAA-flask differences (mean -94 per meg for

$\delta(Ar/N_2)$ and –5.5 for $\delta^{29}N_2$) should reflect fractionation introduced during sampling or analytical procedures. A closer examination of correction factors applicable to retained data (i.e. where observed fractionation is relatively small) and comparison of $\delta(O_2/N_2)$ values calculated using $\delta(Ar/N_2)$ and $\delta^{29}N_2$ as tracers of fractionation artefacts (Section 3.5.2 below) follows discussion of other causes of major O_2/N_2 modification.

3.4.2 Modification of O_2/N_2 by N_2 contamination

From 1986 some samples were collected in 48 and 24 L, Spectra-seal passivated aluminium cylinders (prefix "AL") supplied by Commonwealth Industrial Gases (CIG, now trading as British Oxygen Corporation, BOC) to CSIRO containing high purity N_2 rather than air. As these cylinders were fitted with a single valve, the flushing procedure was modified from that previously used for dual-valve, 35 L cylinders. Rather than "through-flushing" (where air is swept through the length of the cylinder by using one valve with a diptube as the inlet and the other valve as the outlet) a volume of ambient air many times the volume of the cylinder, the aluminium cylinders were flushed by an initial evacuation (using a rotary vane pump and a liquid N_2 cooled trap to prevent back-streaming of oil vapour) followed by several pressurise/vent (P&V) cycles. This method of flushing was far less effective in removing pre-fill contents, with drastic consequences for integrity of resultant sample O_2/N_2 ratio (Figure 3.6b). In the extreme case (sample 870003), a dilution factor of only 1×10^3 (ambient air / residual pre-fill contents) was achieved, implying an error in $\delta(O_2/N_2)$ of -1300 per meg, calculated assuming perfect mixing during flushing. The measured anomaly in this sample was -2700 per meg, double that

predicted, with the difference probably due to either imperfect mixing or error in pressure measurement. Results from all cylinders in this category are rejected.

3.4.3 Flushing procedure dependence

The flushing procedure employed for 35 L cylinders filled between 1988 and mid-1996 (prefixes "S35L-B" and "S35L-C") was different to that used for earlier "S35L-A" collections, more closely following that described above for Spectra-seal treated cylinders. Because the pre-fill gas was natural air and not pure N_2, error due to inadequate dilution of the pre-fill contents is negligible. However, the observed offset and scatter of $\delta(O_2/N_2)$ is larger relative to contemporary flask records (mean difference = -28 ± 56 (std. dev., n = 20) per meg relative to the SIO smooth curve) than for samples collected from mid-1996 onwards using the original procedure of "through-flushing" large volumes of clean air through the cylinders at ambient pressure (mean difference = 1 ± 15 per meg, n = 22; Figure 3.6c).

The cause of this effect is yet to be identified. However, it is clear that processes other than mass-dependent fractionation are responsible. Residuals of $\delta(Ar/N_2)$ and $\delta^{29}N_2$ from the flask records are relatively small and their relationships with $\delta(O_2/N_2)$ residuals are inconsistent with mass dependence. The 1991-2001 CGAA data in Figure 3.6c have been corrected, using mostly $\delta(Ar/N_2)$ anomalies (also $\delta^{29}N_2$ for 7 samples in this period that were not analysed on the Delta^{plus}XL) as tracers of fractionation. The correction accounts for most of the scatter in $\delta(O_2/N_2)$ residuals for samples collected after mid-1996 but has little impact on data before mid-1996. Data from all samples collected using the evacuation/P&V flushing procedure are rejected.

3.4.4 Multi-species evidence of contamination

One further sample (880003; represented by a circle in Figure 3.6c) is rejected on the grounds of anomalous (but stable) composition of other trace species by comparison to another CGAA sample collected the same day and to independent Cape Grim records (e.g. CO_2, CH_4 and N_2O depleted by 1 ppm, 36 ppb and 2 ppb respectively). The large anomalies indicate non-representative sampling. Other retained samples show CO_2 anomalies relative to the CSIRO in-situ record (Steele et al., 1999) within ± 0.9 ppm, except for two drifting samples (-4, -19 ppm; see below). Anomalies in CH_4 relative to the CSIRO flask record (Steele et al., 1996) over the period of overlap from 1986 are within ± 3 ppb except for one drifting sample (+11 ppb). There is no indication of erratic behaviour in the older samples, one of which has recently begun to drift after demonstrated earlier stability.

3.4.5 Dissolution of O_2 and N_2 in condensed water

All data retained to this point are from samples collected in 35 L, stainless steel, internally electropolished cylinders, pre-filled with natural air, "through-flushed" without evacuation before sampling and filled cryogenically. Most samples were filled wet with the bulk of the condensed water (typically 8 ml, maximum 14 ml) being expelled after 1-2 days by inverting the cylinder and briefly opening the valve. Comparison of the volume of water actually expelled with that calculated to have been trapped (from final sample pressure and ambient humidity) for a batch of 6 samples collected in January 1997, suggests that about 1 ml of liquid water remains after venting, presumably either attached as a thin film on the walls of the cylinder or trapped around the edge of the valve orifice. One sample (870004) was dried through

a trap cooled by ethanol/dry ice trap to about -75°C. Another sample, for which collection documentation is unavailable (780001), appears to contain no liquid water as indicated by measurement of $\delta^{18}O$ in CO_2 (Francey et al., 1999a). Exchange of oxygen between CO_2 and water modifies $\delta^{18}O$ by typically -5 to –10 ‰ in "wet" archive samples while 780001 shows a markedly smaller depletion of 1 ‰, relative to measurements from in situ collection of (dried) CO_2 in glass flasks.

Dissolution of air in water alters sample O_2/N_2 ratio owing to different solubilities of O_2 and N_2 (Lide, 1993). The magnitude of the effect on $\delta(O_2/N_2)$ in the air sample is a linear function of the volume of water present with a proportionality factor of -0.47 per meg ml^{-1}, after equilibration at 20°C. This formulation is specific to air contained within a fixed 35 L volume, whereby the relationship can be expressed independently of sample pressure. Small corrections (up to +6 per meg) are applied to all retained data according to volume of water trapped which is estimated from sample volume, pressure and humidity. Where humidity data is unavailable for some of the early samples, a value of 8 g m^{-3} is assumed.

Although estimation of the magnitude of $\delta(O_2/N_2)$ modification by this process appears straightforward, it is noted that unexplained anomalies in $\delta^{13}C$ of CO_2 have been observed in wet CGAA samples. The sign is consistent with fractionation by dissolution into water but with larger than expected magnitude (Francey et al., 1999a). If actual $\delta(O_2/N_2)$ changes were different to those calculated, errors would most likely reflect trapping of more water than expected, equilibration at less than 20°C before venting of the water or incomplete gas-liquid phase equilibration before venting.

3.4.6 Constraints on modification of O_2 by surface processes

Validity of the retained data relies on the assumption of long-term sample stability. Repeat analyses of some CGAA samples have given no clear indication of any instances of drifting O_2/N_2 to within attainable precision. The sample (960051) most frequently analysed (for calibration purposes) has been stable to within about 10 per meg over 5 years (Figure 2.18), but variability of similar magnitude in records of many of the calibration standards, and uncertainty in stability of the primary reference standard (950051) due to usage-related fractionation (Section 2.6.7), complicates identification of any real drift in 960051. These data are of little value in constraining O_2/N_2 stability in CGAA samples to a degree that is useful for global carbon budgeting purposes.

Evidence supporting suitability of these samples is provided by demonstrated stability of other trace species. For example, measurements of CO_2 and CH_4 over periods of up to 9 years show most of these samples to be stable in CO_2 to within ± 0.1 ppm/yr and in CH_4 to within ± 1 ppb/yr. The exceptions are samples 780002 and 790001 which have recently exhibited CO_2 loss at the rate of 0.5 and 0.8 ppm yr^{-1}, respectively and 810002 and 860003 which are growing CH_4 at 3 and 4 ppb yr^{-1}, respectively. Mechanisms responsible for these drifts remain unidentified but there is no evidence to indicate that O_2/N_2 is directly affected. Absence of CO_2 growth excludes the possibility of O_2 depletion by processes leading to complete oxidation of available reduced carbon, such as that present in the form of surface organic residues. Potential for incomplete carbon oxidation can be assessed using measurements of CO. Most samples are stable in CO and all retain mole fractions below 100 ppb, limiting possible O_2 depletion by this process to insignificant levels.

Even allowing for the possibility that CO is formed and bound to the metal surface, thus not appearing in the gas phase, the effect on O_2 can be considered negligible. In the extreme case that the entire internal cylinder surface is covered by a monolayer of CO, formed entirely with the sample at 1 atm. pressure (for maximum possible influence on O_2 mole fraction), O_2 would be depleted by only 15 per meg. This value provides an extreme upper limit. Any actual depletion must be far smaller because 1) CO production would occur at sample pressures higher than 1 atm. with less impact on O_2 mole fraction, 2) extent of surface coverage will be less than 100 % and 3) gas phase levels would be expected to show larger than measured rates of growth due to some desorption of CO from the surfaces. These arguments suggest that any O_2 loss through oxidation of surface organic residues should be negligible.

3.4.7 Corrosion of old CGAA cylinders

A more serious concern is the possibility that O_2 may have been depleted in some samples by formation of metal oxides on the cylinder surfaces, as some cylinders show visible signs of rust on the external surfaces and have developed leaks. This could occur through either dry or wet corrosion (Jastrzebski, 1964). In the absence of water, dry corrosion may proceed through chemisorption of O_2 at the metal-gas interface to form an oxide layer. On stainless steel surfaces, while they remain free of impurities and mechanical stress, such layers are strongly adherent, continuous and relatively impermeable to diffusion of O_2 or metal ions. Thus, once formed, the layers are thin and highly protective, retarding further corrosion.

An important factor is the pre-treatment of the stainless steel, CGAA cylinders. All were internally electropolished before use, a passivation process that electrochemically smooths the metal surface, thereby reducing surface area and

removing impurities. A thin oxide layer is rapidly formed after the treatment, mostly within hours to days. In addition, "S35L-A" series cylinders used for the earliest samples were used as air standards for periods of some years after electropolishing but before CGAA collection. All cylinders used from 1996, and probably also the S35L-B and S35L-C cylinders used from 1990 were exposed to air for periods of at least several months before filling. It is therefore likely that protective oxide layers were established on their surfaces long before they were filled with CGAA air. Even if some dry corrosion has occurred during the life of the CGAA samples, the effect on O_2/N_2 is likely to be small if the oxide layers are thin. This is demonstrated by the above calculation for a monolayer of CO, though noting that oxide layers can be of greater than molecular thickness.

While the protective oxide layers should be well preserved in dry air, this may not hold true for wet CGAA samples that retain traces of liquid water. The nature of the oxidation process changes under these conditions. Wet corrosion can occur at the metal-liquid interface and may penetrate deeper into the surface, thus providing greater scope for O_2 consumption over long periods of storage. Unlike dry corrosion, the oxidation products can become visible as rust. For example, the general governing equation for formation of hydrated ferric oxide is:

$$4Fe + 3O_2 + 2H_2O = 2Fe_2O_3H_2O \qquad (3.2)$$

It is possible to calculate the minimum change in $\delta(O_2/N_2)$ that would occur if all of the retained liquid water (1 ml) was consumed through corrosion. For production of $Fe_2O_3H_2O$ and assuming O_2 is removed from the sample at an initial

pressure of 30 atm., $\delta(O_2/N_2)$ would be depleted by 9000 per meg. This figure is two orders of magnitude larger than the maximum possible change actually encountered in CGAA cylinders, as constrained by the range of atmospheric O_2/N_2 histories that would be consistent with existing knowledge of the global carbon/oxygen cycles. Also, after allowance for fractionation indicated by $\delta(Ar/N_2)$ and $\delta^{29}N_2$, the close agreement in $\delta(O_2/N_2)$ of wet CGAA and dry glass flask samples after mid-1996 shows that corrosion does not result in measurable depletion of O_2 within a few years of collection. While these arguments provide no guarantee that O_2/N_2 in the wet CGAA samples has not been modified by corrosion to a lesser degree, they do demonstrate that even under wet conditions where corrosion is more likely to occur, the internal surfaces have proved to be highly resistant. Together, these lines of evidence give one confidence that, as a minimum case, effects of dry corrosion in the dry samples are likely to be insignificant.

Some rust is visible on the external (not electropolished) surfaces of "S35L-A" cylinders filled between 1978 and 1988 with small leaks resulting in some cases at welded sites. The present reasoning is that the corrosion commenced at Cape Grim around the time of collection, when CGAA cylinders were stored in a shed exposed to the marine atmosphere and in boxes packed with padding (foam and/or newspaper) with cylinders laid on their sides. This would be consistent with observations that a) rust-affected areas are along only one side of the length of those cylinders that were stored at Cape Grim as part of the CGAA and b) no rust is evident on one cylinder which was not filled as a dedicated archive sample but rather as a laboratory standard and was thus presumably returned to CSIRO immediately after collection. One cylinder, for which the sample had leaked away, was cut open

and showed no sign of rust on its internal surface except for the point near the weld site where the leak had developed. By this reconstruction of events, leaks that have formed in rust-affected cylinders have been caused by corrosion migrating inwards, and thus potential impacts of the corrosion on stored air are minimal.

3.4.8 Fractionation corrections applied to retained data

The inter-species relationships in retained data are plotted in Figures 3.9 and 3.10. Here the magnitude of residuals and their range of variation are much smaller than for the full CGAA data set as plotted in Figures 3.7 and 3.8. These inter-species relationships may differ from values observed in heavily fractionated CGAA air because effusion may not be the dominant cause of modification. The retained data could be subject to significant fractionation from other processes, such as those affecting high pressure cylinder air due to usage (Section 2.6.4), to the use of regulators where fractionation was observed to be dependent on the flow rate of air drawn from cylinders (Section 2.6.5), or to sampling techniques.

Data are plotted separately for the older, 1978-1987 (Figure 3.9) and more recent, 1996-2001 (Figure 3.10) CGAA samples because the two sets of samples differ in cylinder type, propensity for leaks, extent of sample consumption and hence susceptibility to fractionation due to different processes. For the older samples, each of the three plots shows behaviour consistent with mass-dependent fractionation. Lines of best fit are plotted 1) for all data and 2) excluding one sample (780002, which appears as an outlier in subsequent time series plots, suggestive of modification by other processes). Occasional, recorded pressure measurements show two of the retained samples (810002 and 840004) to have lost most of their original contents through leaks. One cylinder (870004) shows no signs of either corrosion or

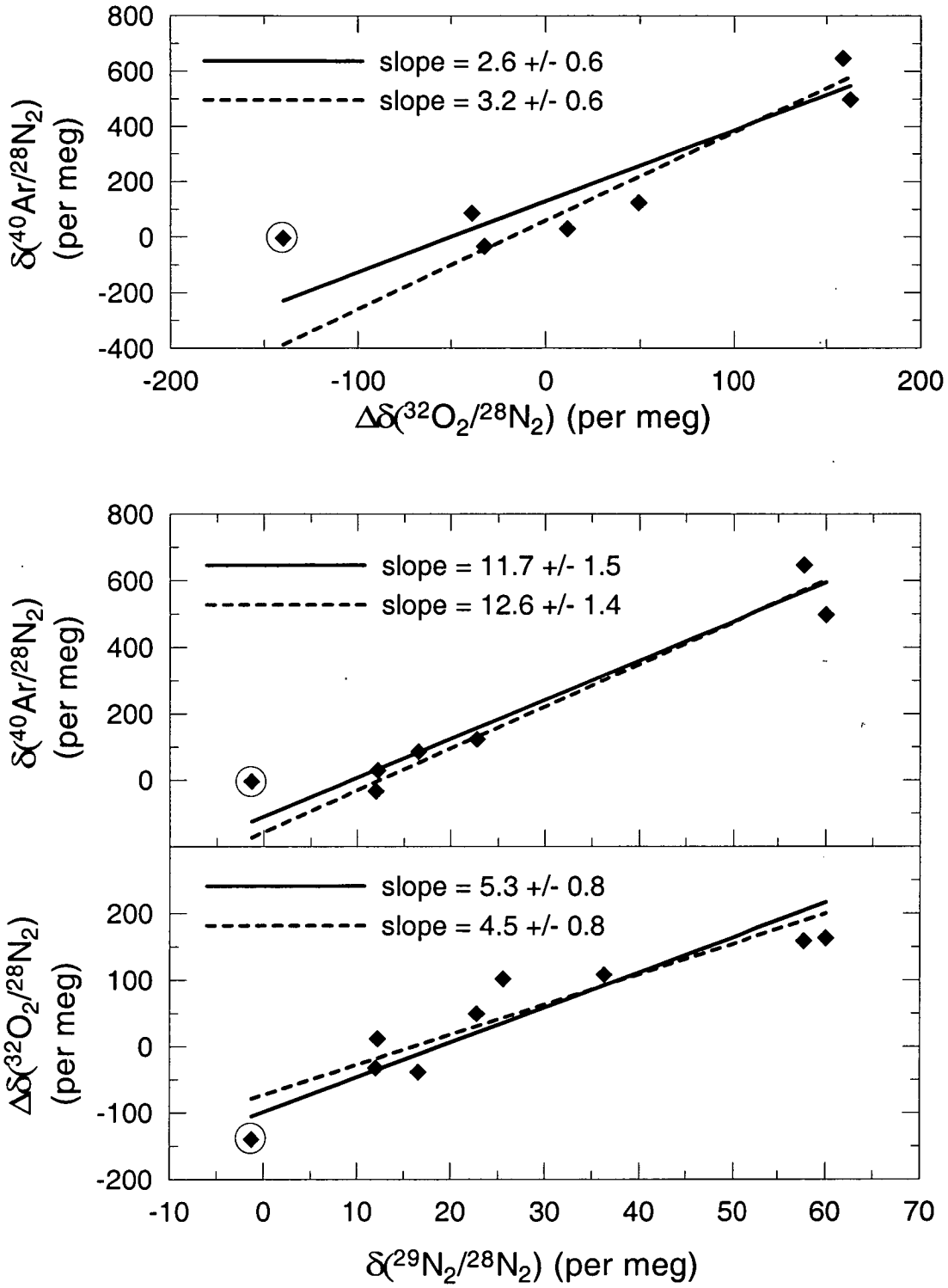

Figure 3.9 Inter-species relationships of $\delta(Ar/N_2)$ and $\delta^{34}O_2$ with respect to $\delta^{29}N_2$ of CGAA data that survive preliminary quality assessment. Lines of best fit were obtained by ODR fits to all plotted data (solid lines) and to all data excluding sample 780002 (dashed lines). 780002 data are circled.

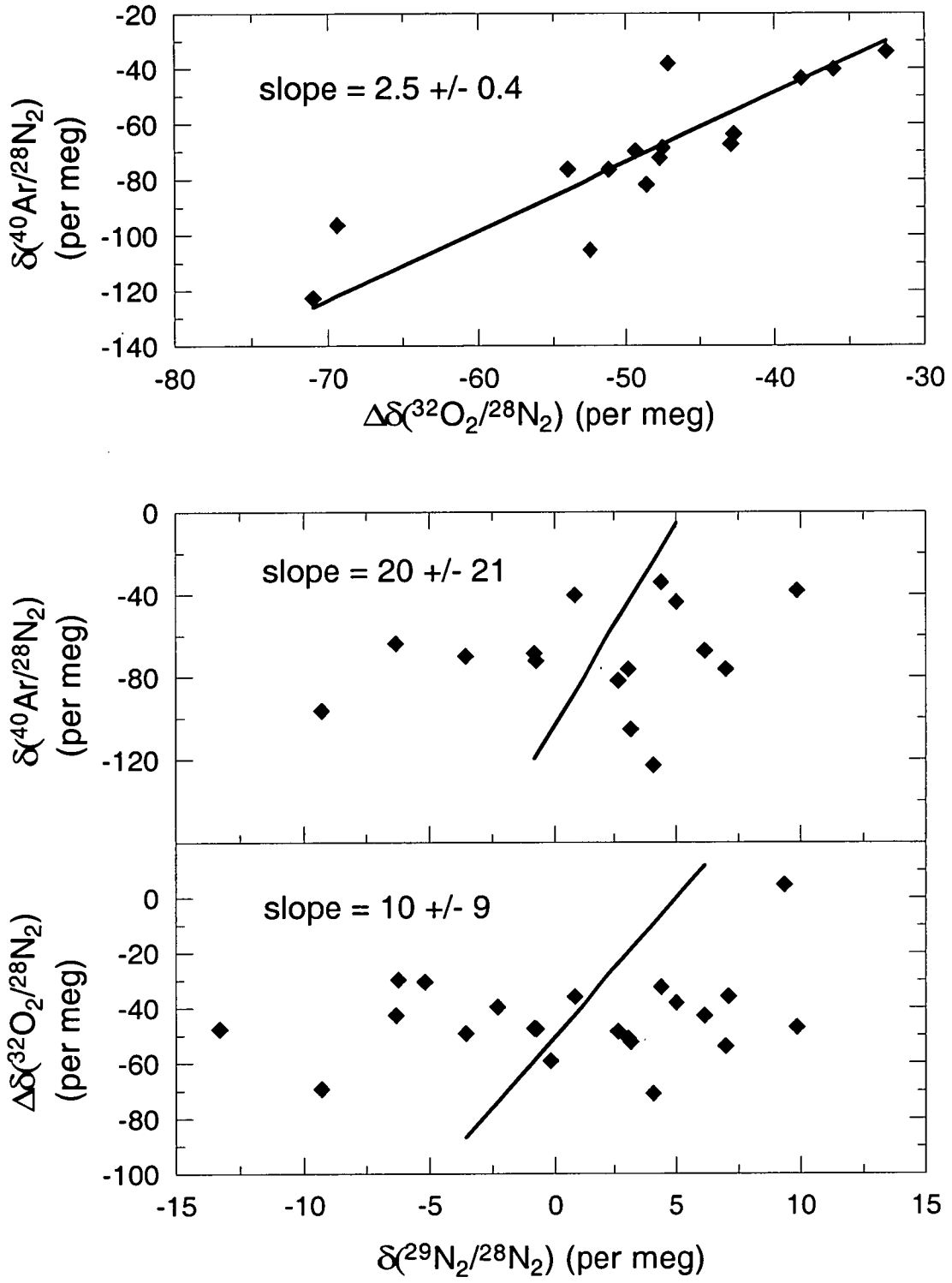

Figure 3.10 Inter-species relationships of $\delta(O_2/N_2)$, $\delta(Ar/N_2)$ and $\delta^{29}N_2$ of CGAA data that survive preliminary quality assessment. Lines of best fit were obtained by ODR. The $\delta(O_2/N_2)$ residuals are calculated here with respect to a hypothetical back-extrapolated curve giving a preliminary estimate of atmospheric $\delta(O_2/N_2)$ at Cape Grim.

leaks. Consumption of air in the remaining six samples appears to have been mainly due to analytical usage. Some loss due to small leaks cannot be discounted, but if this has occurred it has depleted cylinder contents by < 10% over 5-20 years. Thus it is possible that effusion, usage and analysis-related fractionation all contribute to $\delta(O_2/N_2)$ modification in these samples. The data in Figure 3.9 do not distinguish relative contributions from these processes.

The range of variation is much smaller in Figure 3.10, and hence a statistically significant relationship is obtained only for $\delta(Ar/N_2)/\delta(O_2/N_2)$ with a slope of 2.5 ± 0.4. This value is lower than expected for all diffusive processes listed in Table 2.2. Effusion should not be an important influence on these samples because they are not subject to corrosion-related leaks. Any fractionation is more likely to reflect artefacts associated with sampling or analytical techniques. The $\delta(Ar/N_2)/\delta(O_2/N_2)$ slope is close to that observed for regulator-related flow rate dependence (2.2 ± 0.2; Section 2.6.5). This link supports the fractionation being related to the gas handling procedures used to extract air from the cylinders, although the physical nature of the fractionating process remains obscure.

In light of uncertainty as to the specific cause of fractionation and to the precise $\Delta\delta(Ar/N_2)/\Delta\delta(O_2/N_2)$ and $\Delta\delta(O_2/N_2)/\Delta\delta^{29}N_2$ ratios in retained CGAA samples, corrections are applied to all CGAA $\delta(O_2/N_2)$ data using correction factors based on theoretical values for effusion, i.e. 2.8 for $\Delta\delta(Ar/N_2)/\Delta\delta(O_2/N_2)$ and 3.9 for $\Delta\delta(O_2/N_2)/\Delta\delta^{29}N_2$. Allowance is made for uncertainty in the ranges 2.2-3.9 and 2.6-4.5 respectively, which encompass the theoretical values for diffusive processes (Table 2.2) and empirical values for various experimental artefacts reported in this thesis.

3.5 Determination of a 23-year trend in atmospheric O_2/N_2

3.5.1 $\delta^{13}C$ constraints on interannual variability

The relatively small number of selected CGAA samples, and their uneven distribution over the two decades seriously limits the ability to assess the influence of interannual variability on derived trends (and associated assessment of the internal consistency of the retained data). Fortunately, constraints on interannual variability can be explored by comparison with a higher time resolution record of $\delta^{13}C$ in CO_2 extracted from Cape Grim marine air (Francey et al., 1999a). The $\delta^{13}C$ trend can be used to predict variations in the associated $\delta(O_2/N_2)$ trend using a simple 1-box model (Francey et al., 1995; Keeling and Shertz, 1992):

$$\frac{d}{dt}(C_a) = F + N_s + N_b \tag{3.3}$$

$$\frac{d}{dt}(C_a\delta_a) \approx F\delta_f + N_s(\delta_a + \varepsilon_{as}) + N_b(\delta_a + \varepsilon_{ab}) + G_s(\delta_a^s - \delta_a) + G_b(\delta_a^b - \delta_a) \tag{3.4}$$

$$\frac{d}{dt}(O_2)_a \approx R_f F + R_b N_b \tag{3.5}$$

where C_a and $(O_2)_a$ are the atmospheric burdens of CO_2 (in PgC) and O_2 (calculated from $\delta(O_2/N_2)$ assuming negligible change in N_2 and converted to units of PgC equivalent on a mol/mol CO_2:O_2 basis so that 1 per meg $\delta(O_2/N_2)$ = 0.45 PgC equivalent); F, N and G denote carbon fluxes due to fossil fuel emission and cement manufacture, net and gross exchange respectively; subscripts a, f, s and b refer to atmosphere, fossil fuel, oceans and terrestrial biosphere; δ_a^s and δ_a^b represent atmospheric $\delta^{13}C$ in equilibrium with the oceans and terrestrial biosphere; ε_{as} = -1.8

and ε_{ab} = -14.8 represent isotopic discrimination associated with net air-sea (Keeling et al., 1989) and air-biosphere (Lloyd and Farquhar, 1994) fluxes; R_f and R_b are O_2/CO_2 exchange ratios for fossil fuel combustion and cycling through terrestrial biomass. R_f has a mean value of -1.39 but varies with time according to the relative proportions of fuel types combusted (Keeling, 1988; Marland et al., 2001) and R_b = -1.1 (Severinghaus, 1995).

The major uncertainty in applying Equation 3.4 has been the size of the isotopic disequilibrium terms arising from increasing emissions of fossil fuel CO_2. This affects the ability to directly partition net oceanic and terrestrial carbon uptake using $\delta^{13}C$. It has generally been assumed that apart from a steady increase in the global disequilibria in response to continued fossil fuel emissions, their contributions to decadal or shorter period variations in atmospheric $\delta^{13}C$ are negligible. This assumption is supported by recent studies of interannual variability in the global carbon cycle (Francey et al., 2001; Le Quéré et al., submitted) and is also made here, thus enabling use of $\delta^{13}C$ to predict O_2/N_2 variations due to net terrestrial carbon exchange. A "predicted" $\delta(O_2/N_2)$ curve is constructed using isotopic disequilibria values independently estimated for the terrestrial biosphere (Enting et al., 1993) and oceans (based on Tans et al., 1993), mean seasonal cycle defined by the harmonic component of a fit to the SIO $\delta(O_2/N_2)$ record and rates of O_2 consumption by fossil fuel use that allow for transport time of the predominantly NH signal to Cape Grim, with an interhemispheric exchange time of about 1 year (Figure 3.11a).

The CGAA data record a decline in $\delta(O_2/N_2)$ that is broadly consistent with the observed flask sampling records from 1991 – 2001 and with the predicted record

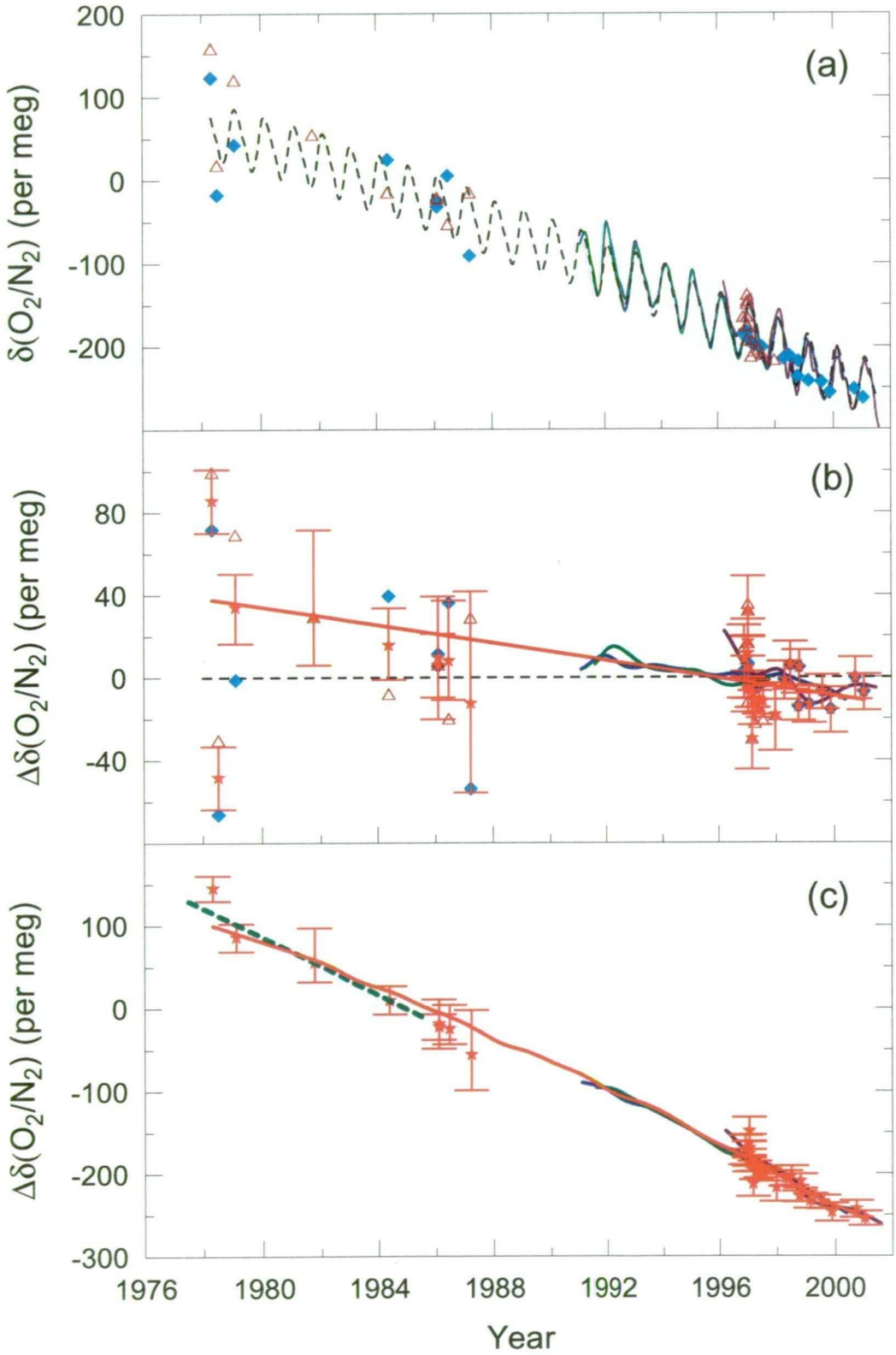
(a)
(b)
(c)
δ(O2/N2) (per meg)
Δδ(O2/N2) (per meg)
Δδ(O2/N2) (per meg)
200
100
0
-100
-200
80
40
0
-40
100
0
-100
-200
-300
1976
1980
1984
1988
1992
1996
2000
Year

Figure 3.11 a) Observations of $\delta(O_2/N_2)$ at Cape Grim. CGAA data are from measurements on the MAT252, corrected for fractionation using $\delta^{29}N_2$ (brown triangles) and the Delta^{plus}XL, corrected using $\delta(Ar/N_2)$ (blue diamonds). Flask sampling records of SIO (blue), URI/PU (green) and CSIRO (magenta) are represented as smooth curves adjusted to the SIO scale. The dashed line shows a predicted $\delta(O_2/N_2)$ curve derived from the Cape Grim $\delta^{13}C$ trend, aligned with the mean of 1996-2001 CGAA data. b) Difference from the predicted $\delta(O_2/N_2)$ curve of panel a). Symbols and lines correspond to those of panel a) with additional data showing mean CGAA data (averaged over both mass spectrometers; red stars), also fitted by linear regression (fit to all CGAA data excluding sample 780002; red line). Error bars (1σ) allow for measurement precision, correction for fractionation and uncertainty in correcting for the seasonal cycle (std. dev. of flask data residuals from the harmonic function = ±5 per meg), assuming negligible temporal change in the phase or amplitude of the mean seasonal cycle. c) Cape Grim $\delta(O_2/N_2)$ data from panel a) with the seasonal cycle removed and showing only retained CGAA data. Symbols and lines are as for a). An optimal fit to CGAA data is shown by the red line. Arbitrarily located above it is the slope of the firn-derived $\delta(O_2/N_2)$ trend of Battle et al. (1996) (green, dashed).

prior to 1991. However, to be useful as a constraint of terrestrial and oceanic carbon uptake, the CGAA trend must be quantified more precisely. Resolution of net carbon fluxes to ±1 PgC yr^{-1} (1σ) averaged over the 23 year period requires that the $\delta(O_2/N_2)$ intercept in 1978 be known to within ±20 per meg if other sources of uncertainty (in fossil fuel emissions etc.) are taken into account. Scatter among the 1978 - 1987 data is larger than expected from analytical uncertainty or on biogeochemical grounds, implying that all sources of modification have not yet been accounted for.

Figure 3.11b shows differences relative to the predicted curve of Figure 3.11a. If $\delta(O_2/N_2)$ interannual variability is well-described by that in the $\delta^{13}C$ record then residuals in this plot would form a straight line through the mean of 1996-2001 CGAA data. A negative slope on the line would imply that the mean disequilibria terms used to generate the predicted curve are underestimated. Much of the

interannual variability in the SIO and URI trends is accounted for by this procedure. The remaining variability in SIO and URI records of Figure 3.11b might reflect oceanic contributions to $\delta(O_2/N_2)$ interannual variability, possibly related to variations in upper ocean ventilation rates or marine biological cycling (Keeling and Severinghaus, 2000; Bender et al., 1996). This is the subject of ongoing studies. For the present purposes, however, the $\delta(O_2/N_2)$ curve predicted from the Cape Grim $\delta^{13}C$ record provides a useful benchmark against which to assess the integrity of the remaining CGAA O_2/N_2 measurements.

3.5.2 Comparison of $\delta(O_2/N_2)$ corrected using $\delta(Ar/N_2)$ and $\delta^{29}N_2$

Figures 3.11a and 3.11b show CGAA $\delta(O_2/N_2)$ values obtained with both MAT252 and Delta^{plus}XL instruments. MAT252 data are corrected for fractionation using $\delta^{29}N_2$. Both $\delta(Ar/N_2)$ and $\delta^{29}N_2$ are measured on the Delta^{plus}XL but $\delta(Ar/N_2)$ is preferred for fractionation corrections owing to superior precision of correction. Significant differences emerge for some 1978-1987 data obtained using the two instruments (and correction procedures), and are too large to be attributed to random measurement uncertainty. Part of the difference for some samples could be due to variation in the true inter-species fractionation ratios among samples, as reflected by error bars for individual points. Some error may also be introduced by uncertainty in $\delta^{29}N_2$ calibration arising from factors other than mass-dependent fractionation. For example, $\delta^{29}N_2$ of 1996-2001 CGAA samples analysed on both mass spectrometers was higher by average 3.6 per meg in Delta^{plus}XL measurements but was not accompanied by differences in $\delta(O_2/N_2)$ expected for effects of fractionation. Such discrepancies would produce errors in corrected $\delta(O_2/N_2)$ of 14 (3.6 x 3.9) per meg

and are probably responsible for the positive 1997 outliers in Figure 3.11b. However, these factors are unlikely to account for all of the differences in 1978-1987 data, suggesting modification of one or more of the measured species by unidentified processes.

The impact of uncertainty in fractionation corrections on determination of the CGAA $\delta(O_2/N_2)$ trend and in inferred carbon fluxes can be estimated for two scenarios. First, if the true $\delta(Ar/N_2)/\delta(O_2/N_2)$ and $\delta(O_2/N_2)/\delta^{29}N_2$ fractionation ratios were identical for all retained CGAA samples and within the range of values defined in Section 3.4.8, inferred carbon fluxes would be in error by up to ±0.4 PgC yr^{-1}. In this case, potential errors are a consequence of the "old" (1978-1987) set of CGAA samples being on average more fractionated than the "recent" (1996-2001) set. Second, if the "old" (1978-1987) and "recent" sets of CGAA samples were subject to fractionation ratios at opposite extremes of the defined ranges, errors would be ±0.8 PgC yr^{-1}. This scenario would require the two sets of samples to be fractionated by different processes and should be viewed as an upper limit to uncertainty due to mass-dependent fractionation.

Ideally, repeat analyses could be used to verify stability or quantify the rate of drift of $\delta(O_2/N_2)$ in the CGAA samples. However, measurements made to this point in time do not reliably constrain any possible drifts due to processes other than fractionation through leaks. A key limitation is that the measurements span a relatively short period compared to the storage time of the older CGAA samples, and uncertainties, perhaps reflecting inconsistency in correction for fractionation using $\delta^{29}N_2$ and $\delta(Ar/N_2)$, are too large to resolve any drift. Most of the "retained", 1978-1987 samples were analysed on 2-3 occasions on the MAT252 in 1996/97 and once

on the Delta^{plus}XL in 2001. As indicated in Figure 3.11, mean $\delta(O_2/N_2)$ values obtained using both instruments show significant differences, after correction for fractionation effects. If these differences were interpreted as genuine $\delta(O_2/N_2)$ drift due to processes other than fractionation, extrapolation of $\delta(O_2/N_2)$ back to the times of sampling would dramatically increase the scatter in Figure 3.11.

A further limitation of this approach relates to stability of calibration over the period of monitoring. One CGAA sample (960051) has been used as a surveillance standard and has thus been analysed more frequently. It exhibits good $\delta(O_2/N_2)$ and $\delta(Ar/N_2)$ relative stability against the other high pressure, metal cylinder standards (Figures 2.18 and 2.19), thus supporting integrity of the 35 L, SS cylinders for faithful preservation of $\delta(O_2/N_2)$ ratio. However uncertainty of ± 1.5 per meg yr^{-1} in stability of the CSIRO2001 $\delta(O_2/N_2)$ scale (see Section 2.6.7) implies uncertainty of the same magnitude in directly establishing any drift in CGAA samples, at least until concurrent records of $\delta(Ar/N_2)$ are long enough to isolate fractionation effects.

Langenfelds et al. (1999b), using MAT252 data only, argued that of the 1978-1987 data, those obtained from the two dry samples (780001 and 870004) were most reliable for defining the long term trend in $\delta(O_2/N_2)$. The assessment was based on three points: 1) that the main potential for error in the 1978-1997 CGAA data was through O_2 loss in the wet samples due to either corrosion or larger than expected dissolution effects, 2) that $\delta(O_2/N_2)$ of the old, wet samples was systematically depleted relative to the two dry samples, consistent with water-related loss and 3) that "wet" CGAA values could not be reconciled with SIO and URI/PU flask sampling records as this would imply biogeochemically unrealistic interannual variability

between 1986 and 1991 (equivalent to a net 1.8 GtC yr^{-1} ocean source sustained over more than 4 years).

In light of the new information gained from reprocessing CSIRO's CGAA and flask sampling data using improved algorithms, and especially with the benefit of $\delta(Ar/N_2)$ measurements, the arguments favouring reliability of the old, "dry" CGAA data no longer carry the same weight. While point 1) above remains a valid concern, points 2) and 3) can no longer be justified. The differences in old CGAA values obtained by $\delta(Ar/N_2)$ and $\delta^{29}N_2$-based corrections, and the larger range of possible correction factors that accommodates fractionation by different processes, cast doubt on there being genuine differences in determination of the trend between old, "wet" and "dry" values, at least for sample 870004. Allowance for systematic, fractionation-related differences between CGAA and flask sampling records has removed the apparent discrepancy between contemporary flask sampling records and the old, "wet" CGAA data. Therefore, subsequent determination of $\delta(O_2/N_2)$ trends is based on both wet and dry, 1978-1987 CGAA data. There is still disagreement among 1978/79 CGAA data that indicates unaccounted modification of at least sample 780002, for which $\delta(O_2/N_2)$ appears substantially depleted. This point is rejected as a 3σ outlier. Best estimates of reconstructed $\delta(O_2/N_2)$ for all samples are taken from the mean of MAT252 and Delta^{plus}XL data, where both are available.

All retained data are plotted in Figure 3.11c after adjustment for the seasonal cycle. The data yield a best estimate of the mean 23-year trend of -15.6 ± 0.5 per meg yr^{-1}. The corresponding curve constructed from $\delta^{13}C$ is in reasonable agreement with both contemporary and firn-air derived slopes. Over the common period of

contemporary records (1991.56 – 1997.76), SIO, URI/PU and CGAA best-fit slopes are –16.2, -15.9 and –17.0 per meg yr^{-1} respectively.

3.5.3 Oceanic influences on atmospheric O_2/N_2

Equations 3.3–3.5 assume no change in atmospheric $\delta(O_2/N_2)$ due to air-sea fluxes on longer than seasonal timescales. However, there is mounting evidence that air-sea O_2/N_2 fluxes might be large enough to significantly impact O_2-based derivation of global carbon budget terms. The 23-year budget evaluated here is subject to uncertainty from both "random" effects on interannual timescales and systematic effects on longer (e.g. decadal) timescales. Keeling and Severinghaus (2000) speculated that $\delta(O_2/N_2)$ variations of order ±10 per meg might plausibly occur on ENSO timescales due to changes in ocean dynamics or biological activity. Observed interannual variations in $\delta(O_2/N_2)$ indicated by SIO and URI/PU records, after allowance for terrestrial forcing as deduced from $\delta^{13}C$ (Figure 3.11b), are within ±10 per meg, thus providing an upper limit for interannual oceanic influences. When applied to a 23-year carbon budget, these effects translate to an upper limit in carbon flux uncertainty of ±0.2 PgC yr^{-1}.

Three mechanisms have been proposed as possible causes of net air-sea O_2/N_2 fluxes on longer (e.g. decadal) timescales. All involve a net source of O_2 to the atmosphere, thus partly offsetting the trend due to fossil fuel combustion.

1. The marine organic carbon pool may have grown due to fertilisation by anthropogenic nitrogen (N) deposited in the oceans (Keeling, 1988). If so, some of the O_2 that is evolved by photosynthesis would be released to the atmosphere. Sequestration of all anthropogenic N through biological

uptake at Redfield C:N ratios of 6.6 would account for uptake of 0.4 PgC yr^{-1} although the actual value is likely to be smaller due to rapid remineralisation of a large fraction of the N (Galloway et al., 1995).

2. Following calculations by Keeling (1988), changes in the ocean's physical capacity to store O_2 can be estimated from observed changes in sea level (Warrick et al., 1996). Assuming sea level has risen by 1.8 mm yr^{-1} with 50% of the rise caused by thermal expansion of water at a mean temperature of 8°C, the resulting O_2 flux into the atmosphere leads to a small budget error of 0.1 ± 0.1 PgC yr^{-1} which would be incorrectly allocated to terrestrial carbon uptake.
3. Some ocean biogeochemical models predict net outgassing of oceanic O_2 to the atmosphere due to changes in ocean dynamics and biology forced by climate change (Matear et al., 2000; Bopp et al., 2001). After allowance for concomitant changes in the oceanic N_2 inventory, the impact on carbon budget calculations is for oceanic carbon uptake to be overestimated by about 0.2-0.5 PgC yr^{-1}.

3.5.4 Partitioning of terrestrial and oceanic CO_2 fluxes

Using the CGAA-derived $\delta(O_2/N_2)$ trend of -15.6 ± 0.5 per meg yr^{-1} (-7.1 PgC yr^{-1} equivalent) and known values for the mean CO_2 trend (1.53 ppm yr^{-1}, equivalent to 3.2 PgC yr^{-1} from CSIRO measurements at Cape Grim) and mean fossil fuel carbon emissions (5.8 PgC yr^{-1}; Marland et al., 2001) between 1978 and 2001, Equations 3.3 and 3.5 give mean net uptake of $+1.6 \pm 0.7$ and $+1.0 \pm 0.8$ PgC yr^{-1} by the oceans and terrestrial biosphere, respectively. Uptake terms represent net storage

of carbon such that the oceanic uptake includes a contribution of 0.4–0.7 PgC yr^{-1} transported by rivers (Sarmiento and Sundquist, 1992). Uncertainties are calculated by quadratically adding components arising from the $\delta(O_2/N_2)$ trend measurement of ±0.5 per meg yr^{-1} (±0.2 PgC yr^{-1}), allowance for possible systematic error due to fractionation correction of CGAA data (±0.6 PgC yr^{-1}) and other experimental artefacts (±0.1 PgC yr^{-1}, summed over multiple effects described in Chapter 2), ±5 % (1σ) in fossil fuel emissions (±0.3 PgC yr^{-1}) (Marland and Rotty, 1984), allowance for ±0.05 in R_b and ±0.04 in R_f (±0.3 PgC yr^{-1}) and ±0.2 PgC yr^{-1} for interannual variability of air-sea O_2/N_2 fluxes. No allowance is made in these calculations for oceanic influences on longer timescales.

The partitioning of net fluxes for the 5-year period 1996-2001 deduced from the CSIRO flask sampling record gives oceanic uptake of 3.2 ± 1.8 and net terrestrial release of 0.2 ± 1.9 PgC yr^{-1}. Larger uncertainties in fluxes derived from the flask sampling record are mainly a consequence of the greater potential impact of interannual variability in oceanic influence on O_2/N_2 (±0.8 PgC yr^{-1}), uncertainty in long term calibration of the CSIRO2001 $\delta(O_2/N_2)$ scale, particularly in relation to stability of standards (±0.6 PgC yr^{-1}) and possible sampling-related artefacts indicated by differences in surface and aircraft-based flask data (±1.5 PgC yr^{-1}). The flask-derived budget does not agree closely with those of SIO and URI/PU for the 1990s, although differences are accommodated by uncertainties (Table 3.2). It is likely that flux differences are partly due to different measurement periods, especially for net terrestrial fluxes that exhibit larger interannual variability (Chapter 4). Although the CSIRO flask sampling data are not as precise as those of SIO and URI/PU, the record presented here nevertheless provides an independent estimate of

Reference	Experimental Method	Time period	Inferred net carbon sink (PgC yr^{-1})	
			Oceans	Land Biosphere
Manning (2001)	flask sampling	1991-1999	1.5 ± 0.4	1.6 ± 0.6
Battle et al. (2000)	flask sampling	1991-1997	2.0 ± 0.6	1.4 ± 1.0
Battle et al. (1996)	South Pole firn	1977-1985	3.0 ± 1.1	-0.4 ± 1.1
This study	Cape Grim Air Archive	1978-2001	1.6 ± 0.7	1.0 ± 0.8
This study	flask sampling	1996-2001	3.2 ± 1.8	-0.2 ± 1.9

Table 3.2 Partitioning of oceanic and terrestrial uptake of fossil carbon from studies using observed of trends in atmospheric O_2. Positive values indicate removal from the atmosphere. All budgets are shown here exclusive of possible long-term oceanic influences on atmospheric O_2/N_2.

the atmospheric $\delta(O_2/N_2)$ trend with extensive consideration given to possible experimental biases.

CGAA-derived flux estimates are not strongly sensitive to a data selection that excludes results obtained using either of the two instruments (and use of $\delta(Ar/N_2)$ or $\delta^{29}N_2$ for fractionation corrections). Analysis of MAT252 data only, gives a slightly steeper $\delta(O_2/N_2)$ trend of -16.3 ± 0.9 per meg yr^{-1} and net oceanic and terrestrial uptake of 1.8 ± 0.8 and 0.8 ± 0.9 PgC yr^{-1}. Delta^{plus}XL data, with fractionation corrections based on $\delta(Ar/N_2)$ give a $\delta(O_2/N_2)$ trend of -15.1 ± 0.6 per meg yr^{-1} and net oceanic and terrestrial uptake of 1.3 ± 0.7 and 1.3 ± 0.8 PgC yr^{-1}.

The main unquantified uncertainties relate to the possibility that old CGAA samples were subject to either 1) modification by an unidentified process and/or 2) possible water-related depletion of O_2, for example through corrosion of cylinder surfaces. If the old, wet CGAA data have been depleted in O_2/N_2, the inferred trend is a lower limit to the rate of O_2/N_2 depletion in the atmosphere and the inferred carbon budget gives lower (upper) limits to the rate of oceanic (terrestrial) uptake of fossil carbon.

If allowance is made for possible long term oceanic influences on atmospheric O_2/N_2, the effect on inferred carbon fluxes is to give higher (lower) rates of net oceanic (terrestrial) carbon uptake by approximately 0.4 ± 0.4 PgC yr^{-1}. Best estimates of carbon fluxes in the 23-year budget then become 2.0 ± 0.9 and 0.6 ± 1.0 PgC yr^{-1} for oceanic and terrestrial uptake respectively.

3.5.5 Estimation of the $\delta^{13}C$ isoflux

The mean 23-year $\delta^{13}C$ isotopic disequilibrium flux (isoflux) is calculated to be 91 ± 16 PgC ‰ yr^{-1} (Table 3.3). This estimate is within the range of values obtained from recent budgeting studies (Tans et al., 1993; Battle et al., 2000; Trudinger, 2000) employing various approaches, including constraints from observations of atmospheric $\delta(O_2/N_2)$. However, because of the trend in atmospheric $\delta^{13}C$, isofluxes vary with time and are thus sensitive to the time period being investigated. A meaningful comparison of independent estimates would need to make allowance for the different time periods.

	ΔCO_2	$\Delta\delta^{13}C$	Product (PgC ‰ yr^{-1})
Atmosphere			-17.2 ± 1.5[a]
Fossil Fuel	5.8 ± 0.3 (PgC yr^{-1})	-20.6[b] ± 0.5[c] (‰)	-119.5 ± 6.8
Oceans	-2.0 ± 0.9 (PgC yr^{-1})	-1.8 ± 0.2[c] (‰)	3.6 ± 1.7
Biosphere	-0.6 ± 1.0 (PgC yr^{-1})	-14.8 ± 2[c] (‰)	8.9 ± 14.8
Disequilibrium Flux (= A-F-O-B)			91 ± 16

Table 3.3 Calculation of the mean $\delta^{13}C$ isoflux for the period 1978-2001 using the CGAA-derived carbon budget that includes allowance for long-term oceanic influence on atmospheric $\delta(O_2/N_2)$.
[a]calculated from the average CO_2 content of the atmosphere for 1978-2001 (744 PgC) and the mean $\delta^{13}C$ trend (-0.023 ± 0.002 ‰ yr^{-1}).
[b]mean annual difference for the period 1982 - 1992 between $\delta^{13}C$ in the atmosphere and from emissions by fossil fuel combustion and cement manufacture (Andres et al., 1996); while $\delta^{13}C$ declined in the atmosphere, the difference remained fairly stable due to consumption of an increasingly higher proportion of lighter carbon fuels.
[c]Uncertainties quoted for oceanic and terrestrial ^{13}C isotopic discrimination and for the difference between atmospheric and fossil $\delta^{13}C$ are estimated from the range of values reported in recent literature.

3.6 Anthropogenic impacts on atmospheric O_2 since pre-industrial times

The knowledge gained from recent decades can be used to estimate the change in atmospheric O_2 over the period of industrialization (Figure 3.12). This calculation uses the land/ocean partitioning of CO_2 uptake determined by Trudinger et al. (1999) based on a deconvolution of the ice core/firn CO_2 record from Law Dome, Antarctica (Etheridge et al., 1996). They determine oceanic CO_2 uptake using a box-diffusion model, calibrated against ^{14}C and assessed against the Law Dome

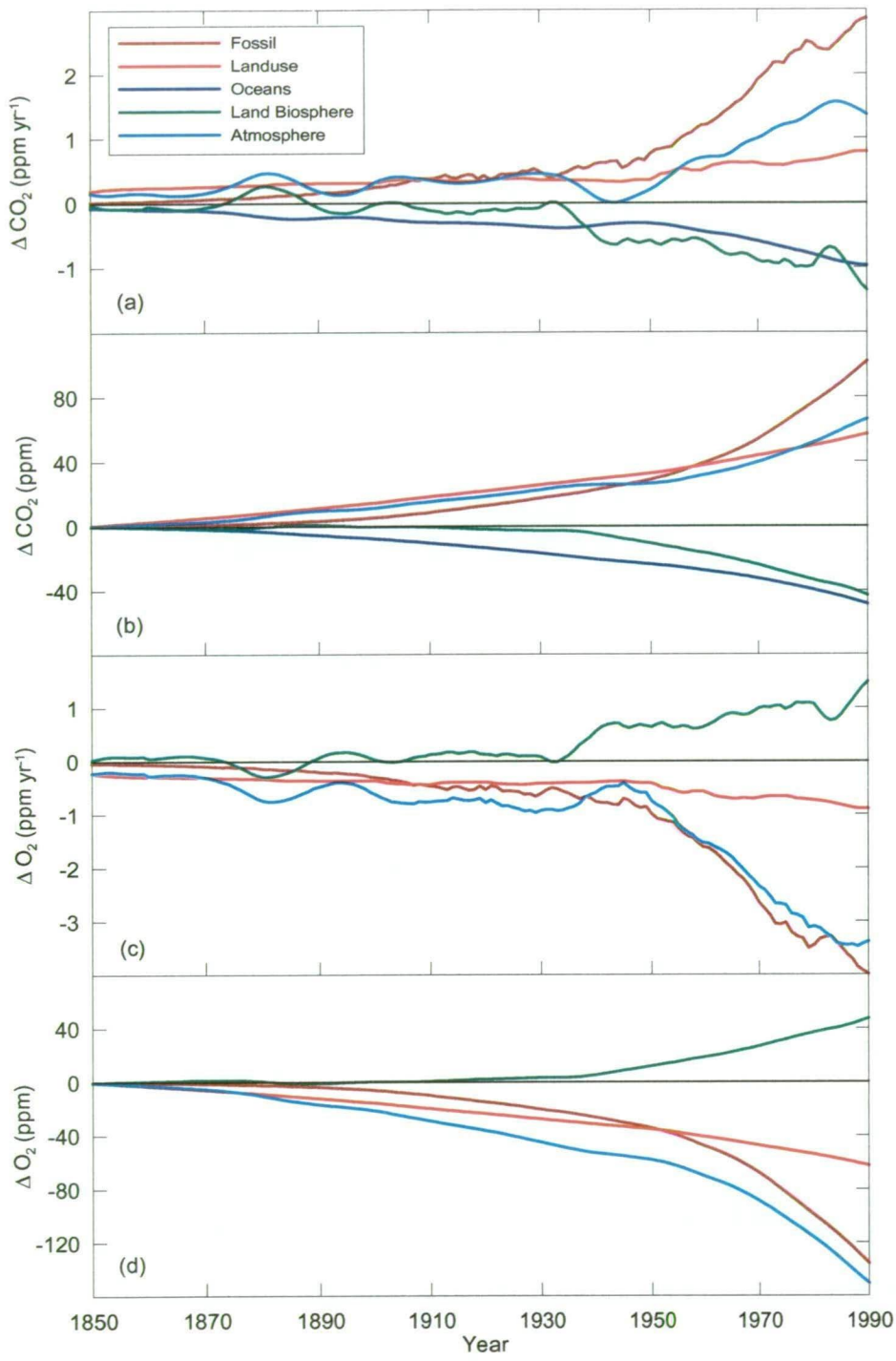

Figure 3.12 Changes in atmospheric CO_2 and O_2 over the period 1850-1990. CO_2 changes are described in terms of a) annual and b) cumulative fluxes. They represent observations of the atmospheric increase from air in Law Dome firn/ice, independent estimates of emissions due to fossil fuel use and land use change, modelled oceanic CO_2 uptake and inferred land biospheric exchange. The land biosphere curves are net of land use change. Corresponding c) annual and d) cumulative O_2 fluxes are calculated assuming no change in oceanic O_2 inventory and known stoichiometric relationships of O_2/CO_2 exchange for terrestrial vegetation (Severinghaus, 1995) and for different fuel types (Keeling, 1988).

$\delta^{13}C$ record of Francey et al. (1999a). The modelled rate of CO_2 uptake at the end of the record is in close agreement with budgets derived from measured $\delta(O_2/N_2)$ trends Table 3.2). Records of fossil fuel use and land use change allow determination of net terrestrial exchange or, as displayed in Figure 3.12, exchange with land biota not including land use change. Corresponding changes in O_2 can be calculated for each of these terms. Depletion of the atmosphere by 151 ppm O_2 is implied for the period 1850-1990. Small, additional changes must also have been incurred before 1850, but early rates of land use change are not well known. An assumed history, involving linear extrapolation of the 1850 estimate back to 0.2 PgC yr^{-1} at 1765 (Enting et al., 1994), would imply pre-1850 O_2 loss of ≥12 ppm. Comparable depletion in earlier centuries is unlikely as the Law Dome CO_2 record shows no significant trend between 1000 and 1800 with variations spanning a range of ±5 ppm. Any CO_2 increase due to land use change is masked by natural variability, for example as observed during the Little Ice Age (Etheridge et al., 1996). Estimates of early fossil fuel use back to 1750 account for a further loss of 1 ppm. Recent observations indicate a trend of approximately –3.5 ppm yr^{-1} during the 1990s. Not included in Figure 3.12 are effects of other, mostly oceanic processes that may have partially offset O_2 consumption (Section 3.5.3). The estimated sum of their cumulative contributions carries large uncertainty, with a best estimate of about 20 ppm.

Thus, by the end of the 20th century, atmospheric O_2 has fallen by an estimated 180 ppm. Over the same time, CO_2 has increased by some 90 ppm. The growth in CO_2 represents a large relative change in concentration of 30% compared to pre-industrial levels. This has significantly changed the radiative balance of the atmosphere and has major implications for Earth's climate. By contrast, the relative

change in O_2 is just –0.1% of its atmospheric burden (approximately 209,500 ppm). A change as small as this is unlikely to be of any direct environmental significance.

Looking to the future, a hypothetical calculation is possible of the maximum depletion that would result from oxidation of all accessible biogenic material. At the end of 1998, proved world fossil fuel reserves (BP Amoco, 1999) amounted to potential O_2 consumption of 600 ppm; however this figure will continue to grow as fuel reserves are boosted by future exploration. Estimates of total carbon stocks (biomass and soils) among four terrestrial biosphere models lie in the range 1150-2300 PgC (Kicklighter et al., 1999), representing a further potential O_2 sink of 600-1200 ppm. If all of the material in both reservoirs were oxidized, atmospheric O_2 would be reduced by upwards of 1200 ppm. This is equivalent to reducing the atmospheric mole fraction from 20.95 to below 20.83%. The extent to which the potential loss is realised depends overwhelmingly on energy and land use practices of future generations.

3.7 Conclusions

Trends in atmospheric $\delta(O_2/N_2)$ have been determined from flask sampling of Cape Grim air between 1996 and 2001, and from analysis of archived Cape Grim air that was collected between 1978 and 2001. The CGAA has provided a unique opportunity to establish the $\delta(O_2/N_2)$ trend over a period double the length of contemporary flask sampling records and with less susceptibility to uncertainties in long term calibration. A multi-species diagnostic approach has identified several causes of significant O_2/N_2 modification in subsets of CGAA samples and enabled correction of data for effects of mass-dependent fractionation.

The CGAA data give a best estimate of the mean 23-year $\delta(O_2/N_2)$ trend of – 15.6 ± 0.5 per meg yr^{-1}. This trend implies net oceanic and terrestrial uptake of fossil carbon of 1.6 ± 0.7 and 1.0 ± 0.8 PgC yr^{-1}, respectively, assuming no oceanic contribution to the $\delta(O_2/N_2)$ trend. The partitioning of carbon fluxes based on the flask sampling results is less precise owing to the shorter length of record and larger experimental uncertainties, mostly relating to gas handling procedures. These data imply net oceanic uptake of 3.2 ± 1.8 and land biosphere release of 0.2 ± 1.9 PgC yr^{-1} between 1996 and 2001.

Possible oceanic influence on atmospheric O_2/N_2 due to processes acting on decadal timescales may involve an O_2 flux to the atmosphere that would otherwise be misinterpreted as being of terrestrial origin. Allowance for such influences would imply oceanic and terrestrial carbon uptake of 2.0 ± 0.9 and 0.6 ± 1.0 PgC yr^{-1} in the 23-year budget, and mean $\delta^{13}C$ isoflux over the same period of 91 ± 16 PgC ‰ yr^{-1}.

These results provide observational evidence of significant uptake of anthropogenic CO_2 by both the oceans and the land biosphere. The rate of oceanic carbon sequestration is in close agreement with results from ocean carbon cycle modelling (e.g. 1.9 PgC yr^{-1} for 1980-1989; Sarmiento et al., 1992) and from observation of the changing oceanic ^{13}C inventory between 1970 and 1990 (2.1 PgC yr^{-1}; Quay et al., 1992), forced by the decline in atmospheric $\delta^{13}CO_2$ due to burning of fossil fuels. The land biosphere is favoured to have been a small net carbon sink, notwithstanding an ongoing source of about 2 PgC yr^{-1} to the atmosphere through predominantly tropical deforestation (Houghton, 1999). Compensating growth of the biosphere is implied, attributable to reforestation, higher rates of net production in

response to climatic trends, fertilisation by elevated levels of atmospheric CO_2 or nitrogen deposition or a combination of these factors (Houghton et al., 1998).

CHAPTER 4

INTERANNUAL VARIABILITY IN ATMOSPHERIC GROWTH RATES OF MULTIPLE TRACE GAS SPECIES

4.1 Introduction

An increasing long-term trend in atmospheric CO_2 and a decreasing trend in its $^{13}C/^{12}C$ isotopic ratio is well established (e.g. Etheridge et al., 1996; Francey et al., 1999a) and can be attributed to combustion of fossil fuels (Marland and Rotty, 1984; Marland et al., 2001) and a significant net flux of CO_2 to the atmosphere as a consequence of land use change (Houghton, 1999). However, the rate of CO_2 increase is not steady, with prominent growth rate variations observed on time scales of 2-5 years. Year-to-year variations in fossil fuel related emissions are relatively small and cannot account for this behaviour. The variations in rates of land use change are also too small, although accounting procedures are not as precise as for fossil fuel emissions so that such carbon flux estimates carry larger uncertainty.

Atmospheric methods to attribute CO_2 exchange between oceanic and terrestrial reservoirs have often employed the observed covariation of CO_2 with either its $\delta^{13}C$ (C.D. Keeling et al., 1989) or the O_2/N_2 ratio (R.F. Keeling et al., 1996). Both tracers preferentially reflect CO_2 exchange with the terrestrial biosphere, $\delta^{13}C$ by way of the much stronger isotopic fractionation associated with terrestrial photosynthesis compared to air-sea exchange, and O_2/N_2 by way of the low solubility of O_2 in the oceans compared to that of CO_2. Early studies of interannual growth rate variations (IAV) in CO_2 using $\delta^{13}C$ drew conflicting conclusions (e.g. Keeling et al., 1995; Francey et al., 1995; Nakazawa et al., 1997). Francey et al. (2001) now report

a consistent relationship between CO_2 and $\delta^{13}C$, indicative of mainly terrestrial IAV forcing, over two decades, with the possible exception of the 1991-93 period.

Results from direct monitoring of O_2/N_2 between 1991 and 1999 also suggest most of the IAV in carbon fluxes is due to terrestrial exchange, with highest net carbon release centred on 1994 and 1998 (Battle et al., 2000; Manning, 2001). While both $\delta^{13}C$ and O_2/N_2 are subject to second-order interactions that potentially complicate interpretation on interannual timescales, both tracers indicate similar estimates of terrestrial IAV forcing over the last decade. Using an inverse model constrained by the spatiotemporal distribution of CO_2 alone, Bousquet et al. (2000) concluded that IAV in terrestrial exchange was twice as large as that of oceanic exchange.

Variations of CO_2 growth rate have been linked to variations in climatic parameters associated with the El Niño Southern Oscillation (ENSO) (e.g. Dettinger and Ghil 1998; Rayner et al., 1999a). Early studies noted the potential for ENSO-related oceanic circulation perturbations to influence atmospheric CO_2 (e.g. Bacastow, 1976). However, recent assessment of ocean processes via CO_2 partial pressure differences (ΔpCO_2) suggests that air-sea fluxes can account for only a minor fraction of the observed variability (Lee et al., 1998; Feely et al., 1999; Le Quéré et al., 2000). These studies indicate suppressed release of CO_2 from tropical ocean upwelling during El Niño periods and a contribution to global IAV of opposite sign to what is observed in the atmosphere. The implication is that the terrestrial contribution to IAV, favouring higher emissions during El Niño periods, must be larger than the net atmospheric signal. On the other hand, climate driven ecosystem models seem able to accommodate much of the observed CO_2 IAV through an ENSO effect on photosynthesis/respiration in terrestrial ecosystems (Kindermann et al.,

1996; Tian et al., 1998; Gerard et al., 1999; Knorr, 2000; Yang and Wang, 2000) with El Niño periods favouring net CO_2 release and La Niña periods net uptake in tropical regions.

This chapter examines the IAV (defined here as perturbations sustained over longer than seasonal timescales, but less than the 8-year period of the data set) of CO_2 between 1992 and 1999 using CSIRO flask sampling data. The analysis includes records of $\delta(O_2/N_2)$ from Cape Grim and of four additional species from CSIRO's global flask sampling network: $\delta^{13}C$ of CO_2, H_2, CH_4 and CO, all of which are measured in the same air samples. Compared to CO_2, interpretation of variations in H_2, CH_4 and CO is complicated by greater uncertainty in global budgets involving a larger number of source/sink processes. Nevertheless, there are common processes and thus, a multi-species analysis can provide additional information for interpretation of IAV.

The monitoring of atmospheric H_2, CH_4 and CO has not been as prolonged or as extensive as is the case for CO_2. IAV in these species has been noted before, but generally related to anomalous events rather than any general climate factor such as ENSO over the whole period of records. For example, Dlugokencky et al., (1994) suggested that observed anti-correlation of IAV in CH_4 growth rate between Northern (NH) and Southern Hemispheres (SH) in 1987-1990 might be explained by variations in the rate of inter-hemispheric exchange. High CH_4 growth rates observed in later years were attributed to other factors, in 1991/92 to a reduced hydroxyl (OH) sink in the tropics resulting from the Mt Pinatubo volcanic eruption (Dlugokencky et al., 1996) and in 1998 to increased emissions from wetlands and boreal biomass burning (Dlugokencky et al., 2001). In the latter case, the increased wetland emissions were linked to climatic variations involving positive temperature and

precipitation anomalies. Brunke et al. (1990) reported IAV in CO at Cape Point, South Africa, over the period 1978-1987 and speculated about a link to ENSO through affected source/sink or atmospheric circulation processes. Novelli et al. (1998) suggested that IAV in CO between 1990 and 1995 included contributions from perturbations to OH due to the Pinatubo eruption and also from biomass burning. IAV in H_2 was observed over a similar period but its causes were not addressed (Novelli et al., 1999).

4.2 Methods

4.2.1 Potential causes of IAV artefacts

Equipment and techniques used for CSIRO GASLAB sample collection and analysis have been documented in Chapter 2 for O_2/N_2, and elsewhere for other species (Francey et al., 1996; Allison and Francey, 1999; Langenfelds et al., 2001a and references therein) and are therefore described only briefly here. Discussion focuses on the extent to which changes in experimental procedure and instrument calibration may produce spurious IAV in atmospheric records. For the global network, some differences in sampling methodology exist among sampling sites and minor variations have been implemented since 1992, involving upgraded pump units and changes in flask type. Extensive testing has established a high level of agreement among collection techniques and characterized trace gas modification due to storage of air in different flask types. Furthermore, these changes were phased in over a period of several years so that any errors would not appear as concerted IAV at all sites and their significance would therefore be diluted in terms of global mean observations. There have been no major changes to analytical equipment or techniques since 1992.

Measurements are supported by rigorous calibration strategies that permit quantification of uncertainties in IAV. For the O_2/N_2 data presented here, it can be shown that experimental uncertainties are large relative to the atmospheric signals of interest, so that the CSIRO O_2/N_2 record from Cape Grim is not a strong constraint of IAV in the carbon cycle. However, for the other species considered here, changes in sampling methodology and uncertainties in calibration are of second-order significance compared to their atmospheric variability.

4.2.2 Sampling techniques

Sampling units currently used at most CSIRO global network sites are similar to that used for O_2/N_2 sampling at Cape Grim (Section 2.8), but are not operated with an absolute pressure relief device. They consist of a diaphragm pump which draws air through a chemical drying agent (anhydrous $Mg(ClO_4)_2$). They were introduced at network sites between 1992 and 1997, superseding older units constructed around metal bellows pumps and employing the same drying technique. Parallel operation of old and new pump units at Cape Grim (CGA) in 1994/95 demonstrated close agreement between the techniques. Similar units, specifically configured for aircraft-based applications have been in service and unchanged since 1992. The two Canadian sites, Alert (ALC) and Estevan Point (EPC), are operated by the Meteorological Service of Canada (formerly Atmospheric Environment Service) and employ a different sampling technique. Air is drawn through a cold trap held below –60°C by a diaphragm pump. Samples are then sent to CSIRO for analysis.

Air is generally collected in glass flasks, though a small number of samples are also collected in electropolished, stainless steel flasks at Cape Grim. The glass flasks are sealed with valves that are fitted with one of three types of O-ring material, PFA (perfluoroalkoxy), PTFE (polytetrafluoroethene) or Viton. Results of parallel

sampling in multiple flask/O-ring combinations at CGA between 1994 and 1999 have been used to evaluate data consistency among different flask types. Laboratory tests have examined stability of sample composition in different flask types for varying periods of up to about 1 year for 0.5 L flasks and more than 2 years for 5 L flasks. Flask storage effects have been shown to be an important consideration for O_2/N_2 (Section 2.7). Measurable drifts have also been observed in some flask types for CO_2, $\delta^{13}C$ and CO (see Cooper et al., 1999 for preliminary results). Relative rates of change among glass flasks have been linked to O-ring material and flask volume. Where drift rates were modest and consistent among flasks of the same type, storage corrections were established and routinely applied to all network data. CO and $\delta^{13}C$ data were rejected from 0.5 L glass flasks with Viton O-rings and CO data from metal flasks, due to drifts being too large or variable to permit reliable correction. Effectiveness of storage drift corrections has been tested by parallel use of different flask types at South Pole (SPU) and Macquarie Island (MQA) where any storage-related errors are accentuated by long storage times of up to 1 year.

If the drift corrections do not precisely capture actual flask storage drifts or if systematic errors are introduced by use of different pumps or flask types, errors can be manifested as false IAV. By using mean differences in measurements obtained from parallel pump unit operation at CGA and flask type comparisons at CGA, SPU and MQA as a constraint of experimental uncertainty, it is possible to estimate uncertainties in inferred changes in atmospheric composition and hence in the fluxes driving global mean IAV. This calculation accounts for actual experimental changes (in equipment and the timing of such changes) implemented at each individual site and makes allowance for mean flask storage times particular to each site. Uncertainties are calculated in a way that is consistent with the treatment of

atmospheric variations (see below). They refer to changes in mixing ratio (or isotopic composition), integrated over a time window of 1.8 years and are calculated to be (1σ) ±0.04 ppm for CO_2, ±0.001 ‰ for $\delta^{13}C$ and ±0.1 ppb for H_2, CO and CH_4. These numbers are within measurement precision for individual samples and suggest that uncertainties introduced by changes in sampling techniques have negligible impact on characterization of IAV in these species.

Other than tests involving overlapping sampling with different drying techniques, the equipment and techniques used for O_2/N_2 sampling at Cape Grim have remained unchanged, and are thus not expected to be a source of spurious IAV. However, there is unexplained systematic variability of about ±20 per meg in $\delta(O_2/N_2)$ differences between ground and aircraft-based sampling in the Cape Grim region that suggests unidentified sources of experimental artefacts (Section 5.3.4). If this were entirely due to time-variant artefacts in Cape Grim data, it would imply uncertainty of ±6 per meg in $\delta(O_2/N_2)$ changes forcing IAV, integrated over 1.8 years. Mean uncertainties associated with drift due to storage in flasks with Viton O-rings are calculated to be ±2 per meg, based on the 1σ uncertainty indicated by the linear regression to test results in Figure 2.20. However, there is a suggestion of larger errors in storage drift correction applying to samples collected in mid-1998 and stored for up to 1 year before analysis (Section 3.3.3).

4.2.3 Analysis

Mixing ratios of CO_2, CH_4, H_2 and CO were determined by gas chromatography (GC). Carbon dioxide and CH_4 were measured on a Carle Series 400 instrument with flame ionization detection (FID), where the separated CO_2 is converted to CH_4 prior to detection by a heated (400°C) nickel catalyst in the

presence of H_2. Carbon monoxide and H_2 were measured on a Trace Analytical Reduction Gas Analyzer (model RGA3), in which the separated CO and H_2 react with heated mercuric oxide (HgO) to produce Hg vapour that is detected by UV absorption. The isotopic composition of CO_2 was determined using a Finnigan MAT252 isotope ratio mass spectrometer (MS), equipped with a Finnigan MT Box C for cryogenic separation of CO_2 from air. The same instruments have been in service since before 1992.

Measurements of all species, including O_2/N_2, are supported by calibration strategies that monitor long term stability of the reference scale, non-linearity in instrument response, and sample handling procedures. Calibration of GC measurements is centred on regular analysis of suites of standards stored in high pressure cylinders with mixing ratios spanning the range of background atmospheric variations. Calibration of $\delta^{13}C$ involves regular analysis of both whole air and pure CO_2 reference gases for characterization of variations due to CO_2 extraction and mass spectrometric influences (Allison and Francey, 1999). Isotopic data are reported in the VPDB-CO_2 scale, CO_2 in the WMO mole fraction scale and CH_4 in the CSIRO94 CH_4 scale, which is derived from and almost identical to the CH_4 scale maintained at National Oceanic and Atmospheric Administration's Climate Monitoring and Diagnostics Laboratory (NOAA/CMDL). The CSIRO CO scale is linked to the scale of NOAA/CMDL by way of a single high pressure cylinder standard near 200 ppb; however measurements are not closely aligned at lower mixing ratios. Hydrogen data are referenced to a scale established at CSIRO by "bootstrapping" to a gravimetrically derived CH_4 scale. Comprehensive descriptions are provided elsewhere of CSIRO GC measurement programs (Langenfelds et al.,

2001a and references therein) and intercomparison with measurements of these species made by NOAA/CMDL (Masarie et al., 2001).

Uncertainties due to instrument calibration and analytical techniques can be estimated from measurements of regularly analyzed, natural air standards that are not actively used for routine calibration and thus provide an independent evaluation of overall instrument performance. Residuals from the long-term mean of each standard were compiled into a single time series per species, and processed in a similar way to that described above for changes in sampling techniques to give uncertainties consistent with the treatment of atmospheric data. Calculated uncertainties (1σ) due to instrument calibration and analytical techniques are ±0.04 ppm for CO_2, ±0.015 ‰ ($\delta^{13}C$), ±0.4 ppb (H_2) ± 1.6 ppb (CO) and ±0.2 ppb (CH_4).

For $\delta(O_2/N_2)$, the corresponding estimates are ±5 per meg based on data from air standards stored in high pressure, metal, cylinders (Table 2.1) and ±6 per meg for the three standards stored in 20 L, glass flasks, which also take into account variability associated with gas handling procedures that is specific to glass flask samples. The value of ±6 per meg for standards in glass flasks implies that $\delta(O_2/N_2)$ calibration and analytical techniques alone account for uncertainty of about ±2.7 PgC in inferred CO_2 fluxes integrated over a timeframe of 1.8 years: Differences between Cape Grim and low altitude, aircraft-sourced data (Section 4.2.2) imply similar uncertainty in carbon flux estimates, to the extent that these differences relate to Cape Grim (rather than aircraft) data and to sampling (rather than analytical) artefacts. Flask storage drift corrections account for a further ±0.9 PgC uncertainty. Added in quadrature, the total experimental uncertainty is in the range ±3-4 PgC, of comparable magnitude to fluxes driving CO_2 IAV on ENSO timescales.

4.3 Atmospheric observations

4.3.1 Global network data (CO_2, $\delta^{13}C$, H_2, CH_4, CO)

The CSIRO global flask network sites used in this study are displayed in Figure 4.1 and listed in Table 4.1 (see also Francey et al., 1996; 1998). They are distributed across latitudes from 90°S to 82°N and, under suitable meteorological conditions, provide access to "background" air that, for this purpose, is representative of zonal mean atmospheric composition. With the exception of MLU and SPU, all surface sites are coastally situated and often encounter air masses characterized by long marine back-trajectories that are far removed from anthropogenic sources and exchange with terrestrial vegetation. Air mass histories of the inland sites MLU and SPU are of similar character, due to little or no surrounding vegetation. Air is routinely sampled under background conditions at all sites. Since 1992, approximately monthly light aircraft flights have sampled the troposphere above Cape Grim to altitudes of 6-8 km, also under background conditions. Data from the 4-8 km altitude range are used here to complement the surface records.

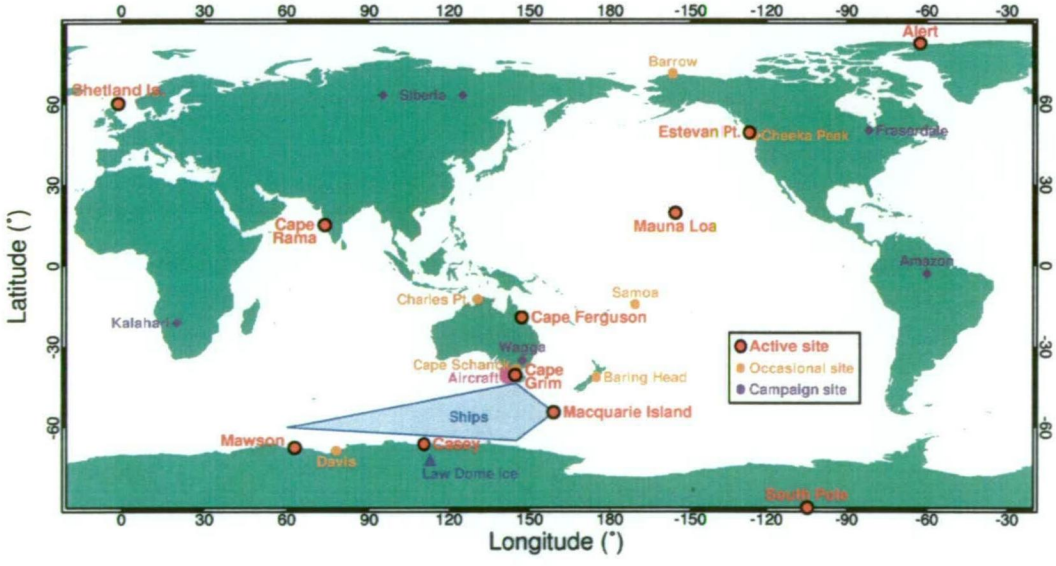

Figure 4.1 CSIRO global flask sampling network sites.

Code	Site[a]	Latitude (°N)	Longitude (°E)	Altitude (m)	Mean Sampling Frequency[b] (samples yr^{-1} / days yr^{-1})
ALC	Alert	82.5	-62.5	6	42 / 21
SIS	Shetland Islands	60.2	-1.2	30	25 / 25
EPC	Estevan Point	49.4	-126.5	39	24 / 12
MLU	Mauna Loa	19.5	-155.6	3397	41 / 21
CFA	Cape Ferguson	-19.3	147.1	2	47 / 17
AIA	Aircraft	-40.5	144.3	4000-8000	97 / 11
CGA	Cape Grim	-40.7	144.7	94	170 / 48
MQA	Macquarie Island	-54.5	159.0	12	51 / 25
MAA	Mawson	-67.6	62.9	32	49 / 29
SPU	South Pole	-90.0	-24.8	2810	30 / 21

Table 4.1 CSIRO global flask sampling network sites.

[a]Selected sites exhibit unbroken records over most or all of the period 1992-1999. Two long-running network sites have been excluded, Cape Rama in India and Charles Point in northern Australia, as they are heavily affected by local continental influences that obscure the smaller IAV signal. Aircraft data are from approximately monthly flights over Cape Grim. Only data from the 4-8 km altitude range are considered here.

[b]Mean sampling frequency refers both to the number of individual air samples collected and the number of days in which air is sampled, averaged over 1992-1999.

Examples of trace gas records for one site, CGA, are shown in Figure 4.2. Points represent measurements from individual flask samples. Two curves are fitted to the data and used in subsequent data analysis: a "smooth" curve that tracks short term variations including the seasonal cycle, and a "trend" curve that is smoothed over a longer period, thus highlighting IAV (see Section 3.3.1). Growth rate curves used for subsequent analysis are the first derivative of the trend curves.

Ability to detect large-scale IAV varies significantly among sites. There are two main factors accounting for this, sampling frequency (Table 4.1) and short term atmospheric variability (Table 4.2). The combination of these factors favours higher resolution of IAV in the high southern hemisphere (HSH) records (CGA and sites to its south). CSIRO sampling frequency is comparatively low at NH sites and northern

air masses are subject to larger short term variability due to closer proximity to continental regions and stronger latitudinal gradients (e.g. Harris et al., 1992).

The contrasting sensitivity of respective hemispheres to detection of global IAV is illustrated by comparison of precision statistics at CGA and MLU in Table 4.2. Similar experimental techniques are employed at both sites but data scatter is larger at MLU, by up to a factor of 7 for CO. This reflects higher short term

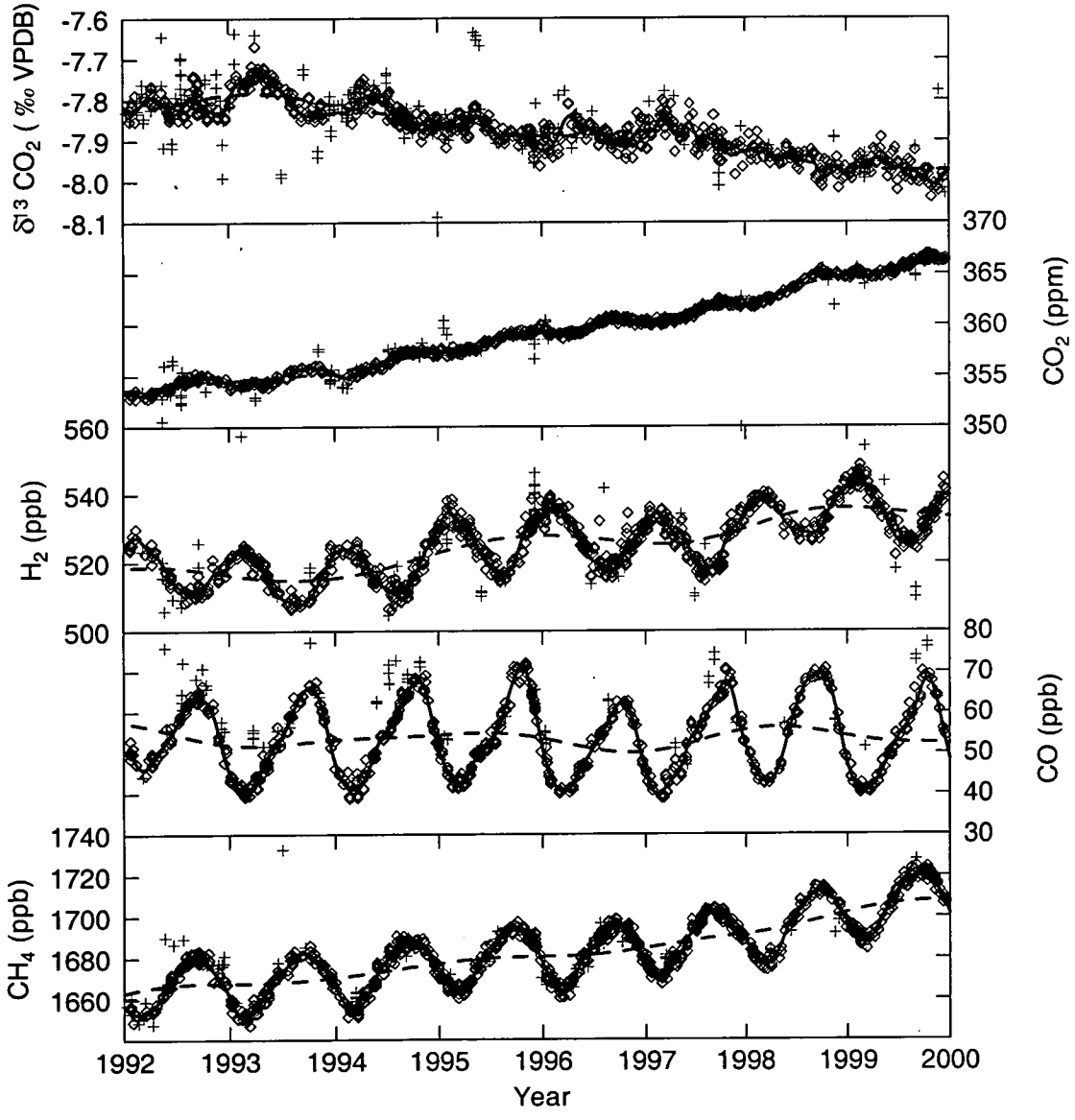

Figure 4.2 Trace gas records from flask sampling at Cape Grim. Data are classified as retained (◇) or rejected (+).

Species	Measurement Precision[a]	External Precision[b]	RSD[c] (Cape Grim)	RSD[c] (Mauna Loa)
$\delta^{13}CO_2$ (‰)	0.01	0.02	0.02	0.03
CO_2 (ppm)	0.09	0.16	0.18	0.46
H_2 (ppb)	1.5	2.0	1.9	4.6
CO (ppb)	0.6	1.5	1.3	9.1
CH_4 (ppb)	2.3	2.4	2.1	10.2
$\delta(O_2/N_2)$ (per meg)	6	18	13	-

Table 4.2 Experimental uncertainties for CSIRO measurements from selected sites in either hemisphere.

[a]Measurement precision is defined here for $\delta^{13}C$ and GC-measured species as the mean (over 7 years) standard deviation of repeat aliquots taken from high pressure cylinders. For $\delta(O_2/N_2)$ it is the standard error of one analysis block on the MAT252 instrument.

[b]External precision is the mean standard deviation in flask pair differences from Cape Grim.

[c]RSD is the residual standard deviation of retained flask data with respect to the smooth curve (see Figure 4.2).

atmospheric variability at MLU and hence better resolution of global IAV at CGA, at least for long-lived species.

In Figure 4.3, 1992-1999 growth rates are plotted for the species measured at all global network sites, as functions of time and latitude. A striking feature is strong correlation in the main component of temporal variations of all species (see also Figure 4.4; discussed further below). All show maxima in 1994/95 and 1997/98 and minima in 1995/96 (note that $\delta^{13}C$ growth rate is inverted in this plot). This feature is somewhat unexpected given that correlations among these species on a global scale have not been previously reported and also because their global budgets are not dominated by the same exchange processes. The link between CO_2 and $\delta^{13}C$ need not come as a surprise, though quantitatively the relationship is important in that it constrains relative contributions of terrestrial and oceanic exchange.

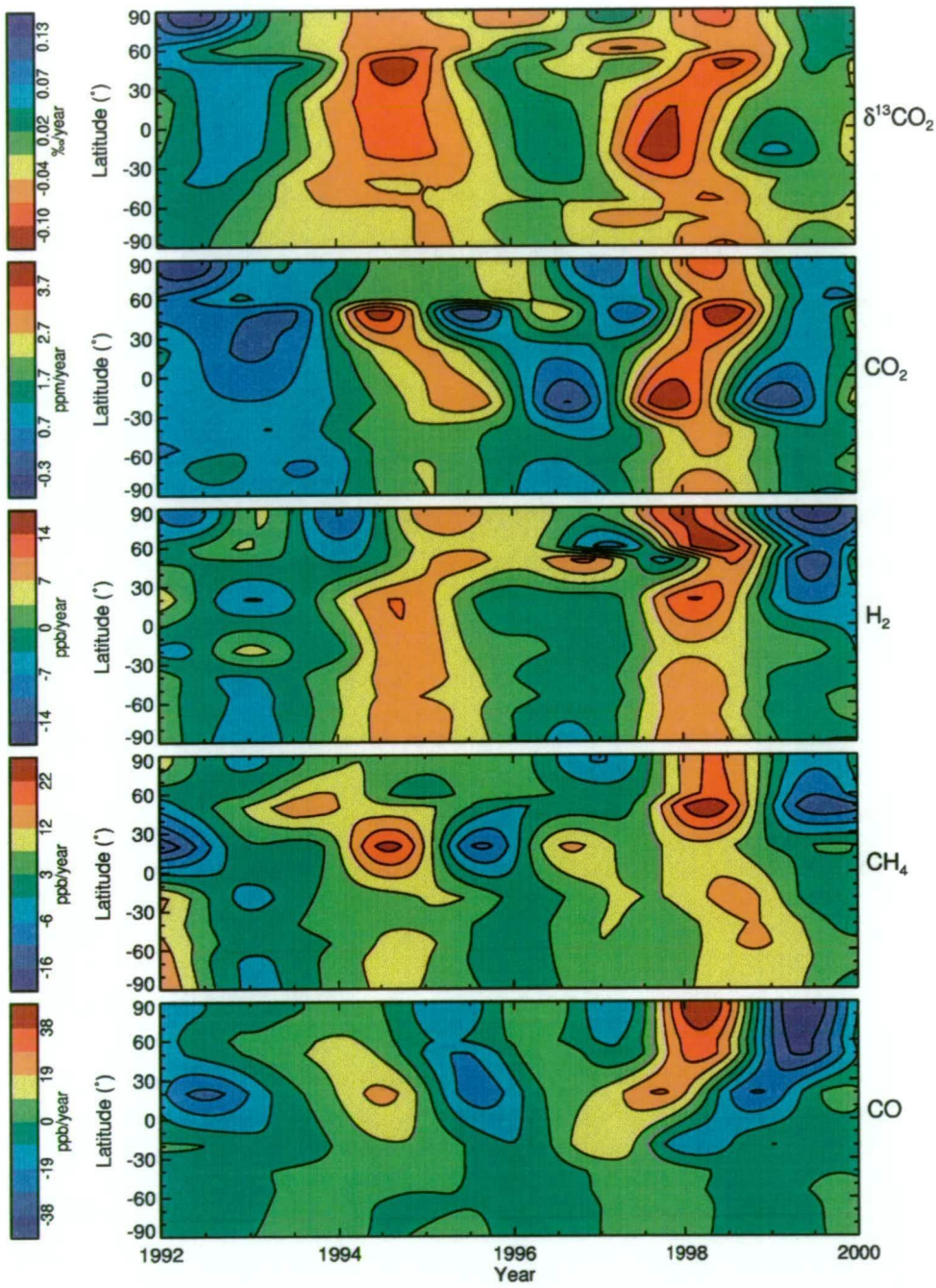

Figure 4.3 Growth rate variations of multiple trace gas species with time and latitude. Each plot is constructed using growth rate curves for the 9 surface sites (Table 4.1; but excluding aircraft data), and by linear interpolation between adjacent sites. There is no smoothing across latitudes. Data from ALC have been extrapolated to 90°N. The $\delta^{13}CO_2$ scale is inverted to show positive correlation with CO_2 through biological exchange.

Differences among sites in the intensity and phase of growth rate variations may hold information about the origins of the IAV forcing but should be viewed with more caution. This is especially the case for the NH where uncertainties are larger. The expectation of better resolution of global IAV in the SH is supported by greater uniformity of growth rate variations among the sites south of 40°S in Figure 4.3. It is suggested that for this study, interpretation of growth rate variations in terms of genuine and significant atmospheric features requires that they be consistent at two or more neighbouring sites.

There is some evidence of latitudinal dependence in the phase of growth rate maxima. A leading tropical signal is suggested for $\delta^{13}C$, CO_2 and CO in 1997/98 while there is no clear dependence in 1994/95. One point that can be made is that the main component of the variability for all species and through both periods is a global phenomenon and is not isolated to limited sites or latitude bands. It cannot be explained by anomalies in meridional transport, which would induce near simultaneous growth rate variations of opposite sign at different latitudes.

There are some instances of growth rate anomalies that are not common to all five tracers. They indicate that even if the main component of IAV for all species is due to a common or closely linked forcing, there are other contributions to IAV from unrelated processes. One prominent example is an increase in CH_4 growth rate during 1996 at MLU and sites to its south that is not mirrored by the other species. This might be due to an anomaly in either a CH_4 source that is independent of the other species or in the rate of inter-hemispheric exchange. The latter possibility would require an anomalously large injection of CH_4-rich NH air into the SH in 1996 and for this to have occurred at a time of the year when the inter-hemispheric CH_4 gradient is large by comparison to the other species (relative to experimental

precision). A preliminary assessment of MLU/CGA differences suggests that such conditions might exist at some times of the year, however a more thorough investigation of this hypothesis would require a transport model and possibly additional data from more suitably located sites.

The multi-species correlation can also be displayed in the form of global mean growth rate variations, obtained by re-applying the curve fit to a mean "smooth curve" averaged over all 9 surface sites (Figure 4.4) after the average seasonal cycle at each site is removed. The phase of both 1994/95 and 1997/98 maxima is closely consistent among all species. Carbon monoxide shows the largest departure with earlier maxima in both years, most notably in 1994 where its maximum precedes that of CO_2 by 7 months. Some of this difference is due to the short lifetime of CO. More specifically, this study uses "adjustment times" (the global average value for CO is about 3 months), which relates to the rate of decay of perturbations in atmospheric mixing ratio rather than the turnover time of total atmospheric burden (Prather et al., 1996a). A simple test using a single box model (described in more detail below), and employing the same algorithms used to generate the growth rate curves of Figures 4.3 and 4.4 shows that CO growth rate maxima inferred from the curve fitting procedure lead actual fluxes by about 3 months. This artefact is a consequence of the smoothing time used by the curve fit being much longer than the CO adjustment time. Growth rates of CO_2 and $\delta^{13}C$ in Figure 4.4 are scaled so as to highlight forcing by terrestrial exchange (with mainly C_3 vegetation). Over the 8-year timeframe, similar amplitude of both curves implies that a major fraction of the variation involves terrestrial forcing.

Also plotted in Figure 4.4 is the (inverted) SOI. Maximum trace gas growth rates in 1994 and 1997/98 coincide with the latter part of El Niño events. This

relationship resembles that observed for CO_2 and the SOI in earlier decades (e.g. Keeling et al., 1989; Rayner et al., 1999a; 1999b), although the absence of elevated CO_2 growth rates during the early part of the extended 1991-1994 event appears as an anomaly in more than 40 years of continuous monitoring of both parameters.

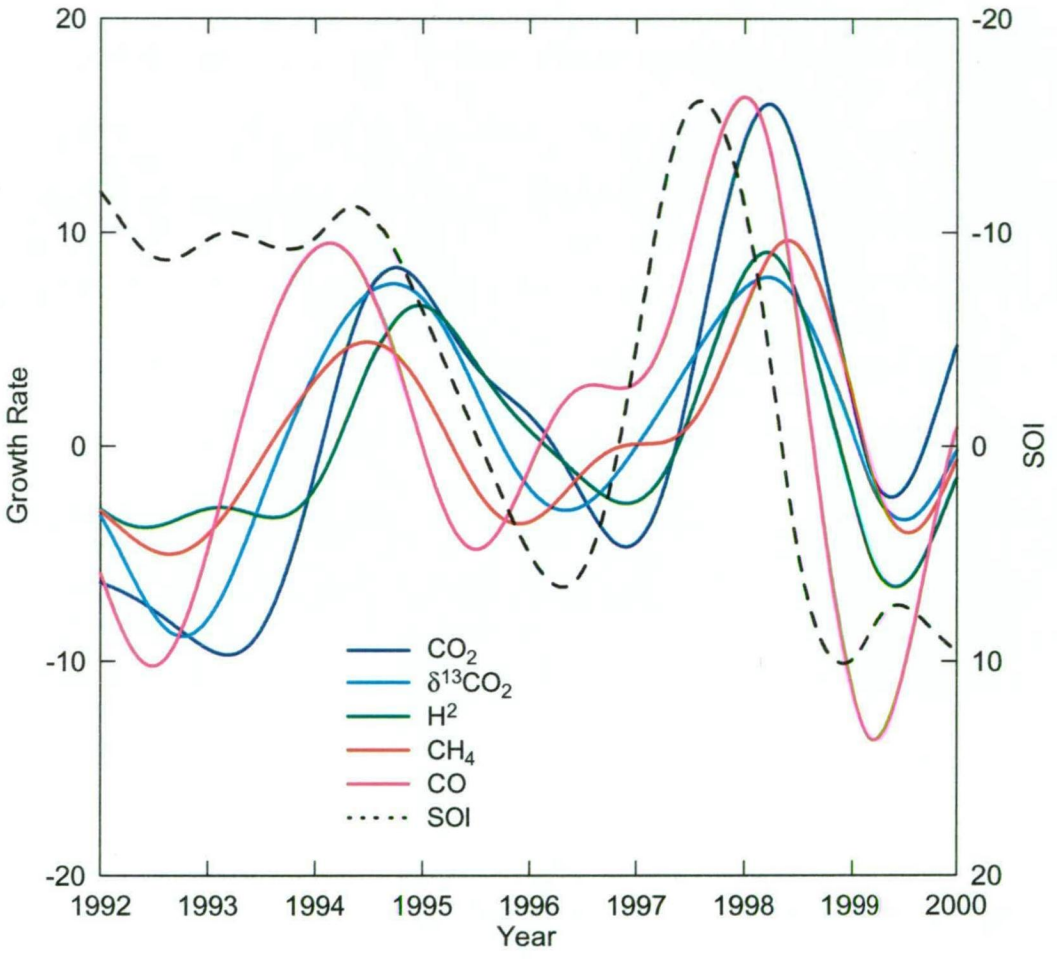

Figure 4.4 Comparison of global mean growth rate curves of multiple trace gas species and the SOI (plotted against the right-hand axis which is inverted). Each growth rate curve is constructed by averaging "smooth curves" from the 9 surface sites (with seasonal cycles removed) and re-applying the curve-fitting procedure. To facilitate direct comparison of the multi-species correlation, mean growth rates (1992.0 – 2000.0) are first subtracted from each curve. CO_2 is scaled by a factor 10 and $\delta^{13}CO_2$ by a factor –160 to make their growth rate variations visible on the same scale and to highlight forcing by terrestrial exchange. Units are: H_2, CH_4 and CO (ppb yr^{-1}); CO_2 (ppm yr^{-1} x 10); $\delta^{13}C$ (‰ yr^{-1} x -160). Perfect correlation between CO_2 and $\delta^{13}C$ in this plot would imply CO_2 exchange characterized by $\delta^{13}C$ discrimination of –17 ‰ with allowance made for modification of $\delta^{13}C$ by isotopic disequilibrium fluxes over the smoothing time.

4.3.2 $\delta(O_2/N_2)$ at Cape Grim

The growth rate of $\delta(O_2/N_2)$ at Cape Grim is plotted in Figure 4.5, as inferred from CSIRO data and from the published records of SIO and URI/PU. The CSIRO curve shows the largest variability due to systematic influences associated with experimental techniques (Section 4.2.3), and thus does not provide a reliable constraint of IAV in $\delta(O_2/N_2)$. Corresponding experimental uncertainties in SIO and URI/PU data are likely to be much smaller, but cannot be easily quantified with available information. A general point is that exacting demands must be placed on $\delta(O_2/N_2)$ measurements for them to be useful in constraining IAV signals. The error analysis for $\delta^{13}C$ in Section 4.2 indicates that CSIRO data carry experimental uncertainty of ±0.015 ‰ (15 per meg) in terms of anomalies integrated over 1.8 years. This translates to uncertainty of about ±0.8 PgC in partitioning of terrestrial and oceanic carbon exchange. For measurements of $\delta(O_2/N_2)$ to deliver the same outcome, they must be robust to ±2 per meg. This differentiation is a consequence of (C_3) terrestrial exchange being characterized by a $\Delta\delta^{13}C/\Delta CO_2$ signature in the atmosphere of about –0.04‰ ppm^{-1} (or –40 per meg ppm^{-1}; as determined by Trudinger (2000) for the ratio of $\delta^{13}C$ and CO_2 responses smoothed over 1.8 years) as compared to a $\Delta\delta(O_2/N_2)/\Delta CO_2$ signature of –5 per meg ppm^{-1}.

Furthermore, there are limitations related to the time span of data in Figure 4.5. The main period of interest for this study (1992-1999) is defined by the timeframe of the CSIRO, multi-species, global network data, but only the SIO $\delta(O_2/N_2)$ record spans the entire period. The CSIRO $\delta(O_2/N_2)$ record only commences in 1996 and the published URI/PU record extends only to 1997.

For these reasons, it is concluded that the available $\delta(O_2/N_2)$ data do not represent as strong a constraint of carbon cycle IAV as the other species used in this study. Instead, $\delta^{13}C$ is used as the primary tracer of IAV in net terrestrial carbon exchange and the remainder of this chapter focuses on the global network CO_2, $\delta^{13}C$, H_2, CH_4 and CO data.

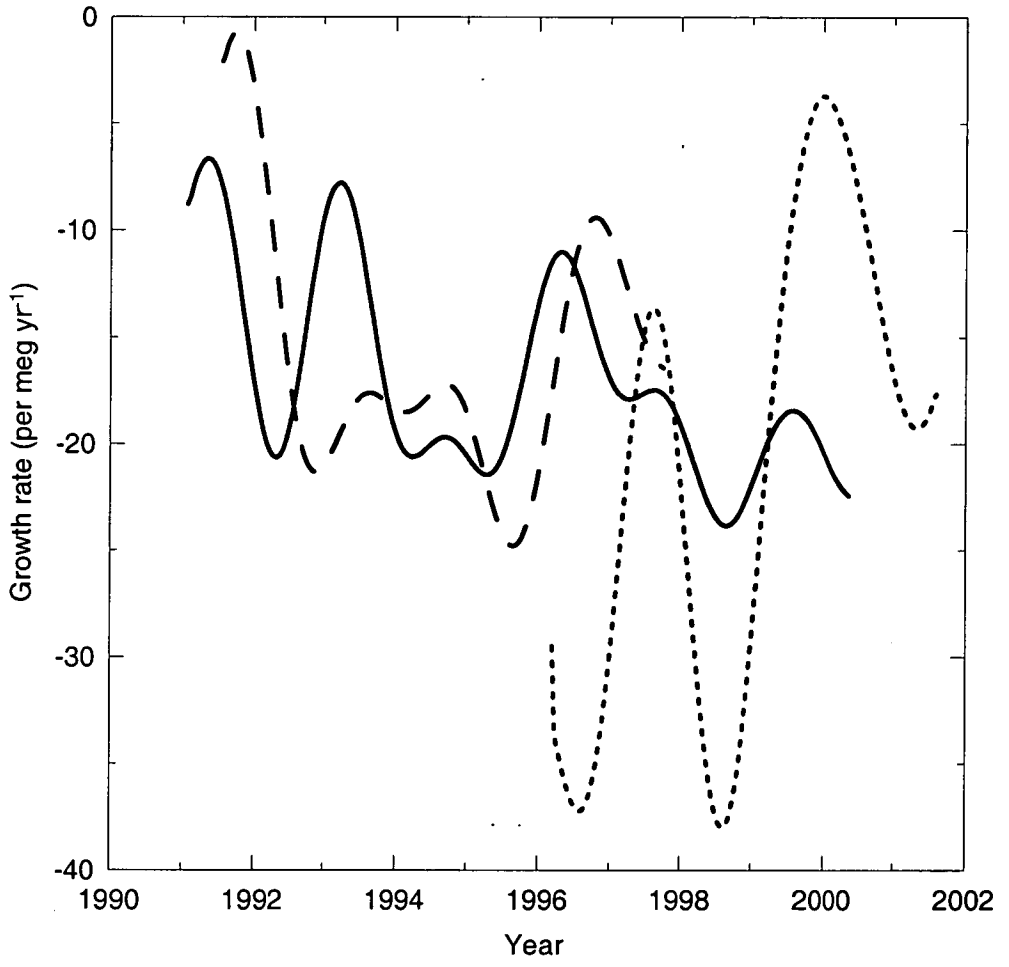

Figure 4.5 Observed $\delta(O_2/N_2)$ growth rate at Cape Grim from flask sampling by SIO (solid), URI/PU (dashed) and CSIRO (dotted).

4.3.3 Aircraft sampling data

Aircraft-based vertical sampling of the troposphere above Cape Grim has revealed large seasonal variations in trace gas composition between 4 and 8 km altitude. Between July and November, vertical profiles frequently show distinct plumes in limited altitude bands that are enriched in CO_2, CO, CH_4, H_2 and depleted in $\delta^{13}C$ of CO_2 with respect to background surface air. Through analysis of inter-species relationships and air mass histories for 1992-1997 data, Pak (2000) attributed the observed trace gas enrichment to emissions from biomass burning. Plume back-trajectories were traced to the SH tropics where they crossed land masses subject to extensive biomass burning during the dry season. Transit times to Cape Grim were typically 8 and 13 days from southern Africa and South America, respectively. Longer times apply to transport from northern Australia and South-east Asia.

The vertical profile data exhibit IAV in the magnitude of trace gas enrichment of the mid-tropospheric plumes. This is most dramatically illustrated by CO (Figure 4.6) for which the phase of IAV was similar to that observed globally at the surface but with amplitude substantially larger than at Cape Grim and other SH sites. There was marked enrichment in mid-tropospheric CO with respect to Cape Grim surface data, centred on 1994 and 1997. High values were also observed in 1999 but appeared during a period of low sampling frequency and were dominated by data from a single profile. Growth rate curves for other species were generally well correlated with surface data, however uncertainties are larger because of the relatively low sampling frequency (mean 11 days yr^{-1}) and the episodic nature of enriched plumes. The aircraft data suggest that the SH mid-troposphere carries strong evidence of emissions from the same source(s) forcing the global IAV but with greater intensity, at least for the short-lived species CO.

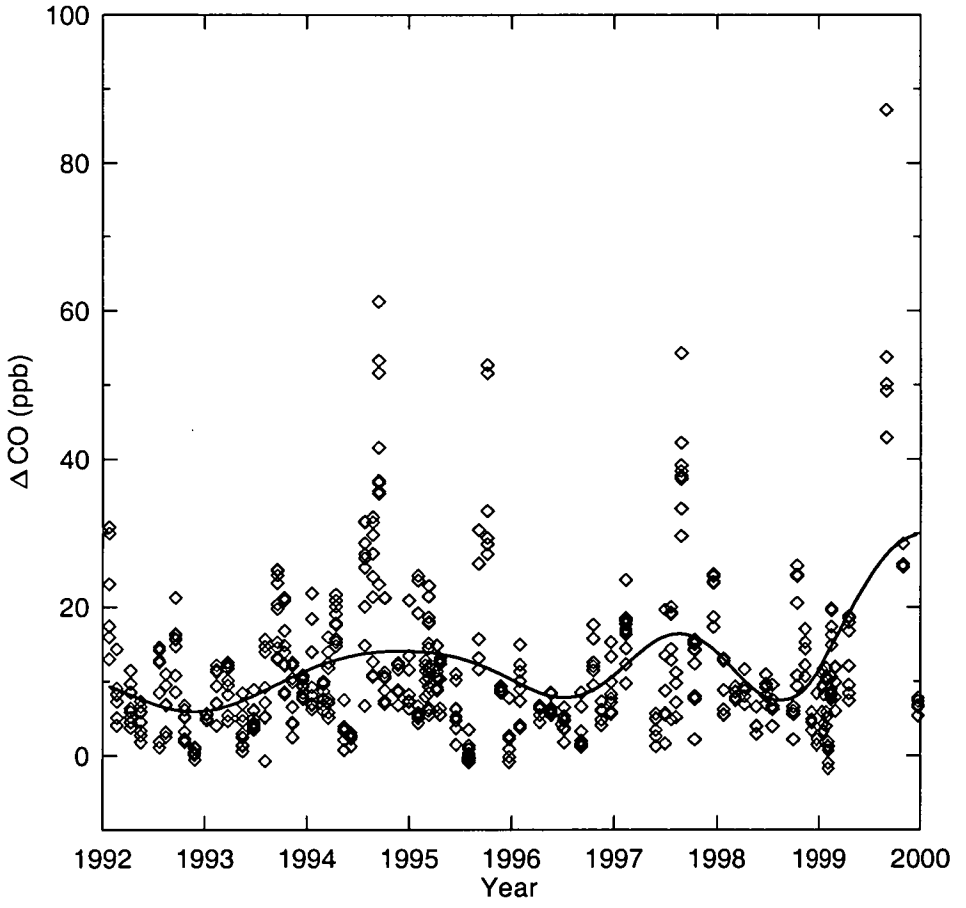

Figure 4.6 The difference in mid-tropospheric CO with respect to the surface at Cape Grim. Points are from aircraft-based flask sampling in the 4-8 km altitude range above Cape Grim, with the Cape Grim "smooth curve" subtracted. The residuals are fitted with a "trend curve".

4.4 Source attribution

4.4.1 Global trace gas budgets

A central issue for this study is whether all species are responding to the same biogeochemical process or perhaps a combination of processes closely linked to a common climatic forcing such as ENSO. Consider the sources (Table 4.3). Substantial amounts of CO_2 are released to the atmosphere by combustion of fossil fuels and biomass burning. Oceans and terrestrial ecosystems may be either net sources or sinks, reflecting imbalance in large, opposing fluxes. Sources of H_2 and CO are closely linked; major sources are photochemical production through

	CO_2 (PgC y^{-1})	H_2 (Tg y^{-1})	CO (Tg y^{-1})	CH_4 (Tg y^{-1})
Sources:				
Fossil fuels:				
combustion	6 - 7	15 -20	300 - 800	0 - 2
fugitive emissions				50 - 80
Terrestrial:				
vegetation/soils	60 - 120		50 - 160	
biomass burning	1 - 3	15 - 20	370 - 1250	25 - 70
landfills				20 - 40
rice paddies				40 - 280
natural wetlands				40 - 150
Animals:				
termites				20 - 150
ruminant animals				60 - 160
Photochemical:				
oxidation of CH_4		7 - 29	600 - 950	
oxidation of NMHCs		14 - 25	290 - 1000	
Oceans	60 - 100	3 - 4	10 - 100	4 - 65
Sinks:				
Terrestrial:				
photosynthesis	60 - 120			
soils		56 - 90	180 - 390	10 - 30
Photochemical:				
tropospheric OH		6 - 19	2000 - 3200	380 - 490
stratosphere			80 - 140	40 - 70
Oceans	60 - 100			

Table 4.3 Trace gas fluxes by source/sink type. Values are shown as approximate ranges from recent budgeting studies of CO_2 (Tans et al., 1993; Siegenthaler and Sarmiento, 1993; Schimel et al., 1996; Heimann and Maier-Reimer, 1996; Waring et al., 1998; Kicklighter et al., 1999), H_2 (Novelli et al., 1999; Warneck, 1988), CO (Warneck, 1988; Bergamaschi et al., 2000a, 2000b; Holloway et al., 2000) and CH_4 (Fung et al., 1991, Warneck, 1988, Prather et al., 1996a).

oxidation of CH_4 and non-methane hydrocarbons (NMHCs) by OH, and combustion of both fossil fuels and biomass. Oceans are a minor source of both gases and a small amount of CO is emitted directly from vegetation. The global CH_4 budget comprises a wider range of sources falling within the broader categories of microbial (natural wetlands, rice paddies, oceans, ruminant animals and landfills), fossil fuel (natural gas leakage, coal mining) and biomass burning. Other than biomass burning, the only sources common to all species on these timescales are fossil fuel use and oceans, both of which can be excluded as sole forcing mechanisms on the grounds that magnitudes of implied flux variations are unrealistically high for at least some of the species. A primary oceanic forcing of CO_2 IAV is further contradicted by the $\delta^{13}C$ data.

Similar arguments rule out changes in sink processes. The main sink of CO and CH_4 is oxidation by OH. Although H_2 is itself destroyed by OH, it is also a by-product of CH_4 destruction and a net product of OH photochemistry (Novelli et al., 1999). CO_2 is the end-product of both CO and CH_4 (via CO) oxidation. Thus variations in OH concentration would produce anti-correlation in growth rates of CO and CH_4 (net loss due to higher OH) against those of H_2 and CO_2 (net gain). Soils are a major sink of H_2 but only minor sinks of CH_4 and CO, and are a source of CO_2. Thus, if the observed IAV were to be explained by a single exchange process, the current state of knowledge of the global budgets of these trace gases dictates that biomass burning is the only plausible candidate. While biomass burning has previously been associated with IAV of CO and CH_4, it has not been identified as a major contributor to IAV in CO_2 or H_2. However, it is known that biomass burning is a significant source of these and other gases (e.g. Crutzen and Andreae, 1990;

Andreae and Merlet, 2001) and that the extent of emissions can vary dramatically from year to year, at least on regional scales.

4.4.2 Other mid-tropospheric observations

It was shown in Figure 4.6 that CO in the mid-troposphere above Cape Grim exhibits IAV of similar phase to that at the surface but with larger amplitude. Concordant IAV has previously been reported for products of biomass burning in the free troposphere. Intense, seasonal CO maxima were observed in 1994, 1995 and 1997 above Lauder, New Zealand, and linked to seasonal maxima in aerosol (Jones et al., 2001). Regular flask sampling from aircraft in the 8.5-13 km altitude range above the western Pacific showed prominent CO maxima in late 1994 and late 1997 (Matsueda et al., 1999). Positive tropospheric ozone (O_3) anomalies were found in spectroscopic and ozonesonde data over Indonesia at the same times (Fujiwara et al., 1999; 2000) and from satellite-based measurements above South-east Asia in 1997 (Thompson et al., 2001). Spectroscopic measurements of CO, hydrogen cyanide (HCN) and ethane (C_2H_6) above Mauna Loa between 1995 and 1998 showed correlated enhancement in late 1997 (Rinsland et al., 1999). Using similar techniques, Rinsland et al. (2000) further reported elevated CO, HCN and C_2H_6 above Jungfraujoch, Switzerland, peaking in early to mid 1998. In each case the anomalies were linked to major biomass burning events in South-east Asia in 1994 and 1997/98. The phase lag in anomaly maxima between Mauna Loa and Jungfraujoch in 1997/98 may be consistent with either tropical emissions being transported northward and/or a contribution from northern, extra-tropical emissions in 1998. Spaceborne measurements from three 10-day space shuttle missions showed dramatically elevated CO over the tropics in October 1994 by comparison to both

April 1994 and October 1984 (Connors et al., 1999), with largest enhancements over South-east Asia and tropical South America. The total atmospheric CO burden in October 1994 was calculated to exceed that of October 1984 by 90 Tg. This value can be used to approximate emissions of other trace gases. Assuming the entire difference was due to biomass burning with a molar CO/CO_2 emission ratio of 0.1 (Pak, 2000) and negligible long term CO trend, a lower limit for 1994 CO_2 emissions is 0.4 PgC. Total CO_2 emissions integrated over the whole burning event would likely be higher if allowance is made for emissions after the October observations and for the short adjustment time of CO. It is likely that a significant fraction of the CO emitted earlier in the burning event would already have been oxidized by OH.

4.4.3 Biomass burning

Major tropical biomass burning events, linked to ENSO dry periods, have been reported for both 1994/95 and 1997/98. However, the magnitude of emissions is not well known as there are large uncertainties in the parameters that determine the total trace gas emissions, such as the area burned, biomass loading per unit area and combustion efficiency. South-east Asia was one affected region with areas of 50,000 km^2 or more burned in each of 1994 (Nichol, 1997; Folkins et al., 1997) and 1997/98 (Liew et al., 1998; Levine, 1999; Legg and Laumonier 1999; Siegert and Hoffmann, 2000). One estimate of area burned in Indonesia alone in 1997/98 amounted to 90,000 km^2 (Page et al., 2000 and references therein). Most of the trace gas emissions from these fires were attributed to combustion of peat. A lower limit of 0.2 and a range of 0.4-0.9 PgC were estimated for 1997/98 carbon emissions by Levine (1999) and Page et al. (2000), respectively.

Large fires also occurred in South America in 1997/98, although the total areal extent is not well known. The Brazilian state of Roraima alone accounted for a burned area of 15,000 km^2 (Nepstad et al., 1999; Andreae et al., 2001), contributing towards a possible doubling of net emissions from deforestation for the Brazilian Amazon relative to other years (Nepstad et al., 1999). This would imply an additional release of about 0.2 PgC following the estimates of Houghton et al. (2000). Potter et al. (2001) suggest that in the early 1990s, emissions from the same region varied by up to 1 PgC yr^{-1} with highest emissions occurring during El Niño years. IAV in African biomass burning emissions was reported by Barbosa et al. (1999) for the earlier period 1981-1991, with mid-range estimates of annual emissions varying by up to 0.4 PgC. However, maximum emissions were not directly correlated with El Niño as was the case for South-east Asia and South America. Interannual variability in biomass burning has been reported not only for the tropics, but also for boreal regions (Kasischke et al., 1999). More than 110,000 km^2 of forest covering both North America and Eurasia were burned in the severe fire year of 1998 and both 1994 and 1995 were also major fire years, at least in North America. A best estimate of 1997/98 carbon emissions of 0.3 PgC is implied by Kasischke et al. (1999), assuming consumption of 5000 tons km^{-2} of biomass containing 50 % carbon.

4.4.4 Covariations

While biomass burning appears to be the only process that by itself might plausibly satisfy the observed multi-species IAV, this does not exclude the possibility that climate driven covariations might exist among otherwise independent sources and sinks. Covariations with biomass burning are likely. One could

contemplate many permutations involving sources and sinks of different species and external forcing factors, but an exhaustive analysis is not attempted here. Rather, discussion is limited to covariations that might involve fluxes of sufficient magnitude to account for a major fraction of the observed IAV, and which could be linked to ENSO.

Covariations of CO_2 with ENSO have previously been identified and may include both oceanic and terrestrial components. We can use $\delta^{13}C$ to investigate this partitioning (see below). The terrestrial component may involve fluxes due to both biomass burning and imbalance in photosynthesis/respiration. Perturbations favouring net respiration are predicted by some ecosystem models for warm/dry conditions associated with El Niño (Kindermann et al., 1996; Tian et al., 1998; Gerard et al., 1999; Knorr, 2000; Yang and Wang, 2000), so that a positive correlation with biomass burning is possible. It seems unlikely that photosynthesis/respiration could account for all of the CO_2 variability because positive correlations with all three species, H_2, CO and CH_4 are not expected. The absence of a direct link among emission of H_2, CO and CH_4 and respiration of CO_2 is supported by results of ground-based flask sampling in terrestrial ecosystems (Figure 4.7; Lloyd et al., 1996; Miranda et al., 1997; Lloyd et al., in press). The samples were collected over several years from 13 individual campaigns on 5 different continents by 1) the Australian National University (ANU), Canberra, Australia, 2) The University of Edinburgh, Edinburgh, Scotland and 3) the Max Planck Institute (MPI) for Biogeochemistry, Jena, Germany. All samples were analyzed by CSIRO. The highly elevated CO_2 values result from a combination of net respiration and stable boundary layer conditions. Hydrogen is strongly anti-correlated with CO_2 due to uptake of H_2 by soils while CO and CH_4 show little dependence. Thus, when natural

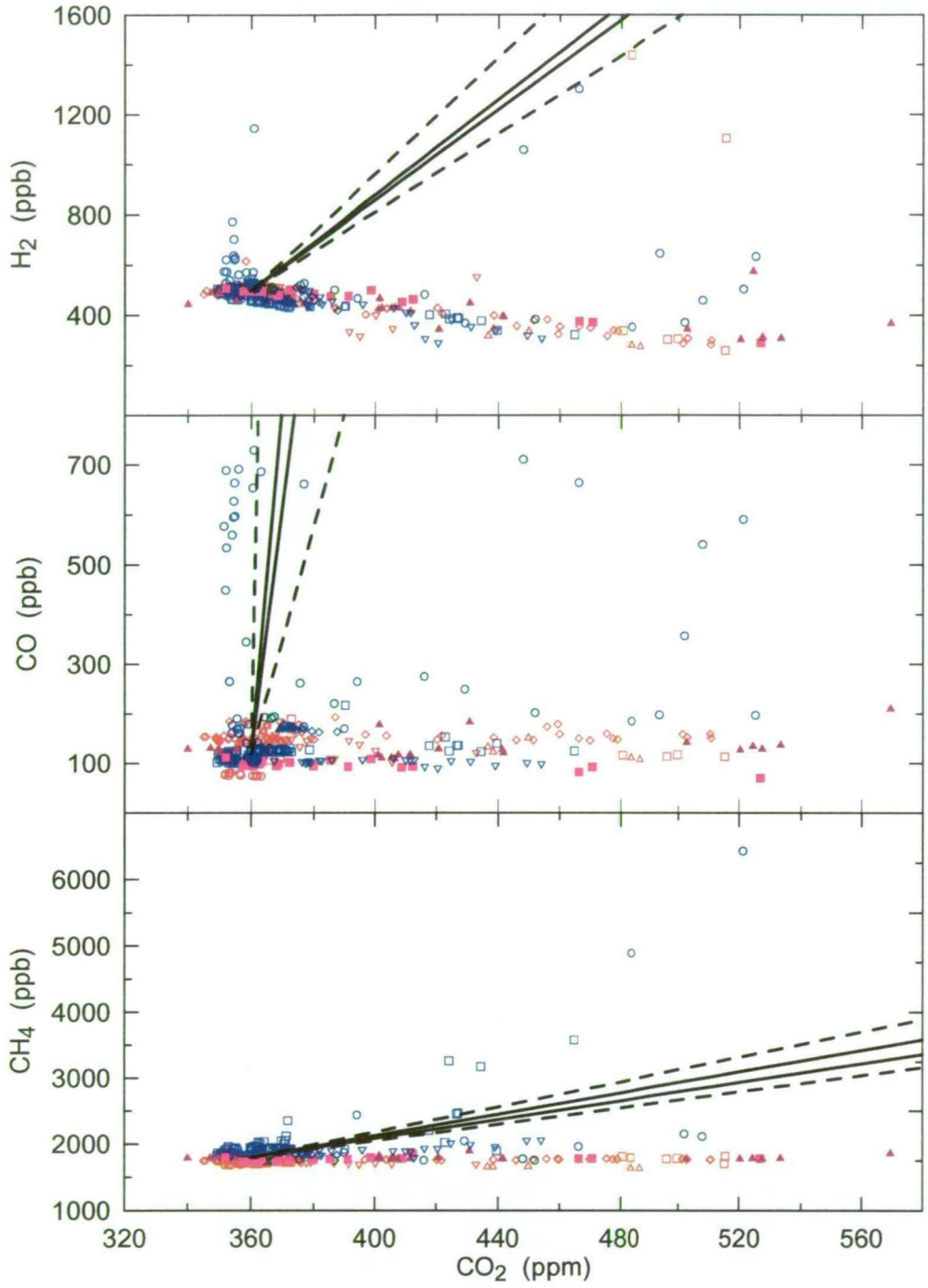

Figure 4.7 Observed relationship of changes in H_2, CO and CH_4 with changes in CO_2 in natural, terrestrial ecosystems. Data are from near-surface flask sampling of air from terrestrial ecosystems in 5 different countries, Brazil (red; 5 individual campaigns distinguished by symbol type, includes sampling in regions of Jaru Forest and Cerrado), Siberia, Russia (blue; 5 campaigns), Cameroon (green; 1), Wagga, Australia (pink, 1) and Saskatchewan, Canada (magenta, 1). Solid lines represent mean emission ratios implied by our atmospheric observations for the 2 periods, 1994/95 and 1997/98 (see Modelling section) and are forced through approximate "background" values of 360 ppm (CO_2), 500 ppb (H_2), 120 ppb (CO) and 1800 ppb (CH_4). Dashed lines show the full range of uncertainty covering both periods. Anomalously high ratios observed during one Siberian campaign (blue circles) were due to local biomass burning. CH_4 in Siberia is also known to be significantly elevated by emission from bogs.

variations in terrestrial gas exchange are the prime source of variability, the relationship of CO_2 exchange with that of H_2, CO and CH_4 is very different to the large scale relationships characterizing the observed global IAV (or the multi-species, biomass burning signals identified by Pak, 2000).

Uptake by soils is the largest single term in the global H_2 budget and might be influenced by climate, though the nature of any covariation with CO_2 fluxes is not known. Carbon monoxide global budget terms for direct emission from vegetation and consumption by soils are too small. Plants are known to release some NMHC's (isoprene and terpenes) that are oxidized in the atmosphere and produce H_2 and CO via formaldehyde. This process represents a substantial global source of both species. The factors controlling NMHC emissions by plants are complex, but include climatic variables such as temperature and humidity (Zimmerman et al., 1978; Guenther et al., 1993; 1995, Goldstein et al, 1998; Schade et al., 1999; Pétron et al., 2001). It is conceivable that increased NMHC production could be linked to net respiration of CO_2. However, even if this link did exist, the resulting CO/H_2 ratio (2.8 as calculated from Novelli et al., 1999) would be lower than indicated by the IAV observations presented here (best estimates 5-8, see below), though not excluded when all uncertainties are factored in. Microbial production of CH_4 from wetlands and rice paddies is a major term in the global CH_4 budget. Global emissions might be significantly perturbed by ENSO-related climatic variations, with emissions promoted by higher temperatures and soil moisture (via precipitation). Dlugokencky et al. (2001) used a global, process-based model to account for most of the 1998 CH_4 growth rate anomaly through increased wetland emissions, responding to positive temperature and precipitation anomalies.

4.4.5 Influences on $\delta^{13}C$ and $\delta(O_2/N_2)$

A key use of atmospheric $\delta^{13}CO_2$ and $\delta(O_2/N_2)$ in carbon cycle studies is as tracers of net CO_2 exchange with the terrestrial biosphere. However, it is possible that some contribution to IAV in both tracers results from other processes. Changes in the mixing ratio and $\delta^{13}C$ of atmospheric CO_2 can be described by separate mass budgets for ^{12}C ($\approx[C_a]$) and ^{13}C ($\approx[C_a\delta_a]$) (Enting et al., 1993),

$$\frac{d[C_a]}{dt} = F + N_{lb} + N_o \tag{4.1}$$

$$\frac{d[C_a\delta_a]}{dt} = F\delta_f + N_{lb}(\delta_a + \varepsilon_{lb}) + N_o(\delta_a + \varepsilon_o) + G_{lb}(\delta_a^{lb} - \delta_a) + G_o(\delta_a^{o} - \delta_a) \tag{4.2}$$

where F, N_{lb} and N_o are net CO_2 fluxes from fossil fuels, exchange with the land biosphere and oceans; ε terms represent isotopic discrimination with respect to atmospheric $\delta^{13}C$; G_{lb} and G_o are the gross fluxes of CO_2 through land biosphere and oceans, and δ_a^{lb} and δ_a^{o} are the values of atmospheric $\delta^{13}C$ that would be in equilibrium with the land biosphere and ocean reservoirs (Tans et al., 1993).

An issue for this study is how much IAV might be contributed by terms other than N_{lb} at the right hand side of Equations 4.1 and 4.2. It has been established elsewhere that peak-to-peak IAV of F (Marland et al., 2001) and N_o (Le Quéré et al., 2000) in the 1990s was ≤ 0.7 PgC yr^{-1}, implying that most of the IAV in $d[C_a]/dt$ of up to several PgC yr^{-1} was of terrestrial origin. Francey et al. (2001) use a revised 20-year record of δ_a to reach a similar conclusion, which implies little contribution to IAV from the N_o and G terms on the right hand side of Equation 4.2. Some authors (e.g. Kaplan, 2001; Thompson and Randerson, 1999) have suggested that IAV in the ε_{lb} and $G_{lb}(\delta_a^{lb} - \delta_a)$ terms might be important if $\delta^{13}C$ is used for partitioning. It is

easy to demonstrate that possible variations in global ε_{lb} of 1-2 ‰ due to climatic influences (Kaplan, 2001) have a small (< 10 %) influence on the N_{lb} term on interannual timescales (e.g. Enting et al., 1993). The $G(\delta - \delta_a)$ terms represent an isotopic disequilibrium flux (isoflux), and combined are the largest term on the right hand side of Equation 4.2. The terrestrial isoflux component represents about 1/3 of the total isoflux (Trudinger, 2000). Thompson and Randerson (1999) have estimated IAV of < 10 PgC‰ yr^{-1} in the terrestrial isoflux due to atmospheric $\delta^{13}C$ variations. If this component is misinterpreted as a $\delta^{13}C$ variation due to net terrestrial exchange with discrimination of –17 ‰ (exchange with predominantly C_3 vegetation), the error is < 0.6 PgC yr^{-1}, again small compared to the total net terrestrial IAV. Succession of C_3 photosynthesizing plants by C_4 species in tropical terrestrial regions following ENSO-induced fires has been raised as another possible source of IAV in the terrestrial isoflux (Ciais et al., 1999). However, this effect will only be significant if the average lifetime of respired detritus in tropical regions is long compared to the 1.8-year lifetime of this study. In terms of a perturbation pulse model discussed below for the 1994/95 and 1997/98 high CO_2 growth rates, it is pertinent that the mid-tropospheric CO_2 and $\delta^{13}C$ anomalies reported by Pak (2000), and attributed to tropical biomass burning, are consistent with the release of carbon from C_3 vegetation (-0.048 ‰ ppm^{-1}, characteristic of photosynthetic discrimination of about –17 ‰), and give no indication of significant isoflux or C_4 vegetation effects. Here we assume that other possible sources of IAV in isoflux, including an oceanic component about which little is known, are small in the 1.8-year smoothed global average.

The known influences on atmospheric O_2 can be written:

$$\frac{d[O_2]}{dt} \approx R_f F + R_{lb} N_{lb} \qquad (4.3)$$

with R_f and R_{lb} representing O_2/CO_2 exchange ratios for fossil fuel combustion and cycling through terrestrial biomass respectively. Mean R_f during the 1990s was about −1.39 taking into account exchange ratios for different fuel types (Keeling, 1988) and the fuel mix (Marland et al., 2001). The ratio R_{lb} is about -1.1 (Severinghaus, 1995).

It has been suggested that some IAV in atmospheric $\delta(O_2/N_2)$ may result from air-sea exchange due to variability in ocean dynamics or biological activity. Any such effects are not included in Equation 4.3. Keeling and Severinghaus (2000) explored the sensitivity of atmospheric $\delta(O_2/N_2)$ and CO_2 to hypothetical variations in oceanic productivity. They speculated that $\delta(O_2/N_2)$ variations of order ±10 per meg might plausibly occur on ENSO timescales, although the hypothesis is yet to be tested. If variations of this magnitude did exist, they would limit the value of using $\delta(O_2/N_2)$ as a tracer of terrestrial forcing of IAV in CO_2.

4.5 Modelling

4.5.1 Model construction

A simple 1-box model, representing a well-mixed global atmosphere, is used to quantify flux anomalies forcing the observed IAV. This approach is designed to test the hypothesis that a significant fraction of the IAV is due to the major biomass burning events of 1994/95 and 1997/98. Specifically, 1) can the observed IAV be reproduced by a release of pulses at these times? and 2) are the implied emission ratios consistent with biomass burning? For CH_4, CO and H_2, the model tracks time

variation in the composition of the pulses by taking account of atmospheric adjustment times and incorporating the main interactions involving destruction/formation by OH photochemistry. Modelled mixing ratios take the form:

$$C = C_o + at + \sum bR(t) \tag{4.4}$$

obtained by adding a set of pulses (with each pulse defined by a response function R(t) and weighting coefficient b) to "base curves" (C_o + at) that are defined to have zero IAV, but may have constant, non-zero growth rate (as defined by the coefficient a and determined by the optimization procedure described below). The base curves represent the sum of all other processes and include a contribution from biomass burning that is equivalent to the mean seasonal emissions of other years.

4.5.2 CH_4, H_2 and CO response functions

The evolution of CH_4, H_2 and CO pulse mixing ratios are described by the following set of equations, which are solved analytically:

$$\frac{d[CH_4]}{dt} = \frac{-[CH_4]}{\tau_{CH_4}} \tag{4.5}$$

$$\frac{d[CO]}{dt} = \frac{-[CO]}{\tau_{CO}} + \frac{a_1[CH_4]}{\tau_{CH_4}} \tag{4.6}$$

$$\frac{d[H_2]}{dt} = \frac{-[H_2]}{\tau_{H_2}} + \frac{a_2[CH_4]}{\tau_{CH_4}} \tag{4.7}$$

Because the model addresses the evolution of perturbations to the background atmosphere, it is appropriate to use atmospheric adjustment times rather than lifetimes (Prather et al., 1996a; 1996b). Adjustment times (τ) are taken to be 12.2,

0.25, and 2.3 years for CH_4, CO and H_2 (Warneck, 1988; Prather et al., 1996a; Novelli et al., 1999). The constants are set to: $a_1 = 0.85$ assuming OH destruction in the troposphere represents 85 % of the CH_4 sink and all CH_4 is oxidized to CO, and $a_2 = 0.58$ (0.68 x 0.85) assuming 0.68 moles of H_2 are produced per mole of CH_4 destroyed (Warneck, 1988). Production of CO and H_2 from OH destruction of NMHCs emitted by biomass burning are not explicitly treated in the model because 1) there are limited observational constraints of NMHC emissions for these events and 2) the lifetimes of NMHCs are generally very short with respect to transport times from emission sources to our measurement sites and the smoothing time employed in this analysis. Thus the inferred fluxes include the CO and H_2 both emitted directly by fires and produced later as by-products of NMHCs emitted by the fires.

4.5.3 CO_2 and $\delta^{13}C$ response functions

Response functions for pulses of CO_2 and $\delta^{13}C$ cannot be described in terms of a single lifetime because equilibration with different compartments of oceanic and land biosphere reservoirs involves various timescales. Response curves for small perturbations to the contemporary atmosphere were obtained from the box-diffusion model of Enting and Lassey (1993; see also Trudinger et al., 1999; Trudinger, 2000). The model is calibrated against ^{14}C and assessed against the Law Dome $\delta^{13}C$ record of Francey et al. (1999a), and includes enhancement of net primary production (NPP) in terrestrial ecosystems due to CO_2 fertilization (Trudinger, 2000). On the timescales of interest (i.e. < 6 years), the main influences are equilibration with the surface ocean and the "young" terrestrial biosphere. Response curves are fitted by functions comprising a sum of exponential terms, which for CO_2 (approximately)

represent distinct "pools" of CO_2 that are removed from the atmosphere on different timescales (e.g. Wigley, 1991) and where t is in years:

$$[CO_2] = (0.19 + 0.27e^{-t/1.02} + 0.32e^{-t/4.65} + 0.22e^{-t/322}) \quad (4.8)$$

$$[\delta\,^{13}C] = (0.58e^{-t/1.26} + 0.33e^{-t/4.89} + 0.09e^{-t/274}) \quad (4.9)$$

These equations represent the evolution of a pulse of CO_2 per unit emission and of unit change in $\delta^{13}C$ in a well-mixed atmosphere. Advantage is taken of the fact that for small perturbations, the shape of the response is not strongly dependent on pulse strength. For $\delta^{13}C$, the response functions for injections of terrestrial and oceanic CO_2 pulses are almost identical (Trudinger, 2000). Uncertainties are estimated here by allowing for ±20 % variation in the time constants, reflecting approximate uncertainty in gross flux (G) terms.

4.5.4 Detection of pulse perturbations at measurement sites

It is important to note that signal strengths detected at measurement sites will be modified from their initial values, especially for short-lived species. Figure 4.8a shows the decay in airborne fraction of all species as a fraction of an initial pulse at t = 0, here ignoring production from OH-destruction of precursor species. There is dramatic depletion of CO over the time scales of interest. Most is destroyed within a few months so that only a small fraction of a CO pulse is captured by the 1.8-year smoothing time. This situation is exacerbated by the fact that some depletion will occur between the time of emission and arrival of the signal at the measurement sites. Assuming a mean transport time of 2 months (equivalent to 50 % response at Cape Grim of a signal released at the equator; P. J. Rayner, personal communication), a

CO pulse would already have decayed to just half its initial value. Depletion of other species over these time scales is not as dramatic, but is taken into account for quantification of emissions and emission ratios.

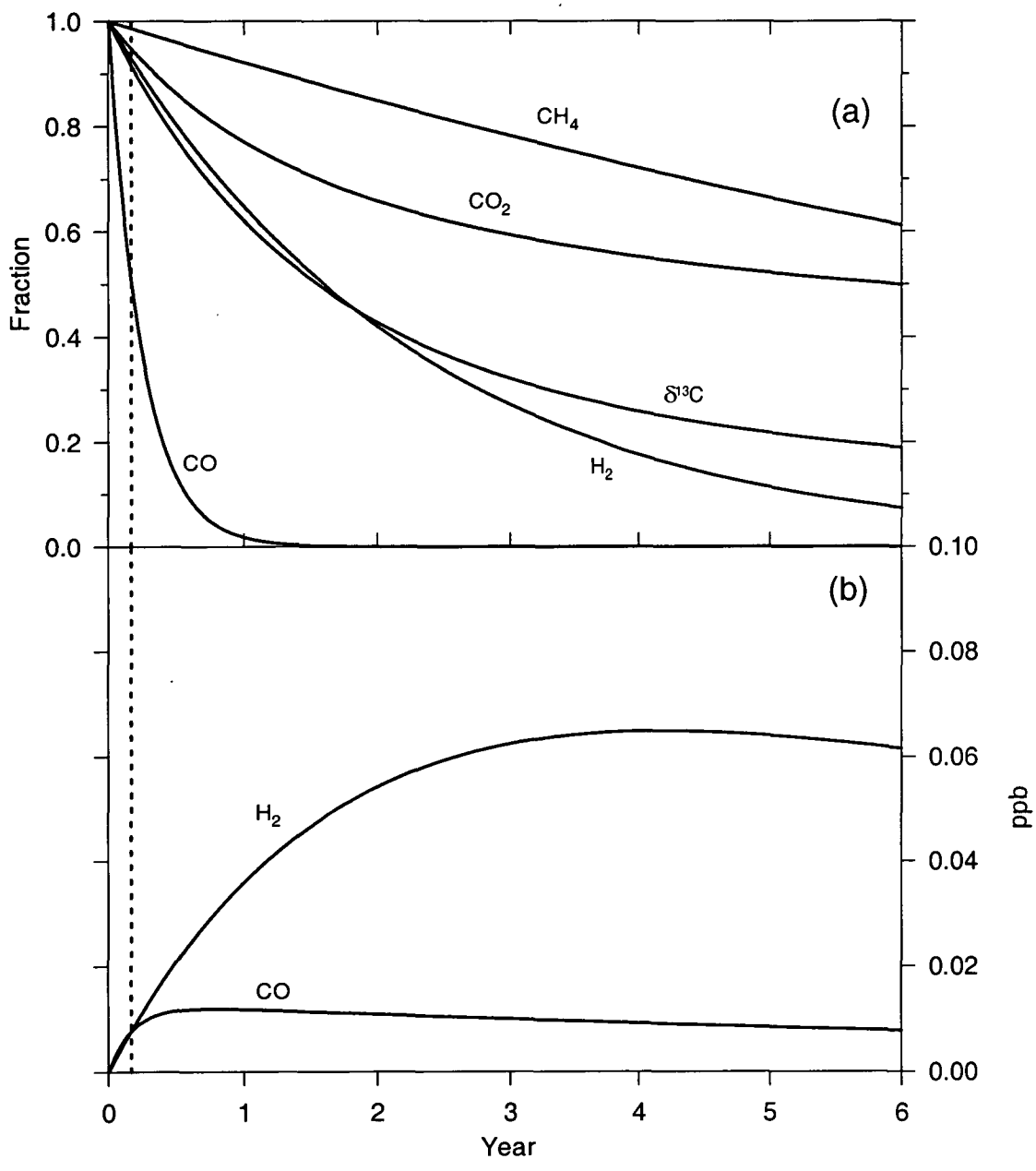

Figure 4.8 (a) Airborne fraction as a function of time after emission, according to pulse response functions used in the model. For $\delta^{13}C$, the curve represents the fractional change in a perturbation to $\delta^{13}C$ in a well-mixed atmosphere. The dashed line at 2 months represents the assumed mean transport time between source and measurement sites. (b) Response of H_2 and CO to an emission pulse of 1 ppb CH_4, taking into account their respective adjustment times and production of H_2 and CO through destruction of CH_4 by OH.

4.5.5 H_2 and CO response to a CH_4 pulse

By making allowance for adjustment time and OH-related interactions that include production from CH_4 oxidation, it is possible to calculate the response of H_2 and CO to an initial pulse of 1 ppb CH_4 (Figure 4.8b). Maximum response is < 0.08 and < 0.02 ppb for H_2 and CO respectively, confirming that observed IAV of H_2 and CO is largely independent of this source. For CO this represents a negligible fraction of observed IAV, while for H_2 it accounts for < 10 %. Similarly, oxidation of CO and CH_4 (via CO) can account for only a small fraction of CO_2 IAV. The model explicitly accounts for these interactions in the treatment of CH_4, H_2 and CO. The major contributions to CO_2 and $\delta^{13}C$ through CO occur within the first few months after release (Figure 4.8a) and due to the 1.8-year smoothing time are not treated explicitly but rather are counted as part of the initial CO_2 and $\delta^{13}C$ pulses..

4.5.6 Time distribution of pulse emissions

Modelled mixing ratio (and δ) curves are constructed by taking the first year (1992) of observations, appending "base curves" (1993-1999) with zero IAV but non-zero trend, and adding two sets of emission pulses each of 1-year duration. The first year of observations are used in the model to minimize errors from not resolving growth rate variations in 1994/95 from those of 1992/93. Each set of pulses is divided into equal, monthly parts centred on August, 1994 and February, 1998, thus matching the mean times of observed growth rate maxima. The 1-year duration of pulses approximates the duration of anomalous biomass burning activity. This period was well defined in 1997/98 with major fires starting in August, 1997 in the tropics and continuing through to September, 1998 in boreal forests. The same duration is assumed for 1994/95, although the time distribution is not as clearly defined in these

years and may involve above average biomass burning emissions from different regions over a period of more than 1 year. The objective, for each species, is to find the magnitude of both sets of pulses to best fit observed growth rate variations while maintaining integrity in the long-term trend. An iterative procedure optimizes two variables, pulse strength and growth rate of the base curve (i.e. coefficients b and a in Equation 4.4). Pulse strengths are adjusted to match the area beneath modelled and observed growth rate curves with respect to the growth rate of the base curve. The base curve growth rate is adjusted to maintain consistency of observed and modelled mixing ratios (and δ) before and after each period of modelled pulses (1993.0 and 1996.5 for 1994/95 pulses, 1996.5 and 2000.0 for 1997/98 pulses). Calculations for the two sets of pulses are thus independent except for the response to the 1994/95 emissions which continues through 1997/98. This procedure does not require modelled and observed curves to be perfectly in phase.

4.5.7 Model results

Modelling results are listed in Table 4.4 and plotted in Figure 4.9. The model successfully reproduces the main features of the observed global mean growth rate curves. Largest discrepancies appear for CO_2 and H_2 in 1994/95. The shape of the 1994/95 H_2 growth rate peak is well reproduced by the model but leads the observations by 3 months. The same feature is manifested as an offset between observed and modelled mixing ratios during the period of modelled pulses. This discrepancy appears to be related to a HNH perturbation that was specific to H_2. Peak H_2 growth rates in 1994/95 at the three northernmost sites showed a phase lag with respect to other sites (Figure 4.3). A secondary maximum/minimum cycle was observed at ALC and SIS in 1993/94, suggesting a contribution to IAV from another

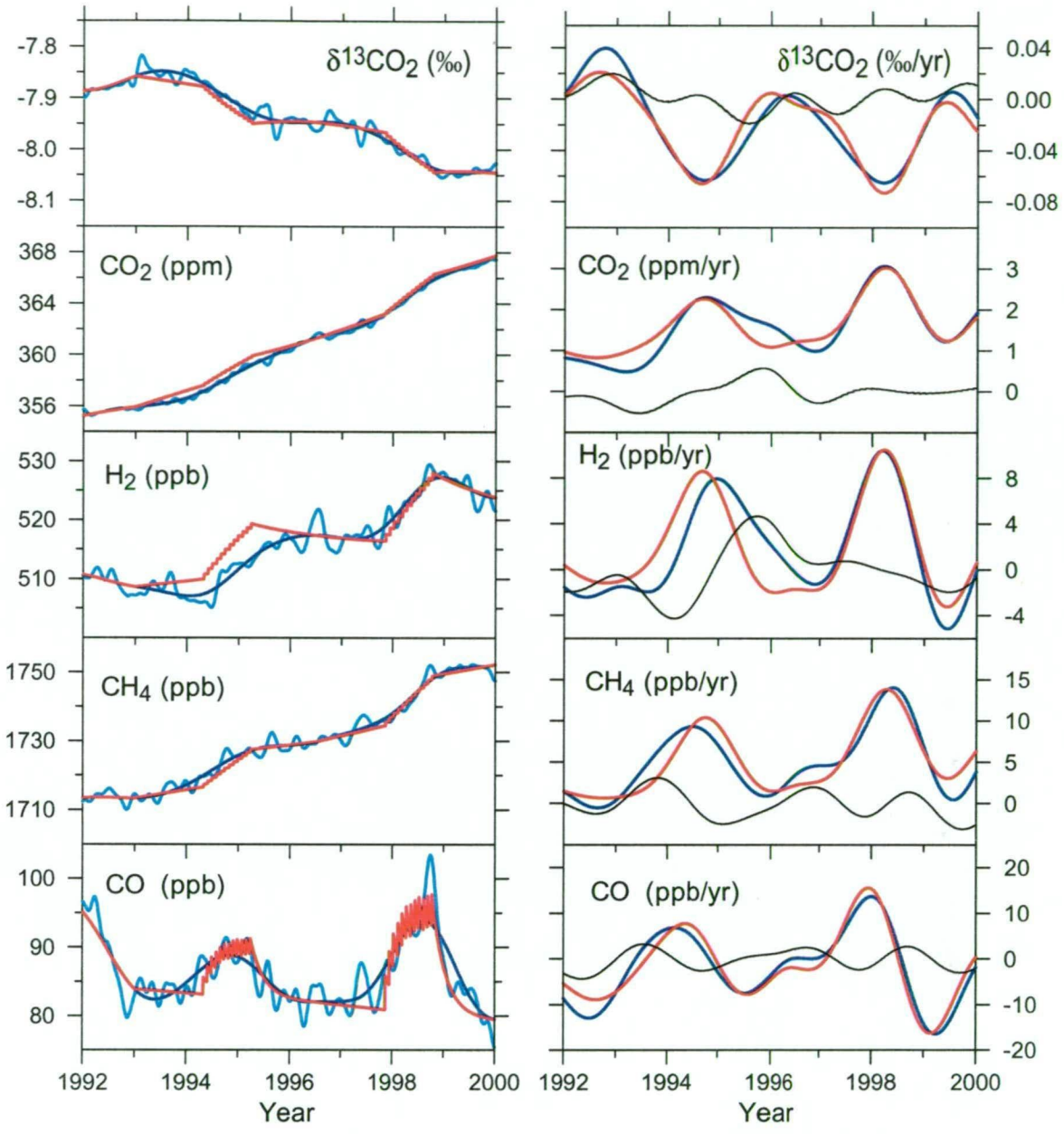

Figure 4.9 Global mean records (left hand side) represented by observed "trend" (dark blue), observed "smooth" (light blue; averaged "smooth curves" from all sites with seasonal cycle removed) and modelled (red) curves. The right hand side compares observed (blue) and modelled (red) growth rates and their difference (observed-modelled; black).

	CO_2	$\delta^{13}CO_2$	H_2	CO	CH_4
Observations:					
Global mean growth rate 1992-1999	1.46 ppm yr^{-1}	-0.016 ‰ yr^{-1}	1.4 ppb yr^{-1}	-2.6 ppb yr^{-1}	4.4 ppb yr^{-1}
[a]Resolution of interannual variations among sites integrated over 1.8 years (1σ)	0.12 ppm	0.009 ‰	1.4 ppb	13 ppb	1.3 ppb
[b]Uncertainty due to instrument calibration and changes in sampling procedure (1σ)	0.07 ppm	0.015 ‰	0.5 ppb	1.6 ppb	0.3 ppb
Model input:					
Atmospheric adjustment time (years)			2.3 ± 0.5	0.25 ± 0.1	12.2 ± 3
Model output:					
[c]Base curve growth rate 1993.0 - 1996.5	1.27 ppm yr^{-1}	-0.016 ‰ yr^{-1}	1.0 ppb yr^{-1}	-0.6 ppb yr^{-1}	2.5 ppb yr^{-1}
[c]Base curve growth rate 1996.5 - 2000.0	1.51 ppm yr^{-1}	-0.023 ‰ yr^{-1}	0.8 ppb yr^{-1}	-0.8 ppb yr^{-1}	4.1 ppb yr^{-1}
[d]Emission error factor	0.95 – 1.06	0.90 – 1.14	0.90 – 1.17	0.47 – 4.4	0.98 – 1.04
[e]1994/95 emission	$1.30^{+0.17}_{-0.16}$ ppm	$-0.077^{+0.019}_{-0.021}$ ‰	$10.8^{+2.4}_{-1.9}$ ppb	57^{+194}_{-33} ppb	$9.2^{+1.3}_{-1.3}$ ppb
	(2.8 Pg C)		(3.8 Tg H_2)	(283 Tg CO)	(26 Tg CH_4)
[e]1997/98 emission	$2.02^{+0.19}_{-0.18}$ ppm	$-0.082^{+0.019}_{-0.021}$ ‰	$14.9^{+3.0}_{-2.1}$ ppb	117^{+398}_{-63} ppb	$11.7^{+1.3}_{-1.3}$ ppb
	(4.3 Pg C)		(5.3 Tg H_2)	(581 Tg CO)	(33 Tg CH_4)
1994/95 emission ratio (ppm^{-1} CO_2)		$-0.059^{+0.016}_{-0.018}$ ‰	$8.3^{+2.2}_{-1.7}$ ppb	44^{+149}_{-26} ppb	$7.1^{+1.5}_{-1.3}$ ppb
1997/98 emission ratio (ppm^{-1} CO_2)		$-0.041^{+0.010}_{-0.011}$ ‰	$7.4^{+1.7}_{-1.2}$ ppb	58^{+197}_{-32} ppb	$5.8^{+0.9}_{-0.9}$ ppb

Table 4.4 Modelled pulse strengths and emission ratios for 1994/95 and 1997/98 events.

[a]Calculated from the difference in growth rate between records of individual sites and the global mean by integrating over a time window of 1.8 years.

[b]See Methods for derivation of experimental uncertainty.

[c]Growth rates that are independent of modelled emission pulses, as determined by the iterative optimization procedure.

[d]The range of uncertainty in modelled emission pulses due to uncertainty in pulse response functions and in mean transport time between source and measurement sites (2 ± 1 months).

[e]Modelled emission pulses, expressed as a change in mixing ratio (or δ) in a well-mixed atmosphere. Uncertainties are calculated by adding in quadrature the contributions from signal resolution[a], calibration[b] and response/transport times[d].

process (the discrepancy in Figure 4.9 is almost entirely removed when the observed global mean growth rate curve is calculated without data from the three northernmost sites).

For CO_2, the model does not adequately reproduce that part of the growth rate peak that extends into 1995 and which is not mirrored by CO or CH_4 (H_2 is inconclusive). For this reason, the results shown in Figure 4.9 and Table 4.4 were obtained by restricting integration of CO_2 growth rate peaks to the 12-month period of modelled pulses. $\delta^{13}C$ was treated in the same way to maintain integrity between these species for partitioning of terrestrial and oceanic fluxes. This modified procedure provides a better fit to observations at the time of multi-species correlation in growth rate in 1994 but neglects that part of the CO_2 IAV occurring in 1995. The difference between observed and modelled curves implies an unaccounted net CO_2 release of 1.5 PgC in 1995. There is a corresponding $\delta^{13}C$ residual that, at face value, implies the 1995 CO_2 release is approximately equally due to terrestrial and oceanic exchange, though this source allocation must be viewed with caution as the implied fluxes are smaller than their uncertainties.

The discrepancies for CO_2 (and other species) preceding the 1994 maximum are likely due in part to the assumption of no other contributions to IAV between 1993 and mid-1996. Growth rate perturbations observed for CO_2, H_2, CO and CH_4 during 1991-93 were linked, at least for CO and CH_4 to the 1991 Mt Pinatubo volcanic eruption (Conway et al., 1994; Dlugokencky et al., 1996; Novelli et al., 1998; 1999). These variations may not be fully resolved from the 1994/95 event, especially in light of the 1.8-year smoothing time used in this analysis.

A high level of agreement between observed and modelled curves was obtained for all species in 1997/98. One feature worthy of mention is the 1998 spike

in observed CO mixing ratio indicated by the light blue curve in Figure 4.9. Maximum values were recorded in late 1998, mainly reflecting a HNH signal that was distinct from CO variations at other latitudes (Figure 4.3). Growth rate maxima in the HNH occurred substantially later than in the tropics but were more intense. This suggests anomalously high CO emissions occurred in more than one latitude band. It is consistent with emissions peaking in the tropics in late 1997 and in higher latitudes of the NH in mid-1998, a distribution that corresponds to times of major biomass burning activity in both tropical (at least in South-east Asia) and boreal regions.

4.5.8 Uncertainties

Pulse strength estimates in Table 4.4 allow for experimental uncertainty and for signal-to-noise in detection of IAV, as determined by consistency among sites and illustrated by the light blue curves at the left hand side of Figure 4.9. They partly allow for assumptions relating to trace gas adjustment times and transport times between source regions and measurement sites. Of the species considered here, modelled CO emissions carry the largest uncertainty, owing to the short CO adjustment time. They are strongly sensitive to transport time, which will vary with latitude, and the season when emissions occur. The assumed transport time of 2 ± 1 months approximates an equatorial source but becomes less satisfactory for higher latitude emissions. Because OH is not uniform through the troposphere, the simplistic treatment of CO destruction (which assumes constant global OH) also contributes uncertainty. Actual adjustment times are shorter in the tropics and longer at high latitudes and in the upper troposphere. These factors have far weaker impact on modelled emissions of other species.

There are other potentially large uncertainties that cannot be quantified and are thus not explicitly included in these calculations. They relate to the assumption that the IAV can be largely attributed to two sets of emission pulses. It is likely that some contributions to IAV forcing result from other processes with a different time distribution. For example, the CH_4 growth rate anomaly commencing in 1996 at Mauna Loa and sites to its south is inconsistent with modelled 1997/98 pulses. One way to gauge the possible significance of interfering processes is by comparison of the model-derived base curve growth rates for the two periods before and after mid-1996 (Table 4.4). If all of the IAV were fully explained by the modelled pulses, these terms should be equal. Significant differences do emerge for CO_2 (i.e. 1.27 and 1.51 ppm yr^{-1}), $\delta^{13}C$ and CH_4 which translate to errors in modelled pulse strengths of as much as 30 %.

4.5.9 Post-burning fluxes

An additional factor not included in the model is the response of terrestrial ecosystems to a burning event. Decomposition of the dead plant matter that remains after a fire is a source of CO_2 (and a sink of O_2) to the atmosphere and is opposed by CO_2 uptake (and O_2 release) through regrowth (Ward et al., 1992; Poth et al., 1995; Houghton et al., 2000). Of greatest significance here is the net response in the first 1-2 years because this quantity is not distinguished from the initial pulse emissions of the model. Over longer time scales, the response to fires in earlier years forms part of the modelled base curves. The net response is governed by the combustion factor (the fraction of dead vegetation burned), the rate of decomposition of the remaining dead vegetation and the rate of regrowth. These factors can depend heavily on the nature of the fire, such as the type of biomass fuel and fire intensity. The net

response to fires in forests (e.g. variable combustion factor dependent on fire intensity; rate of regrowth dependent on mortality rate of trees), peat swamps (effectively slow rate of decomposition and maybe slow regrowth) and savanna (high combustion factors and rapid regrowth) is likely to vary significantly. The potential impact on the results was explored by constructing a range of response scenarios using possible ranges of each parameter. Uncertainties are large and even the sign of the response in early years is uncertain, although an initial net release of CO_2 to the atmosphere is favoured. The scenario representing the upper extreme for net respiration of CO_2 suggests that within the first year, this source could even exceed the initial release through combustion. However, a response as large as this is not supported by Figure 4.9 where both a phase lag in growth rate maxima and tailing of the CO_2 and $\delta^{13}C$ growth rate peaks would be expected relative to those of H_2, CH_4 and CO. The sustained CO_2 and $\delta^{13}C$ flux anomalies in 1995 are consistent with a smaller contribution from net respiration while there is no evidence for post-burning fluxes in 1997/98 that are not captured by the model.

4.6 Flux Estimates

4.6.1 Partitioning of terrestrial and oceanic CO_2 fluxes

Model results for CO_2 alone give optimal pulse strengths of 2.8 and 4.3 PgC in 1994/95 and 1997/98 respectively. The corresponding signal in $\delta^{13}C$ can be used to separate terrestrial and oceanic components, using estimates for ε_{lb} and ε_o of -17 ± 2 and -1.8 ± 0.3 ‰ respectively. Significant net terrestrial release of 3.5 ± 1.1 and 3.7 ± 1.1 PgC is indicated for the two periods (Table 4.5). Implied oceanic releases of -0.8 ± 1.1 and 0.6 ± 1.1 PgC are smaller and within uncertainty. The assumed value for ε_{lb} of -17‰ represents CO_2 exchange with predominantly C_3 vegetation. Mean

CO_2 Source	Constraint	Biomass Burning Emission Ratio (mol mol^{-1})	1994/95 (PgC)[a]	1997/98 (PgC)[a]
Oceans	$\delta^{13}C$		-0.8 ± 1.1	0.6 ± 1.1
Terrestrial Biosphere[b]			3.5 ± 1.1	3.7 ± 1.1
Biomass Burning	CH_4 / CO_2 (Pak, 2000; all fires)	0.006 – 0.016	1.1 – 3.8[c]	1.4 – 4.7[c]
	H_2 / CO_2 (Pak, 2000; all fires)	0.008 – 0.034	0.6 – 3.5[c]	0.8 – 4.8[c]
	CO / CO_2 (Pak, 2000; all fires)	0.06 – 0.16	0.3 – 8.9[c]	0.7 – 18.3[c]
	CH_4 / CO_2 (Matsueda et al.; Japan-Australia aircraft transects at 10km altitude)	0.0089		~2.8[d]
	CO / CO_2 (Matsueda et al.; Japan-Australia aircraft transects at 10km altitude)	0.077		~3.2[d]
	CH_4 / CO_2 (Matsueda and Inoue; aircraft sampling above Singapore, October 1997)	0.0045		~5.5[d]
	H_2 / CO (Sawa et al.; aircraft sampling above Indonesia, October 1997)	0.06 – 0.10		1.7 – 10.6[e]

Table 4.5 Partitioning of CO_2 pulses.

[a]Positive pulses are into the atmosphere

[b]Includes both biomass burning and imbalance in photosynthesis/respiration.

[c]Allowance is made for the range of literature estimates of emission ratios for biomass burning and for uncertainties in CH_4, H_2 and CO pulses as given in Table 4.4.

[d]Only the "best estimate" is quoted due to weakly constrained uncertainty in the biomass burning emission ratio.

[e]Calculated assuming a biomass burning CO/CO_2 emission ratio range of 0.06-0.16.

global values for photosynthetic discrimination, weighted by gross primary productivity (GPP), were estimated by Lloyd and Farquhar (1994) to be -17.8 and -3.6 ‰ for C_3 and C_4 plants respectively. A heavy bias towards C_3 exchange in the 1994/95 and 1997/98 flux anomalies is expected if biomass burning played a significant role. The major fires in these years occurred in forests of South-east Asia, South America and boreal regions, all of which are dominated by C_3 vegetation (Lloyd and Farquhar, 1994). Although large areas of savanna with a higher proportion of C_4 plants are burned seasonally, especially in Africa and to a lesser extent in tropical America (Hao and Liu, 1994), it is only perturbations from mean seasonal biomass burning activity that are relevant here. In any case, Pak (2000) detected no clear influence of C_4 photosynthetic discrimination in the 8 years of mid-troposphere sampling of tropical biomass burning plumes (although the isotopic data are sparse and scattered). Furthermore, C_3 plants account for the major fraction of global GPP (e.g. 79 % as determined by Lloyd and Farquhar, 1994) so that any flux anomalies due to imbalance in photosynthesis/respiration might also be expected to favour C_3 exchange (see also Kindermann et al., 1996; Tian et al., 1998).

4.6.2 Implications for $\delta(O_2/N_2)$

Having estimated the magnitude of terrestrial and oceanic pulses forcing IAV in CO_2, it is possible to calculate an implied growth rate curve for $\delta(O_2/N_2)$. The same modelling approach is used, but with $\delta(O_2/N_2)$ pulses fixed relative to CO_2 so that only the growth rate of the base curve is optimized. Pulses of $\delta(O_2/N_2)$ are given the same time distribution as those of CO_2 and are calculated by scaling the terrestrial CO_2 pulses by a molar O_2/CO_2 exchange ratio (R_{lb}) of –1.1 (Severinghaus, 1995). Total pulses are –8.6 and –9.1 per meg for 1994/95 and 1997/98 respectively.

The smaller contributions to CO_2 IAV from net air-sea exchange are assumed to have no impact on O_2/N_2.

The response function for $\delta(O_2/N_2)$ comprises three components. Firstly, there is a release of O_2 to the atmosphere in response to a pulse emission of CO_2, due to fertilization of the land biosphere by higher atmospheric CO_2 levels. This process contributes to decay of a CO_2 pulse as estimated from the model of Trudinger (2000) (Section 4.5.3). The effect on atmospheric O_2 is expressed here as a response to an initial (negative) O_2 pulse associated with a unit terrestrial pulse emission of CO_2 at t = 0 years (Figure 4.10):

$$[O_2] = R_{lb}\,(0.667 + 0.015e^{-t/0.80} + 0.166e^{-t/2.77} + 0.153e^{-t/14.09}) \qquad (4.10)$$

Second, a pulse in atmospheric O_2/N_2 will be partly offset by re-equilibration of the atmosphere with dissolved O_2 and N_2 in the oceans. However, because of the low solubility of both O_2 and N_2 and slow vertical mixing in the oceans, the effect on the atmosphere is very small. On a 6-year timescale, this mainly involves equilibration with the oceanic surface layer. This process causes an atmospheric perturbation to be offset by less than 0.1 % and is thus not considered any further here. Thirdly, there may be significant O_2 exchange associated with the response of terrestrial ecosystems to fire as discussed for CO_2 in Section 4.5.9. Atmospheric O_2 is consumed by decomposition of dead vegetation and replenished by regrowth. As was the case for CO_2, these fluxes may be significant for the pulse perturbation model used here, but their magnitude and even their sign in the period immediately after a fire, are uncertain. Hence they are not explicitly included in the model calculations.

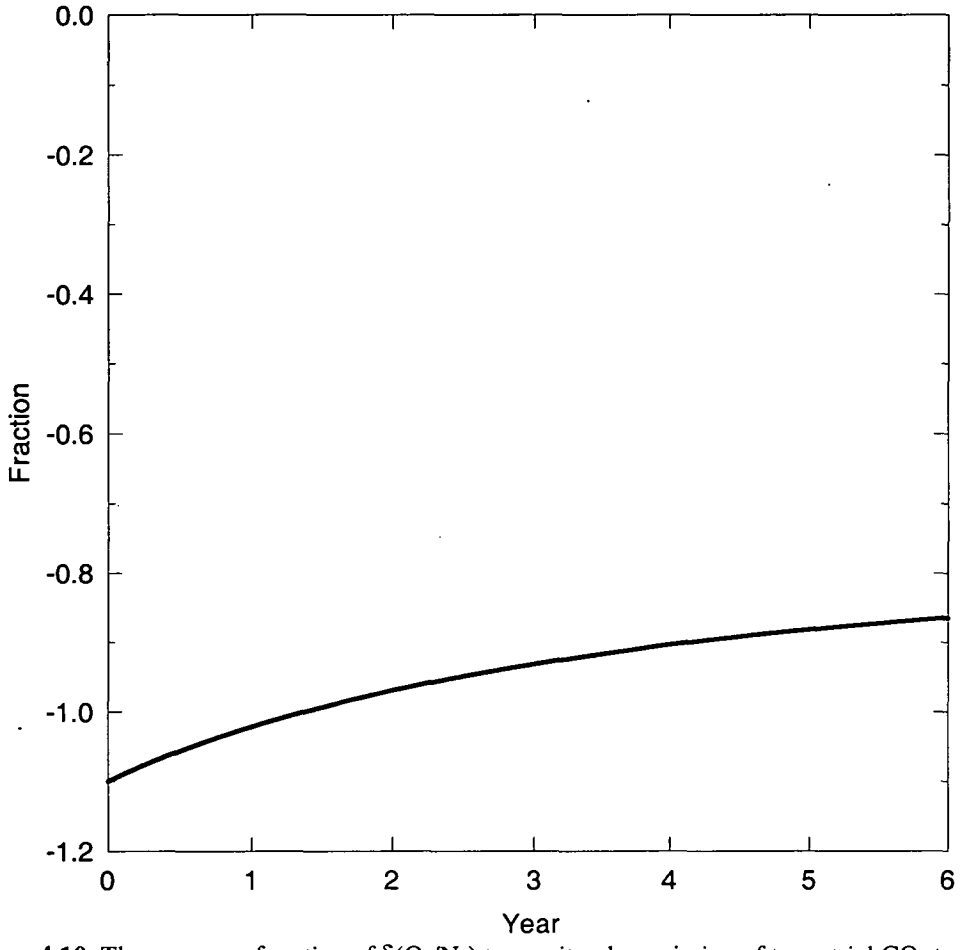

Figure 4.10 The response function of $\delta(O_2/N_2)$ to a unit pulse emission of terrestrial CO_2 to the atmosphere scaled by the terrestrial O_2/CO_2 exchange ratio of –1.1.

Observed Cape Grim $\delta(O_2/N_2)$ curves from the three laboratories are plotted in Figure 4.11. The modelled curve was generated by adding $\delta(O_2/N_2)$ pulses to base curves derived from and optimized against the observed SIO record. The SIO record was best suited to this purpose because of its precision and continuity over the 1992-1999 period. Both the amplitude and the phase of IAV in the modelled curve are broadly similar with the SIO record and also to a lesser extent with the shorter URI/PU record. The comparison is supportive of mainly terrestrial forcing of CO_2 IAV. Whether or not the remaining differences between observed (SIO and URI/PU)

and modelled curves reflect a different time distribution of fluxes forcing IAV or of other processes (e.g. an oceanic contribution to IAV in $\delta(O_2/N_2)$) depends critically on integrity of the SIO and URI/PU records at the ~2 per meg level.

4.6.3 Multi-species constraints on biomass burning CO_2 fluxes

If it is assumed that the modelled H_2, CH_4 and CO emission pulses are entirely due to biomass burning, they can be used with literature estimates of biomass burning emission ratios to directly constrain emissions of CO_2 (Table 4.5). The main limitation to this approach is that literature values show large variations due to dependence of emissions on vegetation type and combustion efficiency (e.g. Crutzen and Andreae, 1990). Although the high CO ratios with respect to other species are a strong indicator of biomass burning, estimated CO pulse strengths are too uncertain to provide a firm quantitative constraint of CO_2 emissions. The best estimates of CO/CO_2 ratios in Table 4.4 are consistent with upwards of 10 % of the terrestrial CO_2 pulses being from biomass burning, based on a molar emission ratio range of 0.06-0.16 from the literature survey of Pak (2000).

The longer-lived species H_2 and CH_4 are better suited to this application but uncertainty in actual source emission ratios becomes a serious limitation. Molar emission ratios for different fire types are mostly in the range 0.006-0.016 and 0.008-0.034 for CH_4/CO_2 and H_2/CO_2 respectively (Pak, 2000). Generally, low values are associated with savanna fires where combustion efficiency is high. Values closer to the upper end of the range might be expected for the 1994/95 and 1997/98 events if emissions came mostly from fires in peat swamp forests with a higher proportion of smoldering combustion. Data for emissions from peat combustion are sparse but an identical range of 0.006-0.016 for CH_4/CO_2 was obtained by Yokelson et al. (1997)

from laboratory experiments. The pulse strength ratios derived from the model are near the lower end of the literature range. Actual source ratios at the upper end of the range would imply minimum biomass burning contributions to terrestrial CO_2 pulses of 17 % in 1994/95 and 22 % in 1997/98 (Table 4.5).

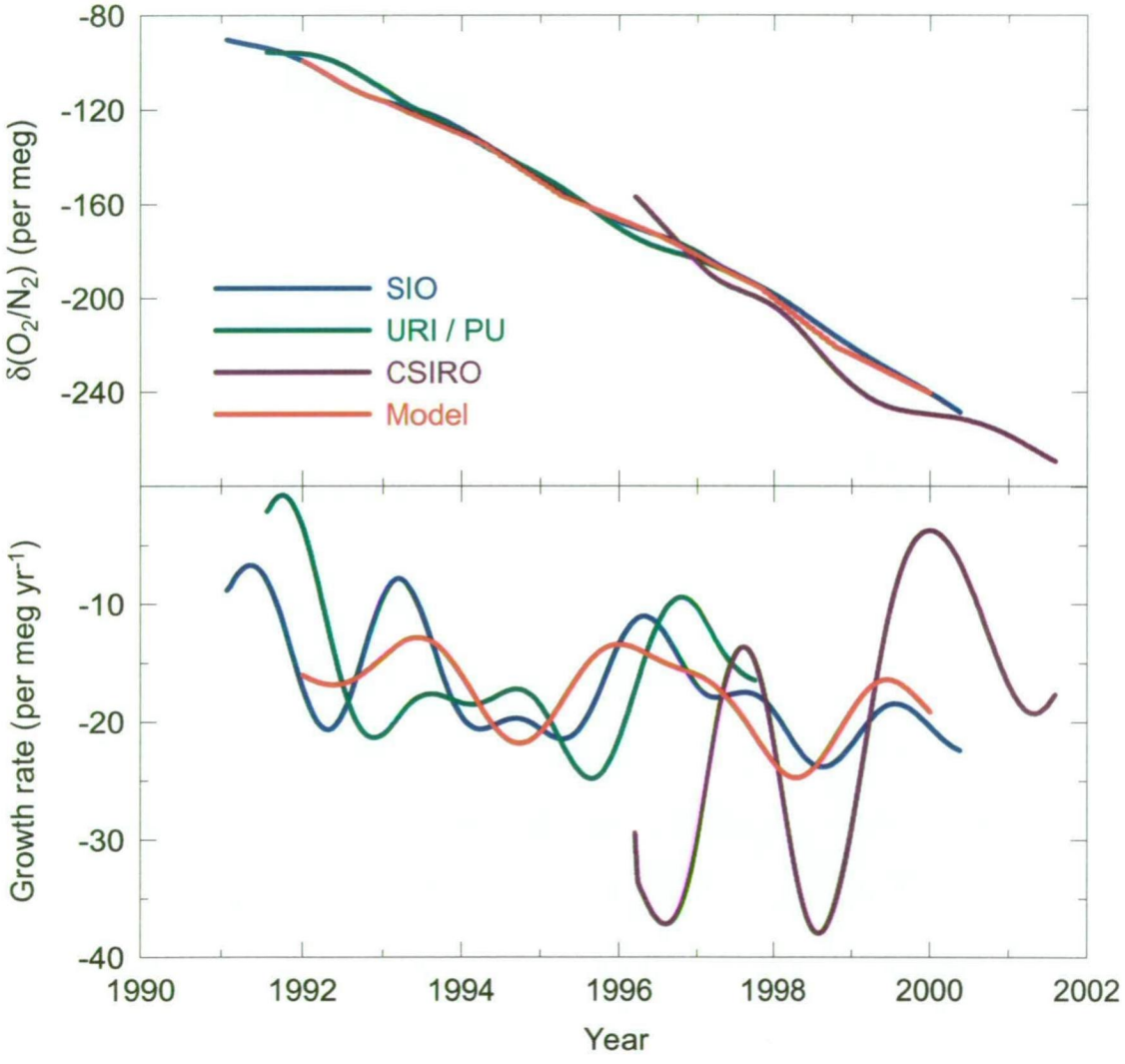

Figure 4.11 $\delta(O_2/N_2)$ trend (upper panel) and growth rate (lower panel) derived from Cape Grim observations of three laboratories, and from the pulse perturbation model, assuming $\delta(O_2/N_2)$ pulses consistent with those inferred for terrestrial CO_2 exchange from global mean observations.

For CH_4, there is also a question of possible interference from covariations involving microbial CH_4 production. The assumption made here, that most or all of the CH_4 IAV can be ascribed to biomass burning, conflicts with the findings of Dlugokencky et al. (2001) who attribute most of the 1998 IAV to wetland emissions and a minor fraction to mostly boreal biomass burning. There are two points to be made about the Dlugokencky et al. analysis. Firstly, it focused on 1998 and did not address the positive growth rate anomaly that commenced in 1996 in the tropics and SH and continued through 1997, in tandem with CO_2, H_2 and CO (see Figure 4.3). Secondly, it may have underestimated global biomass burning flux anomalies during the 1997/98 period. A CH_4 emission of 5.7 Tg was determined for boreal fires but only 1.8 Tg was assumed for fires elsewhere based on the estimate of Levine (1999) for Indonesia. Possible contributions from fires in other regions, e.g. South America, were not included. It is possible that both biomass burning and wetland emissions were responsible for significant and overlapping IAV but, with available information, there is no definitive way of establishing their relative contributions.

Observations of changes in the isotopic composition of atmospheric CH_4 may help to clarify this situation. For example, CH_4 from biomass burning and microbial production carries distinctive isotopic signatures in the $^{13}C/^{12}C$ ratio ($\delta^{13}C \approx$ -25 and –60 ‰) as compared to a background atmospheric value of about –47 ‰. If the 1994/95 CH_4 perturbation were entirely due to biomass burning, it would have been accompanied by a shift in $\delta^{13}C$ of +0.12 ‰. A concordant, positive shift is favoured by the record of Lowe et al. (1997) from Baring Head, New Zealand, the Cape Grim record of Francey et al. (1999b) and the SH record of Quay et al. (1999), but a shift of this magnitude is not well resolved relative to overall precision by any of these records. It remains to be seen whether $\delta^{13}C$ measurements through 1997/98 are able

to distinguish biomass burning from microbial sourced CH_4 or constrain overlapping contributions from both processes.

4.6.4 Emission ratios from Cape Grim vertical profiles

Inter-species relationships of the seasonal source influencing the mid-tropospheric plumes above Cape Grim were obtained by comparing data from individual samples against background concentrations (Pak, 2000). Calculated "emission ratios" with respect to CO_2, averaged over 1992-97, were 0.0086 ± 0.0008 for H_2, 0.0216 ± 0.0020 for CO, 0.0073 ± 0.0007 for CH_4 and -0.048 ± 0.005 ‰ ppm^{-1} for $\delta^{13}C$. These values are consistent with literature estimates for biomass burning emissions, allowing for reduction of the CO/CO_2 ratio by a factor 2 or more due to rapid removal of CO by OH. In some respects, the vertical profile data are well-suited to quantification of biomass burning emission ratios applicable to this study of global IAV. Sampled plumes are sufficiently young to retain high signal-to-noise characteristics, yet are sufficiently old to reduce uncertainties associated with sampling of fresh plumes, in relation to heterogeneity of emissions (e.g. due to source material and burning efficiency) and modification of ageing plumes by chemistry involving short-lived species such as NMHCs (Mauzerall et al., 1998; Holzinger et al., 1999). However, determination of emission ratios directly relevant to this study would require that the excess 1994/95 and 1997/98 components be resolved from mean seasonal signals. These ratios are likely to differ. Regular, seasonal emissions may include a substantial contribution from savanna fires, especially in Africa, which mostly involve flaming combustion and are characterized by low emission of H_2, CO and CH_4. The large 1994 and 1997/98 tropical fires were predominantly in peat swamps (in South-east Asia) and forests (Nichol, 1997;

Levine, 1999; Nepstad et al., 1999). There is limited knowledge of emission ratios from peat combustion (Yokelson et al., 1997) but forest fires generally emit more H_2, CO and CH_4 due to a higher proportion of smoldering combustion (e.g. Laursen et al., 1992). The sparsity of vertical profile data prevents resolution of 1994/95 and 1997/98 emission ratios to a degree that would provide a firm quantitative constraint of global IAV.

4.6.5 Emission ratios from 1997 tropical fires

Some measurements were made of the plumes above the large South-east Asian fires of 1997. Derived emission ratios have the advantage that they directly relate to fires suspected of contributing to much of the IAV in CO_2, but spatial and temporal sampling resolution is low. Matsueda and Inoue (1999) reported large enhancement of CO, CO_2 and CH_4 over Singapore in October 1997 from aircraft-based flask sampling. Measured emission ratios were 0.089 and 0.051 for CO/CO_2 and CH_4/CO implying a CH_4/CO_2 ratio of 0.0045. Aircraft-based, in-situ measurements of H_2 and CO over Indonesia in October, 1997 yielded H_2/CO ratios of 0.06-0.10 (Sawa et al., 1999). This compares with the global best estimate of 0.33 of Andreae et al. (1996) and a range of 0.06-0.52 implied by the survey of Pak (2000). These results give low CH_4/CO_2 and H_2/CO_2 ratios that support a dominant biomass burning contribution to CO_2 IAV (Table 4.5). It must be accepted, however, that their representativeness of large scale behaviour cannot be determined.

A more reliable indication of the large scale emission characteristics of the 1997 tropical fires is available from regular aircraft-based flask sampling of the mid-troposphere (8.5-13 km altitude) between Japan and Australia. Matsueda et al. (1999) reported elevated CH_4 and CO peaking in October to November, 1997, where the

enhanced CH_4/CO ratio was consistent with a dominant biomass burning influence. The enhanced CH_4/CO_2 and CO/CO_2 ratios from the same samples were 0.0089 and 0.077, but peak CO_2 enhancement occurred 1-2 months after CH_4 and CO (H. Matsueda, personal communication). These ratios are also consistent with a dominant biomass burning contribution to CO_2 IAV in 1997/98. However, the decoupling of CO_2 from CH_4 and CO demands an explanation. It would be hard to imagine the CO_2 emissions being independent of CH_4 and CO, as a phase difference of 1-2 months, while not trivial, seems too short for independent and coincidental sources. The CH_4/CO observations alone imply that CO_2 emissions from biomass burning are expected, and of magnitude similar to that observed, albeit by integrating over several months. A more likely explanation is that the phase difference reflects either heterogeneity in emission characteristics of fires during this period and/or some delayed CO_2 emissions due to decomposition of dead vegetation following the combustion phase. It remains unclear as to how representative these observations are of all 1997/98 tropical fires, integrated over all affected regions and over their full duration. Furthermore, no account is taken here of the contribution from 1998 boreal fires. Thus the accuracy of these emission ratios for linking to global IAV-related fluxes is uncertain.

4.6.6 Summary

The ability to precisely quantify biomass burning carbon fluxes is limited by knowledge of actual source H_2/CO_2 and CH_4/CO_2 emission ratios for the 1994/95 and 1997/98 events. However, it is possible to define a range that is consistent with the observations. Upper limits of literature emission ratios imply lower emission limits for CO_2 of 0.6 and 0.8 PgC for 1994/95 and 1997/98. Terrestrial pulses

indicated by the model are 3.5 and 3.7 PgC, which are adopted as likely upper limits for biomass burning. Intermediate values would be consistent with some fraction of the observed terrestrial signal being due to imbalance in photosynthesis/respiration. Higher values for total, terrestrial release would violate agreement in observed and modelled growth rate peak shapes and/or the constraint imposed by $\delta^{13}C$ but cannot be dismissed, especially in 1997/98 where an oceanic release of 0.6 PgC is indicated by the $\delta^{13}C$–based budget. A net oceanic flux of this magnitude is somewhat surprising, especially as ΔpCO_2-based estimates of air-sea flux favour a net flux of opposite sign during El Niño events (Feely et al., 1999; Le Quéré et al., 2000). Any budgeting error in overestimation of the oceanic release would translate to underestimation of the terrestrial release. This is plausible, within the ±1.1 PgC uncertainty, and would require an error in the $\delta^{13}C$-based partitioning of fluxes, involving either random (e.g, signal-to-noise) or systematic influences (e.g. underestimated isotopic disequilibrium flux, or actual ε_{lb} of source material > -17 ‰, which might occur if there was a larger fraction of C_4 exchange).

4.6.7 Comparison with inventory-based estimates

The magnitude of IAV in biomass burning carbon fluxes accommodated by the results presented here is generally higher than allowed for by previous IAV/budgeting studies. This may reflect underestimation of fluxes in previous studies, together with the fact that while anomalously high emissions have been reported from time to time for particular regions, they have generally not been evaluated in terms of combined global fluxes. The available, inventory-based estimates of 1997/98 fires for different regions are not inconsistent with results from the atmospheric, multi-species approach presented here. The more conservative

estimates of a 0.2 PgC release from each of South-east Asia (Levine, 1999) and South America (Houghton et al., 2000) together with a best estimate of 0.3 PgC from boreal fires (Kasischke et al., 1999) gives a total of 0.7 PgC, similar to the lower bound of the range estimated here. Upper bounds of 0.9 PgC for South-east Asia (Page et al., 2000) and about 1 PgC for South America (Potter et al., 2001; if conclusions relating to the early 1990s are extended to the 1997/98 event) would imply a global release of about 2.2 PgC.

It is arguable whether the parameters used in the inventory-based estimates are sufficiently constrained to exclude even larger global fluxes. For example, the Levine (1999) calculations assumed conservative estimates of area burned that were based on satellite imagery for Kalimantan and Sumatra only. Fires on other Indonesian islands and in neighbouring countries were not included. There appears to be substantial uncertainty in values adopted for biomass loading and combustion efficiency. For the 1997/98 Indonesian fires, Levine used conservative values for combustion efficiency of 20 % and above-ground biomass loading of 10,000 tons km^{-2}, though noting a mean value of 23,000 for tropical forests in South-east Asia. These values compare with $\leq$ 50 % and 20,000 tons km^{-2} used by Page et al. (2000). Effective biomass loading of peat was taken as 97,500 and 40,000-100,000 tons km^{-2} by Levine and Page et al., respectively, partly reflecting differences in assumed burning depth (1.5 m and 0.4-1.0 m) and combustion efficiency (50 % and 100 %).

The thickness of peat layers consumed by these fires might be a key parameter. The depth of Indonesian peat ranges from 0.5 to more than 10 m, with about half its total area exceeding 2 m. Field surveys in central Kalimantan following the 1997/98 fires revealed losses of between 0.2 and 1.5 m of the peat surface (Page et al., 2000). Most peat forests in Malaysia are characterized by a greater thickness,

perhaps averaging about 6 m, but with some peat layers being as deep as 16 m (Anderson, 1964; Richards, 1996). Importantly, the peat forests of Sumatra and Kalimantan are considered to be true ombrogenous mires, comparable to the raised bogs of Eurasia (Richards, 1996). Studies of the effects of fires on such bogs in Russia have revealed that complete burning of the organic part of the peat soil often occurs down to its mineral bottom, which in that study was at a depth of about 1 m (Zaidel'man et al., 1999). Although the discussion of uncertainties here has focused on the South-east Asian fires, similar considerations probably apply to the South American and boreal forest fires.

4.6.8 Pre-1993 IAV

This study has focused on the period 1992-1999, owing to the availability of high precision, multi-species data obtained from the same air samples. In light of the conclusion that biomass burning was a major influence on IAV during this period, it is pertinent to further examine earlier multi-species IAV information and links to El Niño or biomass burning events that occurred before 1992. Concurrent, high precision records of $\delta^{13}C$ in CO_2, CH_4 and CO extend back to the early 1980s, allowing comparison over this period with the longer CO_2 records starting in 1958. Measurements of H_2 over 3.5 years between 1985 and 1989 were reported by Khalil and Rasmussen (1990) but the records are too short to clearly resolve any IAV.

High growth rates of CH_4 and CO following the 1991 Pinatubo eruption were linked to perturbations in OH (Dlugokencky et al., 1996; Novelli et al., 1998) but were not accompanied by elevated growth rates of CO_2. The largest positive global CO_2 growth rate anomalies between 1980 and 1993 were observed in 1983 and 1987 (Conway et al., 1994; see also NOAA/CMDL website http://www.cmdl.noaa.gov),

coinciding with the largest CO growth rate anomalies of the decade observed at the SH sites, Cape Point (Brunke et al., 1990) and Cape Grim (Fraser et al., 1994; Langenfelds et al., 2001b). Re-evaluation of the $CO_2/\delta^{13}C$ relationship by Francey et al. (2001) shows these CO_2 variations to be largely from terrestrial forcing. Both 1983 and 1987 anomalies occurred during El Niño events that preceded major fires in Indonesia and elsewhere in the Western Pacific region (Malingreau et al., 1985; Page et al., 2000 and references therein). Extensive fires were also reported for Amazonia (Setzer and Pereira, 1991) and Eurasia in 1987 (Cahoon et al., 1994; Kasischke et al., 1999). Thus there is a substantial body of evidence to indicate a biomass burning influence on IAV of CO_2 and CO during the 1980s. However, CH_4 IAV did not show as strong a correlation with the other species as was observed after 1992. Markedly different behaviour was observed in the Northern and Southern Hemispheres between 1983 and 1990 (Dlugokencky et al., 1994; see also http://www.cmdl.noaa.gov). Positive growth rate anomalies were observed in the SH in 1983 but not in 1987 (Dlugokencky et al., 1994; Fraser et al., 1994). This suggests that processes other than biomass burning probably contributed to forcing of CH_4 IAV during this period.

4.7 Conclusions

Strong correlation in interannual growth rate variations of CO_2, its $\delta^{13}C$, H_2, CH_4 and CO was observed at a network of globally distributed surface sites between 1992 and 1999. The relationship of CO_2 with ENSO was broadly consistent with observations from earlier decades. Growth rate variations were global in extent with a latitude/phase relationship suggesting partly tropical forcing with an additional contribution from high northern latitudes in 1998, at least for CO. Similar variations

were observed in vertical profiles of the troposphere above Cape Grim, where plumes enriched in products of biomass burning are observed seasonally between July and November. Strong enrichment was observed in years coinciding with major biomass burning events in South-east Asia and South America in 1994 and 1997/98, and independent observations of elevated levels of biomass burning products such as CO, O_3, C_2H_6 and HCN in the free troposphere at these times. Larger areas of boreal forest were burned in 1994, 1995 and 1998 than in neighbouring years.

A multi-species, pulse perturbation model shows that the observed global IAV is largely consistent with two emission pulses of 1-year duration centred on August, 1994 and February, 1998 and that the chemical signature is consistent with a significant, perhaps major contribution from biomass burning. However, it does not prove this scenario. The modelling involves an assumed time distribution of perturbations forcing IAV and thus does not attempt to provide a unique solution. Use of a 1-box model and 1.8-year smoothing examines large scale behaviour but does not use all available information on spatiotemporal trace gas variations. More detailed studies may be possible using 3D chemical transport models constrained by higher resolution data sets that also incorporate measurements from other laboratories and perhaps other chemical and isotopic tracers.

Using this approach, estimation of the relative magnitudes of globally integrated fluxes for each species provides a means of assessing possible contributions from different source/sink processes. The relationship between CO_2 and $\delta^{13}C$ implies the major fraction of CO_2 variability is from terrestrial exchange. This conclusion is supported by observations of IAV in $\delta(O_2/N_2)$ at Cape Grim made by SIO and URI/PU, though noting the signal-to-noise ratio for detection of IAV may not be as high for $\delta(O_2/N_2)$ as for $\delta^{13}C$. The CSIRO $\delta(O_2/N_2)$ record exhibits

large variability, probably due to artefacts associated with experimental techniques, and is not a reliable constraint of IAV.

Multi-species signatures involving H_2, CH_4 and CO are consistent with biomass burning and eliminate other sources and sinks as sole forcing mechanisms. However, covariations of other sources/sinks with biomass burning and/or ENSO cannot be excluded. Foremost among these are net respiration of CO_2 from terrestrial ecosystems and CH_4 production from wetlands and rice paddies.

Best estimates of anomalous H_2, CO and CH_4 emissions in 1994/95 and 1997/98 are 3.8 and 5.3 Tg H_2, 280 and 580 Tg CO, 26 and 33 Tg CH_4. If it is assumed that biomass burning is the dominant forcing of IAV in H_2, CH_4 and CO, these species provide a direct, quantitative constraint of CO_2 emissions from biomass burning and distinguish them from any net respiration signal. CO-based budgets are not well constrained due to the short CO adjustment time. Calculations based on H_2 and CH_4 rely on independent knowledge of source H_2/CO_2 and CH_4/CO_2 emission ratios, for which literature estimates show a large range of variation and globally integrated 1994/95 and 1997/98 values are poorly constrained. Consequently, uncertainties in derived carbon fluxes are large and would be reduced if better definition of these ratios became available. Total carbon (effectively CO_2 + CO) pulses from biomass burning of 0.6-3.5 and 0.8-3.7 PgC are implied for 1994/95 and 1997/98 respectively. These pulses represent biomass burning emissions in excess of mean levels of other years. The lower bounds are constrained by the upper limit of literature H_2/CO_2 and CH_4/CO_2 emission ratios while upper bounds represent the full terrestrial component of each pulse, as constrained by $\delta^{13}C$.

CHAPTER 5

SEASONAL AND VERTICAL VARIATIONS OF O_2/N_2 ABOVE CAPE GRIM

5.1 Introduction

Most of our knowledge about the distribution of trace gases in the atmosphere comes from near surface measurements, yet these measurements only describe the lower boundary of the atmosphere. For example, CO_2 is now monitored at more than 100 globally distributed surface sites, providing extensive information about latitudinal and longitudinal gradients at the surface. By comparison, measurements describing variations with altitude are relatively sparse. Improving the definition of vertical gradients in atmospheric composition is a high priority for accurate budgeting of atmospheric trace gas burdens, for calibrating atmospheric transport models and for using such models to infer trace gas fluxes. The importance of vertical gradients is illustrated by observations from CSIRO's ground and aircraft-based sampling in the SH that show larger gradients for some species (such as CO_2) over 8 km altitude above Cape Grim than over 5500 km between Cape Grim and the South Pole in MBL air.

The above-surface data that do exist have been gathered by air sampling from aircraft, balloons or tall towers, or by remote sensing from ground-based or satellite platforms. Each method has its limitations. Many of the aircraft and balloon sampling programs have involved relatively brief campaigns (duration of days to weeks), which only provide a snapshot of vertical structure in atmospheric composition. Balloon sampling programs have focused mainly on the stratosphere where trace gas variations are generally larger than in the troposphere (e.g. Schmidt

and Khedim, 1991). Tall towers have a limited altitude range and thus capture variations forced by surface exchange characteristic of a relatively small footprint (typically over distances of 10s to 100s of kilometres; e.g. Bakwin et al., 1995). Remote sensing techniques primarily measure integrated column densities and have limited ability to resolve vertical structure (e.g. Connors et al., 1996; Rinsland et al., 1999; 2000).

There are few long-running programs, especially in the SH, with data that constrain seasonal and/or interannual changes in vertical gradients of the trace gas species analysed in GASLAB. Several are operated by Japanese groups. The Meteorological Research Institute (MRI) and Japan Meteorological Agency (JMA) obtain latitudinal gradients at 8-13 km altitude from regular commercial airliner transects between Japan and Australia (Matsueda et al., 1999). Regular vertical profiling has been conducted by Tohoku University (TU) above Japan (Tanaka et al., 1988) and Syowa Station, Antarctica (Murayama et al., 1995) and by the National Institute for Environmental Studies (NIES) above Russia (Machida et al., 2001). Similar programs are maintained by NOAA/CMDL who sample above Colorado, USA (Tans et al., 2001) and by a group of laboratories sampling above several sites in Siberia and Western Europe as part of the EuroSib program (Levin et al., 2002). All of these programs include CO_2 among their suite of measured species but as yet there are no reported measurements of vertical O_2/N_2 gradients.

CSIRO has conducted regular aircraft-based sampling of the atmosphere above the south-east Australian region since 1972 (Beardsmore et al., 1978; Pearman et al., 1983). Vertical profiling above Cape Grim commenced in 1989, initially to an altitude of about 4 km. From 1992 the altitude range was extended to a maximum of 6-8 km (Langenfelds et al., 1996a). Air samples were collected mostly in CSIRO's

0.5 L glass flasks and analysed for the full suite of species routinely measured in GASLAB (CO_2 and its isotopes $\delta^{13}C$ and $\delta^{18}O$, CH_4, H_2, CO and N_2O).

A study of vertical profile climatologies of GASLAB-measured species by Pak (2000; see also Pak et al., 1996; 1999) identified several important influences on vertical gradients and their seasonal variation. One of the key findings was observed enrichment of CO_2, CO, CH_4, H_2 and depletion of $\delta^{13}C$ in CO_2 in the 4-8 km altitude range between July and November. The signal was attributed to emissions from seasonal biomass burning in the SH tropics that are convected into the mid to upper troposphere and transported laterally to higher latitudes. Enrichment of CH_4 and CO, and depletion of H_2 between January and June also at high altitudes was found to be consistent with influence of inter-hemispheric exchange and photochemistry involving OH. Mean vertical gradients in CO_2 were related to uptake of anthropogenic CO_2 by the Southern Ocean. Mean gradients in $\delta^{13}C$ were observed to exhibit positive correlation with CO_2. This observation is puzzling as the sign of the relationship is opposite to expectation for net exchange with either the land biosphere or the oceans. Pak (2000) speculated that it might reflect a regional oceanic influence involving isotopic disequilibrium with the atmosphere.

Measurement of O_2/N_2 in a subset of aircraft-based samples commenced in 1995. A key focus of this chapter is to establish a seasonal climatology of vertical profiles in $\delta(O_2/N_2)$ and to interpret the observations in terms of surface exchange and atmospheric transport processes. In conjunction with mean, seasonal surface records from Cape Grim and corresponding records for other species (particularly CO_2 and its $\delta^{13}C$), the multi-species climatologies of surface and vertical variations can be used to explore the contribution to seasonal variations from different processes.

The seasonal cycle of $\delta(O_2/N_2)$ in the SH at the surface, for example at Cape Grim, has previously been interpreted as being mainly forced by SH surface exchange. Keeling et al. (1993) modelled the seasonal variation as a sum of three processes, all acting approximately in phase with one another. There are minor components associated with a thermally forced air-sea flux and seasonal exchange with land biota. The oceanic component reflects the different atmospheric mole fraction and temperature dependent solubility of O_2 and N_2. The terrestrial component is very small in the SH compared to the NH, due to the smaller vegetated land area, as illustrated by the large N-S difference in seasonal cycle amplitude of CO_2.

The major fraction of the SH $\delta(O_2/N_2)$ seasonal cycle was attributed to air-sea exchange forced by cycling of marine biological production and ocean mixed layer depth (see also Bender et al., 1996; Balkanski et al., 1999). Enhanced rates of marine production in spring and summer coincide with shoaling of the mixed layer, leading to super-saturation of O_2 in surface waters. Much of the O_2 escapes into the atmosphere before it can be remineralised. This leads to a seasonal maximum in atmospheric $\delta(O_2/N_2)$ in late summer. Some of the organic material produced in the euphotic zone falls below the mixed layer where waters are effectively isolated from the atmosphere. Remineralisation creates a sub-surface O_2 deficit. In autumn and winter, marine production rates slow as waters cool, and both insolation and nutrient availability are diminished. The stratification of near surface waters breaks down, leading to ventilation of water under-saturated in O_2. This draws down atmospheric $\delta(O_2/N_2)$ leading to a seasonal minimum in late winter.

Improved definition of atmospheric dynamics in the SH should help to better constrain SH ocean carbon cycle processes. Cape Grim O_2/N_2 data have previously

been used to estimate seasonal variations in air-sea fluxes, thus constraining marine production rates (Keeling and Shertz, 1992; Bender et al., 1996). This requires assumptions about the rate of vertical transport in the SH troposphere and contributions to O_2/N_2 and CO_2 seasonal cycles from terrestrial exchange and inter-hemispheric transport. One aim here is to use the O_2/N_2 data, in conjunction with supporting data for other species to better constrain the contributions to observed seasonal cycles from each of these processes.

5.2 Air sampling

5.2.1 Aircraft and sampling equipment

Four individual aircraft were used for the flights from which O_2/N_2 measurements were obtained (Table 5.1). All were equipped with twin, wing-mounted engines and unpressurised cabins. In relation to air sampling, the main distinguishing feature was the configuration of air intake systems. Because three of the aircraft were privately owned and were chartered by CSIRO, there was limited scope to modify, standardise or optimise air intake systems for air sampling applications. Brief descriptions of each system are as follows:

1. The Cessna 310 was fitted with two independent sampling lines (4.5 m of 3/8" O.D. tubing, one of nylon and the other copper) drawing air from under the nose of the aircraft and through the firewall (via stainless steel bulkhead, quick-connect fittings) at the front of the cabin.
2. It was not possible to install dedicated intake lines on the Cessna 401A. Instead, air was drawn from the aircraft's ventilation system by feeding the inlet lines of the pump units into a cavity above the ceiling. This cavity was continually flushed with fresh air during flight. Flow rates

were always far in excess of demand from the pump units, preventing return flow of cabin air into the ceiling cavity. There was no evidence of sample air ever being contaminated by cabin air. On occasions, this did occur in other aircraft and was detected primarily by strong enhancement (by up to hundreds of ppm) in measured CO_2 due to contamination by human respiration.

3. A dedicated intake, similar to that used on the Cessna 310 but with a single port and mounted on the underside of the fuselage, was used on the single Fokker F27 flight.

4. The Piper Navajo was fitted with a dedicated, air intake plate mounted on the front passenger side window of the aircraft. The plate was of stainless steel construction and was equipped with four independent ports to accommodate use of multiple pump units and/or on-board instruments.

Dates	Aircraft	Air source
1/95 – 5/98	Cessna 310	Dedicated air intake plate (2 independent ports) mounted under the nose of the aircraft
6/98 – 9/99	Cessna 401A	Cabin ventilation system; accessed via cabin air ports
24-Sep-98	Fokker F27	Dedicated air intake plate (single port) mounted on underside of fuselage
10/99 – 9/00	Piper Navajo	Dedicated air intake plate (4 independent ports) mounted on side window

Table 5.1 Aircraft and associated air intake systems used for O_2/N_2 sampling above Cape Grim.

Two, nominally identical pump units were used for O_2/N_2 sampling (see Chapter 2). Further details of aircraft and sampling equipment are described by Langenfelds et al. (1996a; 1996c; 2001c; 2002c).

5.2.2 Flight protocol

The standard flight path is shown in Figure 5.1. After taking off from Melbourne's Moorabbin Airport, the aircraft climbs to an altitude of 4.9 km and flies south of Melbourne to a point above Bass Strait (39°08'S, 145°14'E). The first set of samples (usually including one for O_2/N_2 analysis) are collected to a) extend the time series of CO_2 obtained at this location since 1980 and b) monitor latitudinal variations in trace gas composition of the mid-troposphere over 1.4° of latitude (a distance of about 155 km) between Bass Strait and Cape Grim (Langenfelds et al., 2001c). The aircraft then ascends to the maximum altitude of 6-8 km while proceeding to a point (40°33'S, 144°18'E) 35 km west (and upwind) of Cape Grim. A vertical profile is obtained by sampling at multiple altitude levels down to 150 m (Figure 5.2).

While descending through a profile, the plane is flown along a line perpendicular to the wind direction and extending 10 km to either side of a central point. On reaching either end of the 20 km transect the plane is turned through 180°, always by turning the nose into the wind so as to prevent the possibility of sampling air contaminated by the engine exhausts. CSIRO's glass, 0.5 L flasks are flushed for a minimum of 3 minutes at low altitudes, ranging to 7 minutes at higher altitudes. Calculations based on flask volume, flushing flow rates and aircraft speed of travel indicate that samples collected in 0.5 L flasks represent an air parcel integrated over horizontal distances of about 1 km near the surface to about 6 km at 8 km altitude.

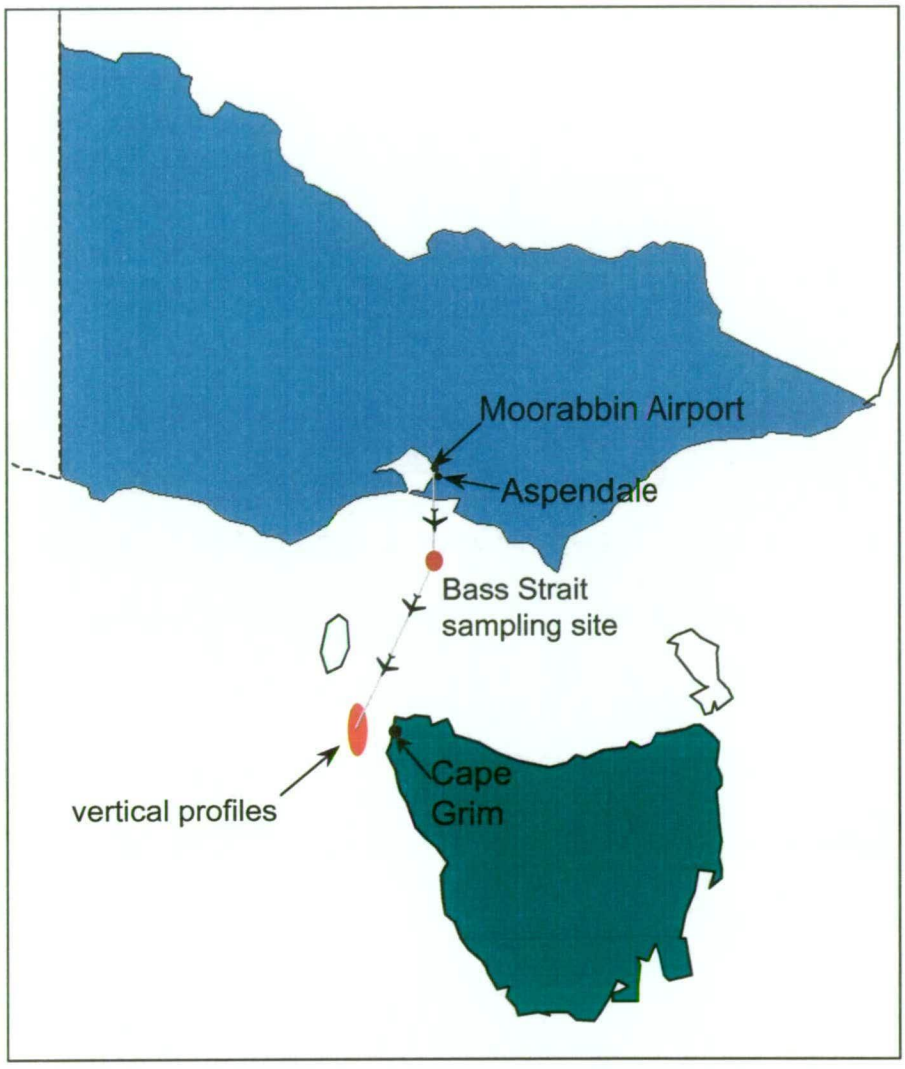

Figure 5.1 The usual flight path and sampling regions of aircraft flights over Bass Strait and Cape Grim between 1995 and 2000.

5.2.3 Sampled air masses

Sampling days were selected on the basis of anticipated clean air conditions at Cape Grim such that the air masses being sampled were free of recent continental influence and therefore representative of a large and well-mixed part of the atmosphere at these latitudes. Flights were typically conducted 1 - 2 days after the passage of a frontal system through the Cape Grim area, allowing sufficient time for

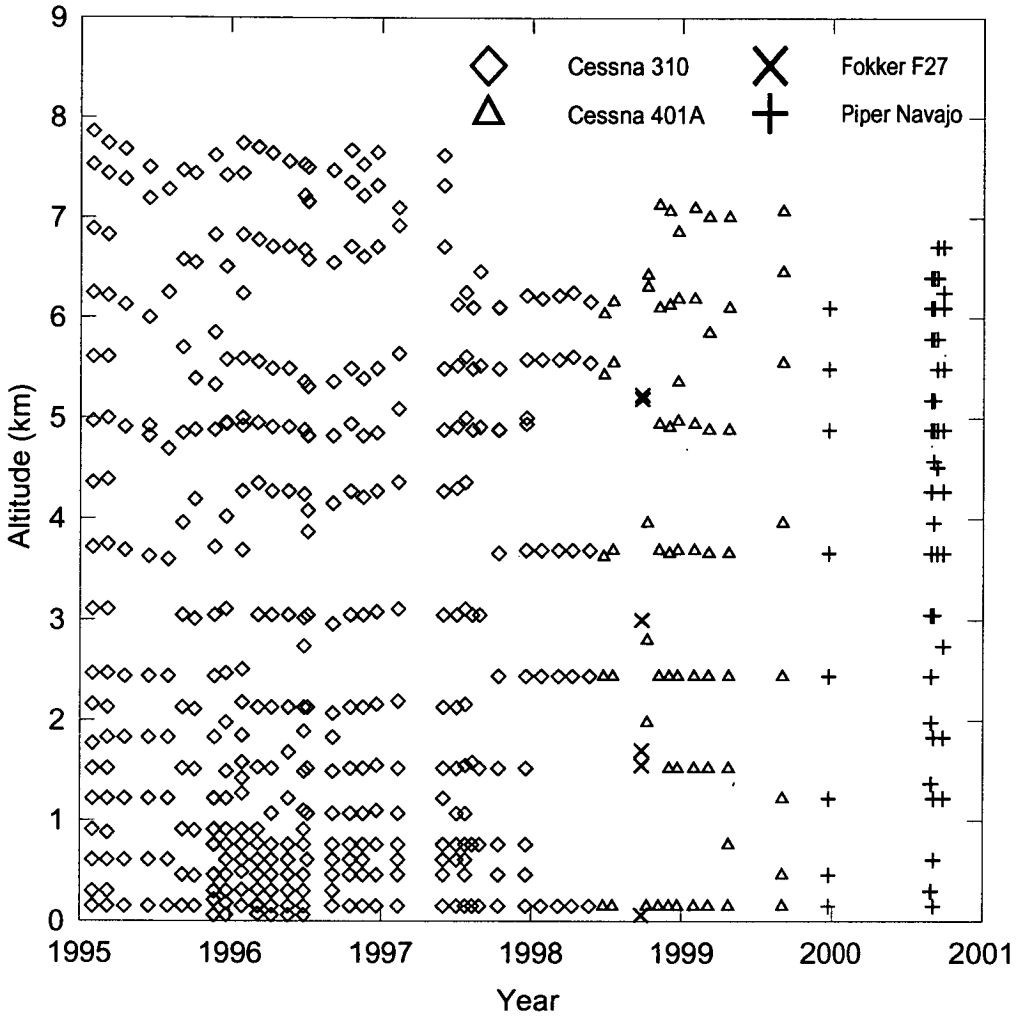

Figure 5.2 Temporal and vertical distribution of aircraft-based air samples analysed for O_2/N_2. Each point represents one sample collection, with symbols distinguishing different aircraft.

stable baseline conditions to become established. Typical back trajectories of air masses sampled for O_2/N_2 at 500 hPa (5.5 km altitude) are plotted in Figure 5.3. The majority of trajectories traverse the Southern Ocean to the south of Australia under the prevailing westerly flow.

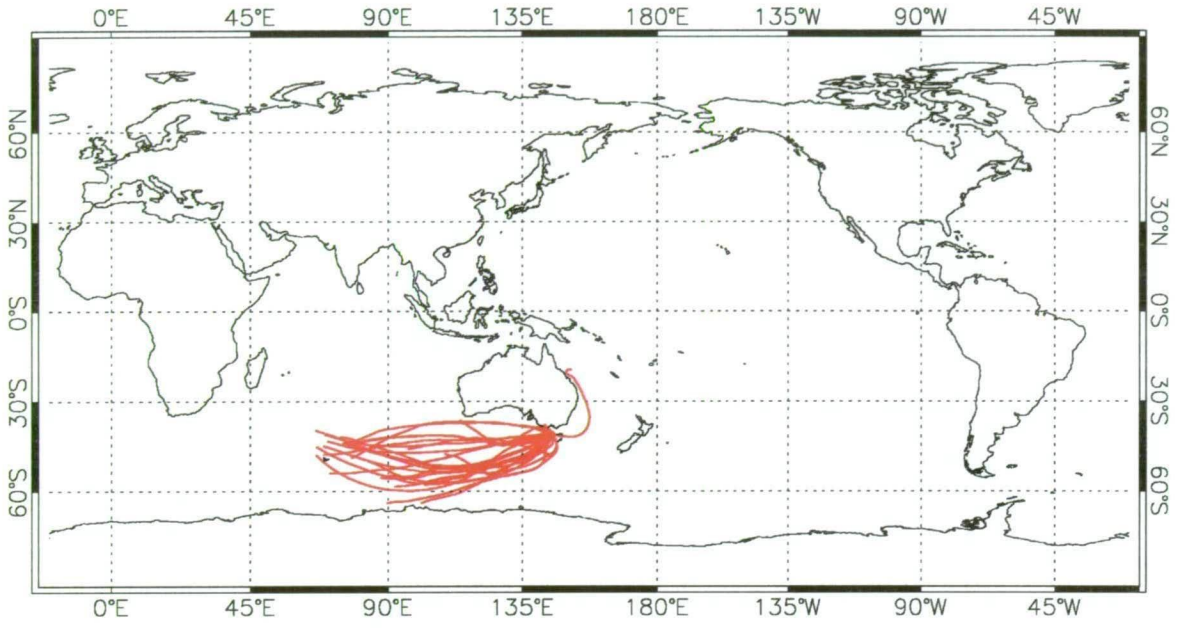

Figure 5.3 4-day back trajectories of air masses at 500 hPa (5.5 km altitude) arriving above Cape Grim for flights in 1998/99.

5.3 Observations

5.3.1 $\delta^{29}N_2$ and $\delta(Ar/N_2)$ artefacts

As demonstrated in Chapters 2 and 3, measurements of $\delta^{29}N_2$ and $\delta(Ar/N_2)$ are a key diagnostic of sample fractionation. By comparison to $\delta(O_2/N_2)$, both tracers are highly inert with respect to biogeochemical processes and are thus expected to exhibit negligible vertical gradients in the troposphere. The main influence is likely to be a small seasonal variation due to thermally forced air-sea fluxes. For example, the peak-to-peak amplitude of the $\delta(Ar/N_2)$ seasonal cycle at the surface in the SH is estimated to be 11 per meg based on the modelling of Keeling et al. (1993). By itself, this could force seasonal cycling in the vertical $\delta(Ar/N_2)$ gradient of up to about ±5

per meg, depending on the rate of vertical mixing. The faster the vertical mixing, the smaller the amplitude of seasonal cycling in the vertical gradient. In terms of annual averages, gradients for both $\delta(Ar/N_2)$ and $\delta^{29}N_2$ are expected to be much smaller. Mean gradients in these tracers are shown in Figure 5.4 for data obtained using each of the four aircraft. Also shown are mean values from Cape Grim surface sampling.

Significant, non-zero gradients are evident for both tracers with some aircraft. Furthermore, there are systematic differences between surface and low altitude, aircraft-derived data. In each case, the relationship between the tracers implicates mass-dependent fractionation as the main influence. By far the largest signal emerges for the Piper Navajo. Linear regressions to the data in Figure 5.4 indicate mean artefacts in vertical gradients over 7 km of -165 ± 32 and -12 ± 3 per meg for $\delta(Ar/N_2)$ and $\delta^{29}N_2$ respectively (Table 5.2). The $\delta(Ar/N_2)/\delta^{29}N_2$ ratio of $13.8^{+5.3}_{-3.8}$ is close to the value (10-12) expected for mass-dependent fractionation. These data imply an artefact in $\delta(O_2/N_2)$ vertical profiles obtained with this aircraft of about –50 per meg (calculated as $\delta(Ar/N_2) / 3$ or $\delta^{29}N_2 \times 4$). The individual vertical $\delta(Ar/N_2)$ profiles are plotted in Figure 5.5. They show significant, non-zero vertical gradients for each flight and significant variability among flights. Samples collected on the Piper Navajo also exhibited artefacts in other trace gas species measured in GASLAB: H_2, CO_2, CH_4 and CO (Langenfelds et al., 2002c). For these species, the artefacts were suggestive of contamination by aircraft-related emissions (though were not clearly associated with cabin air, e.g. human respiration, or engine exhaust), and were not consistent with mass-dependent fractionation. Affected data were linked to a single pump unit on each flight, though not the same unit on all flights, perhaps suggesting a problem with the air intake plate.

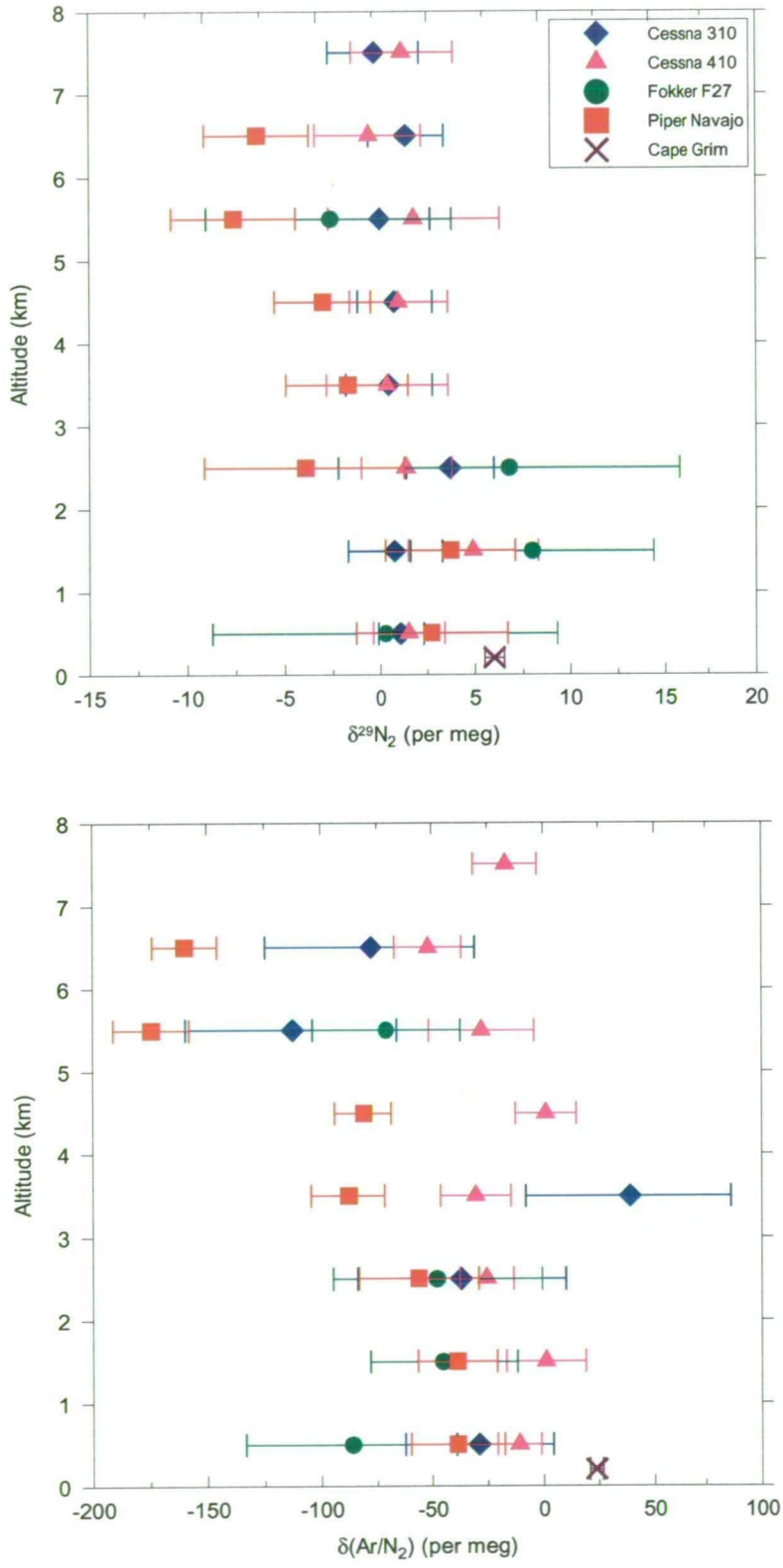

Figure 5.4 Mean $\delta^{29}N_2$ (upper panel) and $\delta(Ar/N_2)$ (lower panel) of aircraft-derived data for each 1 km altitude band, distinguished by aircraft, and from surface sampling at Cape Grim. Error bars represent the standard error of the mean.

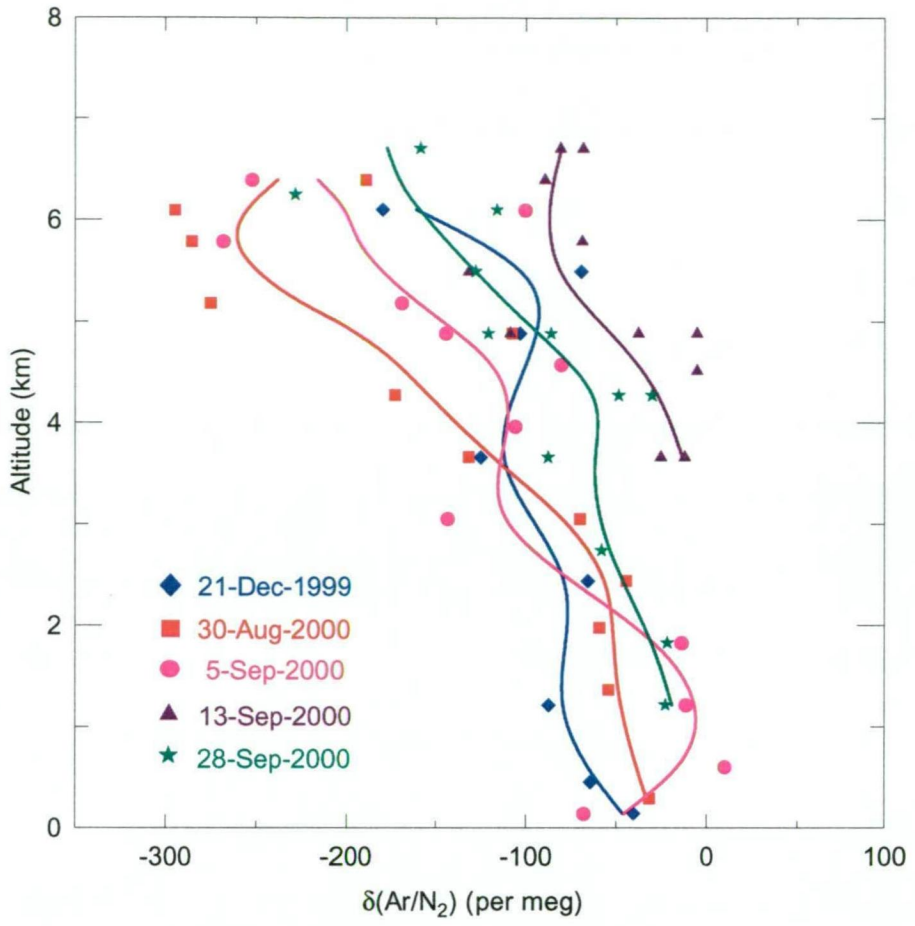

Figure 5.5 Piper Navajo $\delta(Ar/N_2)$ vertical profiles for individual flights. The curves represent spline-fits to data from each flight with 50 % attenuation at 3 km.

Aircraft	No. Flights	$\delta(Ar/N_2)$	$\delta^{29}N_2$	$\delta(Ar/N_2)/\delta^{29}N_2$[a]
Cessna 310	27[b]	-89 ± 81	-1.5 ± 1.1	-
Cessna 401A	10	-23 ± 18	-2.3 ± 1.6	10^{+24}_{-9}
Fokker F27	1	-3 ± 40	-10 ± 8	-
Piper Navajo	5	-165 ± 32	-12 ± 3	$13.8^{+5.3}_{-3.8}$

Table 5.2 Vertical gradient artefacts in $\delta(Ar/N_2)$ and $\delta^{29}N_2$ over a 7 km altitude range as determined by linear regression to data obtained with each of the four aircraft. Negative values indicate decreasing δ with increasing altitude.

[a]Ratios are not meaningful for Cessna 310 and Fokker F27 data due to insufficient data.

[b]$\delta^{29}N_2$ was measured on all 27 flights but $\delta(Ar/N_2)$ was measured on just one Cessna 310 flight.

There are also extensive statistics for both tracers from Cessna 401A flights. Inspection of individual $\delta(Ar/N_2)$ profiles revealed significant, non-zero gradients for only one flight (16-Jul-98) with two samples near 6 km altitude being depleted by about 300 and 500 per meg. There were no irregularities in sampling techniques or conditions for this flight, hence the reason why such fractionation should have occurred on only the one flight with this aircraft remains unknown. Data from this flight are omitted from further analysis. Averaging over all other Cessna 401A data, artefacts in 7 km vertical gradients are -23 ± 18 and -2.3 ± 1.6 per meg for $\delta(Ar/N_2)$ and $\delta^{29}N_2$ respectively, much smaller than observed in Piper Navajo data but again suggestive of a mass-dependent process with a $\delta(Ar/N_2)/\delta^{29}N_2$ ratio of 10^{+24}_{-9}. The implied artefact in measured $\delta(O_2/N_2)$ gradients is about –8 per meg.

A single $\delta(Ar/N_2)$ profile was obtained from the earlier Cessna 310 flights conducted between 1995 and 1998 but experimental precision precludes it from usefully constraining possible artefacts in $\delta(O_2/N_2)$. However, there are extensive $\delta^{29}N_2$ data from samples collected using this aircraft, most of which were analysed on the MAT252 instrument. They give a mean $\delta^{29}N_2$ gradient of -1.5 ± 1.1 per meg over 7 km, slightly smaller than for the Cessna 401A, but with overlapping uncertainties. The implied $\delta(O_2/N_2)$ gradient due to fractionation is about –6 per meg. Statistics for neither tracer from the single Fokker F27 flight were sufficient to usefully constrain possible $\delta(O_2/N_2)$ artefacts.

The cause of the fractionation has not been fully established, but some points can be made about the nature of the effect. Firstly, the dependence on aircraft and the fact that pump units were unchanged throughout, implicates the air intake systems, which differed among the four aircraft. In particular, observed fractionation (and

modification of other trace gases) in samples collected on the Piper Navajo is suspected of being related to the air intake plate mounted on the side window of this aircraft. It is not clear if the problem relates to the design or construction of this plate or its position on the aircraft. It may be significant that samples collected on the Cessna 310 and the Fokker F27 did not exhibit the same degree of fractionation even though the air intakes were of similar design to that used on the Piper Navajo.

Secondly, where non-zero $\delta(Ar/N_2)$ and $\delta^{29}N_2$ gradients were observed, the largest variability among aircraft, and among individual Piper Navajo flights appeared at high altitudes. Furthermore, these high altitude measurements were furthest removed from surface (Cape Grim and cylinder standards filled at Cape Schanck) and near surface aircraft data, obtained with a variety of collection techniques. These factors argue for the fractionation being primarily associated with sampling at high altitudes. If so, it is likely related to vertical gradients in either atmospheric pressure or temperature.

5.3.2 Vertical profile simulation experiment

An experiment designed to simulate sampling under conditions of varying ambient pressure was conducted at CSIRO's Cape Schanck cylinder filling facility on 5 September, 1995. South-west winds brought air to Cape Schanck that was comparable to baseline air at Cape Grim in terms of composition and homogeneity. A Siemens ELMO-G blower was used to draw air through 1½" polyethylene hose from near the top of the 33 m tower at a flow rate of about 400 L min^{-1}. Air was drawn from the main air stream via a tee-junction, at flow rates of between about 5 and 19 L min^{-1} using an electric diaphragm pump (KNF Neuberger type N735.3 AN.18) and through a stainless steel chamber whose pressure was controlled by

variable flow restricting valves at its inlet and outlet. The pressure in this chamber was varied between 350 and 950 hPa to simulate the approximate range of ambient pressure encountered during a vertical profile. Inlet lines of the pump units used for aircraft-based sampling were connected to this chamber. Twenty-four samples were collected in 0.5 L glass flasks and analysed for the full suite of species routinely measured in GASLAB (Langenfelds et al., 1996c). Twelve of the flasks were filled to 1.5 atm and analysed for O_2/N_2 and $\delta^{29}N_2$.

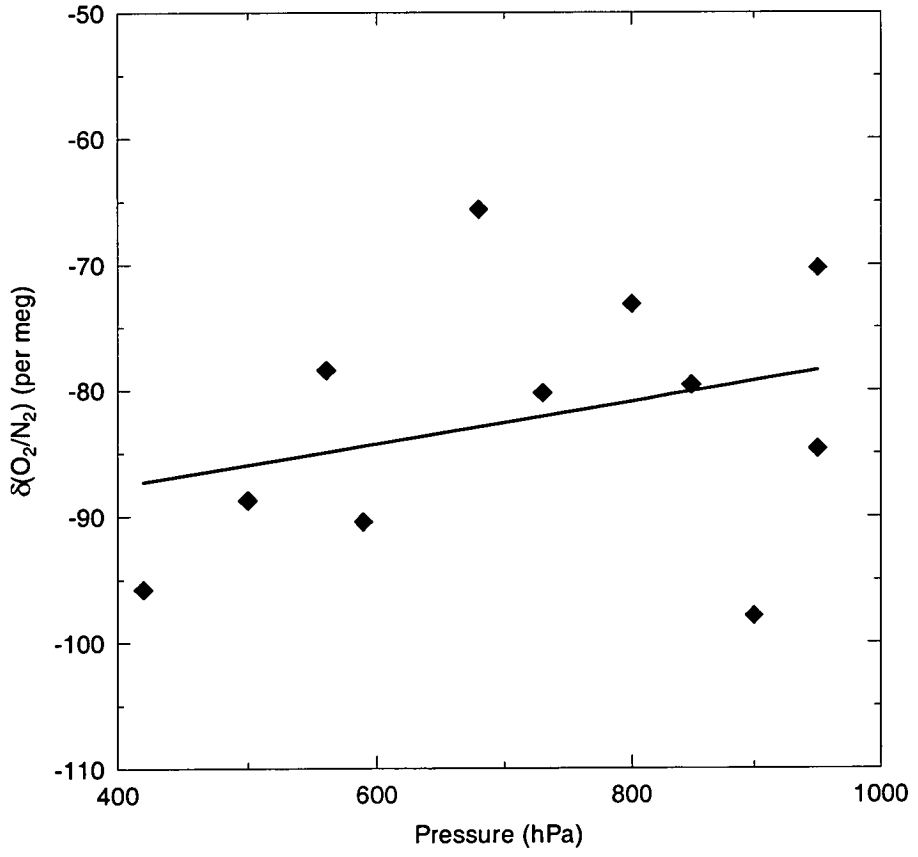

Figure 5.6 Measurements of $\delta(O_2/N_2)$ from 0.5 L glask flask samples filled as part of a vertical profile simulation experiment. Data are plotted as a function of pump unit inlet pressure and are fitted by a linear regression.

Measurements of $\delta(O_2/N_2)$ are plotted in Figure 5.6, excluding one sample at 350 hPa inlet pressure which was rejected due to highly anomalous results for multiple species. The pressure range of 420 to 950 hPa simulates atmospheric pressure at altitudes in the range 6.8 to 0.5 km. A linear regression gives a slope of -0.017 ± 0.018 per meg hPa^{-1}, equivalent to an artefact of -9 ± 9 per meg over a 6.3 km altitude range, or extrapolated to -10 ± 10 per meg over a 7 km range. Measurements of $\delta^{29}N_2$ were not sufficiently precise to usefully constrain $\delta(O_2/N_2)$ with a slope of -1 ± 10 per meg over 7 km. These results give a best estimate of the slope in $\delta(O_2/N_2)$ that only borders on significance but is very close to that implied by observations of $\delta(Ar/N_2)$ and $\delta^{29}N_2$ in vertical profiles obtained with either of the Cessna aircraft. They are consistent with the artefacts observed in aircraft-sourced data being related to fractionation from pressure diffusion effects. However, in light of the fractionations associated with tee-junctions reported by Manning (2001), the possibility of similar interferences being introduced by the plumbing configuration of the simulation experiment cannot be ruled out.

5.3.3 Data selection and corrections

Based on the data quality assessment for $\delta(Ar/N_2)$ and $\delta^{29}N_2$, all Piper Navajo and Fokker F27 data are excluded from further analysis of $\delta(O_2/N_2)$ vertical profiles. It has been established that the Piper Navajo data are compromised by large and variable fractionation of sample air. There is insufficient diagnostic information to verify integrity of $\delta(O_2/N_2)$ data from the single Fokker F27 flight. Only the Cessna 310 and Cessna 401A data are used for interpretation of $\delta(O_2/N_2)$ profiles because altitude-dependent fractionation in $\delta(O_2/N_2)$ is well constrained by the $\delta(Ar/N_2)$ and

$\delta^{29}N_2$ data. A correction of +1 per meg km^{-1}, relative to 150 m altitude, is applied to $\delta(O_2/N_2)$ data obtained using both Cessna aircraft.

Data from the first two flights from which $\delta(O_2/N_2)$ profiles were obtained (in January and March, 1995) are also rejected due to excessive noise in these measurements and inconsistency in calibration procedures in the earliest few months of analyses relative to later years.

5.3.4 Comparison of Cape Grim and 0-1 km aircraft data

Comparison of aircraft data from the 0-1 km altitude band with data from ground-based sampling at Cape Grim in Figure 5.4 shows large differences in both $\delta(Ar/N_2)$ (Cape Grim – aircraft = 41 ± 10 per meg) and $\delta^{29}N_2$ (4.9 ± 1.4 per meg). Again, the $\delta(Ar/N_2)/\delta^{29}N_2$ ratio of $8.3\ ^{+3.8}_{-2.7}$ points to samples collected from one or both platforms being subject to mass-dependent fractionation. Further supporting evidence for such effects comes from data for $\delta^{13}C$ in CO_2 (measured as the ratio of isotopomers of CO_2 with *m/z* 44 and 45, i.e. a 1 mass unit difference as for $\delta^{29}N_2$), which show a mean (Cape Grim – aircraft) difference of 5 ± 4 per meg (std. error, n = 42) in samples collected between 1994 and 1998 (Langenfelds et al., 2001c). The $\delta^{13}C$ value only borders on significance but is consistent with $\delta(Ar/N_2)$ and $\delta^{29}N_2$ in suggesting a fractionation effect.

These results suggest that sampling techniques are responsible for fractionation, either favouring collection of lighter molecules in aircraft-based samples and/or heavier molecules in Cape Grim samples. The fact that fractionations were identified in vertical profiles indicates that the aircraft-based sampling techniques are susceptible to such effects. However, it is also conceivable that air collected at the Cape Grim station might be enriched by fractionation of divided air

streams at tee-junctions (Manning, 2001). Air is supplied to various pump units and in-situ analysers through multiple tee-junctions fitted to a common, high flow rate, air stream.

Aircraft-derived measurements of $\delta(O_2/N_2)$ are plotted in Figure 5.7 and compared to the smooth curve from surface sampling at Cape Grim (Section 3.3.1).

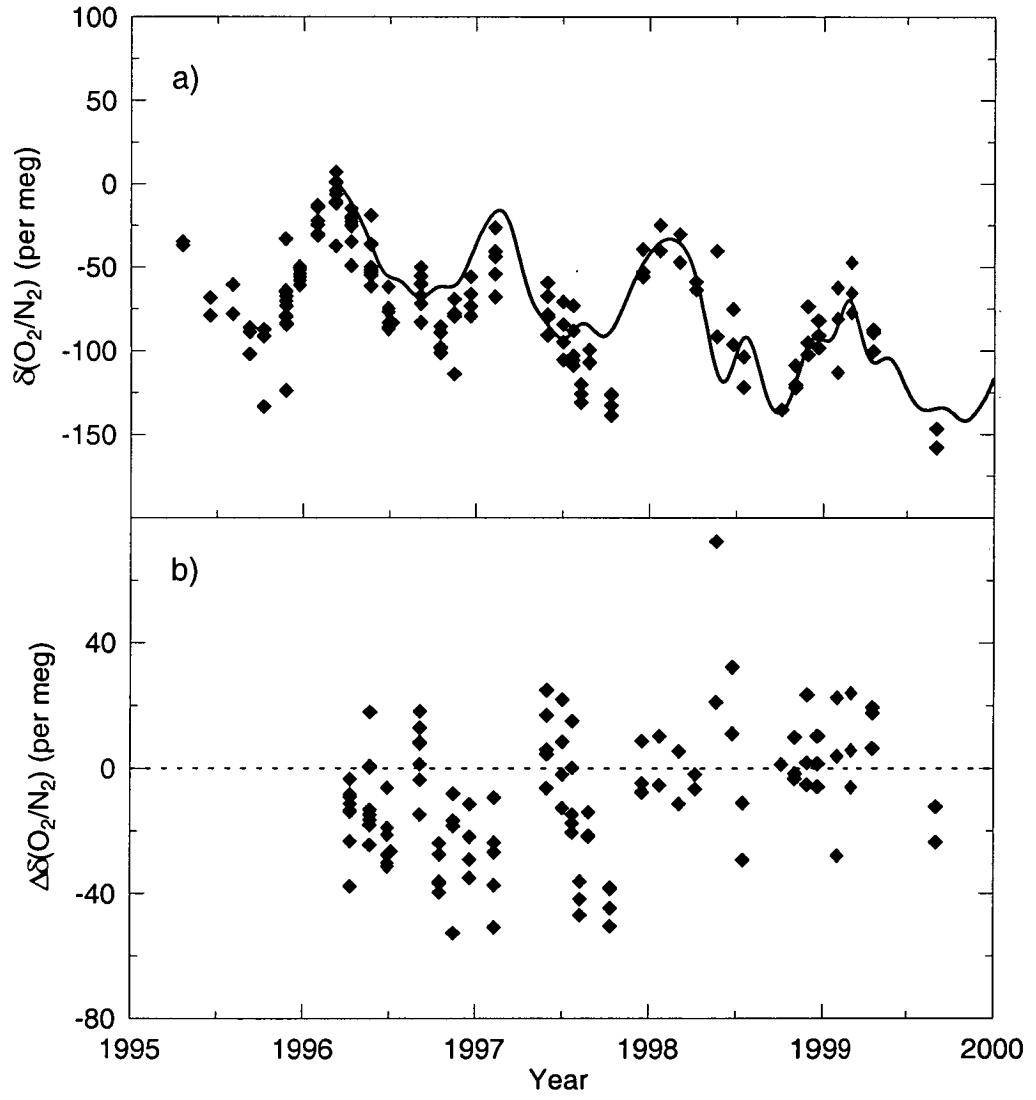

Figure 5.7 a) $\delta(O_2/N_2)$ from aircraft-based sampling in the 0-1 km altitude range (diamonds) and the smoothed curve from surface sampling at Cape Grim. b) $\delta(O_2/N_2)$ differences (aircraft – Cape Grim smoothed).

There is substantial variability in differences between the records. The aircraft data were, on average, lower by about 20 per meg in 1996, consistent with a fractionation-related offset implied by mean $\delta(Ar/N_2)$ and $\delta^{29}N_2$ data. However, differences were large and variable in 1997, while little or no offset was observed in 1998/99. The variations in the difference are difficult to explain. They do not correlate with changes in aircraft or sampling equipment. They cannot be explained by anomalies in sample storage drifts because storage conditions (duration, flask and O-ring type, pressure, surrounding atmosphere) were virtually identical for surface and aircraft-based samples. They are larger than what could be explained by short term (timescale of days) variations in calibration based on cylinder standards (see Figure 2.18). Corresponding records of $\delta^{29}N_2$ do not support the 20 per meg shift in 1997/98 being related to mass-dependent fractionation (Figure 5.8). There are no $\delta(Ar/N_2)$ measurements for samples collected before 1998.

It is possible that some of the difference might reflect coastal air-sea exchange, for example involving anomalous upwelling events as suggested by Manning (2001) for $\delta(O_2/N_2)$ perturbations observed at La Jolla, California and Baring Head, New Zealand. However, it seems unlikely that atmospheric variability could account for much of the aircraft/surface differences reported here, as comparable variability was not observed in the higher precision Cape Grim records of SIO and URI/PU. These arguments point to sample collection related artefacts being the most likely cause of variations in the differences. The absence of a mass-dependent relationship with variations in $\delta^{29}N_2$ suggests a contribution from processes other than fractionation.

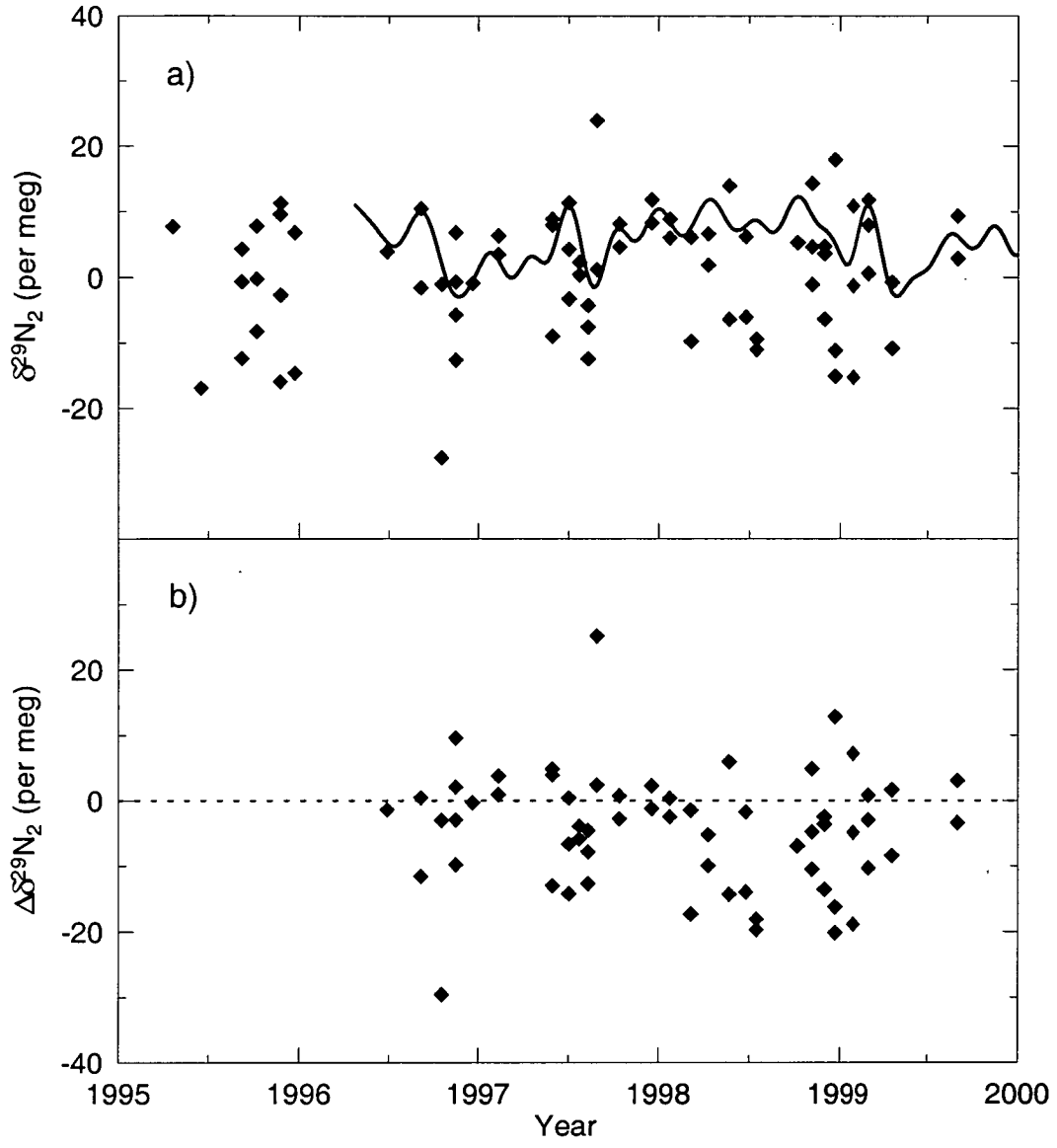

Figure 5.8 a) $\delta^{29}N_2$ from aircraft-based sampling in the 0-1 km altitude range (diamonds) and the smoothed curve from surface sampling at Cape Grim. b) $\delta^{29}N_2$ differences (aircraft – Cape Grim smoothed).

5.3.5 Seasonal climatologies of vertical gradients

The data processing algorithms used here to define seasonal climatologies of $\delta(O_2/N_2)$ vertical profiles closely follow those used by Pak (2000). The lower altitude (0–1 km) data were used to define a trend line with the mean seasonal cycle removed. This was achieved here using the curve-fitting routine of Thoning et al.

(1989). A quadratic and 3-term harmonic function was fit to the data:

$$f(t) = at^2 + bt + c + \sum_{i=1}^{3}[d_i \sin(2\pi it) + e_i \cos(2\pi it)] \quad (5.1)$$

Residuals from the fit were then smoothed by a low pass filter with a cutoff time of 120 days. The trend line is given by the sum of the quadratic function and the smoothed residuals, and excludes the harmonic component of the fit. The trend line suppresses perturbations on timescales less than 120 days but captures variations that are sustained over several months or more, long enough to be well mixed throughout the SH troposphere. Use of the 0-1 km aircraft data to define the trend should largely circumvent the artefacts responsible for the Cape Grim/aircraft differences in Figure 5.7. The key assumption is that any artefacts in the aircraft data (other than the inferred, mean vertical gradient artefact in $\delta(O_2/N_2)$ which is already corrected for) apply equally to all samples collected on each flight.

The number of flights and precision of data are not sufficient to detect year to year variations in cycling of the vertical gradient. However, mean seasonal behaviour can be examined by collating data from all flights as a function of time of year. Residuals from the 0-1 km trend line are plotted in Figure 5.9 for five altitude bands: 0-1, 1-2, 2-4, 4-6 and 6-8 km. Harmonic curves were fit to the residuals by compiling a 4-year data set with successive and identical residuals in each year (to avoid possible end-effects) and applying Equation 5.1. The harmonic curves for all five altitude bands and for the full Cape Grim record (1996-2001) are plotted together in Figure 5.10. Seasonal variations in the vertical gradient are also displayed in Figure 5.11 by mean bimonthly gradients.

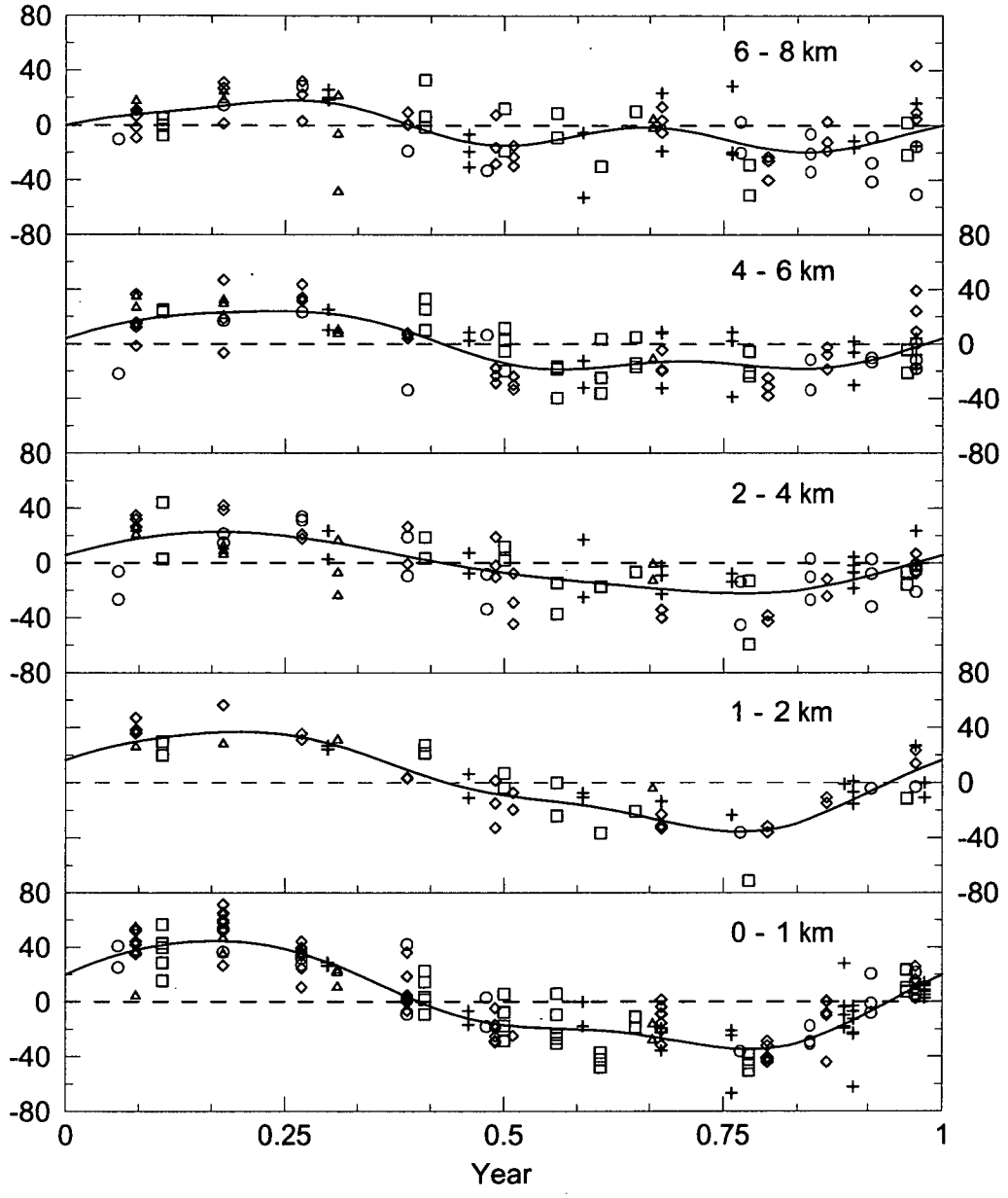

Figure 5.9 $\delta(O_2/N_2)$ residuals from a trend line defined by 0-1 km data with seasonal cycle removed. Residuals are sorted by altitude band and fitted with harmonic function curves. Symbols denote the year of sampling: 1995 (+), 1996 (◊), 1997 (□), 1998 (o) and 1999 (Δ).

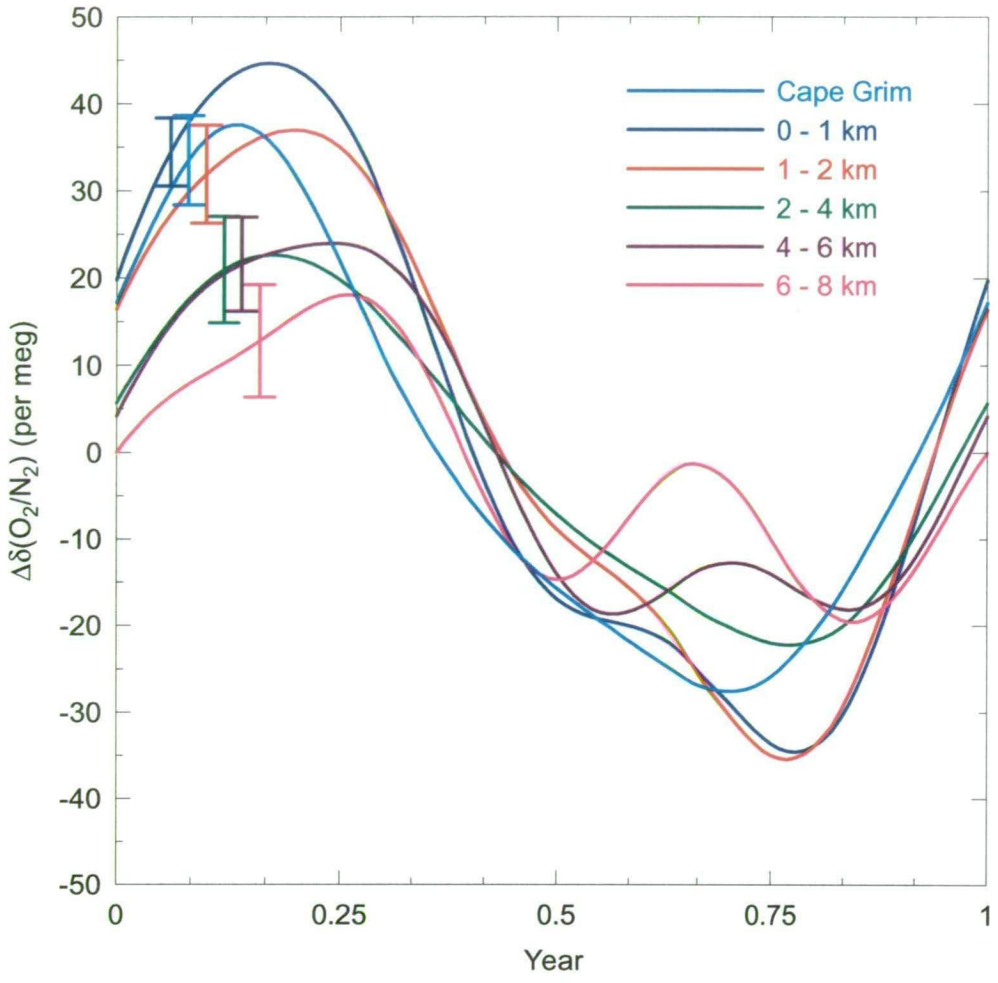

Figure 5.10 Harmonic curves representing the mean seasonal cycle of $\delta(O_2/N_2)$ as inferred from aircraft-sourced data in five altitude bands for the period 1995-1999 and from surface sampling at Cape Grim between 1996 and 2001.

The Cape Grim and lowest altitude (0–1 km) aircraft-derived curves in Figure 5.10 are expected to be similar, yet the Cape Grim curve has substantially smaller peak-to-peak amplitude by 14 per meg. This mainly reflects different averaging periods and interannual variability in the seasonal cycle. When the curves are calculated for the overlapping period only (1996-1999), their amplitudes differ by only 6 per meg. Because the aircraft data predate the commencement of the Cape

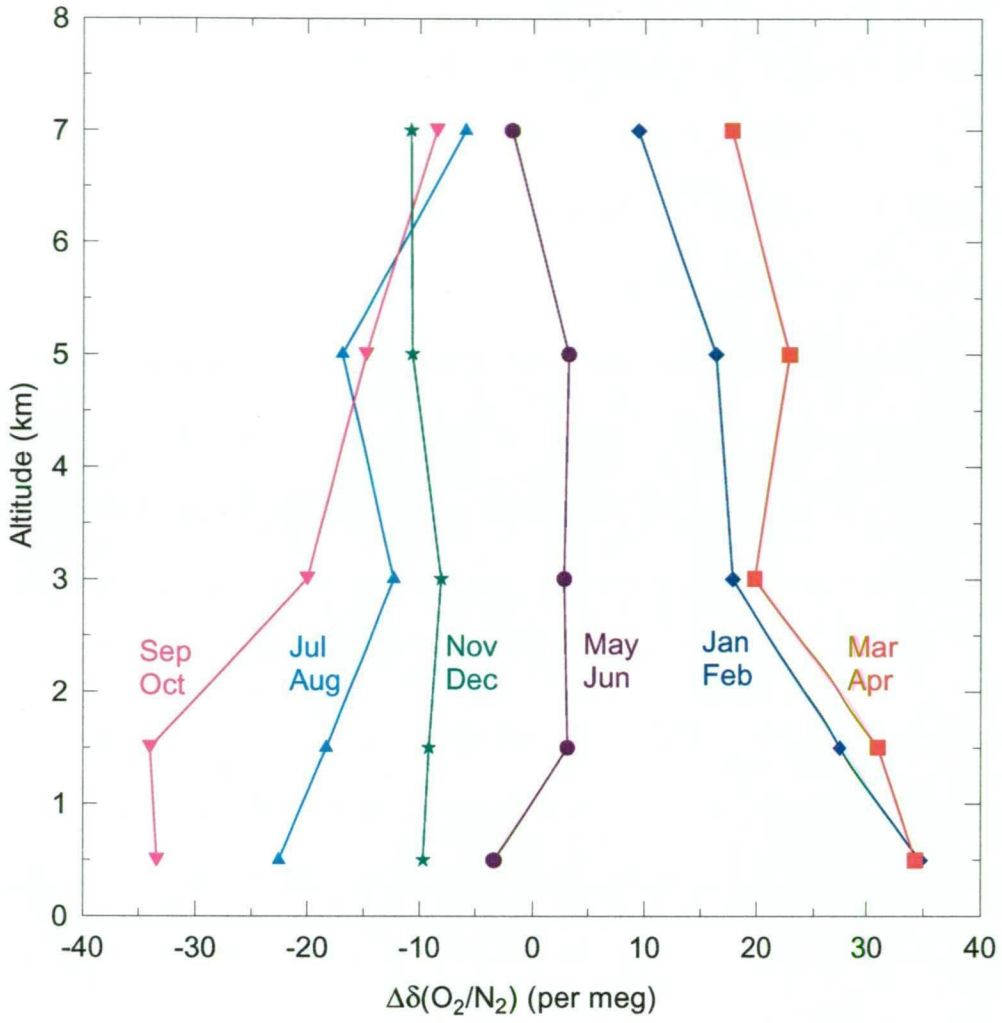

Figure 5.11 Mean, bimonthly $\delta(O_2/N_2)$ vertical profiles calculated from the harmonic curves in Figure 5.10.

Grim record and to avoid possible sampling related biases as indicated by Figure 5.7, the Cape Grim data are not considered any further in this analysis.

The curves in Figure 5.10 show the seasonal cycle amplitude to decrease with altitude from about 80 per meg (peak-to-peak) near the surface to about 35 per meg at 6-8 km. There is a discernible shift in the phase of the seasonal maximum from low to high altitudes with a lag of about 1 month between 0-1 and 6-8 km. These features are qualitatively consistent with the seasonal cycle being forced mainly by

surface exchange in the SH, and damping of the amplitude of the cycle as it is propagated vertically into the troposphere. However, the altitudinal variations around the time of the seasonal minimum in austral winter/spring are not consistent with this simple model. The highest altitude bands at 6-8 and 4-6 km both show perturbations from sinusoidal behaviour between about May and October. The leading phase and larger amplitude of the perturbation at 6-8 km suggests this signal originates in the upper troposphere. Inspection of the flask data in Figure 5.9 shows that perturbations were observed in at least three individual years, suggesting this is a genuine, seasonal atmospheric feature and not an artefact, for example associated with a single flight.

To take advantage of the multi-species, vertical profile measurements, a similar data treatment was carried out for CO_2, its $\delta^{13}C$, H_2, CO and CH_4. Data were collated from the same flights selected for integrity of O_2/N_2 data, to avoid possible inconsistency in multi-species relationships due to interannual variability. Climatologies for all species closely resembled those determined by Pak (2000) for the period 1992-1997. Seasonal climatologies of CO_2 and $\delta^{13}C$ are displayed in Figures 5.12-15.

There are several interesting features in the comparisons of harmonic curves at different altitudes. Throughout the year, CO_2 exhibits a positive (defined here as increasing with altitude) vertical gradient. Between May and July, CO_2 levels above 4 km increase rapidly towards the seasonal maximum. The fact that the 4-6 and 6-8 km curves diverge from MBL curves during this period indicates that CO_2 is being injected into the upper troposphere. Furthermore, the higher altitudes exhibit larger seasonal cycle amplitude than the MBL. Propagation by vertical mixing of seasonal variations in surface fluxes cannot account for these observations. Note that the 1-2

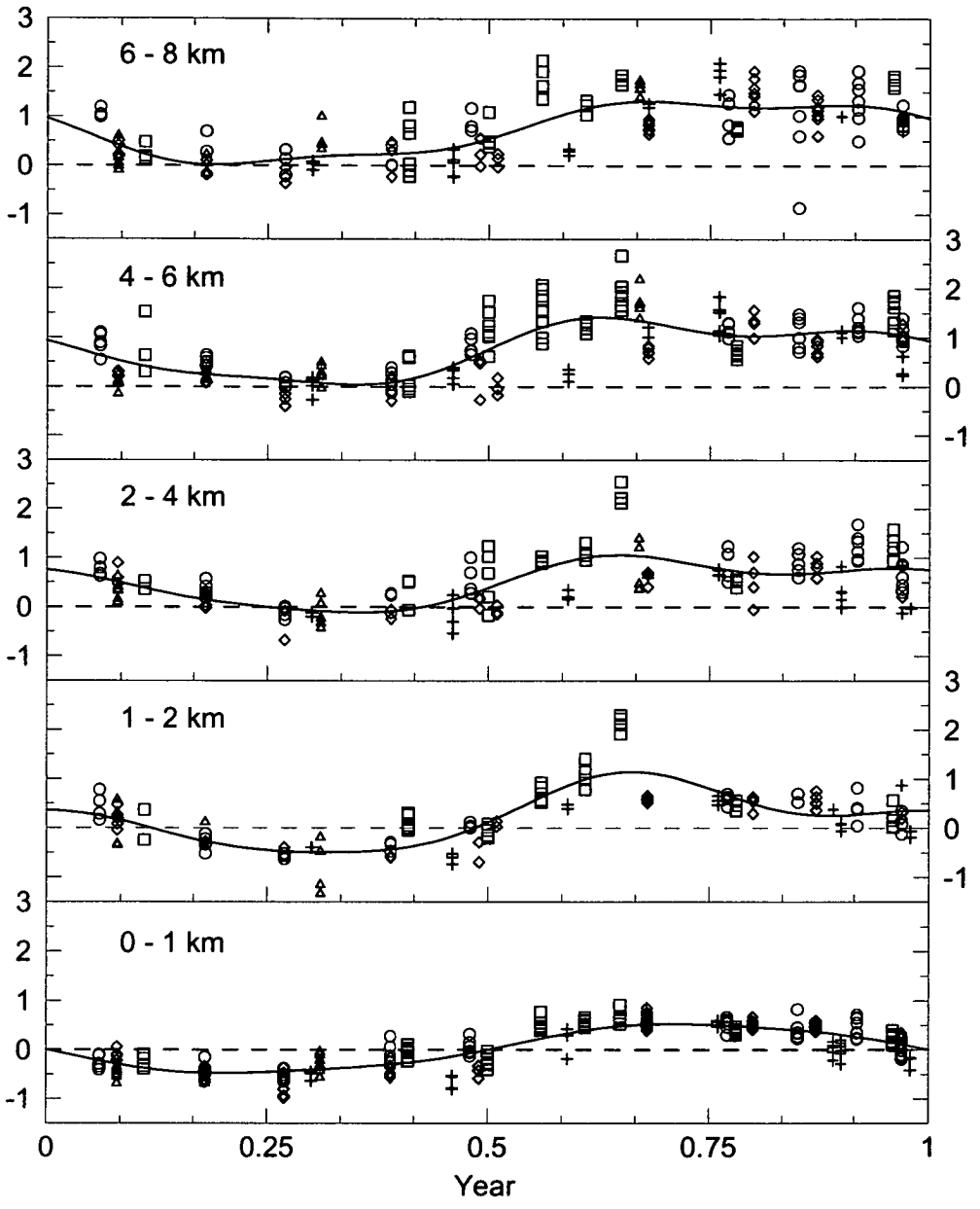

Figure 5.12 CO_2 residuals from a trend line defined by 0-1 km data with seasonal cycle removed. Residuals are sorted by altitude band and fitted with harmonic function curves. Symbols denote the year of sampling: 1995 (+), 1996 (◊), 1997 (□), 1998 (o) and 1999 (Δ).

and 2-4 km seasonal maxima are anomalously high relative to neighbouring altitude bands due to elevated CO_2 data from one flight in August, 1997 (Figure 5.12).

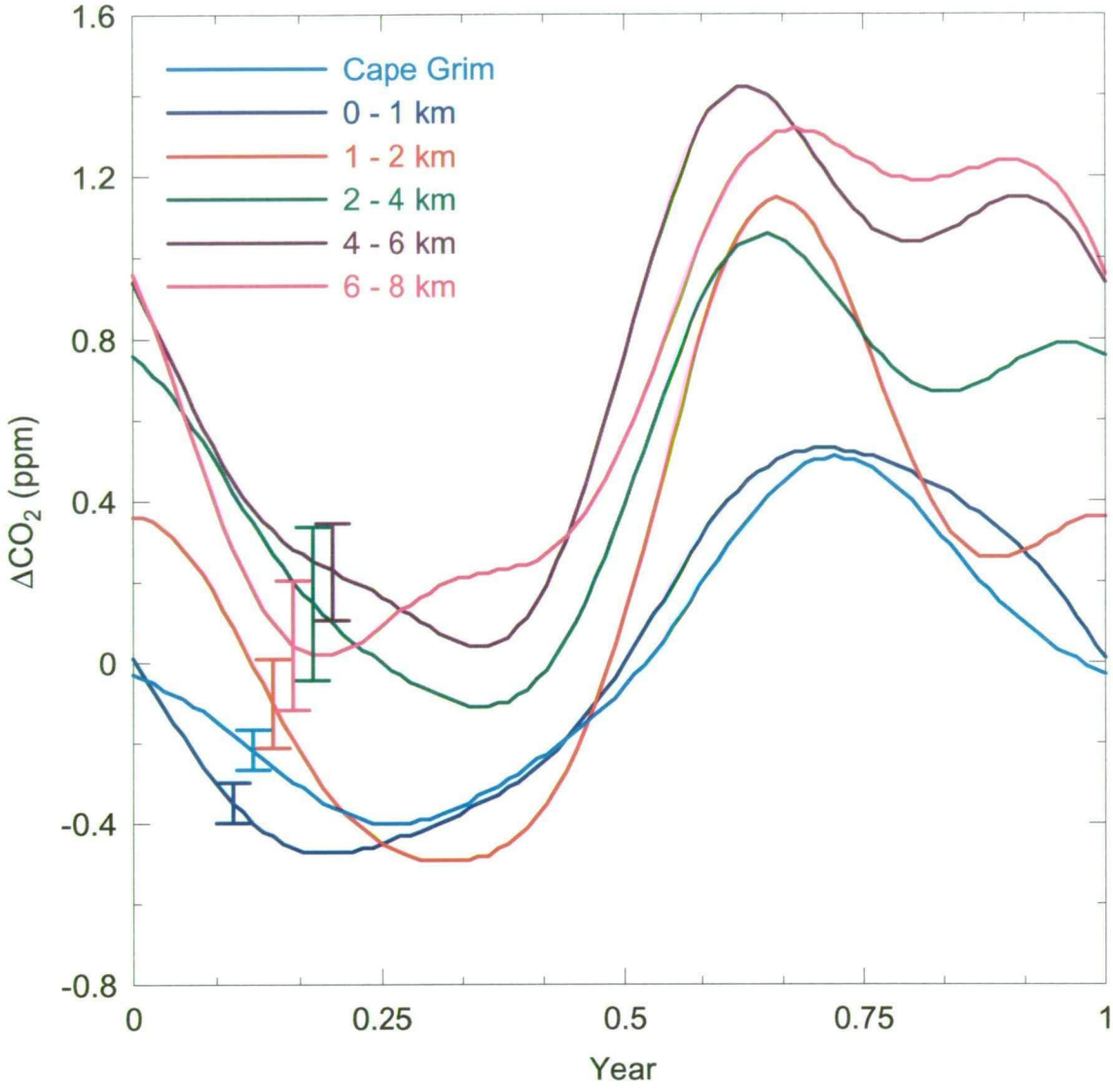

Figure 5.13 Harmonic curves representing the mean CO_2 seasonal cycle as inferred from aircraft-sourced data in five altitude bands for the period 1995-2000 and from surface sampling at Cape Grim between 1992 and 2001.

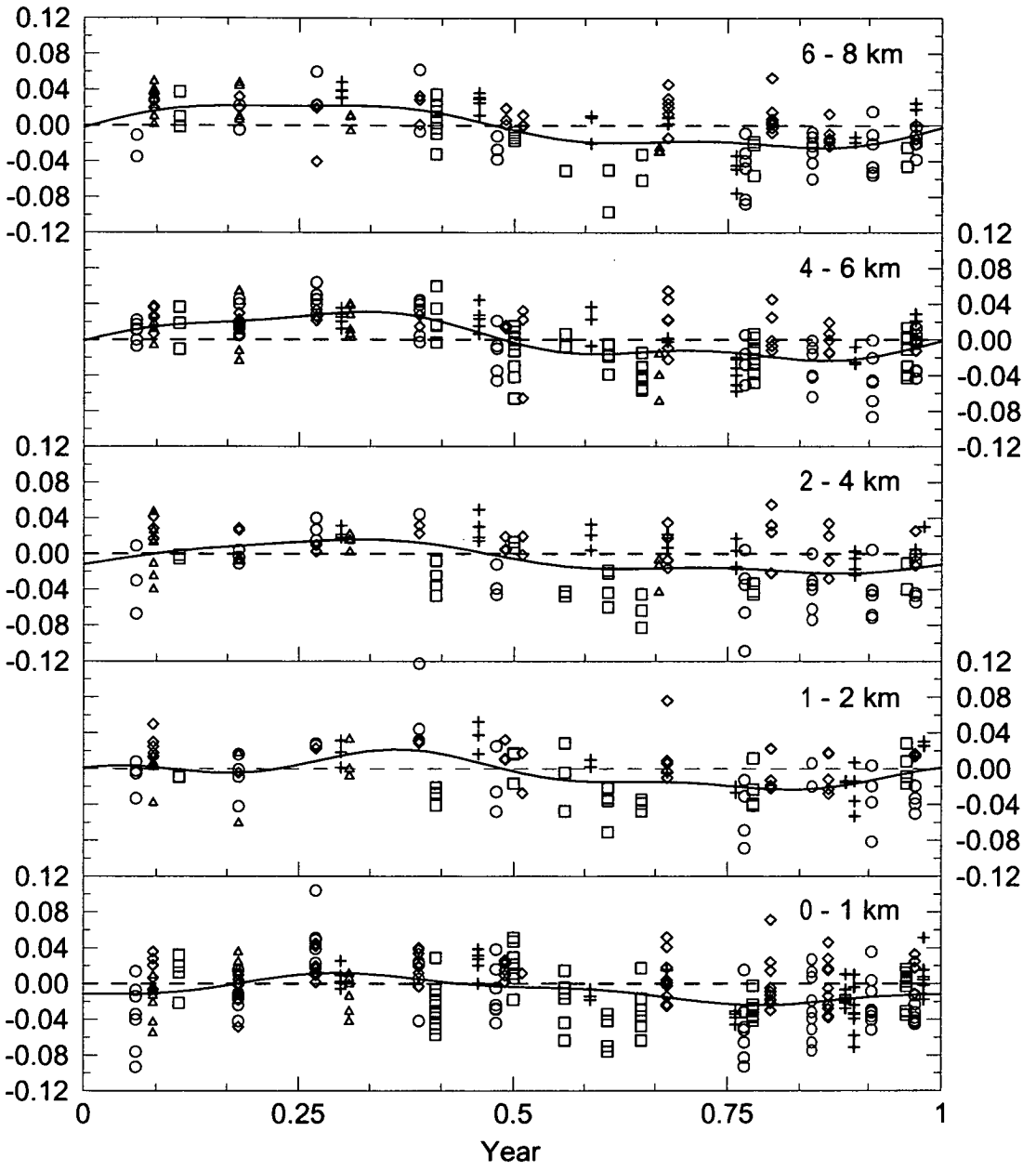

Figure 5.14 $\delta^{13}CO_2$ residuals from a trend line defined by 0-1 km data with seasonal cycle removed. Residuals are sorted by altitude band and fitted with harmonic function curves. Symbols denote the year of sampling: 1995 (+), 1996 (◊), 1997 (□), 1998 (o) and 1999 (Δ).

The $\delta^{13}C$ curves in Figure 5.15 show a systematic difference between 0-1 km and surface data. This is another manifestation of the discrepancies described in Section 5.3.2, that suggest fractionation of sample air associated with either the surface and/or aircraft-based sampling techniques. An interesting feature in this plot

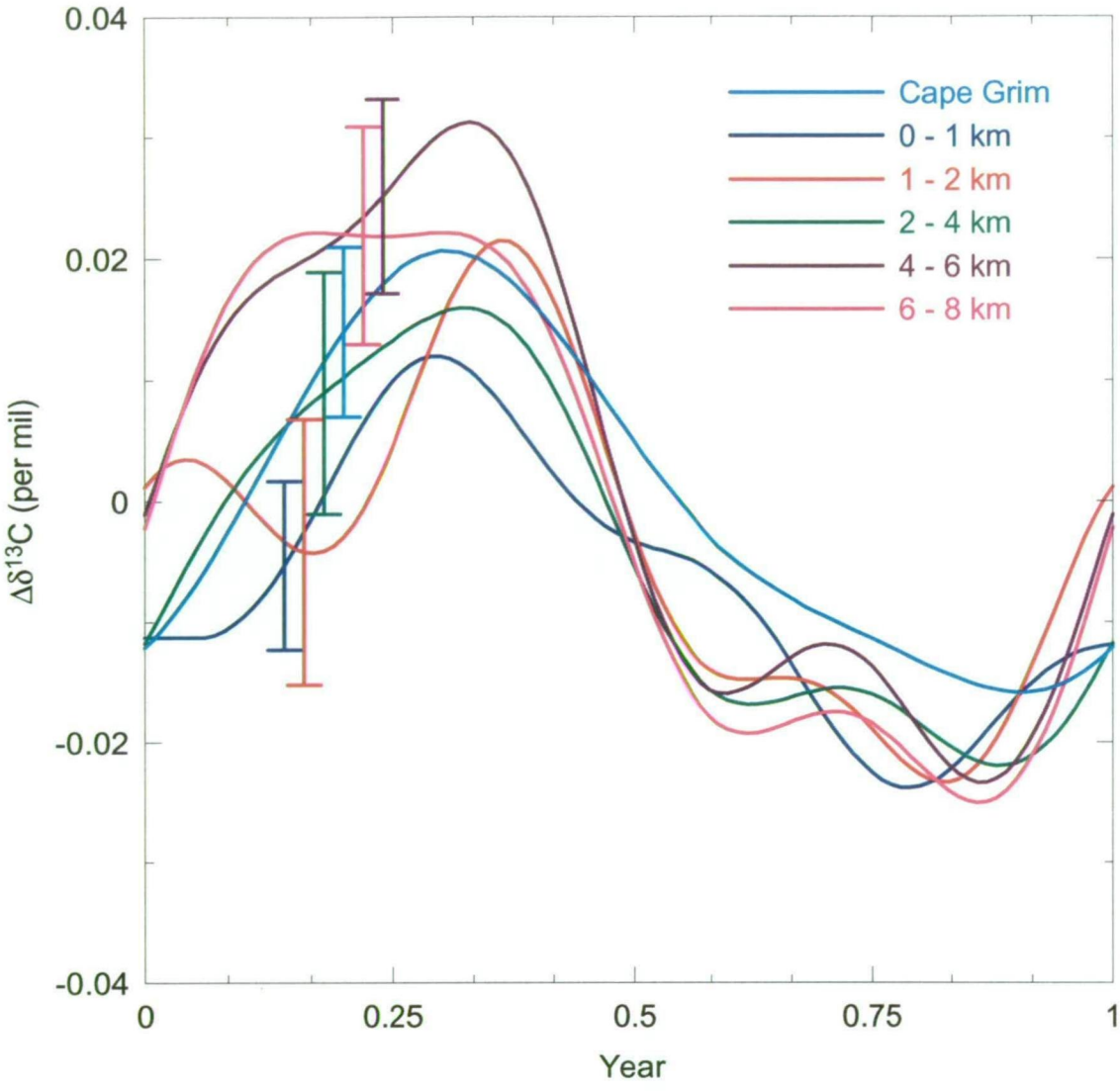

Figure 5.15 Harmonic curves representing the mean seasonal cycle of $\delta^{13}CO_2$ as inferred from aircraft-sourced data in five altitude bands for the period 1995-2000 and from surface sampling at Cape Grim between 1992 and 2001.

is the positive vertical gradient in $\delta^{13}C$ between about January and May. This gradient is of the same sign as that of CO_2, thus showing a relationship that is opposite to expectation for net CO_2 exchange with either the oceans or land biota.

5.4 Tests using an atmospheric transport model

5.4.1 Model description

The observed seasonal climatologies are investigated here using a modified version of the National Center for Atmospheric Research Model of Atmospheric Transport and Chemistry (NCAR-MATCH; Rasch et al., 1997). The version used here is the CRC-MATCH model as described by Law and Rayner (1999). It has resolution of 3° latitude x 5.6° longitude, 24 vertical levels extending into the stratosphere, uses the vertical diffusion scheme of Holtslag and Boville (1993), the convection scheme of Hack (1994) and is driven by winds from the Middle Atmosphere Community Climate Model version 2 (MACCM2).

The transport model was used to simulate the atmospheric distribution of O_2/N_2 and CO_2 based on global, surface flux distributions of O_2 and N_2 from air-sea exchange (Garcia and Keeling, 2001), CO_2 from air-sea exchange (Takahashi et al., 1999), CO_2 from exchange with the terrestrial biosphere as obtained from the CASA model and used by Gurney et al. (2002) and CO_2 from fossil fuel use and cement production (Brenkert, 1998).

Variations in atmospheric O_2/N_2 and $\delta^{13}C$ due to terrestrial biosphere and fossil fuel related fluxes were estimated by scaling to modelled CO_2 fluxes using fixed O_2/CO_2 molar exchange ratios of –1.1 (Severinghaus, 1995) and –1.39 (Keeling, 1988; Marland et al., 2001) respectively, and assuming $\Delta\delta^{13}C$ of –17 ‰ (for mainly C_3 vegetation) and –20.6 ‰ (Andres et al., 1996) relative to the atmosphere for carbon exchange with biotic and fossil fuel reservoirs. Thus fluxes from all known, significant exchange processes for O_2/N_2, CO_2 and $\delta^{13}C$ are included in the model, except for oceanic influences on $\delta^{13}C$, which are likely to be important but which are not well understood. Results were taken from the 3rd year of the model

run, were detrended with respect to net carbon release from fossil fuel use of 6.2 PgC yr^{-1} and oceanic uptake of 2.2 PgC yr^{-1}, and were filtered to remove "non-baseline" data.

5.4.2 Comparison of observed and modelled variations

Modelled seasonal cycles at three altitude levels (500, 3000, 6500 m) above a grid point to the south-west of Cape Grim are plotted alongside the aircraft-derived observations for $\delta(O_2/N_2)$ (Figure 5.16), CO_2 (Figure 5.17) and $\delta^{13}C$ (Figure 5.18). The model results are referenced to the "trend curves" at 500 m so as to be consistent with the treatment of observed data as described in Section 5.3.3. Model results at 6500 m are compared with observations from the 6-8 km altitude band, for which the average altitude of all sample collections was 6900 m.

The broad features of the seasonal and altitudinal $\delta(O_2/N_2)$ variations are well simulated by the model. The phase of seasonal cycles in $\delta(O_2/N_2)$ and in the vertical $\delta(O_2/N_2)$ gradient are close to observations. The amplitude of the seasonal cycle decreases with altitude from 100 per meg at 500 m to 43 per meg at 6500 m. The ratio of amplitudes at 6500 and 500 m is 0.43, slightly lower than for the observations (38/79 = 0.48). The main differences are 1) in the seasonal cycle amplitude, which is larger in the modelled curves by 27, 60 and 13 % at 500, 3000 and 6500 m respectively (Table 5.3), and 2) the model does not reproduce the perturbation observed at 6500 m around the time of the seasonal minimum. The fact that modelled amplitudes exceed those of the observations in each altitude band suggests that the seasonal variation in the fluxes used here are probably overestimated.

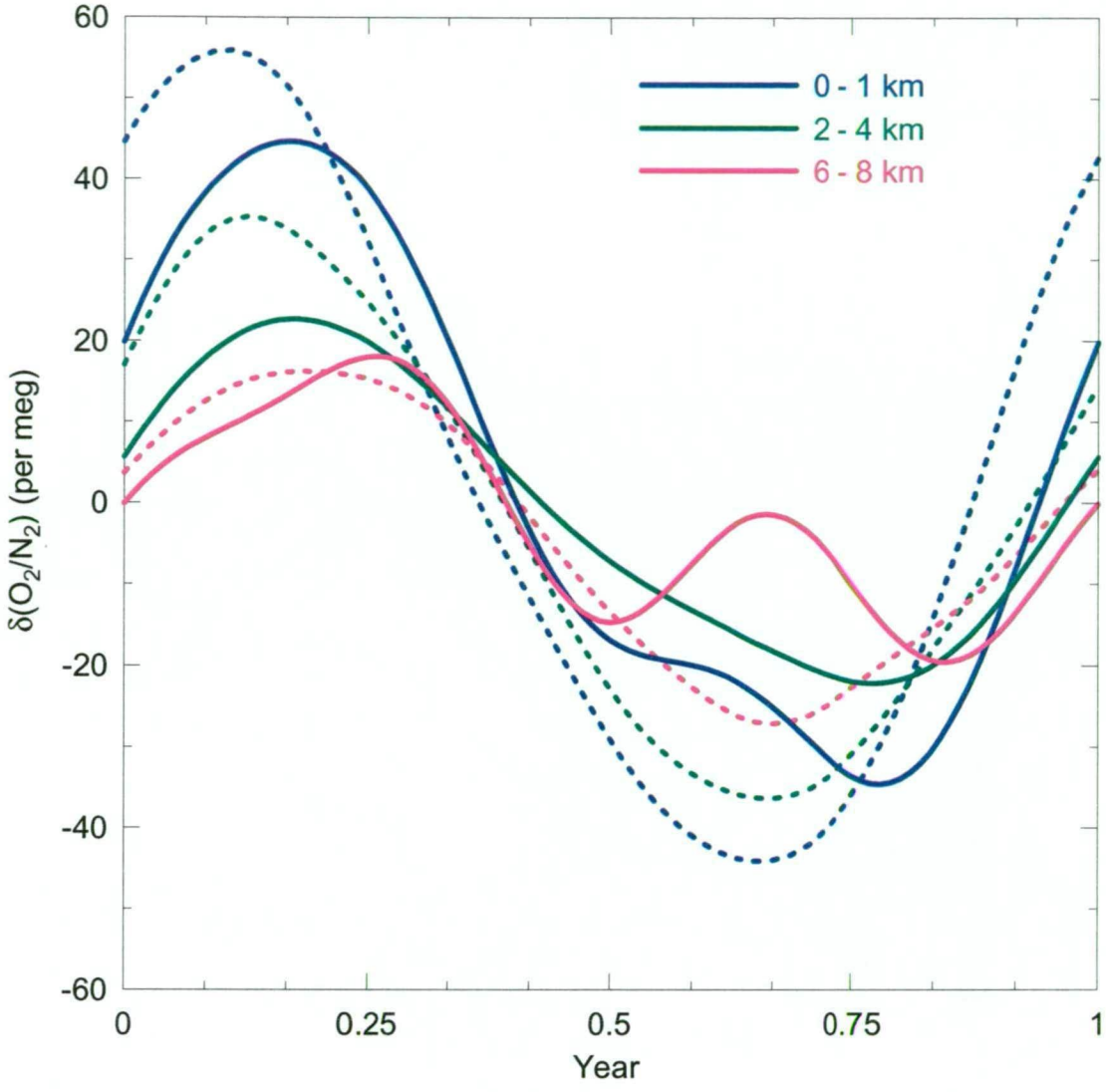

Figure 5.16 Observed (solid) and modelled (dashed) seasonal cycles of $\delta(O_2/N_2)$ above Cape Grim.

Agreement among modelled and observed curves is not as good for CO_2 or $\delta^{13}C$. Modelled seasonal cycle amplitude for both species at 500 m is too large by more than a factor of two. The magnitude of the vertical gradient is also significantly overestimated, and for $\delta^{13}C$ is even of the wrong sign. Part of the discrepancy in $\delta^{13}C$ curves is likely due to oceanic influences that are not included in the model.

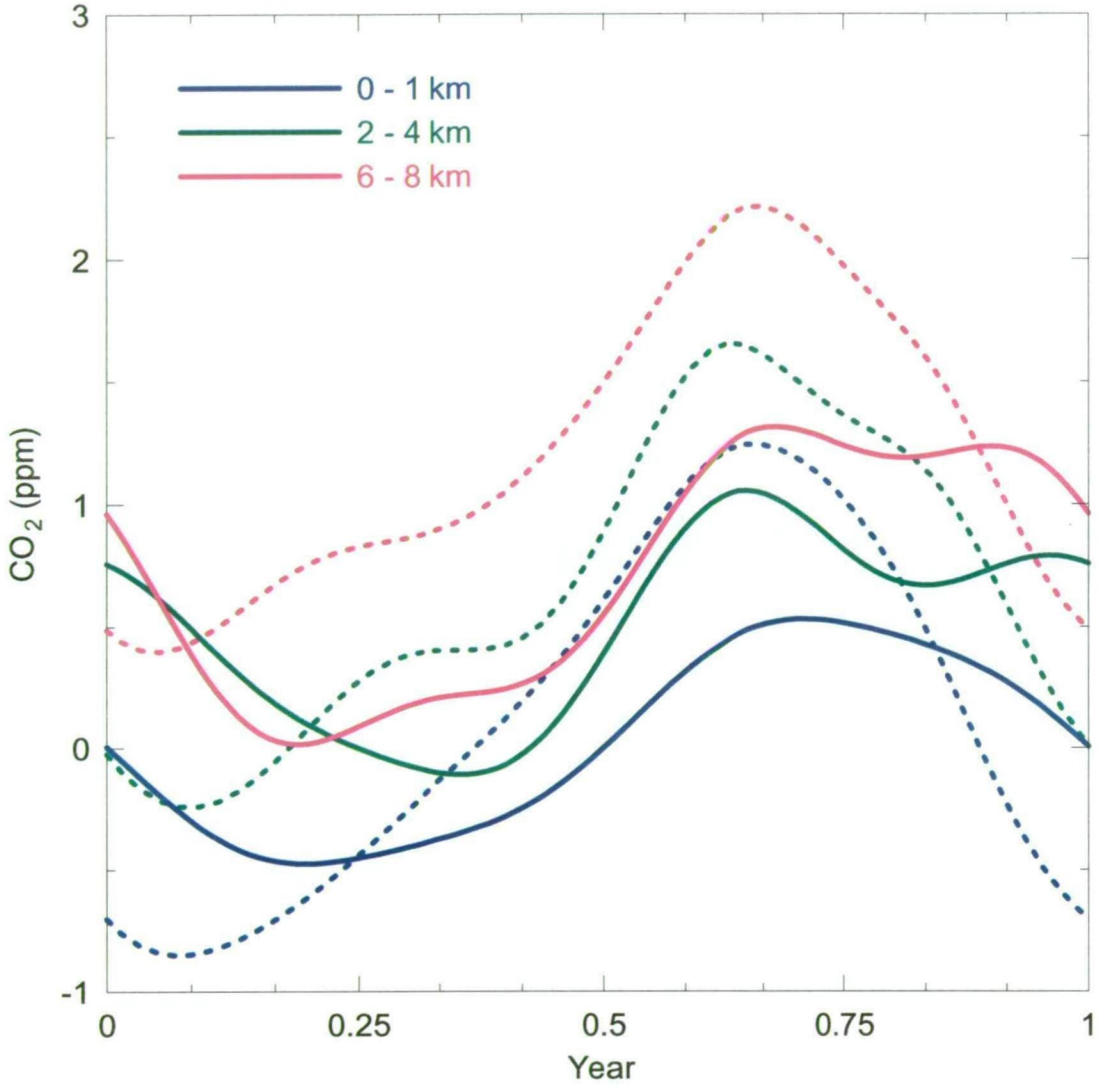

Figure 5.17 Observed (solid) and modelled (dashed) seasonal cycles of CO_2 above Cape Grim.

Species	Seasonal cycle amplitude				Mean vertical gradient	
	Observed 500 m	Modelled 500 m	Observed 6500 m	Modelled 6500 m	Observed	Modelled
$\delta(O_2/N_2)$ (per meg)	79	100	38	43	-4	-8
CO_2 (ppm)	1.0	2.1	1.3	1.8	0.7	1.1
$\delta^{13}C$ (‰)	0.036	0.083	0.047	0.091	0.006	-0.018

Table 5.3 Comparison of seasonal cycle peak-to-peak amplitude and mean, annual vertical gradient (6500 – 500 m) in observed and modelled data.

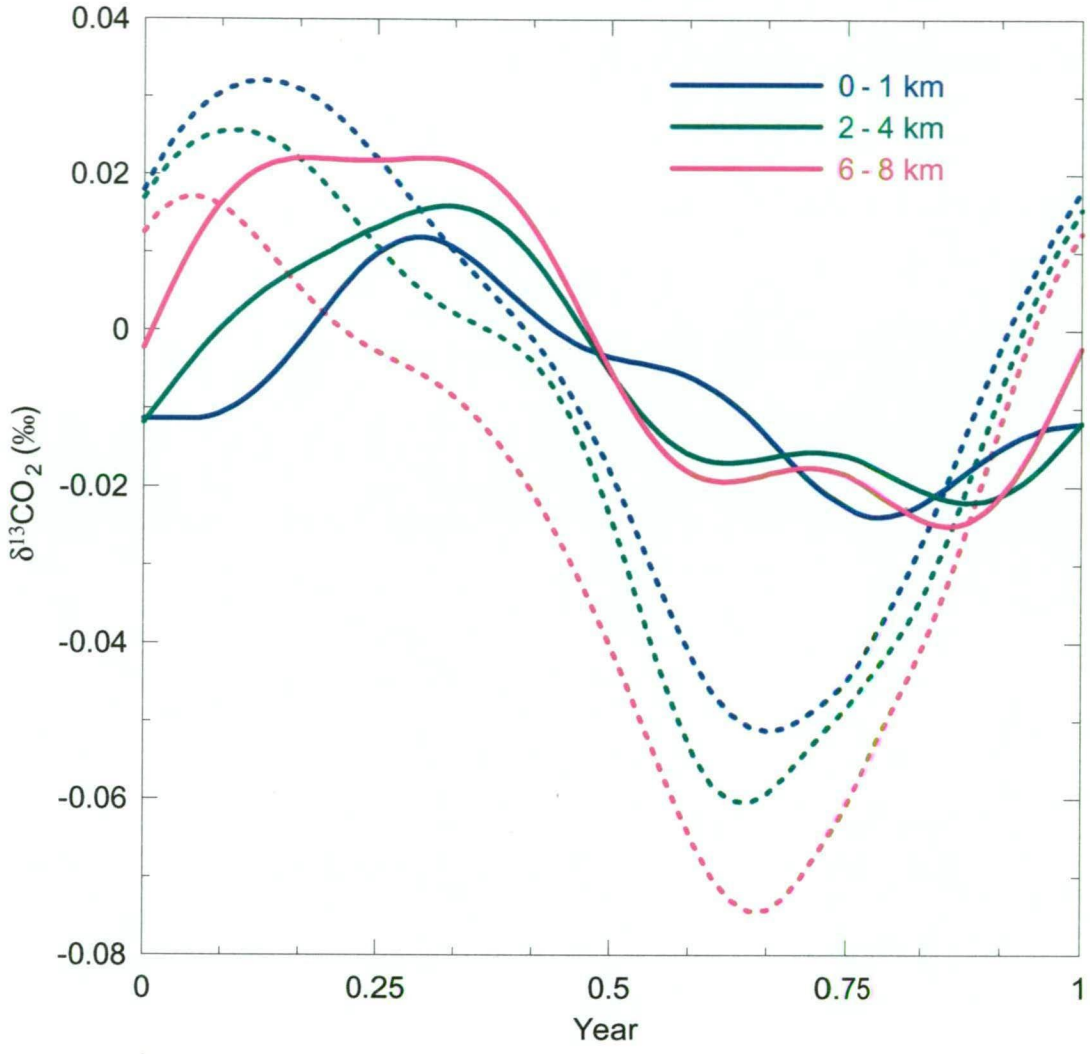

Figure 5.18 Observed (solid) and modelled (dashed) seasonal cycles of $\delta^{13}C$ in CO_2 above Cape Grim.

5.4.3 Surface fluxes

The sensitivity of modelled variations to different transport and exchange processes can be examined by separating the modelled curves into subset components. Figures 5.19 and 5.20 show $\delta(O_2/N_2)$ and CO_2 seasonal cycle contributions from surface fluxes in three latitude bands: SH (south of 18°S), the tropics (18°S-18°N) and NH (north of 18°N), and from oceanic, land biotic and fossil

fuel use fluxes. The $\delta(O_2/N_2)$ seasonal cycles are dominated by SH air-sea fluxes. This is especially the case at 500 m altitude. At 6.5 km, the relative contributions from NH and land biosphere fluxes increase to about 30 % (calculated from seasonal cycle amplitude) of SH and air-sea fluxes respectively, as compared to about 10 % at 500 m.

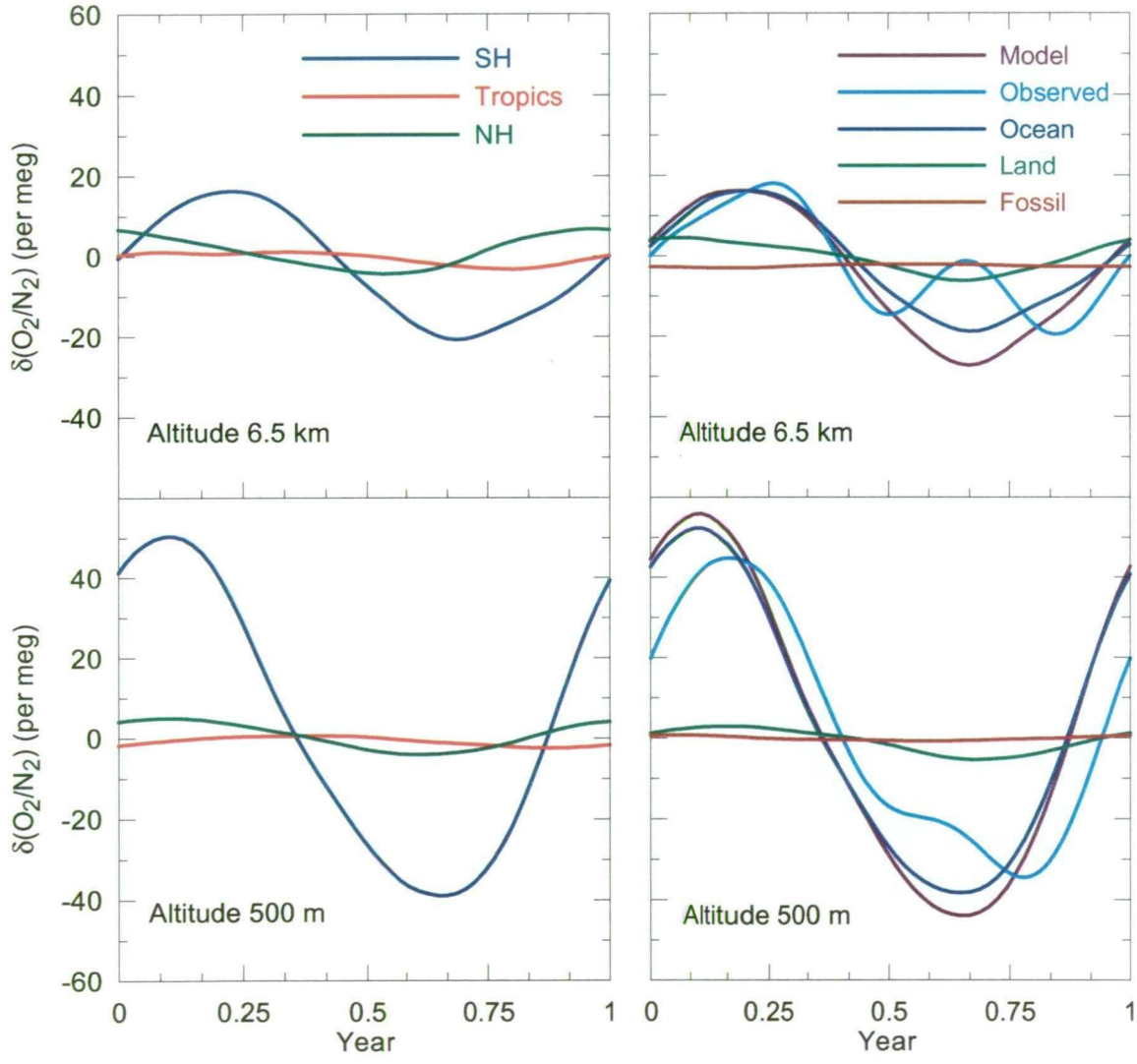

Figure 5.19 Contributions to modelled seasonal cycles in $\delta(O_2/N_2)$ at two altitude levels (6.5 km and 500 m), from fluxes in different latitude bands (left hand side) and with different reservoirs (right). The sum of ocean, land and fossil components ("model") and observed curves are plotted on the right hand side for comparison.

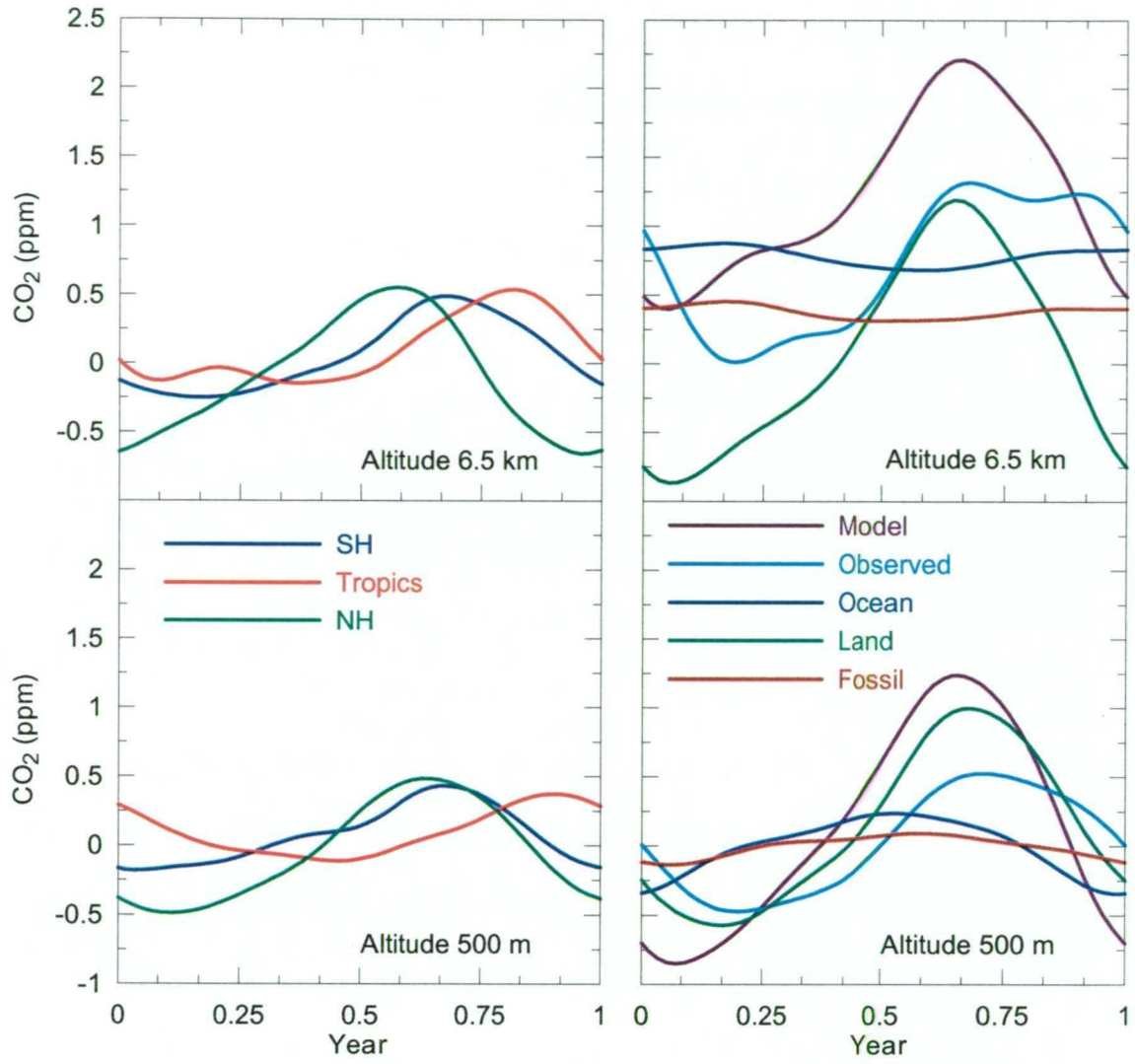

Figure 5.20 Contributions to modelled seasonal cycles in CO_2 at two altitude levels (6.5 km and 500 m), from fluxes in different latitude bands (left hand side) and with different carbon reservoirs (right). The sum of ocean, land and fossil components ("model") and observed curves are plotted on the right hand side for comparison.

Unlike $\delta(O_2/N_2)$, the breakdown of modelled CO_2 seasonal cycle components in Figure 5.20 shows significant influence from each of the three latitude bands with the largest single contribution from the NH at both altitude levels. Oceanic, terrestrial and fossil fuel use fluxes all show discernible seasonal variation at 500 m with the single largest contribution from terrestrial exchange. The terrestrial contribution

becomes more pronounced at 6.5 km, while both oceanic and fossil fuel use fluxes show little seasonality but contribute to a mean positive vertical gradient (increasing concentration with altitude) due to preferential transport of NH air, rich in fossil carbon, through the upper troposphere and a net Southern Ocean sink of CO_2.

5.4.4 Biomass burning plumes

A key finding from the study of multi-species, vertical profile data by Pak (2000) was that tropical biomass burning plumes contribute to significant enhancement of CO_2 (also CO, H_2 and CH_4) and depletion of $\delta^{13}C$ in the mid-troposphere above Cape Grim during the tropical SH dry season between about July and November. Affected trace gas measurements cannot be considered representative of large scale (e.g. zonal) behaviour because such plumes are coherent on horizontal, spatial scales of order 100 km and are not well mixed with background air within the altitude band. Estimation of the magnitude and time distribution of the contribution to mean seasonal cycles in the 4-8 km altitude range was based on a multi-species method. It involved the calculation of residuals in CO_2, $\delta^{13}C$, CO, H_2 and CH_4 from smooth curves of near surface data. Two critical tests were applied to these residuals. First, the ratio of $\Delta CH_4/\Delta CO$ was required to be < 1, to distinguish biomass burning influence from that of photochemistry and/or interhemispheric exchange. Second, the residuals were divided by the standard deviation of all residuals from the smooth curve for each species. The sum of the quotients was used as a measure of the strength of biomass burning influence. The optimum value of the sum for defining the contribution of biomass burning plumes to trace gas seasonal cycles was determined so as to give close agreement between the observed, mean annual vertical

gradient of CO_2 and that simulated by the University of Melbourne Tracer Model run with the global CO_2 surface flux distribution of Ramonet (1994).

The magnitude and distribution of biomass burning fluxes is not well known. Their impact on vertical profiles considered here is therefore not assessed with the

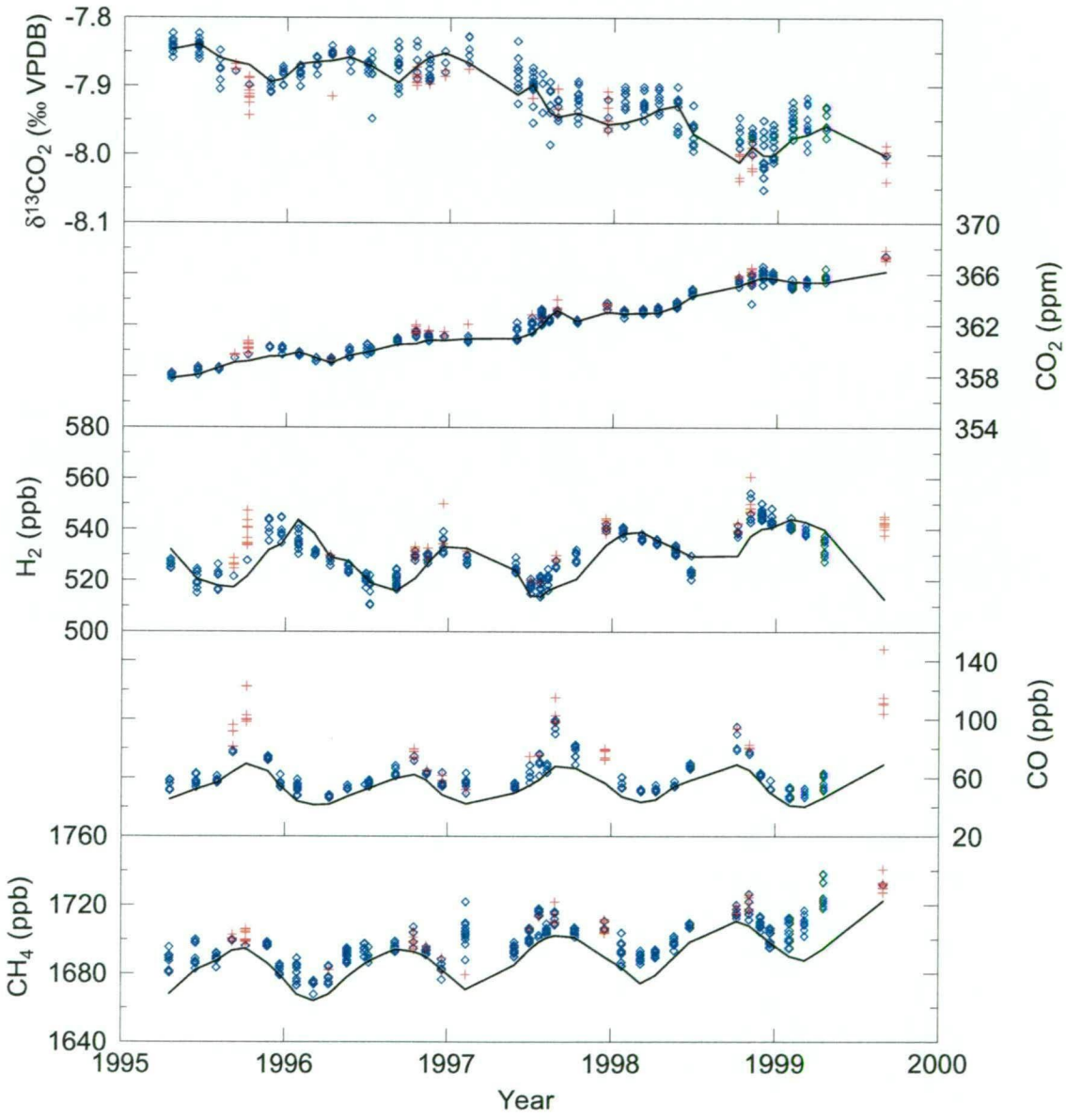

Figure 5.21 Aircraft-sourced data represented by a smooth curve fit to 0-1 km data (solid line), and individual flask data from the 4-8 km altitude band classified as either strongly (red crosses) or not strongly (blue diamonds) influenced by biomass burning plumes.

transport model. Rather, the algorithm of Pak (2000) is used to identify the data from 1995-1999 aircraft flights that were significantly influenced by biomass burning plumes (Figure 5.21). The vast majority (97 %) of these samples were collected between July and December, consistent with the findings of Pak (2000).

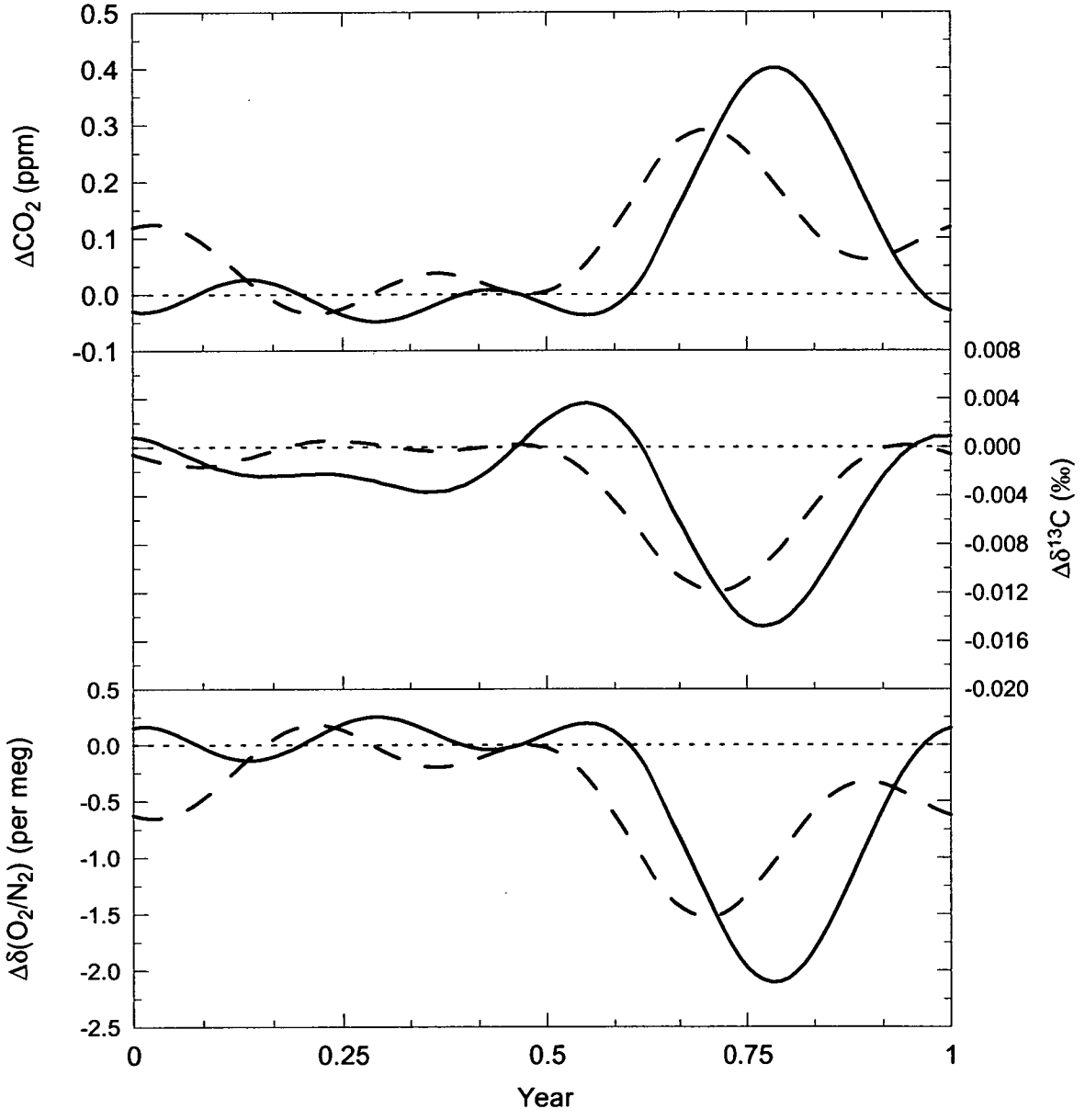

Figure 5.22 Inferred contributions from biomass burning plumes to seasonal cycles of CO_2, $\delta^{13}C$ and $\delta(O_2/N_2)$ at 6-8 km (solid) and 4-6 km (dashed).

The impact of biomass burning plumes on mean seasonal cycles of CO_2 and $\delta^{13}C$ (Figure 5.22) can be estimated as the difference in seasonal cycle curves calculated with and without data from the flagged samples in Figure 5.21. The impact on CO_2 and $\delta^{13}C$ is significant in relation to observed seasonal cycles between about August and November. The amplitude of CO_2 variations attributed to biomass burning plumes at 6500 m is about 0.4 ppm, slightly larger than the value of 0.3 ppm determined by Pak (2000) for the 1992-1997 period. This represents 30 % of the observed CO_2 seasonal cycle amplitude at this altitude. The $\delta^{13}C/CO_2$ relationship of –0.037 ‰ ppm^{-1} implies input of carbon with $\delta^{13}C$ of about -21 ‰ VPDB. This $\delta^{13}C$ value is higher than that determined by Pak (2000) (-25 ‰) and is consistent with a larger contribution from C_4 vegetation.

The impact on $\delta(O_2/N_2)$ is estimated in Figure 5.22 from the CO_2 curve, using an O_2/CO_2 exchange ratio of –1.1. The maximum deviation in October is only –2 per meg, or only about 3 % of the observed seasonal cycle at this altitude. A discrepancy of this magnitude is too small to be resolved in observed $\delta(O_2/N_2)$ data. These calculations show that biomass burning plumes are expected to contribute to seasonal $\delta(O_2/N_2)$ cycles in the mid to upper troposphere but that unlike CO_2 and $\delta^{13}C$, the magnitude of the effect is small by comparison to other processes.

5.4.5 Interhemispheric exchange

Figure 5.20 suggests a major contribution to seasonal cycles of CO_2 and $\delta^{13}C$ above Cape Grim from seasonally varying NH surface fluxes that are dominated by exchange with the land biosphere. Thus interhemispheric exchange likely plays an important role in determining seasonal cycles of these species in the SH, yet the rate

of interhemispheric exchange and its seasonal and altitudinal variations are not well constrained in transport models (Law et al., 1996).

The sensitivity of observed SH seasonal cycles to interhemispheric exchange is addressed in Figure 5.23, which shows observations and the modelled influence of NH fluxes at 500 and 6500 m above Cape Grim, and observations and/or modelled seasonal cycles at Mauna Loa. On the basis of its tropical location (latitude 20°N)

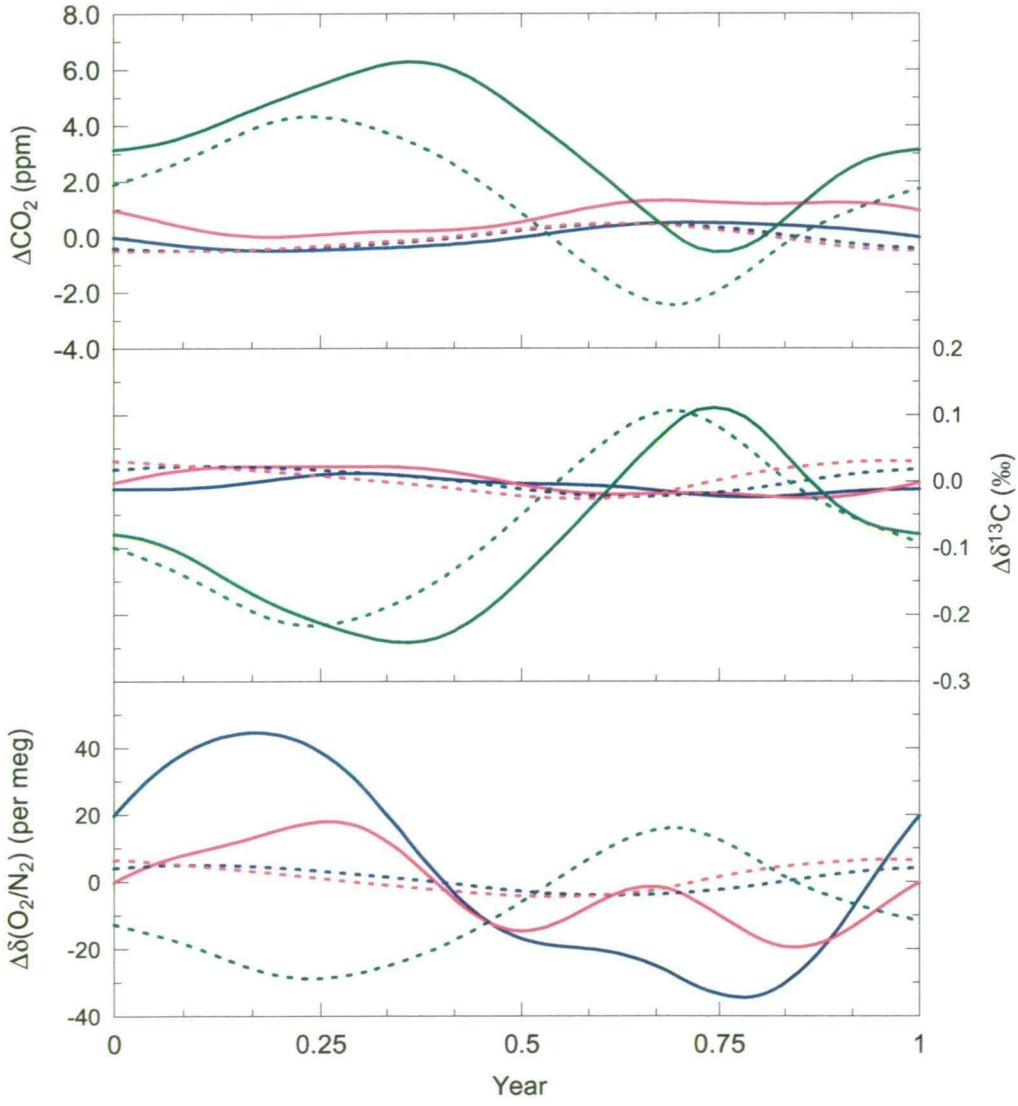

Figure 5.23. Observed seasonal cycles of CO_2, $\delta^{13}C$ and $\delta(O_2/N_2)$ in the 0-1 km (blue solid line) and 6-8 km altitude bands (pink solid) above Cape Grim, and at Mauna Loa (green solid). Also plotted are the modelled seasonal cycle contributions from NH fluxes at 500 m (blue dashed) and 6.5 km (pink dashed) and the seasonal cycle due to all processes and regions at Mauna Loa (green dashed).

and altitude (3.4 km; above the MBL), Mauna Loa is treated here as representing atmospheric conditions that approximate NH air at the interface with the SH. The phase and amplitude of the modelled "NH-influence" curves relative to the Mauna Loa curves provide insight into the nature of interhemispheric exchange described by the CRC-MATCH model. The modelled curves for 500 and 6500 m above Cape Grim show increasing CO_2 values between about February and July. The observations above Cape Grim also show increasing CO_2 during this period. Furthermore, Figure 5.13 shows the 6500 m observations to record a higher rate of CO_2 increase and to diverge from the 500 m curve during this period. This behaviour must reflect preferential entrainment of CO_2-rich, NH air into the upper troposphere above Cape Grim. The phase difference with respect to Mauna Loa curves suggests a transport time from Mauna Loa of around 3-4 months.

Declining CO_2 levels above Cape Grim between December and February might also partially reflect transport of NH air that is depleted in CO_2 relative to Cape Grim around the time of the seasonal CO_2 minimum at Mauna Loa in August. However, any NH influence is harder to isolate as the interhemispheric gradient around August is much smaller than around the time of the NH seasonal CO_2 maximum in the first half of the year, and SH terrestrial and oceanic sinks are also likely important influences in the December to February period.

In many respects, the $\delta^{13}C$ curves mirror those for CO_2, which is expected from the common forcing by NH terrestrial exchange. However, there is one differing feature of the interhemispheric gradient that helps to explain the positively correlated vertical gradients of CO_2 and $\delta^{13}C$ above Cape Grim. Between August and October the observed interhemispheric $\delta^{13}C$ gradient is more pronounced than for

CO_2. This decoupling of CO_2 and $\delta^{13}C$ points to an influence separate from the relationship assumed for terrestrial exchange. It probably involves a net Southern Ocean sink of CO_2 that has little impact on atmospheric $\delta^{13}C$. Allowing for a lag time of a few months, preferential transport of NH air, enriched in $\delta^{13}C$, through the upper troposphere, is a likely contributor to the observed positive vertical $\delta^{13}C$ gradient above Cape Grim between about January and May.

The modelled influence of interhemispheric exchange on CO_2 and $\delta^{13}C$ seasonal cycles above Cape Grim is small by comparison to the seasonal cycle amplitude at Mauna Loa. It follows that in proportional terms, $\delta(O_2/N_2)$ seasonal cycles above Cape Grim should not be very sensitive to interhemispheric exchange, because the amplitude of the (modelled) seasonal cycle at Mauna Loa is similar to that observed at the 6-8 km altitude level and is smaller than that at 500 m.

Figure 5.23 is also useful for assessing the possibility of the May-October perturbation in the $\delta(O_2/N_2)$ seasonal cycle at 6-8 km being related to interhemispheric exchange. If the perturbation was to be explained by injection of O_2-rich air into the upper troposphere around September, the multi-species data in Figure 5.23 rule out an interhemispheric exchange signal for two reasons. First, transport from the NH would have to be almost instantaneous. Second, larger variations would be expected in CO_2 and $\delta^{13}C$ curves at 6-8 km. If on the other hand, the perturbation mainly reflects a negative excursion in $\delta(O_2/N_2)$ centred on June, such a signal is more consistent with effects of interhemispheric exchange. The phase is consistent with a lag of a few months after a period of significant interhemispheric gradient with lower $\delta(O_2/N_2)$ in the NH. Observed CO_2 and $\delta^{13}C$ curves exhibit higher rates of change in June than expected from the model simulation, consistent

with a larger NH influence. Even so, it seems unlikely that interhemispheric exchange could account for much of the mid-tropospheric $\delta(O_2/N_2)$ perturbation.

5.4.6 Hadley circulation

An interesting feature of atmospheric transport indicated by the CRC-MATCH model is the efficiency of transmission of tropical surface flux variations into the upper troposphere above Cape Grim. The effect is demonstrated in Figure 5.24 by the relationship of modelled latitudinal (Cape Ferguson minus Cape Grim) and vertical (6500 – 500 m) gradients in $\delta(O_2/N_2)$ in response to tropical surface fluxes. There is dramatic difference in sensitivity of the vertical gradients to terrestrial and oceanic fluxes. Terrestrial fluxes produce larger vertical gradients above Cape Grim than they do latitudinal gradients between the sites compared here. By contrast, air-sea fluxes have much larger impact on the latitudinal gradient, probably in part due to the close proximity of Cape Ferguson to the Pacific Ocean. These results emphasise the importance of Hadley circulation for transporting air from near the surface at low latitudes to the SH upper troposphere, and demonstrate the role of deep convection over the tropical continents.

The magnitude of vertical gradients in Figure 5.24 is small relative to observations above Cape Grim. Thus if the modelled transport and the assumed tropical $\delta(O_2/N_2)$ fluxes are reasonably accurate, measured $\delta(O_2/N_2)$ vertical gradients above Cape Grim should not be very sensitive to this effect. Nevertheless, the Hadley circulation does contribute to vertical mixing and could potentially be a major influence on vertical gradients of other trace gas species with proportionally larger flux variations in the tropics.

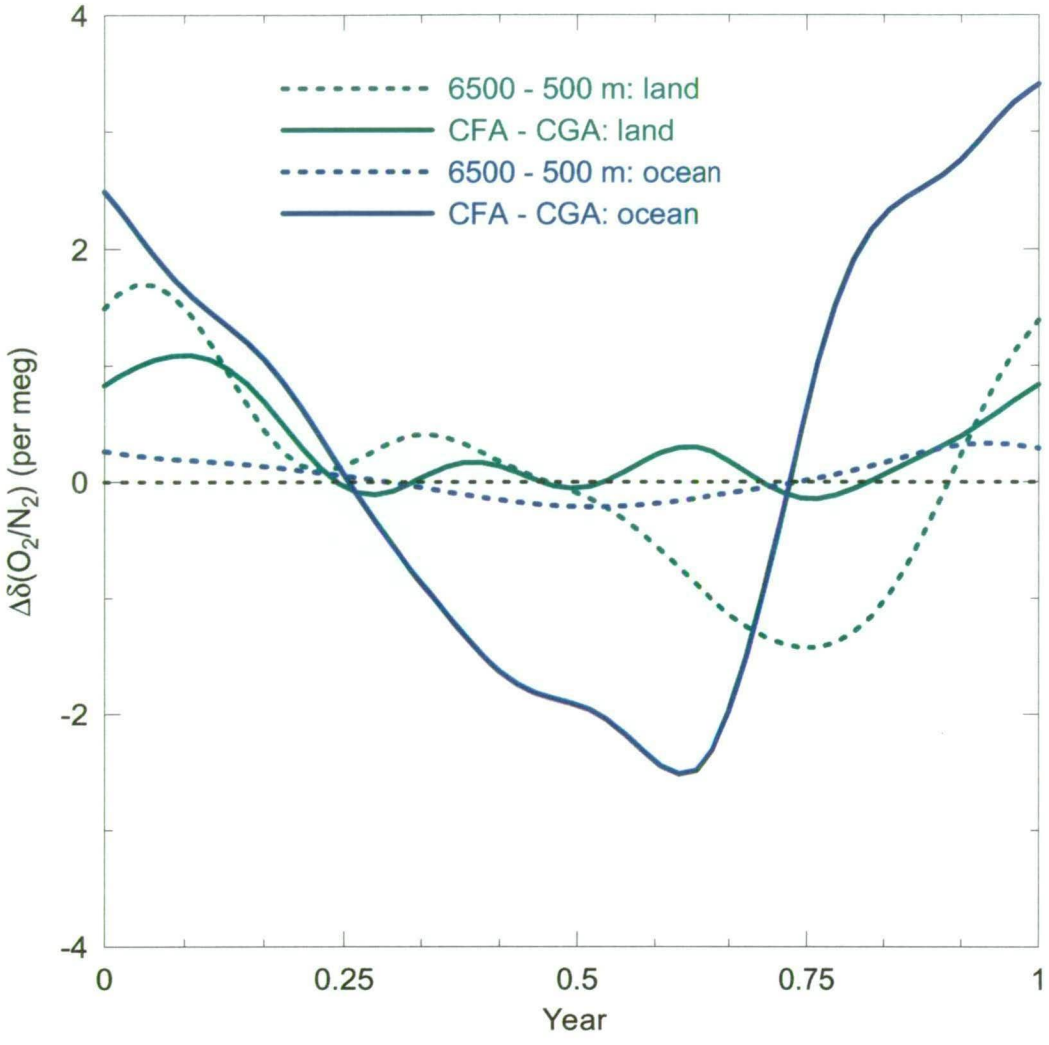

Figure 5.24. Modelled latitudinal (solid lines) and vertical (dashed) gradients of $\delta(O_2/N_2)$ due to surface exchange with oceans (blue) and the terrestrial biosphere (green) in the tropics. The latitudinal gradients are for Cape Ferguson (19°S) minus Cape Grim (41°S). The vertical gradients are for 6500 m – 500 m above Cape Grim.

5.5 Discussion

A general difficulty in relating observed trace gas variations to large scale effects of specific processes is that models such as the one used here, are under-constrained. This situation reflects the paucity of observational data with sufficient spatiotemporal resolution to usefully constrain the various transport and exchange processes that significantly influence atmospheric composition. For example, trace

gas variations are dependent on the distribution of fluxes from biogeochemical exchange processes, and transport parameters such as horizontal and vertical mixing. Vertical mixing in the troposphere involves transport both by eddy diffusion and convection. There are large uncertainties regarding the seasonal and altitudinal distribution of interhemispheric exchange.

The CSIRO vertical profile data have the potential to better constrain such models, as they provide high precision, multi-species information of vertical tropospheric gradients in composition of background SH, mid-latitude air. More observations of the vertical structure of the troposphere have been identified as a high priority for improving model performance (Denning et al., 1999). The long duration of the CSIRO program and the frequency of flights provides extensive information about mean seasonal trace gas behaviour up to 8 km altitude.

Observed vertical/seasonal variations include contributions from numerous processes, many of which are poorly constrained by independent information. This complicates interpretation of observations in terms of specific transport and exchange processes. Nevertheless, there is scope to usefully constrain such processes, especially by using observations of different species as tracers of processes to which they are strongly sensitive. In this context, the main potential of $\delta(O_2/N_2)$ is to constrain SH air-sea fluxes (e.g. Keeling et al., 1993; Bender et al., 1996) and vertical mixing rates in the SH troposphere.

The model results in Figure 5.19 show $\delta(O_2/N_2)$ seasonal cycles above Cape Grim to be mainly forced by surface exchange in the SH. Figure 5.25 shows best estimates of $\delta(O_2/N_2)$ variations at 500, 3000 and 6500 m altitude due to SH surface exchange only. The curves were constructed by subtracting modelled effects due to NH and tropical fluxes from the aircraft-derived observations. The main uncertainty

in this calculation is likely to be in the estimate of NH influence. Also plotted are the modelled variations due to SH fluxes only, which were scaled by a factor of 0.8 to give equal amplitude of both 500 m curves in this plot. The results show the amplitude of modelled curves to be too large at 3000 m and too small at 6500 m. This is consistent with vertical mixing rates being overestimated between 500 and 300 m, and underestimated between 3000 and 6500 m.

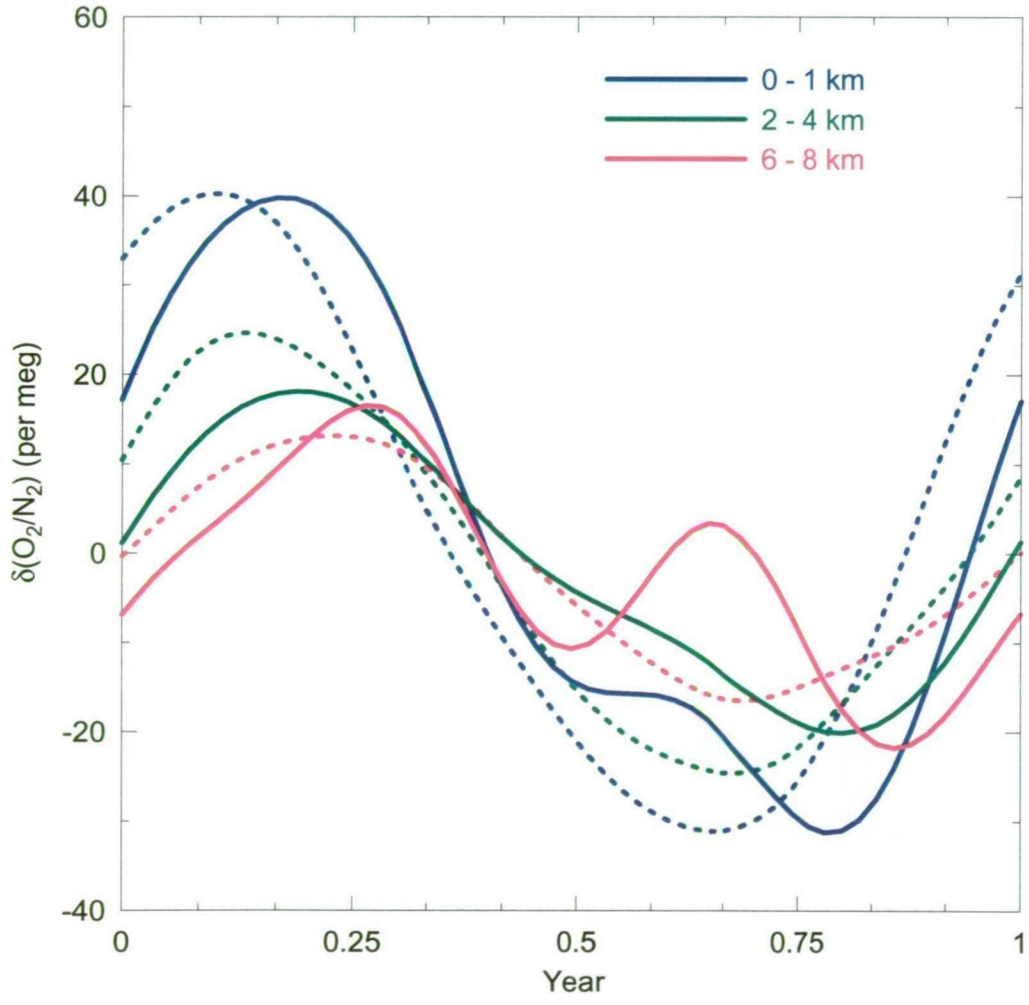

Figure 5.25 Seasonal cycles of $\delta(O_2/N_2)$ above Cape Grim due to SH surface fluxes only. The solid curves represent observations, after subtraction of smaller modelled contributions from NH and tropical fluxes. Dashed curves show model results scaled by a factor of 0.8 (see text).

Interpretation of the $\delta(O_2/N_2)$ data in terms of vertical mixing is complicated by the May-October perturbation at 6.5 km. It has already been shown that this feature is unlikely to be explained by either vertical mixing in the troposphere or interhemispheric exchange. A possible explanation involves injection of stratospheric air into the upper troposphere during austral winter. In the SH, mass transport across the tropopause has a maximum in mid-winter (Appenzeller et al., 1996). The sign of the $\delta(O_2/N_2)$ perturbation is consistent with addition of "old" air enriched in O_2/N_2. If exchange with stratosphere was responsible, significant perturbations would also be expected in other species such as CO_2 and $\delta^{13}C$. There is a hint of small perturbations favouring lower CO_2 and higher $\delta^{13}C$ above 4 km in September. Larger perturbations emerge if the best estimate of influence from biomass burning plumes is subtracted from the observations (Figure 5.26), although the apparent phase of these perturbations varies among species by about a month. The signature of $\delta(O_2/N_2)$, CO_2 and $\delta^{13}C$ perturbations is qualitatively consistent with influence of old air. However, there is substantial uncertainty in the magnitude and shape of the biomass burning influence on seasonal cycles so that possible minor effects from other processes are not well resolved. Thus the data presented here are neither strongly supportive nor dismissive of possible stratospheric influence on the $\delta(O_2/N_2)$ vertical profiles. The nature of stratosphere-troposphere exchange is not well constrained in the CRC-MATCH model and is thus not investigated with the model.

The seasonal cycle of $\delta(O_2/N_2)$ due to SH air-sea exchange can be estimated by subtracting from observations the modelled influence of secondary processes, in this case long range transport from the NH and from the tropics, fossil fuel use, exchange with land biota in the SH, and mid-tropospheric biomass burning plumes (Figure 5.27). This calculation is problematical for the inferred SH ocean curve at

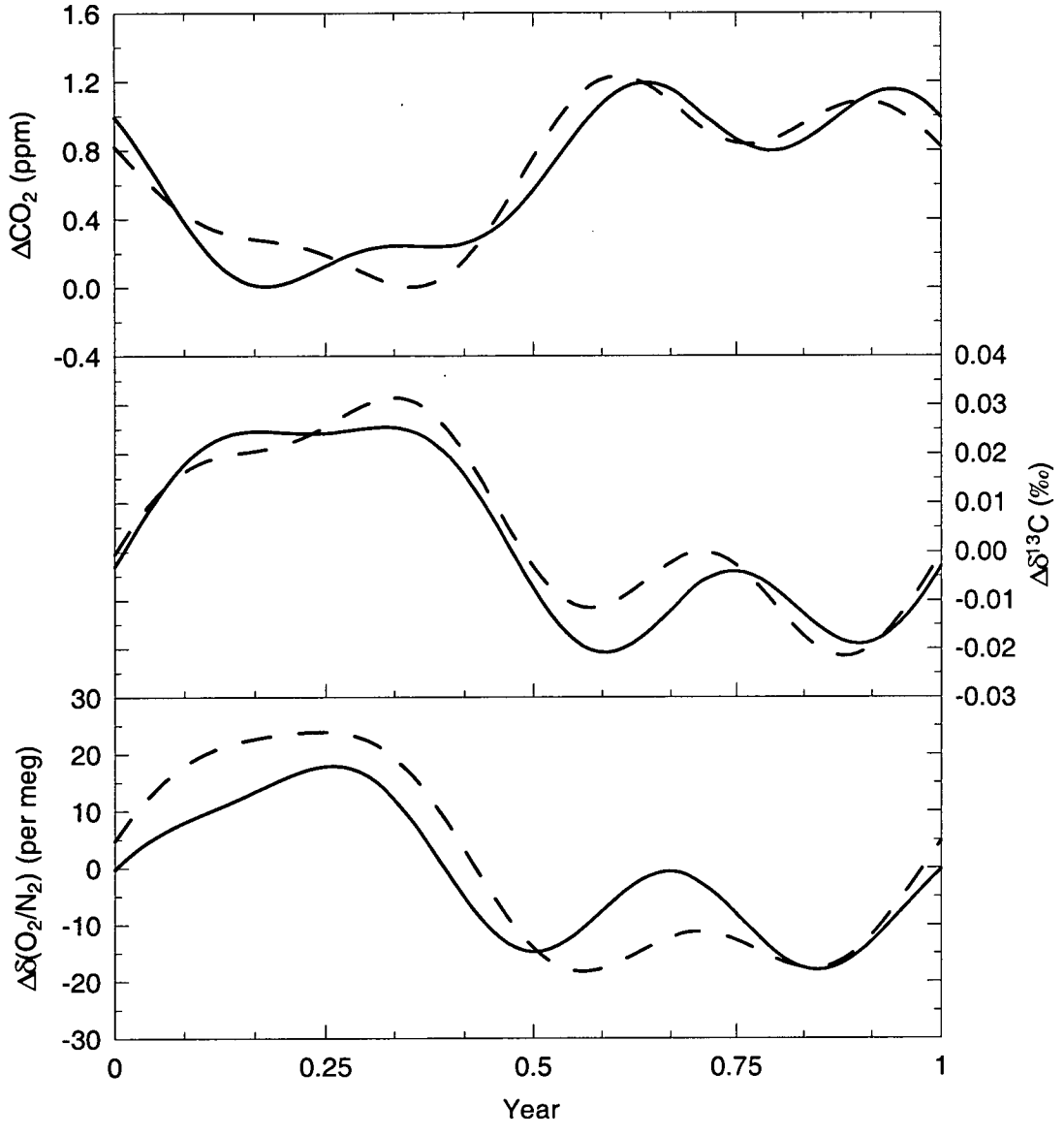

Figure 5.26 Mean seasonal cycles of CO_2, $\delta^{13}C$ and $\delta(O_2/N_2)$ at 6-8 km (solid) and 4-6 km (dashed), after subtraction of the influence due to biomass burning plumes.

6500 m, as the observed May-October perturbation is attributed here to air-sea exchange. The inferred curve at 500 m should be more robust and again demonstrates the dominant contribution of SH air-sea exchange to the $\delta(O_2/N_2)$ seasonal cycle in the SH. The single largest contribution from the secondary components is from NH fluxes. The influence on $\delta(O_2/N_2)$ from exchange with land

biota is estimated in Figure 5.27 using output from the transport model. There is potential to use CO_2 and $\delta^{13}C$ observations to better constrain these terms if oceanic influences on $\delta^{13}C$ can be independently determined.

There are significant discrepancies in observed and modelled seasonal/vertical cycling of CO_2 and $\delta^{13}C$. For example, the model overestimates the seasonal cycle amplitude at Cape Grim by a factor of two. This likely reflects the significant contribution of multiple processes such as SH land biota, SH oceans and covariation in transport with surface fluxes in the NH and in the tropics, and the uncertainties that exist in estimates of each of these terms at this time.

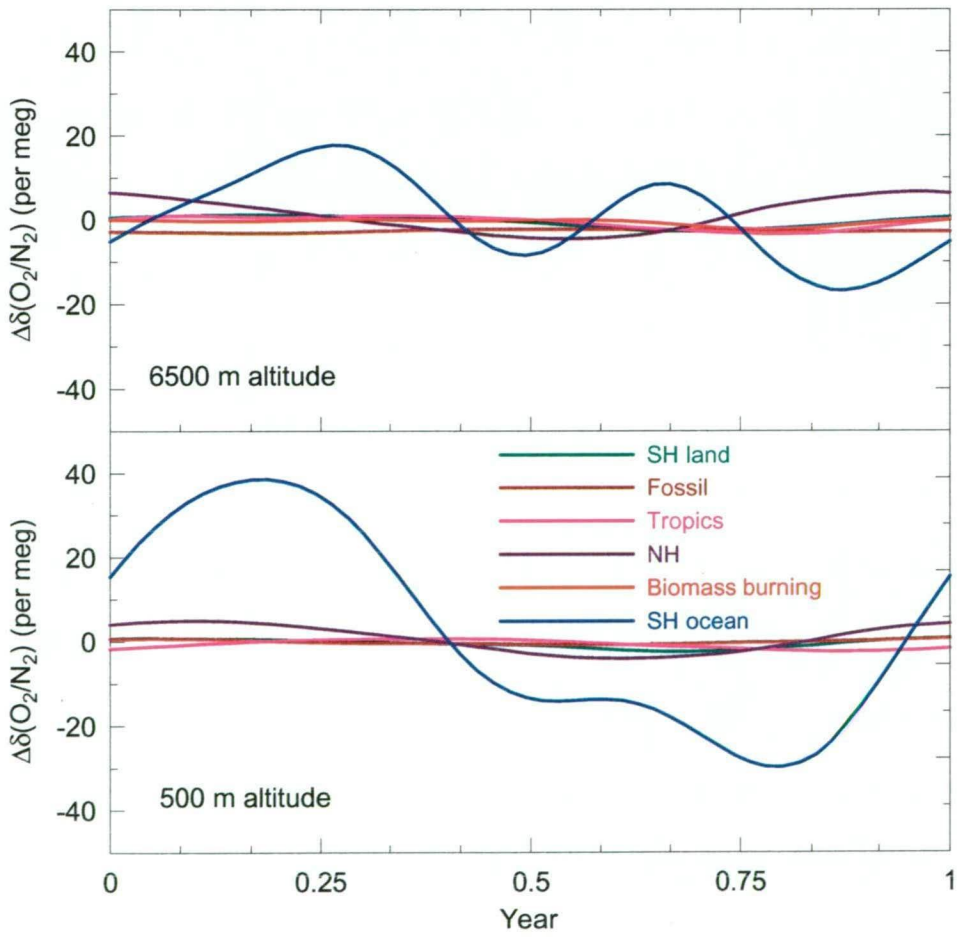

Figure 5.27 Contributions from multiple processes to the $\delta(O_2/N_2)$ seasonal cycle at 500 m above Cape Grim. The SH ocean curve is inferred from the difference of observations and the other modelled secondary components plotted here.

5.6 Summary

Seasonal variations in $\delta(O_2/N_2)$ and its vertical gradient in clean, mid-latitude, SH air were determined from aircraft-based flask sampling of the troposphere above Cape Grim between 1995 and 1999. Data from 43 individual flights were collated to examine mean seasonal behaviour of $\delta(O_2/N_2)$ in five altitude bands between 0 and 8 km.

Measurements of multiple trace gas and isotopic species provide a means to distinguish experimental artefacts from biogeochemical signals. Measurements of $\delta(Ar/N_2)$ and $\delta^{29}N_2$ reveal significant differences between MBL samples collected from aircraft and from surface sampling at Cape Grim due to mass-dependent fractionation. Implied, systematic $\delta(O_2/N_2)$ differences are approximately 20 per meg. There is also evidence of altitude and aircraft-dependent fractionation effects in aircraft sampling data. The artefacts are likely related to subtle differences in sampling techniques.

After allowance for artefacts, the aircraft-derived $\delta(O_2/N_2)$ data show large seasonal and altitudinal variations of biogeochemical origin. Seasonal cycle amplitude diminishes with altitude from 0-1 up to 6-8 km. The sign of the vertical gradient changes seasonally from positive [$\delta(O_2/N_2)$ increasing with altitude] in winter/spring to negative in summer/autumn. There is a departure from sinusoidal behaviour in seasonal cycles above 4 km altitude between May and October.

Observations of $\delta(O_2/N_2)$, CO_2 and its $\delta^{13}C$ were compared with output from the CRC-MATCH atmospheric transport model using independent prior estimates of global surface fluxes from exchange with oceans, land biota and fossil fuel use. There was good agreement in the phase and shape of the $\delta(O_2/N_2)$ seasonal cycle, and to a lesser extent in that of CO_2. Largest discrepancies emerged for $\delta^{13}C$, which

are likely due in part to oceanic influences not addressed by the model. Modelled seasonal cycle amplitudes of $\delta(O_2/N_2)$ and CO_2 were overestimated by about 20 and 110 % respectively in MBL air, and were also overestimated, but to a lesser degree at 6.5 km altitude. Sensitivity tests with the model suggest that seasonal/altitudinal variations in $\delta(O_2/N_2)$ are dominated by SH air-sea exchange and vertical transport in the SH troposphere. The largest contribution from other processes, and the largest influence on the CO_2 seasonal cycle from any process is from transport of seasonally varying NH signals.

The vertical profile $\delta(O_2/N_2)$ data are useful as a constraint of vertical mixing in the SH troposphere. A preliminary assessment suggests that vertical mixing rates in the CRC-MATCH model are overestimated between 500 and 3000 m altitude, and underestimated between 3000 and 6500 m altitude. One objective for future work is to better quantify this link.

CHAPTER 6

CONCLUDING REMARKS

This thesis has addressed scientific issues relating to the global carbon cycle on three different timescales (decadal trends, interannual variability, seasonal cycles) with the investigation focused on two main areas: 1) the measurement of atmospheric O_2 variations and their use for constraining carbon cycle processes and 2) the use of correlations in measurements of multiple trace gas and isotopic species for the interpretation of biogeochemical signatures in atmospheric composition and for the diagnosis of experimental artefacts.

A key result has been elucidation of the role of biomass burning in driving interannual variability of atmospheric CO_2, its isotope $\delta^{13}C$, and other trace gases such as CH_4, CO and H_2. High precision measurements on flask samples from CSIRO's global network show strong correlation in interannual growth rate variations of all these species between 1992 and 1999. High growth rates coincide with El Niño periods, consistent with the observed relationship of CO_2 growth rate and ENSO in earlier decades. Analysis of global mean records using a 1-box pulse perturbation model shows that the observed interannual variability is consistent with forcing by two emission pulses centred on 1994 and 1997/98. In line with other longer term studies of the CSIRO records, the relationship of CO_2 and its $\delta^{13}C$ indicates mainly terrestrial forcing, and implies relatively little oceanic influence on interannual variability of atmospheric CO_2. This conclusion is also consistent with recent studies based on oceanic methods.

Both 1994 and 1997/98 were El Niño years that brought drought to extensive areas of land, especially along the Western Pacific seaboard. Major biomass burning events were reported in South-east Asia, South America and in the boreal forests of Eurasia and North America. Observations of enhanced atmospheric levels of various biomass burning products were linked to these fires. These observations are consistent with the chemical signature of atmospheric perturbations indicated by the CSIRO data in implicating biomass burning as a major influence on interannual variability of global atmospheric composition.

The magnitude of terrestrial CO_2 emissions implied for each of the two periods by the 1-box model calculations is in the order of 3-4 PgC, and may include contributions from both biomass burning and imbalance in photosynthesis and respiration of terrestrial ecosystems. The relative contributions are not distinguished by $\delta^{13}C$ but are constrained by inferred pulse emissions of CH_4, CO and H_2, which are not linked to respiration of CO_2 and thus directly constrain CO_2 emissions from biomass burning. Assuming biomass burning is the dominant influence on interannual variations of these species, the implied total carbon emissions in 1994 and 1997/98 are 0.6-3.5 and 0.8-3.7 PgC respectively. These values represent an excess above mean biomass burning emissions of other years. The main uncertainties with this approach relate to the possibility of indirect covarying flux variations, such as those involving wetland emissions of CH_4, and in estimates of the integrated CH_4/CO_2, CO/CO_2 and H_2/CO_2 ratios of emissions from all of the fires contributing to the large 1994 and 1997/98 trace gas anomalies.

There are several lines of research that could be pursued to better quantify these emissions. Improved estimates of multi-species emission ratios of sources would help to better constrain results using the 1-box model. Use of an atmospheric

transport model and observed spatiotemporal trace gas variations should improve information about the geographical origin of the flux anomalies. Coupled with a model of photochemical processes, this approach could be used to better constrain the magnitude of fluxes of the short-lived species CO, and by extension those of CO_2. Such modelling studies could benefit from inclusion of observational data from other inter-calibrated laboratories, providing greater spatial coverage and of other trace gas species that are effective tracers of biomass burning. Continuous, satellite-based measurements such as those now available for CO and CH_4 (MOPITT; Measurements Of Pollution In The Troposphere) have great potential for elucidating the spatial distribution of some trace gas fluxes from regional sources such as biomass burning events.

Published estimates of carbon emissions from the 1994 and 1997/98 fires, derived from "bottom-up" carbon inventory techniques, vary widely in magnitude. There is scope to better constrain these values. One area deserving of special attention is the peat swamps of South-east Asia. There is evidence from numerous measurement programs of major trace gas emissions from the South-east Asian fires, and the inventory-based studies have attributed the majority of those emissions to combustion of peat.

Another priority for future research is in better quantification of CH_4, CO and H_2 fluxes that may indirectly covary with emissions from biomass burning. Variations in wetland emissions of CH_4 due to temperature and precipitation anomalies have already been identified as a likely significant influence on atmospheric CH_4 growth rate variations on El Niño timescales. There is potential to resolve wetland and biomass burning influences on CH_4 using spatial gradients from global network observations, and observations of covariations with the isotopomers

of CH_4, such as $\delta^{13}C$. The main potential for covariations in CO and H_2 are through 1) photochemical production from NMHCs such as isoprene and terpenes that are emitted by plants and 2) the soil sink of H_2. The sensitivity of both processes to climatic influences is poorly understood.

An important issue concerning the global carbon cycle on decadal timescales is the relative rate of uptake of anthropogenic CO_2 by oceans and the land biosphere. This question was addressed here primarily through reconstruction of a 23-year trend in atmospheric O_2 from measurements of the Cape Grim Air Archive. This reconstruction, closely linked to modern records, represents the longest high precision record of O_2 decline in the contemporary atmosphere. The mean trend in atmospheric $\delta(O_2/N_2)$ between 1978 and 2001 was determined to be -15.6 ± 0.5 per meg yr^{-1}. It implies net carbon uptake of 2.0 ± 0.9 and 0.6 ± 1.0 PgC yr^{-1} by the oceans and land biosphere respectively, after minor adjustment is made for net outgassing of O_2 from the oceans in response to climate change. These results confirm uptake by the oceans at a rate close to that predicted by ocean carbon cycle models and favour a net accumulation of carbon by the land biosphere. The result has also been used to estimate the two-decade contribution of carbon isotope disequilibrium fluxes to the global $\delta^{13}C$ change, so strengthening the use of this complementary tracer of terrestrial exchange on other timescales. A balanced, or growing biosphere implies that ongoing deforestation, especially in tropical regions, has been compensated by growth of vegetation elsewhere. This may be due to reforestation of previously cleared land or increased net production of standing biomes due to fertilisation by enhanced atmospheric CO_2, nitrogen deposition or other climatic influences.

The conclusions drawn here in relation to behaviour of the global carbon cycle on both interannual and multi-decadal timescales highlight the influence of land biosphere processes on atmospheric greenhouse gas levels. They suggest that biomass burning may be a significantly larger source of greenhouse gases than previously thought. Land biota have played an important role in ameliorating the rise of CO_2 in the atmosphere due to human activities. A critical issue for future climate change is the rate at which oceans and land biota can sequester anthropogenic CO_2 in the future. The factors controlling carbon uptake by the land biosphere and its capacity for carbon storage are uncertain. Some studies suggest the biosphere may reach saturation, at which time the rise of atmospheric CO_2 levels would accelerate if anthropogenic emissions are not substantially reduced in the meantime.

There is scope to reduce greenhouse gas emissions by limiting rates of biomass burning. There is an estimated ongoing average release of 2 PgC yr^{-1} to the atmosphere, mainly through the clearing of land for agricultural purposes. Results presented here suggest that emissions from large, uncontrolled fires associated with El Niño-induced droughts may represent an additional significant source. Although these fires are partly the result of climatic influences, it has been suggested that land management practices are also an important contributing factor. A serious concern is that forecast climate change favouring warmer and drier conditions in some areas may be more conducive to fires, with important ramifications for greenhouse gas emissions and for the state of natural ecosystems in general.

The decline in atmospheric O_2 levels is unlikely to have any direct impact on natural ecosystems. The estimated loss since pre-industrial times of 180 ppm represents less than 0.1 % of the atmospheric O_2 burden. Over coming years to decades, further decline is inevitable. Rates of both fossil fuel combustion and land

clearing continue to increase and there is no indication that these trends will be reversed in the near future. Although the land biosphere has partly offset anthropogenic O_2 consumption in recent years, its capacity to sustain this growth is uncertain. However, even if all accessible organic material (known fossil fuel reserves and standing biomass) were combusted, the loss of atmospheric O_2 would still represent a very small fraction (about 0.6 %) of its pre-industrial atmospheric burden.

The data from aircraft-based sampling above Cape Grim represent the first observations of $\delta(O_2/N_2)$ vertical gradients in the troposphere. They show significant seasonal cycling of the vertical gradient. Sensitivity analyses using an atmospheric transport model showed that the $\delta(O_2/N_2)$ variations are mainly controlled by two processes: 1) the seasonal variation of air-sea O_2 and N_2 fluxes in the SH and 2) the rate of vertical mixing in the SH troposphere. Other processes that contribute significantly to seasonal and altitudinal variations in CO_2 and its $\delta^{13}C$ have relatively little impact on $\delta(O_2/N_2)$. Foremost among these is the influence of NH air that is subject to significant seasonal variation in both terrestrial and oceanic fluxes in the NH and to the dynamics of interhemispheric exchange in the atmosphere.

The $\delta(O_2/N_2)$ vertical profile data are expected to provide a valuable constraint of hemispheric-scale, vertical mixing rates in the troposphere. They address a recognised deficiency of observational data that are suitable for constraining vertical mixing parameterisation in atmospheric transport models. The verification or improvement of such models is a high priority for a wide range of atmospheric science applications. For example, the accurate representation of atmospheric transport is critical for reliable inversion of observational data to infer

the surface flux distribution of CO_2. Preliminary tests using one transport model (CRC-MATCH) identified differences between modelled and observed $\delta(O_2/N_2)$ variations that likely reflect the paramaterisation of vertical mixing processes. A more quantitative analysis is planned for the future.

Another potential application of $\delta(O_2/N_2)$ vertical profile measurements is for quantification of surface fluxes on smaller spatial scales, especially involving air-sea exchange. Because O_2 has low solubility in seawater, perturbations in the O_2 concentration of the oceanic mixed layer are rapidly transmitted to the atmosphere. This behaviour contrasts with that of CO_2, for which equilibration with the atmosphere is retarded by inorganic seawater chemistry. Thus, for example, vertical profiles of $\delta(O_2/N_2)$ in the MBL may effectively constrain the marine biological response to iron fertilisation experiments.

Considerable attention has been given in this thesis to the identification of systematic influences on O_2/N_2 measurements. This has been motivated by two factors. One is the knowledge that O_2/N_2 measurements must be very precise to usefully constrain carbon cycle processes. The second is the observation that it is commonplace for discrepancies to exist among inter-laboratory records of other species (e.g. CO_2) that are larger than expected from the laboratories' assessment of uncertainty in their own data. The implication is that significant, systematic influences can go undetected and can result in flawed interpretation of atmospheric measurements.

The experience from this program is that there are many potential pitfalls in trying to measure O_2 in air at a precisionof a few ppm or better. There are difficulties involving the mass spectrometric analysis technique. Of wider significance to trace

gas measurement programs is the identification of artefacts due to mass-dependent fractionation affecting numerous aspects of experimental techniques. Such effects were most clearly manifested in the covariation of ratios of the inert gas pair Ar/N_2, the isotopomer pair $^{29}N_2/^{28}N_2$, and O_2/N_2, which of course also carries biogeochemical information and is thus not a direct tracer of mass-dependent processes. Fractionation effects were linked to gas handling procedures associated with sample collection and analysis, involving both grab sampling of the atmosphere using glass flasks and the use of high pressure cylinders for calibration purposes. Other processes, such as the permeation of gases through the elastomeric O-rings used to seal glass flasks, were also identified as causes of modification of sampled air. These effects are highly significant for measurement of O_2/N_2 and also for other trace gases such as CO_2. For example, the results from this O_2/N_2 program shed light on some previously unexplained CO_2 measurement artefacts (such as drift in cylinder standards and flask samples). Gaining an understanding of the causes of such artefacts is a critical step in meeting the broader scientific objectives that continue to demand higher precision and reliability of observational data.

A common theme of both the experimental and interpretive parts of this thesis is the use of multi-species information. Measurements of Ar/N_2 and $\delta^{29}N_2$ proved to be exceptionally valuable as tracers of mass-dependent experimental artefacts. It is envisaged that this measurement capability will in future be a key element of quality control strategies for various aspects of CSIRO's trace gas measurement programs. It will be used to refine gas handling procedures and to reduce and/or quantify the effects of fractionation in grab samples and calibration standards. The observation of correlated interannual variability among multiple trace gas and isotopic species has shed new light on the biogeochemical forcing of atmospheric composition. This was

achieved with a modest number of tracers whose global atmospheric budgets reflect varying contributions by a range of different processes. It seems likely that the use of multi-species information involving these and other trace gas species holds great potential to resolve other scientific issues.

AUTHOR'S BIBLIOGRAPHY

(relevant to and published during the course of work on this thesis)

Peer-reviewed journal publications:

Cunnold, D.M., L.P. Steele, P.J. Fraser, P.G. Simmonds, R.G. Prinn, R.F. Weiss, L.W. Porter, R.L. Langenfelds and H.J. Wang, GAGE/AGAGE measurements of methane at 5 sites from 1985 to 1999, *J. Geophys. Res.*, in press.

Etheridge, D.M., L.P. Steele, R.L. Langenfelds, R.J. Francey, J.-M. Barnola and V.I. Morgan. Natural and anthropogenic changes in atmospheric CO_2 over the last 1000 years from air in Antarctic ice and firn. *J. Geophys. Res.*, 101, 4115 - 4128, 1996.

Francey, R.J., L.P. Steele, R.L. Langenfelds, M.P. Lucarelli, C.E. Allison, D.J. Beardsmore, S.A. Coram, N. Derek, F.R. deSilva, D.M. Etheridge, P.J. Fraser, R.J. Henry, B. Turner, E.D. Welch, D.A. Spencer and L.N. Cooper. Global Atmospheric Sampling Laboratory (GASLAB): supporting and extending the Cape Grim trace gas programs. *Baseline Atmospheric Program (Australia) 1993*, edited by R.J.Francey, A.L.Dick and N.Derek, Bureau of Meteorology and CSIRO Division of Atmospheric Research, Melbourne, 8-29, Australia, 1996.

Francey, R.J., L.P. Steele, R.L. Langenfelds, C.E. Allison, L.N. Cooper. B.L. Dunse, B.G. Bell, T.D. Murray, H.S. Tait, L. Thompson and K.A. Masarie. Atmospheric carbon dioxide and its isotopes, methane, carbon monoxide, nitrous oxide and hydrogen from Shetland. *Atmos. Environ.*, 32, 3331-3338, 1998.

Francey, R.J., M.R. Manning, C.E. Allison, S.A. Coram, D.M. Etheridge, R.L. Langenfelds, D.C. Lowe and L.P. Steele, A history of $\delta^{13}C$ in atmospheric CH_4 from the Cape Grim Air Archive and Antarctic firn air. *J. Geophys. Res.*, 104, 23631-23643, 1999.

Francey, R.J., C.E. Allison, D.M. Etheridge, C.M. Trudinger, I.G. Enting, M. Leuenberger, R.L. Langenfelds, E. Michel and L.P. Steele, A 1000-year high precision record of $\delta^{13}C$ in atmospheric CO_2, *Tellus*, 51B, 170-193, 1999.

Francey, R.J., L.P. Steele, R.L. Langenfelds and B.C. Pak, High precision long-term monitoring of radiatively-active trace gases at surface sites and from ships and aircraft in the Southern Hemisphere atmosphere. *J. Atmos. Sci.*, 56, 279-285, 1999.

Langenfelds, R.L., R.J. Francey, L.P. Steele, P.J. Fraser, S.A. Coram, M.R. Hayes, D.J. Beardsmore, M.P. Lucarelli and F.R. deSilva. Improved vertical sampling of the trace gas composition of the troposphere above Cape Grim since 1991. *Baseline Atmospheric Program (Australia) 1993*, edited by R.J.Francey, A.L.Dick and N.Derek, Bureau of Meteorology and CSIRO Division of Atmospheric Research, Melbourne, Australia, 45-56, 1996.

Langenfelds, R.L., P.J. Fraser, R.J. Francey, L.P. Steele, L.W. Porter and C.E. Allison. The Cape Grim Air Archive: the first seventeen years, 1978 - 1995. *Baseline Atmospheric Program (Australia) 1994-95*, edited by R.J.Francey, A.L.Dick and N.Derek, Bureau of Meteorology and CSIRO Division of Atmospheric Research, Melbourne, Australia, 53-70, 1996.

Langenfelds, R. R. Francey, P. Steele, M. Battle, R. Keeling and W. Budd, Partitioning of the global fossil CO_2 sink using a 19-year trend in atmospheric O_2, *Geophys. Res. Lett.*, Vol. 26, No. 13, 1897-1900, 1999.

Langenfelds, R.L., R.J. Francey, L.P. Steele, R. Keeling, M. Battle and W. Budd. Measurements of O_2/N_2 ratio from the Cape Grim Air Archive and three independent flask sampling programs, *Baseline Atmospheric Program (Australia) 1996*, edited by J.Gras, N.Tindale and N.Derek, Bureau of Meteorology and CSIRO Atmospheric Research, Melbourne, Australia, 57-70, 1999.

Langenfelds, R.L., Anthropogenic impacts on atmospheric oxygen, in *Encyclopedia of Global Environmental Change, Volume 2: The Earth system: biological and*

ecological dimensions of global environmental change, edited by H. A. Mooney and J. G. Canadell, John Wiley and Sons Limited, United Kingdom, pp 140-143, 2002.

Langenfelds, R.L., R.J. Francey, B.C. Pak, L.P. Steele, J. Lloyd, C.M. Trudinger and C.E. Allison, Interannual growth rate variations of atmospheric CO_2 and its $\delta^{13}C$, H_2, CH_4 and CO between 1992 and 1999 linked to biomass burning, *Global Biogeochem. Cycles*, in press.

Pak, B.C., R.L. Langenfelds, R.J. Francey, L.P. Steele and I. Simmonds. A climatology of trace gases from the Cape Grim overflights, 1992 - 1995. *Baseline Atmospheric Program (Australia) 1994-95*, edited by R.J.Francey, A.L.Dick and N.Derek, Bureau of Meteorology and CSIRO Division of Atmospheric Research, Melbourne, Australia, 41-52, 1996.

Pak, B. C., R. L. Langenfelds, S. A. Young, R. J. Francey, C. P. Meyer, L. M. Kivlighon, L. N. Cooper, B. L. Dunse, C. E. Allison, L. P. Steele, I. E. Galbally and I. A. Weeks, Measurements of biomass burning influences in the troposphere over SE Australia during the SAFARI 2000 dry season campaign, *J. Geophys. Res.*, in press.

Rayner, P.J., I.G. Enting, R.J. Francey and R.L. Langenfelds. Reconstructing the recent carbon cycle from atmospheric CO_2, $\delta^{13}C$ and O_2/N_2 observations, *Tellus*, 51B, 213-232, 1999.

Trudinger, C.M., D.M. Etheridge, P.J. Rayner, I.G. Enting, G.A. Sturrock and R.L. Langenfelds, Reconstructing atmospheric histories from measurements of air composition in firn, *J. Geophys. Res.*, in press.

Other reports and abstracts:

Cooper, L.N., L.P. Steele, R.L. Langenfelds, D.A. Spencer and M.P. Lucarelli, Atmospheric methane, carbon dioxide, hydrogen, carbon monoxide, and nitrous oxide from Cape Grim flask air samples analysed by gas chromatography.

Baseline Atmospheric Program (Australia) 1996, edited by J.Gras, N.Tindale and N.Derek, pp 98-102, Bureau of Meteorology and CSIRO Atmospheric Research, Melbourne, Australia, 1999.

Francey, R., P. Rayner, R. Langenfelds and C. Trudinger, The inversion of atmospheric CO_2 mixing ratios and isotopic composition to constrain large-scale air-sea fluxes, *Proceedings of the Second International Symposium on CO_2 in the Oceans,* National Institute for Environmental Studies, Environment Agency of Japan, 237-250, 1999.

Francey, R.J., L.P. Steele, D.A. Spencer, R.L. Langenfelds, R.M. Law, P.B. Krummel, P.J. Fraser, D.M. Etheridge, N. Derek, S.A. Coram, L.N. Cooper, C.E. Allison, L. Porter and S. Baly, The CSIRO (Australia) measurement of greenhouse gases in the global atmosphere, *report of the 11th WMO/IAEA Meeting of Experts on Carbon Dioxide Concentration and Related Tracer Measurement Techniques*, Tokyo, Japan, September 2001, World Meteorological Organization Global Atmosphere Watch, in press.

Langenfelds, R.L., R.J. Francey, L.P. Steele, M.P. Lucarelli, D.A. Spencer, S.A. Coram and K. Broadhurst. Flask sampling from Cape Grim overflights. *Baseline Atmospheric Program (Australia) 1994-95*, edited by R.J.Francey, A.L.Dick and N.Derek, Bureau of Meteorology and CSIRO Division of Atmospheric Research, Melbourne, Australia, 112-117, 1996.

Langenfelds, R. R. Francey, P. Steele, M. Battle, R. Keeling and W. Budd, Determination of a 19-year O_2/N_2 trend from the Cape Grim Air Archive, *Proceedings of the Fifth International Carbon Dioxide Conference,* Cairns, Australia, September 1997, Fifth International Carbon Dioxide Conference Committee, 39-40, 1997.

Langenfelds,R., R. Francey, P.Steele, and W.Budd. The CSIRO atmospheric O_2/N_2 measurement program. *Report of the Ninth WMO Meeting of Experts on Carbon Dioxide Concentration and Related Tracer Measurement Techniques*, Melbourne, Australia, September 1997, World Meteorological Organization Global Atmosphere Watch, 26-30, 1999.

Langenfelds, R., R. Francey, B. Pak, P. Steele, J. Lloyd, C. Trudinger and C. Allison, The use of multi-species measurements for interpreting interannual variability in the carbon cycle, *Proceedings of the Sixth International Carbon Dioxide Conference,* Sendai, Japan, September 2001, Organizing Committee of Sixth International Carbon Dioxide Conference, 9-11, 2001.

Langenfelds, R.L., L.N. Cooper, L.P. Steele, and D.A. Spencer, Atmospheric methane, carbon dioxide, hydrogen, carbon monoxide, and nitrous oxide from Cape Grim flask air samples analysed by gas chromatography. *Baseline Atmospheric Program (Australia) 1997-98*, pp 69-74, Bureau of Meteorology and CSIRO Atmospheric Research, Melbourne, Australia, 2001.

Langenfelds, R.L., R.J. Francey, L.P. Steele, D.A. Spencer and B.L. Dunse. Flask sampling from Cape Grim overflights. *Baseline Atmospheric Program (Australia) 1997/98*, pp 74-84, Bureau of Meteorology and CSIRO Atmospheric Research, Melbourne, Australia, 2001.

Langenfelds, R.L., P.J. Fraser, L.P. Steele and L.W. Porter. Archiving of Cape Grim air, *Baseline Atmospheric Program (Australia) 1997-98*, pp 84-86, Bureau of Meteorology and CSIRO Atmospheric Research, Melbourne, Australia.

Langenfelds, R.L., R. Keeling, M. Battle and R. Francey. O_2/N_2 from flask sampling, *Baseline Atmospheric Program (Australia) 1997-98*, pp 86-87, Bureau of Meteorology and CSIRO Atmospheric Research, Melbourne, Australia, 2001.

Steele, L.P., R.L. Langenfelds, M.P. Lucarelli, P.J. Fraser, L.N. Cooper, D.A. Spencer, S. Chea and K. Broadhurst. Atmospheric methane, carbon dioxide, carbon monoxide, hydrogen and nitrous oxide from Cape Grim flask air samples analysed by gas chromatography. *Baseline Atmospheric Program (Australia) 1994-95*, edited by R.J.Francey, A.L.Dick and N.Derek, Bureau of Meteorology and CSIRO Division of Atmospheric Research, Melbourne, Australia, 107-110, 1996.

REFERENCES

Allison, C.E., R.J. Francey and H.A.J. Meijer, Recommendations for the reporting of stable isotope measurements of carbon and oxygen in CO_2 gas, in *Reference and intercompasrison materials for stable isotopes of light elements, IAEA-TECDOC-825*, edited by K. Rozanski, Vienna, Austria, 155-162, 1995.

Allison, C.E. and R.J. Francey, $\delta^{13}C$ of atmospheric CO_2 at Cape Grim: The *in situ* record, the flask record, air standards and the CG92 calibration scale, in *Baseline Atmospheric Program (Australia) 1996*, edited by J. Gras, N. Tindale and N. Derek, pp. 45-56, Bureau of Meteorology and CSIRO Division of Atmospheric Research, Melbourne, Australia, 1999.

Anderson, J.A.R., The structure and development of the peat swamps of Sarawak and Brunei, *J. Trop. Geog.*, 18, 7-16, 1964.

Andreae, M.O., E. Atlas, H. Cachier, W.R. Cofer III, G.W. Harris, G. Helas, R. Koppmann, J-P. Lacaux and D.E. Ward, Trace gas and aerosol emissions from savanna fires, *in Biomass Burning and Global Change, Volume 1, Remote Sensing, Modeling and Inventory Development, and Biomass Burning in Africa*, edited by Joel S. Levine, The MIT Press, Cambridge, Massachusetts, USA, 278-295, 1996.

Andreae, M.O., P. Artaxo, H. Fischer, S.R. Freitas, J.-M. Grégoire, A. Hansel, P. Hoor, R. Kormann, R. Krejci, L. Lange, J. Lelieveld, W. Lindinger, K. Longo. W. Peters, M. de Reus, B. Scheeren, M.A.F. Silva Dias, J. Ström, P.F.J. van Velthoven and J. Williams, Transport of biomass burning smoke to the upper troposphere by deep convection in the equatorial region, *Geophys. Res. Lett.*, 28, 951-954, 2001.

Andreae, M.O. and P. Merlet, Emission of trace gases and aerosols from biomass burning, *Glob. Biogeochem. Cycles*, 15, 955-966, 2001.

Andres, R.J., G. Marland and S. Bischof, Global and latitudinal estimates of $\delta^{13}C$ from fossil-fuel consumption and cement manufacture, Carbon Dioxide

Information Analysis Center, Oak Ridge National Laboratory, U.S. Department of Energy, Oak Ridge, Tenn., U.S.A. (http://cdiac.esd.ornl.gov), 1996.

Appenzeller, C., J. R. Holton and K. H. Rosenlof, Seasonal variation of mass transport across the tropopause, *J. Geophys. Res.*,101, 15071-15078, 1996.

Bacastow, R.B., Modulation of atmospheric carbon dioxide by the Southern Oscillation, *Nature*, 261, 116-118, 1976.

Bakwin, P.S., P.P. Tans, C, Zhao, W. Ussler and E. Quesnell, Measurements of carbon dioxide on a very tall tower, *Tellus*, 47B, 535-549, 1995.

Balkanski, Y., P. Monfray, M. Battle and M. Heimann, Ocean primary production derived from satellite data: An evaluation with atmospheric oxygen measurements, *Global Biogeochem. Cycles*, 13, 257-271, 1999.

Barbosa, P.M., D. Stroppiana, J-M. Gregoire and J.M.C. Pereira, An assessment of vegetation fire in Africa (1981-1991): Burned areas, burned biomass and atmospheric emissions, *Glob. Biogeochem. Cycles,* 13, 933-950, 1999.

Battle, M., M. Bender, T. Sowers, P.P. Tans, J.H. Butler, J.W. Elkins, J.T. Ellis, T. Conway, N. Zhang, P. Lang and A.D. Clarke, Atmospheric gas concentrations over the past century measured in air from firn at the South Pole, *Nature*, 383, 231-235, 1996.

Battle, M., M. Bender, P.P. Tans, J.W.C. White, J.T. Ellis, T. Conway and R.J. Francey, Uptake of carbon by the ocean and the terrestrial biosphere inferred from atmospheric O_2 and $\delta^{13}C$, *Science*, 287, 2467-2470, 2000.

Beardsmore, D.J., G.I. Pearman, P.J. Fraser and J.G. O'Toole, The CSIRO (Australia) atmospheric carbon dioxide monitoring program: The first six years of data, CSIRO Division of Atmospheric Physics Technical Paper No. 35, 71 pp., 1978.

Beaumont, V., P. Agrinier, M. Javoy and F. Robert, Determination of the CO contribution to the $^{15}N/^{14}N$ ratio measured by mass spectrometry, *Anal. Chem.*, 66, 2187-2189, 1994.

Bender, M.L., P.P. Tans, J.T. Ellis, J. Orchardo and K. Habfast, A high precision isotope ratio mass spectrometry method for measuring the O_2/N_2 ratio of air, *Geochim. et Cosmochim. Acta*, 58, 4751-4758, 1994.

Bender, M., T. Sowers, and V. Lipenkov, On the concentrations of O_2, N_2 and Ar in trapped gases from ice cores, *J. Geophys. Res.*, 100, 18651-18660, 1995.

Bender, M., T. Ellis, P. Tans, R. Francey and D. Lowe, Variability in the O_2/N_2 ratio of southern hemisphere air, 1991-1994: Implications for the carbon cycle, *Global Biogeochem. Cycles,* 10, 9-21, 1996.

Bergamaschi, P., R. Hein, M. Heimann and P.J. Crutzen, Inverse modeling of the global CO cycle 1. Inversion of CO mixing ratios, *J. Geophys. Res.*, 105, 1909-1927, 2000a.

Bergamaschi, P., R. Hein, C.A.M. Brenninkmeijer and P.J. Crutzen, Inverse modeling of the global CO cycle 2. Inversion of $^{13}C/^{12}C$ and $^{18}O/^{16}O$ isotope ratios, *J. Geophys. Res.*, 105, 1929-1945, 2000b.

Bopp, L., C. Le Quéré, M. Heimann, A.C. Manning and P. Monfray, Climate-induced oceanic oxygen fluxes: Implications for the contemporary carbon budget, in *Sixth International Carbon Dioxide Conference: extended abstracts*, Sendai, Japan, September 2001, Organizing Committee of Sixth International Carbon Dioxide Conference, 1055-1058, 2001.

Bousquet, P., P. Peylin, P. Ciais, C. Le Quéré, P. Friedlingstein and P.P. Tans, Regional changes in carbon dioxide fluxes of land and oceans since 1980, *Science*, 290, 1342-1346, 2000.

BP Amoco statistical review of world energy [http://www/bpamoco.com/worldenergy], 1999.

Brenkert, A. L., Carbon Dioxide Emission Estimates from Fossil-Fuel Burning, Hydraulic Cement Production, and Gas Flaring for 1995 on a One Degree Grid Cell Basis, Carbon Dioxide Information Analysis Center, Oak Ridge National

Laboratory, U.S. Department of Energy, Oak Ridge, Tenn., U.S.A. (http://cdiac.esd.ornl.gov), 1998.

Broecker, W.S., Man's oxygen reserves. *Science*, 168, 1537-1538, 1970.

Brunke, E.G., H.E. Scheel and W. Seiler, Trends of tropospheric CO, N_2O and CH_4 as observed at Cape Point, South Africa, *Atmos. Environ.*, 24A, 585-595, 1990.

Cahoon, D.R. Jnr., B.J. Stocks, J.S. Levine, W.R. Cofer III and J.M. Pierson, Satellite analysis of the severe 1987 forest fires in northern China and southeastern Siberia, *J. Geophys. Res.*, 99, 18627-18638, 1994.

Ciais, P., P.P. Tans, J.W.C. White, M. Trolier, R.J. Francey, J.A. Berry, D.A. Randall, P.J. Sellers, J.H. Collatz and D.S. Schimel, Partitioning of ocean and land uptake of CO_2 as inferred by $\delta^{13}C$ measurements from the NOAA Climate Monitoring and Diagnostics Laboratory global air sampling network, *J. Geophys. Res.*, 100, 5051-5070, 1995.

Ciais, P., P. Friedlingstein, D.S. Schimel and P.P. Tans, A global calculation of the $\delta^{13}C$ of soil respired carbon: Implications for the biospheric uptake of anthropogenic CO_2, *Global Biogeochem. Cycles*, 13, 519-530, 1999.

Chapman, S. and T.G. Cowling, *The mathematical theory of non-uniform gases*, Cambridge Univ. Press, 423 pp, 1970.

Connors, V.S., B.G. Gormsen, S. Nolf and H.G. Reichle Jr., Spaceborne observations of the global distribution of carbon monoxide in the middle troposphere during April and October 1994, *J. Geophys. Res.*, 104, 21455-21470, 1999.

Conway, T.J., P.P. Tans, L.S. Waterman, K.W. Thoning, D.R. Kitzis, K.A. Masarie, and N. Zhang, Evidence for interannual variability of the carbon cycle from the NOAA/CMDL global air sampling network, *J. Geophys. Res.*, 99, 22831-22855, 1994.

Cooper, L.N., L.P. Steele, R.L. Langenfelds, D.A. Spencer and M.P. Lucarelli, Atmospheric methane, carbon dioxide, hydrogen, carbon monoxide and nitrous

oxide from Cape Grim flask air samples analysed by gas chromatography, in *Baseline Atmospheric Program (Australia) 1996,* edited by J.L. Gras, N. Derek, N.W. Tindale and A.L. Dick, pp. 98-102, Bureau of Meteorology and CSIRO Division of Atmospheric Research, Melbourne, Australia, 1999.

Cooper, L.N., R.J. Francey, L.P. Steele, R.L. Langenfelds, D.A. Spencer, C.E. Allison, P.B. Krummel and K.A. Masarie, Flask air sharing program, in *Baseline Atmospheric Program (Australia) 1997/98,* edited by N.W. Tindale, N. Derek and R.J. Francey, pp. 88-89, Bureau of Meteorology and CSIRO Atmospheric Research, Melbourne, Australia, 2001.

Craig, H., Y. Horibe, and T. Sowers, Gravitational separation of gases and isotopes in polar ice caps, *Science*, **242**, 1675-1678, 1988.

Crawford, E., *Arrhenius: From ionic theory to the Greenhouse Effect*, Science History Publications, 320 pp, 1996.

Crutzen, P.J. and M.O. Andreae, Biomass burning in the tropics: Impact on atmospheric chemistry and biogeochemical cycles, *Science*, 250, 1669-1678, 1990.

Denning, A.S., M. Holzer, K.R. Gurney, M. Heimann, R.M. Law, P.J. Rayner, I.Y. Fung, S-M. Fan, S. Taguchi, P. Friedlingstein, Y. Balkanski, J. Taylor, M. Maiss and I. Levin, Three-dimensional transport and concentration of SF_6: A model intercomparison study (TransCom 2), *Tellus*, 51B, 266-297, 1999.

Dettinger, M.D. and M. Ghil, Seasonal and interannual variations of atmospheric CO_2 and climate, *Tellus*, 50B, 1-24, 1998.

Dlugokencky, E.J., L.P. Steele, P.M. Lang and K.A. Masarie, The growth rate and distribution of atmospheric methane, *J. Geophys. Res.*, 99, 17021-17043, 1994.

Dlugokencky, E.J., E.C. Dutton, P.C. Novelli, P.P. Tans, K.A. Masarie, K.O. Lantz and S. Madronich, Changes in CH_4 and CO growth rates after the eruption of Mt Pinatubo and their link with changes in tropical UV flux, *Geophys. Res. Lett.*, 23, 2761-2764, 1996.

Dlugokencky, E.J., B.P. Walter, K.A. Masarie, P.M. Lang and E.S. Kasischke, Measurements of an anomalous global methane increase during 1998, *Geophys. Res. Lett.*, 28, 499-502, 2001.

Enting, I.G., C.M. Trudinger, R.J. Francey and H. Granek, Synthesis inversion of atmospheric CO_2 using the GISS tracer transport model, CSIRO Division of Atmospheric Research Technical Paper No. 29, 44 pp., 1993.

Enting, I.G. and K.R. Lassey, Projections of future CO_2, CSIRO Division of Atmospheric Research Technical Paper No. 27; NIWA/Atmos/R/93-001, 42 pp., 1993.

Enting, I.G., T.M.L. Wigley and M. Heimann, Future emissions and concentrations of carbon dioxide: Key ocean/atmosphere/land analyses, CSIRO Division of Atmospheric Research Technical Paper No. 31, CSIRO Atmospheric Research, Melbourne, Australia, 118 pp, 1994.

Etheridge, D.M, L.P. Steele, R.L. Langenfelds, R.J. Francey, J.-M. Barnola and V.I. Morgan, Natural and anthropogenic changes in atmospheric CO_2 over the last 1000 years from air in Antarctic ice and firn. *J. Geophys. Res.*, 101, 4115-4128, 1996.

Etheridge, D.M., L.P. Steele, R.J. Francey, and R.L. Langenfelds, Atmospheric methane between 1000 A.D. and present: evidence of anthropogenic emissions and climatic variability, *J. Geophys Res.*, 103, 15979-15993, 1998.

Feely, R.A., R. Wanninkhof, T. Takahashi and P. Tans, Influence of El Niño on the equatorial Pacific contribution to atmospheric CO_2 accumulation, *Nature*, 398, 597-601, 1999.

Folkins, I., R. Chatfield, D. Baumgardner and M. Proffitt, Biomass burning and deep convection in southeastern Asia: Results from ASHOE/MAESA, *J. Geophys. Res.*, 102, 13291-13299, 1997.

Francey, R. J. and P. P. Tans, Latitudinal variation in oxygen-18 of atmospheric CO_2, *Nature*, 327, 495-497, 1987.

Francey, R.J., and C.E. Allison, The trend in atmospheric $\delta^{13}CO_2$ over the last decade, in *Isotope variations of carbon dioxide and other trace gases in the atmosphere: final research coordination meeting, coordinated research programme: final report*, Vienna, Austria, K. Rozanski (editor). [Vienna]: International Atomic Energy Agency. 7 pp, 1994.

Francey, R.J., P.P. Tans, C.E. Allison, I.G. Enting, J.W.C. White and M. Trolier, Changes in oceanic and terrestrial carbon uptake since 1982, *Nature*, *373*, 326-330, 1995.

Francey, R.J., L.P. Steele, R.L. Langenfelds, M.P. Lucarelli, C.E. Allison, D.J. Beardsmore, S.A. Coram, N. Derek, F. de Silva, D.M. Etheridge, P.J. Fraser, R. Henry, B. Turner and E.D. Welch, Global Atmospheric Sampling Laboratory (GASLAB): supporting and extending the Cape Grim trace gas programs, in *Baseline Atmospheric Program (Australia) 1993,* edited by R.J. Francey, A.L. Dick and N. Derek, pp. 8-29, Bureau of Meteorology and CSIRO Division of Atmospheric Research, Melbourne, Australia, 1996.

Francey, R.J., L.P. Steele, R.L. Langenfelds, C.E. Allison, L.N. Cooper, B.L. Dunse, B.G. Bell, T.D. Murray, H.S. Tait, L. Thompson and K.A. Masarie, Atmospheric carbon dioxide and its stable isotope ratios, methane, carbon monoxide, nitrous oxide and hydrogen from Shetland Isles, *Atmos. Environ.*, 32, 3331-3338, 1998.

Francey, R.J., C.E. Allison, D.M. Etheridge, C.M. Trudinger, I.G. Enting, M. Leuenberger, R.L. Langenfelds, E. Michel and L.P. Steele, A 1000-year high precision record of $\delta^{13}C$ in atmospheric CO_2, *Tellus*, 51B, 170-193, 1999a.

Francey, R.J., M.R. Manning, C.E. Allison, S.A. Coram, D.M. Etheridge, R.L. Langenfelds, D.C. Lowe and L.P. Steele, A history of $\delta^{13}C$ in atmospheric CH_4 from the Cape Grim Air Archive and Antarctic firn air, *J. Geophys. Res.*, 104, 23631-23643, 1999b.

Francey, R.J., C.E. Allison, C.M. Trudinger, P.J. Rayner, I.G. Enting and L.P. Steele, The interannual variation in global atmospheric $\delta^{13}C$ and its link to net terrestrial exchange, in *Sixth International Carbon Dioxide Conference: extended*

abstracts, Sendai, Japan, September 2001, Organizing Committee of Sixth International Carbon Dioxide Conference, 43-46, 2001.

Francey, R.J., L.P. Steele, D.A. Spencer, R.L. Langenfelds, R.M. Law, P.B. Krummel, P.J. Fraser, D.M. Etheridge, N. Derek, S.A. Coram, L.N. Cooper, C.E. Allison, L. Porter and S. Baly, The CSIRO (Australia) measurement of greenhouse gases in the global atmosphere, *report of the 11th WMO/IAEA Meeting of Experts on Carbon Dioxide Concentration and Related Tracer Measurement Techniques*, Tokyo, September 2001, World Meteorological Organization Global Atmosphere Watch, in press.

Fraser, P.J., R.L. Langenfelds, N. Derek and L.W. Porter, Studies in air archiving techniques. Part 1: Long term stability of atmospheric trace gases in dry, natural air stored in high-pressure surface-treated aluminium cylinders, *Baseline Atmospheric Program (Australia) 1989*, edited by S.R. Wilson and J. L. Gras, pp. 16-29, Bureau of Meteorology and CSIRO Division of Atmospheric Research, Melbourne, Australia, 1991.

Fraser, P., S. Coram and N. Derek, Atmospheric methane, carbon monoxide and carbon dioxide by gas chromatography, *Baseline Atmospheric Program (Australia) 1991*, edited by A. L. Dick and J. L. Gras, pp. 60-64, Bureau of Meteorology and CSIRO Division of Atmospheric Research, Melbourne, Australia, 1994.

Fraser, P.J., D. Cunnold, F. Alyea, R. Weiss, R. Prinn, P. Simmonds, B. Miller and R. Langenfelds, Lifetime and emission estimates of 1,1,2-trichlorotrifluoroethane (CFC-113) from daily global background observations, June 1982 - June 1994, *J. Geophys. Res.*, 101, 12585-12599, 1996.

Fujiwara, M., K. Kita, S. Kawakami, T. Ogawa, N. Komala, S. Saraspriya and A. Suripto, Tropospheric ozone enhancements during the Indonesian forest fire events in 1994 and in 1997 as revealed by ground-based observations, *Geophys. Res. Lett.*, 26, 2417-2420, 1999.

Fujiwara, M., K. Kita, T. Ogawa, S. Kawakami, T. Sano, N. Komala, S. Saraspriya and A. Suripto, Seasonal variation of tropospheric ozone in Indonesia revealed by 5-year ground-based observations, *J. Geophys. Res.*, 105, 1879-1888, 2000.

Fung, I., J. John, J. Lerner, E. Matthews, M. Prather, L.P. Steele and P.J. Fraser, Three-dimensional model synthesis of the global methane cycle, *J. Geophys. Res.*, 96, 13033-13065, 1991.

Galloway, J.N., W.H. Schlesinger, H. Levy II, A. Michaels and L. Schnoor, Nitrogen fixation: anthropogenic enhancement-environmental response, *Global Biogeochem. Cycles*, **9**, 235-252, 1995.

Garcia, H. E. and R. F. Keeling, On the global oxygen anomaly and air-sea flux, *J. Geophys. Res.*, 106, 31155-31166, 2001.

Gerard, J.C., B. Nemry, L.M. Francois and P. Warnant, The interannual change of atmospheric CO_2: contribution of subtropical ecosystems?, *Geophys. Res. Lett.*, 26, 243-246, 1999.

Goldstein, A.H., M.L. Goulden, J.W. Munger, S.C. Wofsy and C.D. Geron, Seasonal course of isoprene emissions from a midlatitude deciduous forest, *J. Geophys. Res.*, 103, 31045-31056, 1998.

Goody, R.M. and Y.L. Yung, *Atmospheric radiation*, Oxford University Press, 519 pp, 1989.

Grew, K.E. and T.L. Ibbs, *Thermal diffusion in gases*, Cambridge Univ. Press, 143 pp, 1952.

Guenther, A., P. Zimmerman, P. Harley, R. Monson and R. Fall, Isoprene and monoterpene emission rate variability: Model evaluation and sensitivity analysis, *J. Geophys. Res.*, 98, 12609-12617, 1993.

Guenther, A., C.N. Hewitt, D. Erickson, R. Fall, C. Geron, T. Graedel, P. Harley, L. Klinger, M. Lerdau, W.A. McKay, T. Pierce, B. Scholes, R. Steinbrecher, R. Tallamraju, J. Taylor and P. Zimmerman, A global model of natural volatile organic compound emissions, *J. Geophys. Res.*, 100, 8873-8892, 1995.

Gurney, K. R., R. M. Law, A. S. Denning, P. J. Rayner, D. Baker, P. Bousquet, L. Bruhwiler, Y. Chen, P. Ciais, S. Fan, I. Y. Fung, M. Gloor, M. Heimann, K. Higuchi, J. John, T, Maki, S. Maksyutov, K. Masarie, P. Peylin, M, Prather, B. C. Pak, J. Randerson, J. Sarmiento, S. Taguchi, T. Takahashi and C. Yuen, Towards robust regional estimates of CO_2 sources and sinks using atmospheric transport models, *Nature*, 415, 626-630, 2002.

Hack, J. J., Paramaterization of moist convection in the NCAR Community Climate model, CCM2, *J. Geophys. Res.*, 99, 5551-5568, 1994.

Hao, W.M. and M.H. Liu, Spatial and tropical distribution of tropical biomass burning, *Global Biogeochem. Cycles*, 8, 495-503, 1994.

Harris, J.M., P.P. Tans, E.J. Dlugokencky, K.A. Masarie, P.M. Lang, S. Whittlestone and L.P. Steele, Variations in atmospheric methane at Mauna Loa Observatory related to long-range transport, *J. Geophys. Res.*, 97, 6003-6010, 1992.

Heimann, M. and E. Maier-Reimer, On the relations between the oceanic uptake of CO_2 and its carbon isotopes, *Global Biogeochem. Cycles*, 10, 89-110, 1996.

Holloway, T., H. Levy II and P. Kasibhatla, Global distribution of carbon monoxide, *J. Geophys. Res.*, 105, 12123-12147, 2000.

Holtslag, A. A. M. and B. A. Boville, Local versus nonlocal boundary-layer diffusion in a global climate model, *J. Clim.*, 6, 1825-1842, 1993.

Holzinger, R., C. Warneke, A. Hansel, A. Jordan, W. Lindinger, D.H. Scharffe, G. Schade, and P.J. Crutzen, Biomass burning as a source of formaldehyde, acetaldehyde, methanol, acetone, acetonitrile and hydrogen cyanide, *Geophys. Res. Lett.*, 26, 1161-1164, 1999.

Houghton, R.A., E.A. Davidson and G.M. Woodwell, Missing sinks, feedbacks and understanding the role of terrestrial ecosystems in the global carbon balance, *Global Biogeochem. Cycles,* **12**, 25-34, 1998.

Houghton, R.A., The annual net flux of carbon to the atmosphere from changes in land use 1850-1990, *Tellus*, 51B, 298-313, 1999.

Houghton, R.A., D.L. Skole, C.A. Nobre, J.L. Hackler, K.T. Lawrence and W.H. Chomentowski, Annual fluxes of carbon from deforestation and regrowth in the Brazilian Amazon, *Nature*, 403, 301-304, 2000.

Houghton, R.A., and J.L. Hackler, *Carbon Flux to the Atmosphere from Land-Use Changes*, In Trends: A Compendium of Data on Global Change, Carbon Dioxide Information Analysis Center, Oak Ridge National Laboratory, U.S. Department of Energy, Oak Ridge, Tenn., U.S.A, 2000.

Jastrzebski, Z.D., *Nature and Properties of Engineering Materials*, John Wiley & Sons, Inc., pp 378-445, 1964.

Jones, N.B., C.P. Rinsland, J.B. Liley and J. Rosen, Correlation of aerosol and carbon monoxide at 45°S: Evidence of biomass burning emissions, *Geophys. Res. Lett.*, 28, 709-712, 2001.

Kaplan, J.O., Geophysical applications of vegetation modeling, PhD thesis, Lund University, Lund, Sweden, 114 pp, 2001.

Kasischke, E.S., K. Bergen, R, Fennimore, F. Sotelo, G. Stephens, A. Janetos and H.H. Shugart, Satellite imagery gives clear picture of Russia's boreal forest fires, *EOS, Transactions*, 80, 141-147, 1999.

Kattenberg, A., F. Giorgi, H. Grassl, G.A. Meehl, J.F.B. Mitchell, R.J. Stouffer, T. Tokioka, A.J. Weaver and T.M.L. Wigley, Climate models – projections of future climate, in *IPCC Climate Change, The Science of Climate Change*, edited by J.T. Houghton, L.G. Meira Filho, B.A. Callander, N. Harris, A. Kattenberg and K.Maskell, Cambridge University Press, Cambridge, 359-405, 1996.

Keeling, C.D., R.B. Bacastow, A.F. Carter, S.C. Piper, T.P. Whorf, M. Heimann, W.G. Mook and H. Roeloffzen, A three-dimensional model of atmospheric CO_2 transport based on observed winds: 1. Analysis of observational data, *Aspects of climate variability in the Pacific and the Western Americas*, Geophysical Monograph 55, American Geophysical Union, Washington DC, pp 165 - 236, 1989.

Keeling, C.D., T.P. Whorf, M. Wahlen, and J. Van Der Plicht, Interannual extremes in the rate and rise of atmospheric carbon dioxide since 1980, *Nature*, 375, 666-670, 1995.

Keeling, C.D., J.F.S. Chin and T.P. Whorf, Increased activity of northern vegetation inferred from atmospheric CO_2 measurements, *Nature*, 382, 146-149, 1996.

Keeling, C.D. and T.P. Whorf, *Atmospheric CO_2 records from sites in the SIO air sampling network,* In Trends: A Compendium of Data on Global Change, Carbon Dioxide Information Analysis Center, Oak Ridge National Laboratory, U.S. Department of Energy, Oak Ridge, Tenn., U.S.A, 2001.

Keeling, R.F., Development of an interferometric oxygen analyzer for precise measurement of the atmospheric O_2 mole fraction, *Ph.D. Thesis, Harvard University*, 178 pp, 1988.

Keeling, R.F. and S.R. Shertz, Seasonal and interannual variations in atmospheric oxygen and implications for the global carbon cycle, *Nature*, 358, 723-727, 1992.

Keeling, R.F., R.P. Najjar, M.L. Bender and P.P. Tans, What atmospheric oxygen measurements can tell us about the global carbon cycle, *Global Biogeochem. Cycles,* 7, 37-67, 1993.

Keeling, R.F., S.C. Piper and M. Heimann, Global and hemispheric CO_2 sinks deduced from changes in atmospheric O_2 concentration, *Nature,* 381, 218-221, 1996.

Keeling, R.F., A.C. Manning, E.M. McEvoy and S.R. Shertz, Methods for measuring changes in atmospheric O_2 concentration and their application in southern hemisphere air, *J. Geophys. Res.,* 103, 3381-3397, 1998a.

Keeling, R.F., B.B. Stephens, R.G. Najjar, S.C. Doney, D. Archer and M. Heimann, Seasonal variations in the atmospheric O_2/N_2 ratio in relation to the kinetocs of air-sea exchange, *Global Biogeochem. Cycles*, 12, 141-163, 1998b.

Keeling, R.F. and J. Severinghaus, Atmospheric oxygen measurements and the carbon cycle, in *The Carbon Cycle*, edited by T.M.L. Wigley and D.S. Schimel, Cambridge University Press, 134-140, 2000.

Khalil, M.A.K. and R.A. Rasmussen, Global increase of atmospheric molecular hydrogen, *Nature*, 347, 743-745, 1990.

Kicklighter D.W, M. Bruno, S. Dönges, G. Esser, M. Heimann, J. Helfrich, F. Ift, F. Joos, J. Kaduk, G.H. Kohlmaier, A.D. McGuire, J.M. Melillo, R. Meyer, B. Moore III, A. Nadler, I.C. Prentice, W. Sauf, A.L. Schloss, S. Sitch, U. Wittenberg and G. Würth, A first-order analysis of the potential role of CO_2 fertilization to affect the global carbon budget: a comparison of four terrestrial biosphere models, *Tellus*, 51B, 343-366, 1999.

Kindermann, J., G. Würth, G.H. Kohlmaier and F.-W. Badeck, Interannual variation of carbon exchange fluxes in terrestrial ecosystems, *Global Biogeochem. Cycles*, 10, 737-755, 1996.

Knorr, W., Annual and interannual CO_2 exchanges of the terrestrial biosphere: process-based simulations and uncertainties, *Glob. Ecol. Biogeog.*, 9, 225-252, 2000.

Langenfelds, R.L., L.P. Steele, P.J. Fraser, R.J. Francey, S.A. Coram, M.A. Hayes, D.J. Beardsmore, M.P. Lucarelli and F.R. de Silva, Improved vertical sampling of the troposphere above Cape Grim since 1991, *Baseline Atmospheric Program (Australia) 1993*, (eds. R.J.Francey, A.L.Dick and N.Derek), 46-57, Bureau of Meteorology and CSIRO Division of Atmospheric Research, Melbourne, Australia, 1996a.

Langenfelds, R.L., P.J. Fraser, R.J. Francey, L.P. Steele, L.W. Porter and C.E. Allison, The Cape Grim Air Archive: the first seventeen years, 1978 - 1995, in *Baseline Atmospheric Program (Australia) 1994-95,* (eds. by R.J. Francey A.L. Dick and N. Derek), 53-70, Bureau of Meteorology and CSIRO Division of Atmospheric Research, Melbourne, Australia, 1996b.

Langenfelds, R.L., R.J. Francey, L.P. Steele, M.P. Lucarelli, D.A. Spencer, S.A. Coram and K. Broadhurst. Flask sampling from Cape Grim overflights. *Baseline Atmospheric Program (Australia) 1994-95*, (eds. R.J.Francey, A.L.Dick and N.Derek), 112 - 117, Bureau of Meteorology and CSIRO Division of Atmospheric Research, Melbourne, Australia, 1996c.

Langenfelds, R.L., R.J. Francey, L.P. Steele, R.F. Keeling, M.L. Bender, M. Battle and W.F. Budd, Measurements of O_2/N_2 ratio from the Cape Grim Air Archive and three independent flask sampling programs, *Baseline Atmospheric Program (Australia) 1996*, (eds W.J. Bouma, A.L. Dick, and N. Derek), 57-70, Bureau of Meteorology and CSIRO, Melbourne, 1999a.

Langenfelds, R.L., R.J. Francey, L.P. Steele, M. Battle, R.F. Keeling and W.F. Budd, Partitioning of the global fossil CO_2 sink using a 19-year trend in atmospheric O_2, *Geophys. Res. Lett*, 26, 1897-1900, 1999b.

Langenfelds, R.L., L.P. Steele, C.E. Allison and R.J. Francey, GASLAB Calibration Information, Internal Report, CSIRO Atmospheric Research, Aspendale, Australia, [http://www.dar.csiro.au], 2001a.

Langenfelds, R.L., L.N. Cooper, L.P. Steele, D.A. Spencer, P.B. Krummel and P.J. Fraser, Atmospheric methane, carbon dioxide, hydrogen, carbon monoxide and nitrous oxide from Cape Grim flask air samples analysed by gas chromatography, in *Baseline Atmospheric Program (Australia) 1997/98,* edited by N.W. Tindale, R.J. Francey and N. Derek, pp. 69-74, Bureau of Meteorology and CSIRO Atmospheric Research, Melbourne, Australia, 2001b.

Langenfelds, R.L., R.J. Francey, L.P. Steele, D.A. Spencer, and B.L. Dunse, Flask sampling from Cape Grim overflights, in *Baseline Atmospheric Program (Australia) 1997/98,* edited by N.W. Tindale, R.J. Francey and N. Derek, pp. 74-84, Bureau of Meteorology and CSIRO Atmospheric Research, Melbourne, Australia, 2001c.

Langenfelds, R.L., R.J. Francey, B.C. Pak, L.P. Steele, J. Lloyd, C.M. Trudinger and C.E. Allison, Interannual growth rate variations of atmospheric CO_2 and its $\delta^{13}C$,

H_2, CH_4 and CO between 1992 and 1999 linked to biomass burning, *Global Biogeochem. Cycles*, 2002a, in press.

Langenfelds, R.L., Anthropogenic impacts on atmospheric oxygen, in *Encyclopedia of Global Environmental Change, Volume 2: The Earth system: biological and ecological dimensions of global environmental change*, edited by H. A. Mooney and J. G. Canadell, pp 140-143, John Wiley and Sons Limited, United Kingdom, 2002b.

Langenfelds, R.L., R.J. Francey, L.P. Steele, B.L. Dunse, T.M. Butler, D.A. Spencer, L.M. Kivlighon and C.P. Meyer, Flask sampling from Cape Grim overflights, in *Baseline Atmospheric Program (Australia) 1999/2000,* Bureau of Meteorology and CSIRO Atmospheric Research, Melbourne, Australia, 2002c, in press.

Langenfelds, R. L., L. P. Steele, L. N. Cooper, D. A. Spencer, D. M. Etheridge and M. P. Lucarelli, CSIRO GASLAB measurement of CO_2, CH_4, CO, H_2 and N_2O by gas chromatography, 1991-2001, CSIRO Atmospheric Research Technical Report, in preparation.

Laursen, K.K., P.V. Hobbs, L.F. Radke and R.A. Rasmussen, Some trace gas emissions from North American biomass fires with an assessment of regional and global fluxes from biomass burning, *J. Geophys. Res.*, 97, 20687-20701, 1992.

Law, R.M., P. J. Rayner, A. S. Denning, D. Erickson, M. Heimann, S. C. Piper, M. Ramonet, S. Taguchi, J. A. Taylor, C. M. Trudinger and I. G. Watterson, Variations in modelled atmospheric transport of carbon dioxide and the consequences for CO_2 inversions, *Global Biogeochem. Cycles*, 10, 783-796, 1996.

Law, R. M. and P. J. Rayner, Impacts of seasonal covariance on CO_2 inversions, *Global Biogeochem. Cycles*, 13, 845-856, 1999.

Lebovits, A., Permeability of polymers to gases, vapors and liquids, *Modern Plastics*, 43, pages 139-142, 144, 146, 150, 194, 196, 198, 200, 202, 205, 206, 208, 210 and 213, 1966.

Lee, K., R. Wanninkhof, T. Tahakashi, S.C. Doney and R.A. Feely, Low interannual variability in recent oceanic uptake of atmospheric carbon dioxide, *Nature*, 396, 155-159, 1998.

Le Quéré, C., J.C. Orr, P. Monfray, and O. Aumont, Interannual variability of the oceanic sink of CO_2 from 1979 through 1997, *Global Biogeochem. Cycles*, 14, 1247-1265, 2000.

Le Quéré, C., O. Aumont, L. Bopp, P. Bousquet, P. Ciais, R. Francey, M. Heimann, C. D. Keeling, R. F. Keeling, H. Kheshgi, P. Peylin, S. C. Piper, I. C. Prentice and P. J. Rayner, Two decades of ocean CO_2 sink and variability, *Tellus*, submitted.

Legg, C.A. and Y. Laumonier, Fires in Indonesia, 1997: a remote sensing perspective, *Ambio*, 28, 479-485, 1999.

Leggett, J., W.J. Pepper and R.J. Swart, Emissions scenarios for the IPCC: an Update, in *Climate Change 1992, the supplementary report to the IPCC scientific assessment*, edited by J.T. Houghton, B.A. Callander and S.K. Varney, Cambridge University Press, Cambridge, 68-95, 1992.

Levin, I., P. Ciais, R. Langenfelds, M. Schmidt, M. Ramonet, M. Gloor, K. Sidorov, N. Tchebakova, M. Heimann, E.D. Schulze, N.N. Vygodskaya, O. Shibistova and J. Lloyd, Two years of trace gas observations over the EuroSiberian domain derived from aircraft sampling – a concerted action, *Tellus*, 2002, in press.

Levine, J.S., The 1997 fires in Kalimantan and Sumatra, Indonesia: Gaseous and particulate emissions, *Geophys. Res. Lett.*, 26, 815-818, 1999.

Lide, D.R., *Handbook of chemistry and physics*, CRC Press, 1993.

Liew, S.C., O.K. Lim, L.K. Kwoh and H. Lim, A study of 1997 fires in South East Asia using SPOT quicklook mosaics, *paper presented at the 1998 International Geoscience and Remote Sensing Symposium*, Seattle, Washington, IEEE Geoscience and Remote Sensing Society, 3pp, July 1998.

Lloyd, J. and G.D. Farquhar, 13C discrimination during CO_2 assimilation by the terrestrial biosphere, *Oecologia*, 99, 201-215, 1994.

Lloyd, J., B. Kruijt, D.Y. Hollinger, J. Grace, R.J. Francey, S.-C. Wong, F.M. Kelliher, A.C. Miranda, G.D. Farquhar, J.H.C. Gash, N.N. Vyogdskaya, I.R. Wright, H.S. Miranda and E.-D. Schulze, Vegetation effects on the isotopic composition of atmospheric CO_2 at local and regional scales: Theoretical aspects and a comparison between rain forest in Amazonia and a boreal forest in Siberia, *Aust. J. Plant Physiol.*, 23, 371-399, 1996.

Lloyd, J., R.J. Francey, A. Sogatchev, J.N. Byers, D. Mollicone, M. Raupach, F.M. Kelliher, A. Arneth, C. Rebmann, R. Valentini, S.-C. Wong and E.-D. Schulze, Vertical profiles, boundary layer budgets and regional flux estimates for CO_2, its $^{12}C/^{13}C$ ratio, and water vapour above a forest/bog mosaic in central Siberia, *Global Biogeochem. Cycles*, in press.

Lowe, D.C., M.R. Manning, G.W. Brailsford and A.M. Bromley, The 1991-1992 atmospheric methane anomaly: Southern hemisphere $\delta^{13}C$ decrease and growth rate fluctuations, *Geophys. Res. Lett.*, 24, 857-860, 1997.

Machida, T., T. Nakazawa, S. Ishidoya, S. Maksyutov, Y. Tohjima, Y. Takahashi, T. Watai, N. Vinnichenko, M. Panchenko, M. Arshinov, N. Fedoseev and G. Inoue, Temproal and spatial variations of atmospheric CO_2 mixing ratio over Siberia, in *Sixth International Carbon Dioxide Conference: extended abstracts*, Sendai, Japan, September 2001, Organizing Committee of Sixth International Carbon Dioxide Conference, 15-18, 2001.

Machta, L. and E. Hughes, Atmospheric oxygen in 1967 to 1970, *Science*, 168, 1582-1584, 1970.

Maiss, M., L.P. Steele, R.J. Francey, P.J. Fraser, R.L. Langenfelds, N.B.A. Trivett, and I. Levin, Sulfur hexafluoride – a powerful new atmospheric tracer, *Atmos. Environ.*, 30, 1621-1629, 1996.

Malingreau, J.P., G. Stephens and L. Fellows, Remote sensing of forest fires: Kalimantan and North Borneo in 1982-1983, *Ambio*, 14, 314-321, 1985.

Manning, A.C., R.F. Keeling and J.P. Severinghaus, Precise atmospheric oxygen measurements with a paramagnetic oxygen analyzer, *Global Biogeochem. Cycles*, 13, 1107-1115, 1999.

Manning, A.C., Temporal variability of atmospheric oxygen from both continuous measurements and a flask sampling network: Tools for studying the global carbon cycle, PhD thesis, University of California, San Diego, USA, 233 pp, 2001.

Marland, G.M. and R.R. Rotty, Carbon dioxide emissions from fossil fuels: a procedure for estimation and results for 1950-1982, *Tellus, 36B*, 232-261, 1984.

Marland, G., T.A. Boden, and R. J. Andres, *Global, Regional, and National Fossil Fuel CO_2 Emissions*, In Trends: A Compendium of Data on Global Change, Carbon Dioxide Information Analysis Center, Oak Ridge National Laboratory, U.S. Department of Energy, Oak Ridge, Tenn., U.S.A., 2001.

Masarie, K.A., R.L. Langenfelds, C.E. Allison, T.J. Conway, E.J. Dlugokencky, R.J. Francey, P.C. Novelli, L.P. Steele, P.P. Tans, B. Vaughn and J.W.C. White, NOAA/CSIRO Flask-Air Intercomparison Experiment: A strategy for directly assessing consistency among atmospheric measurements made by independent laboratories, *J. Geophys. Res.*, 106, 20445-20464, 2001.

Matear, R.J., A.C. Hirst and B.I. McNeil, Changes in dissolved oxygen in the Southern Ocean with climate change, *Geochem. Geophys. Geosyst.*, vol.1, Paper number 2000GC000086, 2000.

Matsueda, H., Intercalibration experiment of methane standard gas scale between NOAA/CMDL and MRI/GRL, *Papers in Meteorology & Geophysics*, 44, 45-56, 1993.

Matsueda, H., H.Y. Inoue and M. Ishii, Large injection of carbon monoxide into the upper troposphere due to intense biomass burning in 1997, *J. Geophys. Res.*, 104, 28867-28879, 1999.

Matsueda, H. and H.Y. Inoue, Aircraft measurements of trace gases between Japan and Singapore in October of 1993, 1996 and 1997, *Geophys. Res. Lett.*, 26, 2413-2416, 1999.

Mauzerall, D.L., J.A. Logan, D.J. Jacob, B.E. Anderson, D.R. Blake, J.D. Bradshaw, B. Heikes, G.W. Sachse, H. Singh and B. Talbot, Photochemistry in biomass burning plumes and implications for tropospheric ozone over the tropical South Atlantic, *J. Geophys. Res.*, 103, 8401-8423, 1998.

Meijer, H.A.J., R.E.M. Neubert, and G.H. Visser, Cross contamination in dual inlet isotope ratio mass spectrometers, *Int. J. Mass Spectrom.* 198, 45-61, 2000.

Miranda, A.C., H.S. Miranda, J. Lloyd, J. Grace, R.J. Francey, P. Riggan and J. Brass, Fluxes of carbon dioxide and water vapour over cerrado vegetation in Central Brazil: An analysis using eddy correlation and stable isotope techniques, *Plant Cell Environ.*, 20, 315-328, 1997.

Moore,W.J., *Physical Chemistry (fourth edition)*, Longmans Green and Co Ltd., 1962.

MOPITT, Measurements Of Pollution In The Troposphere, (http://www.atmosp.physics.utoronto.ca/MOPITT/home.html)

Murayama, S., T. Nakazawa, K. Yamazaki, S. Aoki, Y. Makino, M. Shiobara, M. Fukabori, T. Yamanouchi, A. Shimizu, M, Hayashi, S. Kawaguchi and M. Tanaka, Concentration variations of atmospheric CO_2 over Syowa Station, Antarctica and their interpretation, *Tellus*, 47B, 375-390, 1995.

Nakazawa, T., S. Moromoto, S. Aoki, and M. Tanaka, Temporal and spatial variations of the carbon isotopic ratio of atmospheric carbon dioxide in the Western Pacific region, *J. Geophys. Res.*, 102, 1271-1285, 1997.

Nepstad, D.C., A. Verissimo, A. Alencar, C. Nobre, E. Lima, P. Lefebvre, P. Schlesinger, C. Potter, P. Moutinho, E. Mendoza, M. Cochrane and V. Brooks, Large-scale impoverishment of Amazonian forests by logging and fire, *Nature*, 398, 505-508, 1999.

Nichol, J., Bioclimatic impacts of the 1994 smoke haze event in Southeast Asia, *Atmos. Environ.*, 31, 1209-1219, 1997.

Nicholls, N., G.V. Gruza, J. Jouzel, T.R. Karl, L.A. Ogallo and D.E. Parker, Observed climate variability and change, in *IPCC Climate Change, The Science of Climate Change*, edited by J.T. Houghton, L.G. Meira Filho, B.A. Callander, N. Harris, A. Kattenberg and K.Maskell, Cambridge University Press, Cambridge, 133-192, 1996.

Novelli, P.C., K.A. Masarie, and P.M. Lang, Distributions and recent trends of carbon monoxide in the lower troposphere, *J. Geophys. Res.*, 103, 19015-19033, 1998.

Novelli, P.C., P.M. Lang, K.A. Masarie, D.F. Hurst, R. Myers and J.W. Elkins, Molecular hydrogen in the troposphere: Global distributions and budget, *J. Geophys. Res.,* 104, 30427-30444, 1999.

O'Hanlon, J.F., *A user's guide to vacuum technology, 2nd Edn.*, John Wiley & Sons, 1989.

Oppenheimer, M., Global warming and the stability of the West Antarctic Ice Sheet, *Nature*, 393, 325-332, 1998.

Oram, D.E., P.J. Fraser, C.E. Reeves and S.A. Penkett, Measurements of HCFC-142b and HCFC-141b in the Cape Grim air archive: 1978-1993, *Geophys. Res. Lett.,* 22, 2741-2744, 1995.

Oram, D.E., C. Reeves, W.T. Sturges, S.A. Penkett, P.J. Fraser and R.L. Langenfelds. Recent tropospheric growth rate and distribution of HFC-134a (CF_3CH_2F). *Geophys. Res. Lett.*, 23, 1949 - 1952, 1996.

Page, S.E., J.O. Rieley, H.-D.V. Bohm, F. Siegert and N.Z. Muhamad, Impact of the 1997 fires on the peatlands of central Kalimantan, Indonesia, *paper presented at the International Wetlands Conference*, Quebec, Canada, International Association for Ecology, 2000.

Pak, B. C., R. L. Langenfelds, R. J. Francey, L. P. Steele, and I. Simmonds, A climatology of trace gases from the Cape Grim Overflights, 1992-1995, in *Baseline*

Atmospheric Program (Australia), 1994-95, edited by R. J. Francey, A. L. Dick, and N. Derek, pp. 41-52, Bureau of Meteorology and CSIRO Division of Atmospheric Research, Melbourne, Australia, 1996.

Pak, B. C., M. Ramonet, P. Monfray, R. J. Francey, and I. Simmonds, Assessment of the spatial and temporal representativeness of the Cape Grim Overflight CO_2 data, in *Baseline Atmospheric Program (Australia), 1996*, edited by J. L. Gras, N. Derek, N. W. Tindale, and A. L. Dick, pp. 36-44, Bureau of Meteorology and CSIRO Atmospheric Research, Melbourne, Australia, 1999.

Pak, B.C., Vertical structure of atmospheric trace gases over South-east Australia, PhD thesis, University of Melbourne, 273 pp, 2000.

Pearman, G. I., D.J. Beardsmore and R.C. O'Brien, The CSIRO (Australia) atmospheric carbon dioxide monitoring program: Ten years of aircraft data, CSIRO Division of Atmospheric Physics Technical Paper No. 45, 113 pp., 1983.

Peñuelas, J. and I. Filella, Responses to a warming world, *Science*, 294, 793-795, 2001.

Petit, J.R., J. Jouzel, D. Raynaud, N.I. Barkov, J.-M. Barnola, I. Basile, M. Bender, J. Chappellaz, M. Davis, G. Delaygue, M. Delmotte, V.M. Kotlyakov, M. Legrand, V.Y. Lipenkov, C. Lorius, L. Pépin, C. Ritz, E. Saltzman and M. Stievenard, Climate and atmospheric history of the past 420,000 years from the Vostok ice core, Antarctica, *Nature*, 399, 429-436, 1999.

Pétron, G., P. Harley, J. Greenberg and A. Guenther, Seasonal temperature variations influence isoprene emissions, *Geophys. Res. Lett.*, 28, 1707-1710, 2001.

Peylin, P., P. Ciais, A.S. Denning, P.P. Tans, J.A. Berry and J.W.C. White, A 3-dimensional study of $\delta^{18}O$ in atmospheric CO_2: contribution of different land ecosystems, *Tellus*, 51, 642-667, 1999.

Poth, M., I.C. Anderson, H.S. Miranda, A.C. Miranda and P.J. Riggan, The magnitude and persistence of soil NO, N_2O, CH_4 and CO_2 fluxes from burned tropical savanna in Brazil, *Global Biogeochem. Cycles*, 7, 353-368, 1995.

Potter, C., V. Brooks Genovese, S. Klooster, M. Bobo and A. Torregrosa, Biomass burning losses of carbon estimated from ecosystem modeling and satellite data analysis for the Brazilian Amazon region, *Atmos. Environ.,* 35, 1773-1781, 2001.

Prather, M., R. Derwent, D. Ehhalt, P. Fraser, E. Sanhueza and X. Zhou, Radiative forcing of climate change: Other trace gases and atmospheric chemistry, in *IPCC Climate Change, The Science of Climate Change*, edited by J.T. Houghton, L.G. Meira Filho, B.A. Callander, N. Harris, A. Kattenberg and K.Maskell, Cambridge University Press, Cambridge, Section 2.2, 86-103, 1996a.

Prather, M.J., Time scales in atmospheric chemistry: Theory, GWPs for CH_4 and CO, and runaway growth, *Geophys. Res. Lett.*, 23, 2597-2600, 1996b.

Prinn, R.G., R.F. Weiss, P.J. Fraser, P.G. Simmonds, D.M. Cunnold, F.N. Alyea, S.O'Doherty, P. Salameh, B.R. Miller, J. Huang, R.H.J. Wang, D.E. Hartley, C. Harth, L.P. Steele, G. Sturrock, P.M. Midgley and A. McCulloch, *J. Geophys. Res.*, 105, 17751-17792, 2000.

Quay, P.D., B. Tilbrook and C.S. Wong, Oceanic uptake of fossil fuel CO_2: Carbon-13 evidence, *Science,* 256, 74-79, 1992.

Quay, P., J. Stutsman, D. Wilbur, A. Snover, E. Dlugokencky and T. Brown, The isotopic composition of atmospheric methane, *Glob. Biogeochem. Cycles,* 13, 445-461, 1999.

Ramonet, M., Variabilite du CO_2 atmospherique en regions australes: comparaison modele-mesures, PhD thesis, University of Paris VII, France, 295 pp., 1994.

Rasch, P.J., N.H. Mahowald and B. E. Eaton, Representations of transport, convection and the hydrologic cycle in chemical transport models: Implications for the modelling of short-lived and soluble species, *J. Geophys. Res.*, 102, 28127-28138, 1997.

Rayner, P.J., R.M. Law and R. Dargaville, The relationship between tropical CO_2 fluxes and the El Niño-Southern Oscillation, *Geophys. Res. Lett.*, 26, 493-496, 1999a.

Rayner, P.J., I.G. Enting, R.J. Francey and R.L. Langenfelds. Reconstructing the recent carbon cycle from atmospheric CO_2, $\delta^{13}C$ and O_2/N_2 observations, *Tellus*, 51B, 213-232, 1999b.

Richards, P.W., *The Tropical Rain Forest*, Cambridge University Press, Cambridge, UK, 575 pp, 1996.

Rinsland, C.P., A. Goldman, F.J. Murcray, T.M. Stephen, N.S. Pougatchev, J. Fishman, S.J. David, R.D. Blatherwick, P.C. Novelli, N.B. Jones and B.J. Connor, Infrared solar spectroscopic measurements of free tropospheric CO, C_2H_6 and HCN above Mauna Loa, Hawaii: Seasonal variations and evidence for enhanced emissions from the Southeast Asian tropical fires of 1997-1998, *J. Geophys. Res.*, 104, 18667-18680, 1999.

Rinsland, C.P., E. Mahieu, R. Zander, P. Demoulin, J. Forrer and B. Buchmann, Free tropospheric CO, C_2H_6 and HCN above central Europe: Recent measurements from the Jungfraujoch station including the detection of elevated columns during 1998, *J. Geophys. Res.*, 105, 24235-24249, 2000.

Roth, A., *Vacuum technology*, North Holland Publishing Company, 1976.

Sarmiento, J.L., U. Siegenthaler and J.C. Orr, A perturbation simulation of CO_2 uptake in an ocean general circulation model, *J. Geophys. Res.*, 97, 3621-3645, 1992.

Sarmiento, J.L. and E.T. Sundquist, Revised budget for the oceanic uptake of anthropogenic carbon dioxide, *Nature*, 356, 589-593, 1992.

Sawa, Y., H. Matsueda, Y. Tsutsumi, J.B. Jensen, H.Y. Inoue and Y. Makino, Tropospheric carbon monoxide and hydrogen measurements over Kalimantan in Indonesia and northern Australia during October 1997, *Geophys. Res. Lett.*, 26, 1389-1392, 1999.

Schade, G.W., A.H. Goldstein and M.S. Lamanna, Are monoterpene emissions influenced by humidity?, *Geophys. Res. Lett.*, 26, 2187-2190, 1999.

Schimel, D., D. Alves, I. Enting, M. Heimann, F. Joos, D. Raynaud and T. Wigley, Radiative forcing of climate change: CO_2 and the carbon cycle, in *IPCC Climate Change, The Science of Climate Change*, edited by J.T. Houghton, L.G. Meira Filho, B.A. Callander, N. Harris, A. Kattenberg and K.Maskell, Cambridge University Press, Cambridge, Section 2.1, 76-86, 1996.

Schmidt, U. and A. Khedim, In situ measurements of carbon dioxide in the winter Arctic votrtex and at midlatitudes: An indicator of the 'age' of stratospheric air, *Geophys. Res. Lett.*, 18, 763-766, 1991.

Setzer, A.W. and M.C. Pereira, Amazonia biomass burnings in 1987 and an estimate of their tropospheric emissions, *Ambio*, 20, 19-22, 1991.

Severinghaus, J.P., Studies of the terrestrial O_2 and carbon cycles in sand dune gases and in Biosphere 2, PhD Dissertation, Columbia Univ., 1995.

Severinghaus, J.P., M.L. Bender, R.F. Keeling and W.S. Broecker, Fractionation of soil gases by diffusion of water vapor, gravitational settling and thermal diffusion, *Geochim. et Cosmochim. Acta*, 60, 1005-1018, 1996.

Siegenthaler, U. and J.L. Sarmiento, Atmospheric carbon dioxide and the ocean, *Nature*, 365, 119-125, 1993.

Siegert, F. and A.A. Hoffmann, The 1998 forest fires in east Kalimantan (Indonesia): A quantitative evaluation using high resolution, multitemporal ERS-2 SAR images and NOAA-AVHRR hotspot data. *Remote Sens. Environ.* 72, 64-77, 2000.

Sowers, T., M. Bender and D. Raynaud, Elemental and isotopic composition of occluded O_2 and N_2 in polar ice, *J. Geophys. Res.*, 94, 5137-5150, 1989.

Steele, L. P., R. L, Langenfelds, M. P. Lucarelli, P. J. Fraser, L. N. Cooper, D. A. Spencer, S. Chea and K. Broadhurst, Atmospheric methane, carbon dioxide, carbon monoxide, hydrogen and nitrous oxide from Cape Grim flask samples analysed by

gas chromatography, in *Baseline Atmospheric Program (Australia), 1994-95*, edited by R. J. Francey, A. L. Dick and N. Derek, pp. 107-110, Bureau of Meteorology and CSIRO Division of Atmospheric Research, Melbourne, Australia, 1996.

Steele, L. P., D. J. Beardsmore, G. A. Da Costa and G. I. Pearman, Baseline carbon dioxide monitoring, in *Baseline Atmospheric Program (Australia), 1996*, edited by J. L. Gras, N. Derek, N. W. Tindale and A. L. Dick, pp. 88-89, Bureau of Meteorology and CSIRO Atmospheric Research, Melbourne, Australia, 1999.

Stephens, B.B., R.F. Keeling, M. Heimann, K.D. Six, R. Murnane and K. Caldeira, Testing global ocean carbon cycle models using measurements of atmospheric O_2 and CO_2 concentration, *Global Biogeochem. Cycles*, 12, 213-230, 1998.

Takahashi, T., R. H. Wanninkhof, R. A. Feely, R. F. Weiss, D.W. Chipman, N. Bates, J. Olafsson, C. Sabine and S. C. Sutherland, Net sea-air CO_2 flux over the global oceans: An improved estimate based on the air-sea pCO_2 difference, paper presented at 2nd International CO_2 in the Oceans Symposium, National Institute of Environmental Studies, Tsukuba, Japan, January 18-22, 1999.

Tanaka, M., T. Nakazawa, S. Aoki and H. Ohshima, Aircraft measurements of tropospheric carbon dioxide over the Japanese islands, *Tellus*, 40B, 16-22, 1988.

Tans, P., J. Berry and R. Keeling, Oceanic $^{13}C/^{12}C$ observations: a new window on ocean CO_2 uptake, *Global Biogeochem. Cycles*, 7, 353-368, 1993.

Tans, P.P., P.S. Bakwin, L. Bruhwiler, T.J. Conway, E.J. Dlugokencky, D.W. Guenther, D.R. Kitzis, P.M. Lang, K.A. Masarie, J.B. Miller, P.C. Novelli, K.W. Thoning, M. Trudeau, B.H. Vaughn, J.W.C. White and C. Zhao, Carbon Cycle, in *Climate Monitoring and Diagnostics Laboratory: Summary report No. 25 1998-1999*, edited by R.C. Schnell, D.B. King and R.M. Rosson, NOAA/Clmate and Monitoring Diagnostics Laboratory, Boulder, Colorado, USA, pp 24-46, 2001.

Thompson, T.M., J.W. Elkins, J.H. Butler, S.A. Montzka, R.C. Myers, T.J. Baring, S.O. Cummings, G.S. Dutton, J.M. Gilligan, A.H. Hayden, J.M. Lobert, T.H. Swanson, D.F. Hurst and C.M. Volk, Nitrous oxide and halocarbons division, in

Climate Monitoring and Diagnostics Laboratory No. 22: Summary report 1993, edited by J.T. Peterson and R.M. Rosson, NOAA Environmental Research Laboratories, Boulder, Colorado, USA, pp 72-91, 1994.

Thompson, M.V. and J.T. Randerson, Impulse response functions of terrestrial carbon cycle models: method and application, *Glob. Change Biol.*, 5, 371-194, 1999.

Thompson, A.M., J.C. Witte, R.D. Hudson, H. Guo, J.R. Herman and M. Fujiwara, Tropical tropospheric ozone and biomass burning, *Science,* 291, 2128-2132, 2001.

Thoning, K.W., P. Tans, T.J. Conway and L.S. Waterman, NOAA/GMCC calibrations of CO_2-in-air reference gases: 1979-1985, *NOAA Technical Memorandum ERL-150*, NOAA, Boulder, Colorado, USA, 63pp, 1987.

Thoning, K.W., P.P. Tans and W.D. Komhyr, Atmospheric carbon dioxide at Mauna Loa Observatory, 2, Analysis of the NOAA/GMCC data, 1974 - 1985, *J. Geophys. Res.,* 94, 8549-8565, 1989.

Tian, H., J.M. Melillo, D.W. Kicklighter, A.D. McGuire, J.V.K. Helfrich III, B. Moore III and C.J. Vörösmarty, Effect of interannual climate variability on carbon storage in Amazonian ecosystems, *Nature,* 396, 664-667, 1998.

Tohjima, Y., Method for measuring changes in the atmospheric O_2/N_2 ratio by a gas chromatograph equipped with a thermal conductivity detector, *J. Geophys. Res.,* 105, 14575-14584, 2000.

Trudinger, C.M., I.G. Enting, R.J. Francey, D.M Etheridge and P.J. Rayner, Long-term variability in the global carbon cycle inferred from a high-precision CO_2 and $\delta^{13}C$ ice-core record, *Tellus* 51B, 233-248, 1999.

Trudinger, C.M., The carbon cycle over the last 1000 years inferred from inversion of ice core data, PhD thesis, Monash University, Melbourne, Australia, 2000.

Ward, D.E., R.A. Susott, J.B. Kauffman, R.E. Babbitt, D.L. Cummings, B. Dias, B.N. Holben, Y.J. Kaufman, R.A. Rasmussen and A.W. Setzer, Smoke and fire

characteristics for cerrado and deforestation burns in Brazil: Base-B experiment, *J. Geophys. Res.*, 97, 14601-14619, 1992.

Waring, R.H., J.J. Landsberg and M. Williams, Net primary production of forests: a constant fraction of gross primary production?, *Tree Physiol.*, 18, 129-134, 1998.

Warneck, P., Chemistry of the natural atmosphere, Academic Press Inc., 1988.

Warrick, R.A., C. Le Provost, M.F. Meier, J. Oerlemans and P.L. Woodworth, Changes in sea level, in *IPCC Climate Change, The Science of Climate Change*, edited by J.T. Houghton, L.G. Meira Filho, B.A. Callander, N. Harris, A. Kattenberg and K.Maskell, Cambridge University Press, Cambridge, 359-405, 1996.

Weeks, I.A., R.J. Francey, D.J. Beardsmore and L.P. Steele, Studies in air archiving techniques. Part2: filling high pressure cylinders with baseline air, in *Baseline Atmospheric Program (Australia) 1990,* edited by S.R.Wilson and J.L.Gras, pp. 16-23, Bureau of Meteorology and CSIRO Division of Atmospheric Research, Melbourne, Australia, 1992.

Wigley, T.M.L., A simple inverse carbon cycle model, *Global Biogeochem. Cycles*, 5, 373-382, 1991.

Yang, X. and M.X. Wang, Monsoon ecosystems control on atmospheric CO_2 interannual variability inferred from a significant positive correlation between year-to-year changes in land precipitation and atmospheric CO_2 growth rate. *Geophys. Res. Lett.* 27, 1671-1674, 2000.

Yokelson, R.J., R. Susott, D.E. Ward, J. Reardon and D.W.T. Griffith, Emissions from smoldering combustion of biomass measured by open-path Fourier transform infrared spectroscopy, *J. Geophys. Res.*, 102, 18865-18877, 1997.

Yokohata, A., Y. Makide and T. Tominaga, A new calibration method for the measurement of CCl_4 concentration at 10^{-10} v/v level and the behaviour of CCl_4 in the atmosphere, *J. Bull. Chem. Soc. Jpn.*, 58, 1308-1314, 1985.

Zaidel'man, F.R., M.V. Bannikov and A.P. Shvarov, Properties and fertility of pyrogenic formations on burnt drained peaty soils. *Eurasian Soil Sci.* 32, 1032-1039, 1999.

Zhao, C.L., P.P. Tans and K.W. Thoning, A high precision manometric system for absolute calibrations of CO_2 in dry air, *J. Geophys. Res.,* 102, 5885-5894, 1997.

Zimmerman, P.R., R.B. Chatfield, J. Fishman, P.J. Crutzen and P.L. Hanst, Estimates on the production of CO and H_2 from the oxidation of hydrocarbon emissions from vegetation, *Geophys. Res. Lett.*, 5, 679-682, 1978.